CONF-9410216--Vol.3

NUREG/CP-0140
Vol. 3

Proceedings of the U.S. Nuclear Regulatory Commission

Twenty-Second Water Reactor Safety Information Meeting

Volume 3
- Primary Systems Integrity
- Structural & Seismic Engineering
- Aging Research, Products & Applications

Held at
Bethesda Marriott Hotel
Bethesda, Maryland
October 24–26, 1994

U.S. Nuclear Regulatory Commission

Office of Nuclear Regulatory Research

Proceedings prepared by
Brookhaven National Laboratory

AVAILABILITY NOTICE

Availability of Reference Materials Cited in NRC Publications

Most documents cited in NRC publications will be available from one of the following sources:

1. The NRC Public Document Room, 2120 L Street, NW., Lower Level, Washington, DC 20555-0001

2. The Superintendent of Documents, U.S. Government Printing Office, P. O. Box 37082, Washington, DC 20402-9328

3. The National Technical Information Service, Springfield, VA 22161-0002

Although the listing that follows represents the majority of documents cited in NRC publications, it is not intended to be exhaustive.

Referenced documents available for inspection and copying for a fee from the NRC Public Document Room include NRC correspondence and internal NRC memoranda; NRC bulletins, circulars, information notices, inspection and investigation notices; licensee event reports; vendor reports and correspondence; Commission papers; and applicant and licensee documents and correspondence.

The following documents in the NUREG series are available for purchase from the Government Printing Office: formal NRC staff and contractor reports, NRC-sponsored conference proceedings, international agreement reports, grantee reports, and NRC booklets and brochures. Also available are regulatory guides, NRC regulations in the *Code of Federal Regulations*, and *Nuclear Regulatory Commission Issuances*.

Documents available from the National Technical Information Service include NUREG-series reports and technical reports prepared by other Federal agencies and reports prepared by the Atomic Energy Commission, forerunner agency to the Nuclear Regulatory Commission.

Documents available from public and special technical libraries include all open literature items, such as books, journal articles, and transactions. *Federal Register* notices, Federal and State legislation, and congressional reports can usually be obtained from these libraries.

Documents such as theses, dissertations, foreign reports and translations, and non-NRC conference proceedings are available for purchase from the organization sponsoring the publication cited.

Single copies of NRC draft reports are available free, to the extent of supply, upon written request to the Office of Administration, Distribution and Mail Services Section, U.S. Nuclear Regulatory Commission, Washington, DC 20555-0001.

Copies of industry codes and standards used in a substantive manner in the NRC regulatory process are maintained at the NRC Library, Two White Flint North, 11545 Rockville Pike, Rockville, MD 20852-2738, for use by the public. Codes and standards are usually copyrighted and may be purchased from the originating organization or, if they are American National Standards, from the American National Standards Institute, 1430 Broadway, New York, NY 10018-3308.

DISCLAIMER NOTICE

NUREG/CP–0140
Vol. 3

Proceedings of the U.S. Nuclear Regulatory Commission

Twenty-Second Water Reactor Safety Information Meeting

Volume 3

- Primary Systems Integrity
- Structural & Seismic Engineering
- Aging Research, Product & Applications

Held at
Bethesda Marriott Hotel
Bethesda, Maryland
October 24–26, 1994

Manuscript Completed: March 1995
Date Published: April 1995

Compiled by: Susan Monteleone

Office of Nuclear Regulatory Research
U.S. Nuclear Regulatory Commission
Washington, DC 20555–0001

Proceedings prepared by
Brookhaven National Laboratory

ABSTRACT

This three-volume report contains papers presented at the Twenty-Second Water Reactor Safety Information Meeting held at the Bethesda Marriott Hotel, Bethesda, Maryland, during the week of October 24-26, 1994. The papers are printed in the order of their presentation in each session and describe progress and results of programs in nuclear safety research conducted in this country and abroad. Foreign participation in the meeting included papers presented by researchers from Finland, France, Italy, Japan, Russia, and United Kingdom. The titles of the papers and the names of the authors have been updated and may differ from those that appeared in the final program of the meeting.

PROCEEDINGS OF THE
22nd WATER REACTOR SAFETY INFORMATION MEETING

October 24-26, 1994

Published in Three Volumes

GENERAL INDEX

REGISTERED ATTENDEES (NON-NRC)
22ND WATER REACTOR SAFETY INFORMATION MEETING

H. ABE
NUCLEAR POWER ENGINEERING CORP.
3-13 4-CHOME TORANOMON
MINATO-KU TOKYO, 105 JAPAN

S. AHN
KOREA INSTITUTE OF NUCLEAR SAFETY
PO BOX 114
YUSUNG, TAEJON, 305-600 KOREA

R. ALLEN
BATTELLE PACIFIC NORTHWEST LABS
PO BOX 999, MS P8-10
RICHLAND, WA 99352 USA

R. AMADOR
COMISION NACIONAL DE SEGURIDAD NUC. Y SALVAGUARDIA
DR BARRAGAN NO 779, COL NARVARTE
MEXICO D.F., 03020 MEXICO

J. ANDREWS
B&W FUEL COMPANY
PO BOX 10935
LYNCHBURG, VA 24506-0935 USA

V. ASMOLOV
RUSSIAN RESEARCH CENTER KURCHATOV INST.
KURCHATOV SQUARE
MOSCOW, 123182 RUSSIA

T. BAKER
SHIFTWORK SYSTEMS, INC.
ONE KENDALL SQUARE, BLDG. 200, 4TH FLOOR
CAMBRIDGE, MA 02139 USA

A. BARATTA
PENN STATE UNIV., NUCLEAR ENGINEERING DEPT.
231 SACKETT BLDG.
UNIVERSITY PARK, PA 16802 USA

P. BAYLESS
IDAHO NATIONAL ENGINEERING LABORATORY
PO BOX 1625
IDAHO FALLS, ID 83415-3840 USA

S. BEUS
WESTINGHOUSE BETTIS
P.O. BOX 79
WEST MIFFLIN, PA 15122 USA

D. BHATTACHARYA
NUCLEAR POWER CORP. OF INDIA
BOMBAY, INDIA

S. ADDITON
TENERA (ARSAP)
1901 RESEARCH BLVD., SUITE 100
ROCKVILLE, MD 20850-3184 USA

M. ALAMMAR
GPU NUCLEAR CORP.
ONE UPPER POND RD.
PARSIPPANY, NJ 07054 USA

K. ALMENAS
UNIVERSITY OF MARYLAND
MAT. & NUC. ENERGY DEPT.
COLLEGE PARK, MD USA

L. ANDERMO
SWEDISH NUCLEAR POWER INSPECTORATE
BOX 27106
STOCKHOLM, S-102 52 SWEDEN

W. ANDREWS
SOUTHERN NUCLEAR OPERATING COMPANY
PO BOX 1295
BIRMINGHAM, AL 35201 USA

A. ASRANI
ATOMIC ENERGY REGULATORY BOARD
VIKRAM SARASHAI BHAVAN, ANUSHAKTI NAGAR
BOMBAY, 400 094 INDIA

M. BALE
B&W FUEL COMPANY
3315 OLD FOREST RD., PO BOX 10935
LYNCHBURG, VA 24506 USA

R. BARI
BROOKHAVEN NATIONAL LABORATORY
BLDG. 130, PO BOX 5000
UPTON, NY 11973 USA

L. BELBLIDIA
SCANDPOWER, INC.
101 LAKE FOREST BLVD., STE. 340
GAITHERSBURG, MD 20877 USA

C. BEYER
PACIFIC NORTHWEST LABORATORY
BATTELLE BLVD.
RICHLAND, WA 99352 USA

D. BLEY
BUTTONWOOD CONSULTING INC.
17291 BUTTONWOOD STREET
FOUNTAIN VALLEY, CA 92708 USA

A. AFZALI
NUS
910 CLOPPER ROAD
GAITHERSBURG, MD 20879 USA

A. ALEMBERTI
ANSALDO
C. 30 PERRONE 25
GENOVA, 16161 ITALY

A. ALONSO
POLYTECHNIC UNIVERSITY OF MADRID
JOSE GUTIERREZ ABASCAL, 2
MADRID, 28006 SPAIN

M. ANDOU
HITACHI WORKS, HITACHI LTD.
1-1, SAIWAI-CHO 3-CHOME
HITACHI-SHI, IBARAKI-KEN 317 JAPAN

S. ASAI
MINISTRY OF INT'L TRADE AND INDUSTRY
1-3-1, KASUMIGASAKI
CHIYODA-KU, TOKYO 100 JAPAN

M. AZARM
BROOKHAVEN NATIONAL LABORATORY
PO BOX 5000, BLDG. 130
UPTON, NY 11973-5000 USA

Y. BANG
KOREA INSTITUTE OF NUCLEAR SAFETY
PO BOX 114
YUSUNG, TAEJON, 305-600 KOREA

M. BARRIERE
BROOKHAVEN NATIONAL LABORATORY
PO BOX 5000, BLDG. 130
UPTON, NY 11973-5000 USA

K. BERGERON
SANDIA NATIONAL LABORATORIES
P.O. BOX 5800, MS 0743
ALBUQUERQUE, NM 87185-0743 USA

B. BHASIN
NUCLEAR POWER CORPORATION OF INDIA
TARAPUR ATOMIC POWER STATION
TARAPUR, MAHARASHTRA, INDIA

L. BOLSHOV
RUSSIAN ACADEMY OF SCIENCES/NUC. SAFETY INST.
B. TULSKAYA, 52
MOSCOW, 113191 RUSSIA

M. BONNER
BROOKHAVEN NATIONAL LABORATORY
BLDG. 197C, PO BOX 5000
UPTON, NY 11973-5000 USA

B. BOYACK
LOS ALAMOS NATIONAL LABORATORY
P.O. BOX 1663, MS K551
LOS ALAMOS, NM 87545 USA

R. BOYER
DUKE POWER CO.
8725 HORNWOOD CT.
CHARLOTTE, NC 28215 USA

G. BROWN
AEA TECHNOLOGY
THOMSON HOUSE, RISLEY
WARRINGTON, CHESHIRE WA36AT UK

W. BRUNSON
B&W FUEL COMPANY
PO BOX 10935
LYNCHBURG, VA 24506-0935 USA

R. BUDNITZ
FUTURE RESOURCES ASSOCIATES, INC.
2039 SHATTUCK AVE., SUITE 402
BERKELEY, CA 94704 USA

J. BUTLER
WESTINGHOUSE
P.O. BOX 355
PITTSBURGH, PA 15230 USA

C. CALLAWAY
NUCLEAR ENERGY INSTITUTE - NEI
1776 I ST., N.W., SUITE 400
WASHINGTON, DC 20006-3708 USA

A. CAMP
SANDIA NATIONAL LABORATORIES
PO BOX 5800
ALBUQUERQUE, NM 87185-0747 USA

G. CANAVAN
NEW YORK POWER AUTHORITY
123 MAIN ST.
WHITE PLAINS, NY 10601 USA

F. CARLIN
CIS BIO INTERNATIONAL
BP NO. 32
GIF-SUR-YVETTE CEDEX, F91192 FRANCE

D. CASADA
OAK RIDGE NATIONAL LABORATORY
PO BOX 2009, BLDG. 9102-1
OAK RIDGE, TN 37831-8038 USA

N. CAVLINA
UNIVERSITY OF ZAGREB
FACULTY OF ELEC. ENGINEERING, UNSKA 3
ZAGREB, CRO 41000 CROATIA

D. CHAPIN
MPR ASSOCIATES, INC.
320 KING ST.
ALEXANDRIA, VA 22314-3238 USA

F-B. CHEUNG
PENNSYLVANIA STATE UNIVERSITY
304 REBER BLDG., PENN STATE U.
UNIVERSITY PARK, PA 16802 USA

B. CHO
ILLINOIS DEPARTMENT OF NUCLEAR SAFETY
1035 OUTER PARK DRIVE
SPRINGFIELD, IL 62704 USA

D. CHO
ARGONNE NATIONAL LABORATORY
BLDG. 208, 9700 S. CASS AVE.
ARGONNE, IL 60439 USA

J. CHOI
KOREA INSTITUTE OF NUCLEAR SAFETY
151 DUKJIN-DONG YUSEONG-GU
TAEJON, KOREA, KOREA

S. CHOI
KOREA INSTITUTE OF NUCLEAR SAFETY
PO BOX 114
YUSUNG, TAEJON, 305-600 KOREA

A. CHRISTOU
MATERIALS & NUCLEAR ENG'G., U. OF MARYLAND
2135 BLDG. 090
COLLEGE PARK, MD 20742-2115 USA

T-L. CHU
BROOKHAVEN NATIONAL LABORATORY
BLDG. 130, P.O. BOX 5000
UPTON, NY 11973-5000 USA

T. CHU
SANDIA NATIONAL LABORATORIES
MS 1137, DEPT. 6422
ALBUQUERQUE, NM 87185 USA

N. CHUGO
TOSHIBA CORP.
8, SHINSUGITA-CHO, ISOGO-KU
YOKOHAMA, 235 JAPAN

A. COMBESCURE
CENTRE D'ETUDES DE SACLAY - DRN/DMT/SEMT
CENTRE D'ETUDES DE SACLAY
GIF SUR YVETTE CEDEX, 91191 FRANCE

L. COMES
SCIENCE & ENGINEERING ASSOCIATES, INC.
7918 JONES BRANCH DR., SUITE 500
MC LEAN, VA 22102 USA

L. CONNOR
SOUTHERN TECHNICAL SERVICES, INC.
3 METRO CENTER, SUITE 610
BETHESDA, MD 20814 USA

S. COOPER
SCIENCE APPLICATIONS INT'L. CORP.
11251 ROGER BACON DR., PO BOX 4875
RESTON, VA 22090 USA

R. COPELAND
SIEMENS POWER CORP.
2101 HORN RAPIDS RD.
RICHLAND, WA 99352 USA

B. CORWIN
OAK RIDGE NATIONAL LABORATORY
P.O. BOX 2008
OAK RIDGE, TN 37831-6151 USA

M. COURTAUD
COMMISSARIAT A L'ENERGIE ATOMIQUE
CENTRE D'ETUDES DE GRENOBLE 17, RUE DES MARTYRS
GRENOBLE, 38054 FRANCE

K. COZENS
NUCLEAR ENERGY INSTITUTE - NEI
1776 I ST., N.W., SUITE 400
WASHINGTON, DC 20006-3708 USA

M. CUNNINGHAM
PACIFIC NORTHWEST LABORATORY
PO BOX 999 K8-43
RICHLAND, WA 99352 USA

R. CURTIS
AECL RESEARCH
WHITESHELL LABORATORIES
PINAWA, MB ROE 1LO CANADA

V. DAJI
DUKE POWER COMPANY
9515 PONDSIDE LANE
CHARLOTTE, NC 28213 USA

R. DALLMAN
SCIENTECH, INC.
1700 LOUISIANA BLVD., NE STE. 230
ALBUQUERQUE, NM 87110 USA

J. DANKO
CONSULTANT - UNIVERSITY OF TENNESSEE
15818 SE 35TH ST
VANCOUVER, WA 98684 USA

J. DAVIS
NUCLEAR ENERGY INSTITUTE - NEI
1776 I ST., N.W., SUITE 400
WASHINGTON, DC 20006-3708 USA

B. DE BOECK
AIB-VINCOTTE NUCLEAIR
AVENUE DU ROI, 157
BRUSSELS, B-1060 BELGIUM

J. DE BOR
SCIENCE & ENGINEERING ASSOCIATES, INC.
7918 JONES BRANCH DR., SUITE 500
MC LEAN, VA 22102 USA

L. DEITRICH
ARGONNE NATIONAL LABORATORY
9700 SO. CASS AVE., BLDG. 208
ARGONNE, IL 60439 USA

D. DIAMOND
BROOKHAVEN NATIONAL LABORATORY
BLDG. 130, PO BOX 5000
UPTON, NY 11973-5000 USA

H. DIAMOND
PELCO ENERGY
965 CHESTERBROOK BLVD.
WAYNE, PA 19087 USA

H. DIETERSHAGEN
KNOLLS ATOMIC POWER LAB., INC. - MARTIN MARIETTA
RIVER ROAD - PO BOX 1072
SCHENECTADY, NY 12301-1072 USA

S. DOROFEEV
KURCHATOV INSTITUTE
KURCHATOV SQUARE 1
MOSCOW, RUSSIA, 123182 RUSSIA

R. DUBOURG
CEA-IPSN DES/SEPRI
BP 6
FONTENAY AUX ROSES, 92265 FRANCE

J. DUCO
INSTITUT DE PROTECTION ET DE SURETE NUCLEAIR
CEA, CEN/FAR 60-68 AVE. DU GENERAL LECLERC
FONTENAY AUX ROSES, 92265 FRANCE

R. DUFFEY
BROOKHAVEN NATIONAL LABORATORY
PO BOX 5000, BLDG. 197C
UPTON, NY 11973-5000 USA

J. EATON
NUCLEAR ENERGY INSTITUTE - NEI
1776 I ST., N.W., SUITE 400
WASHINGTON, DC 20006-3708 USA

R. EBERLE
SIEMENS-KWU
HAMMERBACHERSTRASSE 12+14
ERLANGEN, D-8520 GERMANY

M. ELI
LAWRENCE LIVERMORE NATIONAL LAB.
PO BOX 808, L-126
LIVERMORE, CA 94550 USA

F. ELIA
STONE AND WEBSTER ENG. CORP.
PO BOX 2325
BOSTON, MA 02107 USA

T. ENDO
NUCLEAR POWER ENGINEERING CORP.
FUJITA KANKO TORANOMON BLDG. 5F 17-1, 3-CHOME, TORA
MINATO-KU, TOKYO 105 JAPAN

R. ENNIS
TENERA
1901 RESEARCH BLVD., SUITE 100
ROCKVILLE, MD 20850 USA

T. EURASTO
FINNISH CENTRE FOR RADIATION & NUCLEAR SAFETY
PO BOX 14, FIN-00881
HELSINKI, FINLAND

M. FAKORY
S3 TECHNOLOGIES
8930 STAMFORD BLVD.
COLUMBIA, MD 21045 USA

D. FERETIC
UNIVERSITY OF ZAGREB
FACULTY OF ELEC. ENGINEERING, UNSKA 3
ZAGREB, CRO 41000 CROATIA

F. FERON
DIRECTION DE LA SURETE DES INSTALLATIONS NUCLEAIRES
20 AVENUE DE SEGUR
PARIS CEDEX 07 SP, 75353 FRANCE

A. FERRELI
DIR. FOR NUCLEAR SAFETY & HEALTH PROTECTION
VIA VITALIANO BRANCATI 48
ROME, 00168 ITALY

I. FIERO
ABB COMBUSTION ENGINEERING NUCLEAR FUEL
1000 PROSPECT HILL RD.
WINDSOR, CT 06095-0500 USA

M. FIRNHABER
GRS
SCHWERTNERGASSE 1
COLOGNE, 50667 GERMANY

J. FISHER
UTILITY RESOURCE ASSOCIATES, INC.
51 MONROE ST., SUITE 12000
ROCKVILLE, MD 20850 USA

M. FLETCHER
AECL TECHNOLOGIES INC.
9210 CORPORATE BLVD., SUITE 410
ROCKVILLE, MD 20850 USA

J. FOLSOM
GPU NUCLEAR CORP.
ONE UPPER POND RD.
PARSIPPANY, NJ 07054 USA

J. FORESTER
SANDIA NATIONAL LABORATORIES
DEPT. 6412
ALBUQUERQUE, NM 87185 USA

T. FUJISHIRO
JAPAN ATOMIC ENERGY RESEARCH INSTITUTE
TOKAI-MURA, NAKA-GUN
IBARAKI-KEN 319-11, JAPAN

A. FUKUDA
TOSHIBA CORP., ISOGO NUCLEAR ENGINEERING
8 SHINSUGITA-CHO, ISOGO-KU
YOKOHAMA, KANAGAWA 235 JAPAN

R. GAMBLE
GE NUCLEAR ENERGY
175 CURTNER AVE, M.C. 781
SAN JOSE, CA 95125 USA

R. GAUNTT
SANDIA NATIONAL LABORATORIES
PO BOX 5800, M.S. 1139
ALBUQUERQUE, NM 87185-1139 USA

J. GAUTHIER
COMMISSARIAT A L'ENERGIE ATOMIQUE
CE/FAR BP 6
FONTENAY AUX ROSES, 92265 FRANCE

S. GIBELLI
BROOKHAVEN NATIONAL LABORATORY
PO BOX 5000, BLDG. 130
UPTON, NY 11973-5000 USA

C. GIGGER
BETTIS
P.O. BOX 79
WEST MIFFLIN, PA 15122 USA

R. GILLILAND
OAK RIDGE NATIONAL LABORATORY
P.O. BOX 2009, MS 8051
OAK RIDGE, TN 37831-8051 USA

T. GINSBERG
BROOKHAVEN NATIONAL LABORATORY
PO BOX 5000, BLDG. 197D
UPTON, NY 11973-5000 USA

L. GOLDSTEIN
S.M. STOLLER CORP.
485 WASHINGTON AVE.
PLEASANTVILLE, NY 10570 USA

M. GOMOLINSKI
IPSN
321 RUE DE CHARENTON
PARIS, F 75012 FRANCE

A. GOPALAKRISHNAN
ATOMIC ENERGY REGULATORY BOARD
VIKRAM SARASHAI BHAVAN, ANUSHAKTI NAGAR
BOMBAY, 400 094 INDIA

M. GOTO
TOSHIBA CORP., ISOGO NUCLEAR ENGINEERING
8 SHINSUGITA-CHO, ISOGO-KU
YOKOHAMA, KANAGAWA 235 JAPAN

N. GOULDING
B&W NUCLEAR TECHNOLOGIES
PO BOX 10935
LYNCHBURG, VA 24506-0935 USA

M. GRANDAME
ATOMIC ENERGY CONTROL BOARD CANADA
C/O ONTARIO HYDRO, P.O. BOX 160
PICKERING, ONTARIO L1V2r5 CANADA

J. GREEN
UNIVERSITY OF MARYLAND
NUCLEAR ENG'G, 2135 BLDG. 090
COLLEGE PARK, MD 20742 USA

L. GROSSMAN
ABB COMBUSTION ENGINEERING
ADDISON ROAD
WINDSOR, CT 06095 USA

M. GROUNES
STUDSVIK NUCLEAR
S-61182 NYKOPING
NYKOPING, S-61182 SWEDEN

S. HABER
BROOKHAVEN NATIONAL LABORATORY
BLDG. 130, PO BOX 5000
UPTON, NY 11973-5000 USA

G. HACHE
INSTITUT DE PROTECTION ET DE SURETE NUCLEAIRE
CE CADARACHE BAT. 702
ST. PAUL LEZ DURANCE, 13108 FRANCE

R. HALL
BROOKHAVEN NATIONAL LABORATORY
BLDG. 130, PO BOX 5000
UPTON, NY 11973-5000 USA

L. HARROP
NUCLEAR INSTALLATIONS INSPECTORATE
ST. PETER'S HOUSE, BALLIOL RD
BOOTLE, MERSEYSIDE, L20 3LZ UK

E. HARVEGO
IDAHO NATIONAL ENGINEERING LABORATORY
PO BOX 1625
IDAHO FALLS, ID 83415 USA

C. HARWOOD
ATOMIC ENERGY CONTROL BOARD, CANADA
PO BOX 1046 STATION B, 280 SLATER ST.
OTTAWA, ONTARIO K1P 5S9 CANADA

H. HASHEMIAN
ANALYSIS & MEASUREMENT SERVICES CORP
9111 CROSS PARK DR., NW
KNOXVILLE, TN 37923-4599 USA

M. HASSAN
BROOKHAVEN NATIONAL LABORATORY
PO BOX 5000, BLDG. 130
UPTON, NY 11973-5000 USA

H. HAYDEN
OAK RIDGE NATIONAL LABORATORY
P.O. BOX 2008, BLDG. 4500S
OAK RIDGE, TN 37831-6152 USA

J. HENRY
INSTITUT DE PROTECTION ET DE SURETE NUCLEAIRE
BP6
FONTENAY AUX ROSES, 92265 FRANCE

A. HEYMER
NUCLEAR ENERGY INSTITUTE - NEI
1776 I ST., N.W., SUITE 400
WASHINGTON, DC 20006-3708 USA

D. HIDINGER
MARTIN MARIETTA CORP. (KAPL, INC.)
PO BOX 1072
SCHENECTADY, NY 12302 USA

J. HIGGINS
BROOKHAVEN NATIONAL LABORATORY
BLDG. 130, PO BOX 5000
UPTON, NY 11973-5000 USA

A. HO
SIEMENS POWER CORP., NUCLEAR DIV.
PO BOX 130
RICHLAND, WA 99352 USA

R. HOBBINS
RRH CONSULTING
PO BOX 971
WILSON, WY 83014 USA

L. HOCHREITER
WESTINGHOUSE ELECTRIC COMPANY
P.O. BOX 355
PITTSBURGH, PA 15230 USA

S. HODGE
OAK RIDGE NATIONAL LABORATORY
PO BOX 2009 9104-1, MS 8057
OAK RIDGE, TN 37831-8057 USA

P. HOFMANN
NUCLEAR RESEARCH CENTER KARLSRUHE
PO BOX 3640
KARLSRUHE, D-76021 GERMANY

J. HOHORST
IDAHO NATIONAL ENGINEERING LABORATORY
PO BOX 1625
IDAHO FALLS, ID 83415 USA

H. HOLMSTROM
VTT ENERGY, NUCLEAR ENERGY
PO BOX 1604
ESPOO, 02044 VTT FINLAND

R. HOUSER
BETTIS ATOMIC POWER LABORATORY
173 MONTICELLO DR.
MONROEVILLE, PA 15146 USA

A. HOWARD
TOKYO ELECTRIC POWER CO
1901 L ST., NW
WASHINGTON, DC 20036 USA

T. HSU
VIRGINIA POWER
5000 DOMINION BLVD.
GLEN ALLEN, VA 23060 USA

H-Y HUANG
ATOMIC ENERGY COUNCIL, REP. OF CHINA
67 LANE 144, KEELUNG RD., SEC. 4
TAIPEI, TAIWAN ROC

S. HYTEN
WYLE LABORATORIES
PO BOX 077777
HUNTSVILLE, AL 35807-7777 USA

Y. IBE
NUCLEAR POWER ENGINEERING CORP.
3-13 4-CHOME TORANOMON
MINATO-KU TOKYO, 105 JAPAN

R. IRWIN
UNION ELECTRIC CO.
PO BOX 149, MC 470
ST. LOUIS, MO 63166 USA

H. ISBIN
NSRRC
2815 MONTEREY PKWY
MINNEAPOLIS, MN 55416-3959 USA

M. ISHII
PURDUE UNIVERSITY
SCHOOL OF NUCLEAR ENGINEERING
WEST LAFAYETTE, IN 47907 USA

J. JANSKY
BTB JANSKY GMBH
GERLINGER STR. 151
LEONBERG, 71229 GERMANY

T. JAYAKUMAR
INDIRA GANDHI CENTRE FOR ATOMIC RESEARCH
KALPAKKAM, INDIA

M. JIMINEZ
FLORIDA POWER & LIGHT
700 UNIVERSITY BLVD.
JUNO BEACH, FL 33407 USA

Y. JIN
KOREA ATOMIC ENERGY RESEARCH INST.
PO BOX 105, YUSEONG
TAEJON, 305-353 KOREA

J. JO
BROOKHAVEN NATIONAL LABORATORY
BLDG. 130, P.O. BOX 5000
UPTON, NY 11973-5000 USA

G. JOHNSEN
IDAHO NATIONAL ENGINEERING LAB
PO BOX 1625
IDAHO FALLS, ID 83415-3880 USA

R. JOHNSON
PACIFIC GAS & ELECTRIC CO.
333 MARKET ST., RM. 1061
SAN FRANCISCO, CA 94177 USA

A. KAKODKAR
BHABHA ATOMIC RESEARCH CENTRE
REACTOR DESIGN & DEV. GROUP
TROMBAY, INDIA

F. KAM
OAK RIDGE NATIONAL LABORATORY
PO BOX 2009
OAK RIDGE, TN 37831-8250 USA

S-P KAO
SIMULATION EXPERT SYSTEMS
23 HARBOR CLOSE
NEW HAVEN, CT 06519 USA

Y. KARINO
TOSHIBA CORP. (GE NUCLEAR ENERGY)
970 ST. ANDREWS DR., APT. 102
WILMINGTON, NC 28412 USA

H. KARWAT
TECHNISCHE UNIVERSITAT MUNCHEN
FORSCHUNGSGELANDE, D-85748 GARCHING
GARCHING, GARCHING D-85748 GERMANY

H. KASHIMA
MITSUBISHI HEAVY INDUSTRIES, LTD.
3-1, MINATOMIRA1 3CHOME, NISHI-KU
YOKOHAMA, 220 JAPAN

T. KATSUSHIGE
JAPAN POWER ENG'G & INSPECTION CORP.
SHIN-URAYASU BLDG., 9-2, MIHAMA 1 CHOME
URAYASU-SHI, CHIBA-KEN, 279 JAPAN

J. KAYANAGH
ATOMIC ENERGY CONTROL BOARD
280 SLATER ST
OTTAWA, ONTARIO K1P 5S9 CANADA

J. KELLY
SANDIA NATIONAL LABORATORIES
PO BOX 5800, MS 0742
ALBUQUERQUE, NM 87185-0742 USA

S. KERCEL
OAK RIDGE NATIONAL LABORATORY
PO BOX 2008, BLDG. 3508/MS 6318
OAK RIDGE, TN 37831-6318 USA

R. KERN
NETCORP
9 BANNISTER CT.
GAITHERSBURG, MD 20879 USA

B. KIM
KOREA INSTITUTE OF NUCLEAR SAFETY
PO BOX 114
YUSUNG, TAEJON, 305-600 KOREA

H. KIM
KOREA INSTITUTE OF NUCLEAR SAFETY
PO BOX 114
YUSUNG, TAEJON, 305-600 KOREA

I. KIM
BROOKHAVEN NATIONAL LABORATORY
BLDG. 130, PO BOX 5000
UPTON, NY 11973-5000 USA

I. KIM
KOREA ATOMIC ENERGY RESEARCH INSTITUTE
PO BOX 105, YUSEONG
TAEJON, 305-600 KOREA

K. KIM
KOREA INSTITUTE OF NUCLEAR SAFETY
151 DUKJIN-DONG YUSEONG-GU
TAEJON, KOREA, KOREA

S. KIM
KOREA INSTITUTE OF NUCLEAR SAFETY
PO BOX 114
YUSUNG, TAEJON, 305-600 KOREA

W. KIM
KOREA INSTITUTE OF NUCLEAR SAFETY
PO BOX 114
YUSUNG, TAEJON, 305-600 KOREA

S. KINNERSLY
AEA TECHNOLOGY
WINFRITH TECHNOLOGY CENTRE
DORCHESTER, DORSET DT2 8DH UK

J. KLAPPROTH
GE NUCLEAR
PO BOX 780, MC J26
WILMINGTON, NC 28402 USA

P. KLOEG
KEMA
UTRECHTSEWEG 310
ARNHEM, 6812 AR NETHERLANDS

Y. KOBAYASHI
NUCLEAR POWER ENGINEERING CORP.
FUJITA KANKO TORANOMON BLDG. 5F 17-1, 3-CHOME, TORA
MINATO-KU, TOKYO 105 JAPAN

K. KORSAH
OAK RIDGE NATIONAL LABORATORY
PO BOX 2008, BLDG. 3500, MS 6010
OAK RIDGE, TN 37831 USA

M. KOYAMA
JAPAN POWER ENG'G & INSPECTION CORP.
SHIN-URAYASU BLDG., 9-2, MIHAMA 1 CHOME
URAYASU-SHI, CHIBA-KEN, 279 JAPAN

P. KRISHNASWAMY
BATTELLE PACIFIC NORTHWEST LABORATORY
505 KING AVE.
COLUMBUS, OH 43201 USA

B. KUCZERA
KERNFORSCHUNGSZENTRUM NUC. RESEARCH CENTER
PO BOX 3640
KARLSRUHE, D76021 GERMANY

Y. KUKITA
JAPAN ATOMIC ENERGY RESEARCH INSTITUTE
TOKAI, IBARAKI, IBARAKI 319-11 JAPAN

K. KUSSMAUL
MPA STUTTGART
PFAFFENWALDRING 32
STUTTGART, 70569 GERMANY

P. LACY
URA
51 MONROE STREET, SUITE 1600
ROCKVILLE, MD 20850 USA

J. LAKE
IDAHO NATIONAL ENGINEERING LABORATORY
PO BOX 1625
IDAHO FALLS, ID 83415-3895 USA

D. LAMPE
UTILITY RESOURCE ASSOCIATES, INC.
51 MONROE ST., SUITE 1600
ROCKVILLE, MD 20814 USA

P. LANG
U.S. DEPT. OF ENERGY
NE-451
WASHINGTON, DC 20585 USA

S. LANGENBUCH
GESELLSCHAFT FUR ANLAGEN U. REAKTORSICHERHEIT
FORSCHUNGSGELANDE
GARCHING, 85748 GERMANY

V. LANGMAN
ONTARIO HYDRO
700 UNIVERSITY AVE.
TORONTO, ONT M5G1X6 CANADA

D. LANNING
BATTELLE PACIFIC NORTHWEST LAB.
808 W. 22ND AVE.
KENNEWISK, WA 99337 USA

E. LANNING
NEBRASKA PUBLIC POWER DISTRICT
PO BOX 499
COLUMBUS, NE 68602-0499 USA

E. LANNING
NEBRASKA PUBLIC POWER DISTRICT
P.O. BOX 499
COLUMBUS, NE 68602-0499 USA

C. LECOMTE
INSTITUT DE PROTECTION ET DE SURETE NUCLEAIR
CEA, CEN/FAR 60-68 AVE. DU GENERAL LECLERC
FONTENAY AUX ROSES, 92265 FRANCE

C. LEE
KOREA ATOMIC ENERGY RESEARCH INSTITUTE
PO BOX 105, YUSONG
TAEJON, 305-606 KOREA

D. LEE
KOREA ELECTRIC POWER CORPORATION
103-16 MUNJI-DONG, YUSEONG-KU
TAEJEON, KOREA

J. LEE
KOREA INSTITUTE OF NUCLEAR SAFETY
P.O. BOX 114, YUSONG
TAEJON, KOREA, 305-600 KOREA

S. LEE
KOREA ATOMIC ENERGY RESEARCH INST.
PO BOX 105, YUSONG
TAEJON, 305-353 KOREA

J. LEHNER
BROOKHAVEN NATIONAL LABORATORY
PO BOX 5000, BLDG. 130
UPTON, NY 11973-5000 USA

M. LIVOLANT
INSTITUT DE PROTECTION ET DE SURETE NUCLEAIRE
CE/FAR BP M 6
FONTENAY-AUX-ROSES CEDEX, 92265 FRANCE

R. LOFARO
BROOKHAVEN NATIONAL LABORATORY
BLDG. 130, PO BOX 5000
UPTON, NY 11973-5000 USA

F. LOSS
MEA
9700-B M.L. KING JR. HWY.
LANHAM, MD 20706 USA

S. LU
LAWRENCE LIVERMORE NATIONAL LAB.
7000 EAST AVE.
LIVERMORE, CA 94550 USA

W. LUCKAS
BROOKHAVEN NATIONAL LABORATORY
PO BOX 5000, BLDG. 130
UPTON, NY 11973-5000 USA

I. MADNI
BROOKHAVEN NATIONAL LABORATORY
PO BOX 5000, BLDG. 130
UPTON, NY 11973-5000 USA

D. MAGALLON
CEC-JRD ISPRA
JRC-EURATOM
ISPRA, VARESE 21020 ITALY

C. MANUEL
CEA-IPSN DES/SEPRI
BP 6
FONTENAY AUX ROSES, 92265 FRANCE

J. MARCON
FRAMATOME NUCLEAR FUEL
10, RUE JULIETTE RECAMIER
LYON, 69456 FRANCE

Y. MARUYAMA
JAPAN ATOMIC ENERGY RESEARCH INSTITUTE
2-4 SHIRANE, SHIRAKATA
NAKA-GUN, IBARAKI-KEN, 319-11 JAPAN

S. MASAMORI
MITSUBISHI HEAVY INDUSTRIES, LTD.
1-1-1 WADASAKI-CHO, HYOGO-KU
KOBE, 654 JAPAN

M. MASSOUD
BALTIMORE GAS & ELECTRIC
CALVERT CLIFFS NUCLEAR PLANT
LUSBY, MD 20657 USA

B. MAVKO
J. STEFAN INSTITUTE
JAMOVA 39
LJUBLJANA, SLOV. 61111 SLOVENIA

R. McCARDELL
EG&G IDAHO, INC.
167 NORTH 4200 EAST
RIGBY, ID 83442 USA

D. McCULLOUGH
KAPL, INC., MARTIN MARIETTA
RIVER ROAD
SCHENECTADY, NY 12301 USA

K. McDONOUGH
KNOLLS ATOMIC POWER LAB., INC. - MARTIN MARIETTA
RIVER ROAD - PO BOX 1072
SCHENECTADY, NY USA

T. McINTYRE
GE NUCLEAR ENERGY
175 CURTNER AVE, M.C. 781
SAN JOSE, CA 95125 USA

R. McMILLAN
AEA TECHNOLOGY
THOMSON HOUSE, RISLEY
WARRINGTON, CHESHIRE WA38AT UK

K. McMINN
AEA TECNOLOGY
WINFRITH TECHNOLOGY CENTER, DORCHESTER
DORSET, DT28DH UK

C. MEDICH
SOCIETA INFORMAZIONI EXPERIENZE TERMOIDRAULICHE
VIA N. BIXIO 27
PIACENZA, 29100 ITALY

N. MESHKATI
UNIVERSITY OF SOUTHERN CALIFORNIA
INST. OF SAFETY & SYSTEMS MGT, USC
LOS ANGELES, CA 90089-0021 USA

G. MEYER
B&W FUEL COMPANY
PO BOX 10935
LYNCHBURG, VA 24506-0935 USA

A. MEYER-HEINE
INSTITUT DE PROTECTION ET DE SURETE NUCLEAIRE
CE CADARACHE BAT. 702
ST. PAUL LEZ DURANCE, 13108 FRANCE

A. MIAO
CHARLES RIVER ANALYTICS, INC.
55 WHEELER ST.
CAMBRIDGE, MA 02138 USA

M. MILLER
DUKE POWER COMPANY
PO BOX 1439, MS ON01ES
SENECA, SC 29679 USA

R. MILLER
WESTINGHOUSE ELECTRIC CORP.
4350 NORTHERN PIKE WEC W 316
MONROEVILLE, PA 15146-2886 USA

S. MIRSKY
SCIENCE APPLICATIONS INT'L. CORP.
20201 CENTURY BLVD.
GERMANTOWN, MD 20874 USA

D. MITCHELL
B&W FUEL COMPANY
PO BOX 10935
LYNCHBURG, VA 24506-0935 USA

D. MODEEN
NUCLEAR ENERGY INSTITUTE - NEI
1776 I ST., N.W., SUITE 400
WASHINGTON, DC 20006-3708 USA

S. MODRO
INEL LOCKHEED IDAHO TECHNOLOGIES CO.
PO BOX 1625, MS 3890
IDAHO FALLS, ID 83415-3890 USA

D. MONHARDT
FRAMATOME
1 PLACE DE LA COUPOLE
COURBEVOIE, 92400 FRANCE

S. MONTELEONE
BROOKHAVEN NATIONAL LABORATORY
BLDG. 130, PO BOX 5000
UPTON, NY 11973-5000 USA

F. MOODY
GE NUCLEAR ENERGY
175 CURTNER AVE, M.C. 781
SAN JOSE, CA 95125 USA

D. MORRISON
THE MITRE CORPORATION
7525 COLSHIRE DR., MS W768
MCLEAN, VA 22102 USA

A. MOTTA
PENN STATE UNIV., NUCLEAR ENGINEERING DEPT.
231 SACKETT BLDG.
UNIVERSITY PARK, PA 16802 USA

K. MURAYAMA
HITACHI LTD.
1-1, SAIWAI-CHO 3-CHOME, HITACHI-SHI, IBARAKI-KEN
HITACHI-SHI, JAPAN

T. NAGAO
NUCLEAR POWER ENGINEERING CORP.
17-1, 3-CHOME TORANOMON
TOKYO, 105 JAPAN

D. NAUS
OAK RIDGE NATIONAL LABORATORY
PO BOX 2009, BLDG. 9204-1
OAK RIDGW, TN 37831-8058 USA

R. NG
NUCLEAR ENERGY INSTITUTE - NEI
1776 I ST., N.W., SUITE 400
WASHINGTON, DC 20006-3708 USA

M-S NI
ATOMIC ENERGY COUNCIL, REP. OF CHINA
67 LANE 144, KEELUNG RD., SEC. 4
TAIPEI, TAIWAN ROC

G. NIEDERAUER
LOS ALAMOS NATIONAL LABORATORY
M.S. K575
LOS ALAMOS, NM 87545 USA

L. NILSSON
STUDSVIK ECO & SAFETY AB
S-61182 NYKOPING
NYKOPING, S-61182 SWEDEN

S. NOWLEN
SANDIA NATIONAL LABORATORIES
MS/0737, PO BOX 5800
ALBUQUERQUE, NM 87185 USA

A. NUNEZ
COMISION NACIONAL DE SEGURIDAD NUC. Y SALVAGUARDIA
DR BARRAGAN NO 779, COL NARVARTE
MEXICO D.F., 03020 MEXICO

N. ORTIZ
SANDIA NATIONAL LABORATORIES
PO BOX 5800, MS 0738
ALBUQUERQUE, NM 87185-0738 USA

D. OSETEK
LOS ALAMOS TECHNICAL ASSOCIATES
BLDG. 1, SUITE 400, 2400 LOUISIANA BLVD. NE
ALBUQUERQUE, NM 87110 USA

L. OSTROM
IDAHO NATIONAL ENGINEERING LABORATORY
P.O. BOX 1625
IDAHO FALLS, ID 83415-3855 USA

O. OZER
ELECTRIC POWER RESEARCH INSTITUTE
3412 HILLVIEW AVE.
PALO ALTO, CA 94304-1395 USA

B. PALAGI
COM ED COMPANY
P.O. BOX 767
CHICAGO, IL 60601 USA

J. PAPIN
INSTITUT DE PROTECTION ET DE SURETE NUCLEAIRE
CE CADARACHE BAT. 702
ST. PAUL LEZ DURANCE, 13108 FRANCE

B. PARK
KOREA NUCLEAR FUEL COMPANY
DAEJEON, 300 KOREA

Y. PARK
BROOKHAVEN NATIONAL LABORATORY
PO BOX 5000, BLDG. 475C
UPTON, NY 11973-5000 USA

M. PARKER
ILLINOIS DEPARTMENT OF NUCLEAR SAFETY
1035 OUTER PARK DRIVE
SPRINGFIELD, IL 62704 USA

J. PATE
OAK RIDGE NATIONAL LABORATORY
PO BOX 2008
OAK RIDGE, TN 37831-8158 USA

J. PELTIER
COMMISSARIAT A L'ENERGIE ATOMIQUE
BP 6
FONTENAY-AUX-ROSES-CEDEX, 92265 FRANCE

W. PENNELL
AMERICAN SOCIETY OF MECHANICAL ENGINEERS
PO BOX 2009, BLDG. 9204-1, MS-8058
OAK RIDGE, TN 37831-8058 USA

P. PERMEZEL
ELECT. DE FRANCE, SER. ETUDES ET PROJETS THERMIQUES
12-14 AV. DUTRIEVOZ
VILLEURBANNE, LYON 69628 FRANCE

M. PETRASKE
ABB COMBUSTION ENGINEERING
1000 PROSPECT HILL RD.
WINDSOR, CT 06095 USA

M. PEZZILLI
VIA ANGUILLARESE 301
S. MARIA DI GALERIA
ROMA, 60 ITALY

H. PFEFFERLEN
GENERAL ELECTRIC
175 CURTNER AVE. M.C. 781
SAN JOSE, CA 95125 USA

T. PIETRANGELO
NUCLEAR ENERGY INSTITUTE - NEI
1776 I ST., N.W., SUITE 400
WASHINGTON, DC 20006-3708 USA

B. PIKUL
THE MITRE CORPORATION
7525 COLSHIRE DR.
MC LEAN, VA 22102 USA

E. PILAT
YANKEE ATOMIC
580 MAIN ST.
BOLTON, MA 01740 USA

M. PILCH
SANDIA NATIONAL LABORATORIES
PO BOX 5800
ALBUQUERQUE, NM 87185-1137 USA

E. PIPLICA
WESTINGHOUSE
P.O. BOX 355
PITTSBURGH, PA 15230 USA

M. PODOWSKI
RPI
DEPT. OF NUCL. ENG. & ENG. PHYSICS
TROY, NY 12180 USA

S. POPE
SCIENTECH, INC.
11140 ROCKVILLE PIKE
ROCKVILLE, MD 20852 USA

G. POTTS
GE NUCLEAR
PO BOX 780, MC K05
WILMINGTON, NC 28402 USA

R. PRAKASH
EMBASSY OF INDIA
WASHINGTON, DC USA

W. PRATT
BROOKHAVEN NATIONAL LABORATORY
BUILDING 130
UPTON, NY 11973 USA

R. PROEBSTLE
GE NUCLEAR
PO BOX 780, MC A01
WILMINGTON, NC 28402 USA

V. PROKLOV
RRC KURCHATOV INSTITUTE
KURCHATOV SQUARE 1
MOSCOW, RUSSIA, 123182 RUSSIA

J. PUGA
UNESA
FRANCISCO GERVAS 3
MADRID, 28020 SPAIN

C. PUGH
OAK RIDGE NATIONAL LABORATORY
P.O. BOX 2009, MS 8063
OAK RIDGE, TN 37831 USA

T. RAJALA
ABB ATOM
FINNSLATTEN
VASTERAS, SWEDEN

D. RAPP
WESTINGHOUSE BETTIS LAB
P.O. BOX 79
WEST MIFFLIN, PA 15102 USA

J. RASHID
ANATECH RESEARCH CORP.
5435 OBERLIN DR.
SAN DIEGO, CA 92037 USA

S. RAY
WESTINGHOUSE ELECTRIC CORP.
PO BOX 355
PITTSBURGH, PA 15230 USA

K. REIL
SANDIA NATIONAL LABORATORIES
PO BOX 5800, M.S. 1139
ALBUQUERQUE, NM 87185-1139 USA

W. RETTIG
U.S. DOE, IDAHO OFFICE
850 ENERGY DRIVE
IDAHO FALLS, ID 83402 USA

J. RHODE
HEAD, SEVERE ACCIDENTS DEPT., GRS
SCHWERTNERGASSE 1
COLOGNE, 50667 GERMANY

L. RIB
AECL TECHNOLOGIES INC.
9210 CORPORATE BLVD., SUITE 410
ROCKVILLE, MD 20850 USA

A. RODRIGUEZ
COMISION NACIONAL DE SEGURIDAD NUC.Y SALVAGUARDIA
DR BARRAGAN NO 779, COL NARVARTE
MEXICO D.F., 03020 MEXICO

U. ROHATGI
BROOKHAVEN NATIONAL LABORATORY
BLDG. 475B, PO BOX 5000
UPTON, NY 11973-5000 USA

A. ROSCIOLI
PENNSYLVANIA POWER & LIGHT CO.
2 NORTH 9TH ST.
ALLENTOWN, PA 18101 USA

T. ROSS
PSE&G
PO BOX 236, MC n20
HANCOCKS BRIDGE, NJ 08038 USA

P. ROTHWELL
NUCLEAR INSTALLATIONS INSPECTORATE
ROOM 903 ST. PETER'S HOUSE, BALLIOL RD.
BOOTLE, MERSEYSIDE, L20 3LZ UK

T. ROWELL
WESTINGHOUSE ELECTRIC CORP.
PO BOX 353
PITTSBURGH, PA 15230 USA

J. ROYEN
OECD NUCLEAR ENERGY AGENCY
12 BLVD. DES ILES
ISSY-LES-MOULINEAUX, F92130 FRANCE

H. RYU
NUCLEAR POWER ENGINEERING CORP.
8F FUJITAKANKO TORANOMON BLDG. 17-1, 3-CHOME
MINATO-KU, TOKYO, 105 JAPAN

K. SAITO
NUCLEAR POWER ENGINEERING CORP.
17-1, 3-CHOME TORANOMON
TOKYO, 105 JAPAN

O. SANDERVAG
SWEDISH NUCLEAR POWER INSPECTORATE
SEHLSTEDT GT 11
STOCKHOLM, SWEDEN

M. SARRAM
NUCLEAR ENERGY INSTITUTE - NEI
1776 I ST., N.W., SUITE 400
WASHINGTON, DC 20006-3708 USA

K. SATO
HITACHI, LTD
3-1-1 SAIWAI-CHO
HITACHI-SHI, IBARAKI 317 JAPAN

K. SATO
MITSUBISHI ATOMIC POWER INDUSTRIES, INC.
3-3-1, MINATO MIRAI, NISHI-KU
YOKOHAMA-SHI, 220 JAPAN

M. SATO
TOSHIBA NUCLEAR MARKETING DEPT.
1-1-8, UCHISAIWAI-CHO
CHIYODA-KU, TOKYO 100 JAPAN

S. SAVOLAINEN
IMATRAN VOIMA OY/LOVIISA POWER PLANT
PO BOX 23
LOVIISA, FIN-07901 FINLAND

C. SAYLES
SOUTHERN CALIFORNIA EDISON
PO BOX 128
SAN CLEMENTE, CA 92672 USA

P. SCHEINERT
BETTIS ATOMIC POWER LABORATORY
PO BOX 79
WEST MIFFLIN, PA 15122 USA

F. SCHMITZ
CEA/IPSN
F-13108 ST. PAUL LEZ DURANCE CEDEX
FRANCE

R. SCHULTZ
IDAHO NATIONAL ENGINEERING LABORATORY
P.O. BOX 1625
IDAHO FALLS, ID 83415 USA

A. SEKRI
ELECT. DE FRANCE, SER. ETUDES ET PROJETS THERMIQUES
12-14 AV. DUTRIEVOZ
VILLEURBANNE, LYON 69628 FRANCE

C. SEOK
300, CHUN-CHUN-DONG
SUWON, KOREA, 440-748 KOREA

S SETH
THE MITRE CORPORATION
7525 COLSHIRE DR.
MC LEAN, VA 22102 USA

W. SHA
ARGONNE NATIONAL LABORATORY
9700 SOUTH CASS AVENUE
ARGONNE, IL 60439 USA

V. SHAH
IDAHO NATIONAL ENGINEERING LAB.
PO BOX 1625
IDAHO FALLS, ID 83415-3870 USA

J. SHIN
RAYTHEON E&C
2 WORLD TRADE CENTER, 87 FL.
NEW YORK, NY 10048 USA

D. SHURBERG
BROOKHAVEN NATIONAL LABORATORY
BLDG. 130, PO BOX 5000
UPTON, NY 11973-5000 USA

E. SILVER
OAK RIDGE NATIONAL LAB
BLDG. 9201-3, MS 8085, PO BOX 2009
OAK RIDGE, TN 37831-8085 USA

B. SINGH
JUPITER CORP.
2730 UNIVERSITY BLVD. W, STE. 900
WHEATON, MD 20902 USA

S. SNIDER
TU ELECTRIC COMPANY
400 NORTH OLIVE, L.B. 81/24SLIC
DALLAS, TX 75201 USA

M. SONG
KOREA INSTITUTE OF NUCLEAR SAFETY
PO BOX 114
YUSUNG, TAEJON, 305-600 KOREA

B. SOUBIES
INSTITUT DE PROTECTION ET DE SURETE NUCLEAIRE
B.P. 6
FONTENAY AUX ROSES, 92265 FRANCE

G. SRINIVASAN
NUCLEAR POWER CORPORATION OF INDIA
TARAPUR ATOMIC POWER STATION
TARAPUR, MAHARASHTRA, INDIA

K. ST. JOHN
YANKEE ATOMIC ELECTRIC CO.
580 MAIN ST
BOLTON, MA 01740 USA

W. STADTMULLER
MPA STUTTGART
PFAFFENWALDRING 32
STUTTGART, D-70569 GERMANY

D. STARCK
MPR ASSOCIATES, INC.
320 KING ST.
ALEXANDRIA, VA 22314-3238 USA

R. STEELE JR.
IDAHO NATIONAL ENGINEERING LABORATORY
P.O. BOX 1625
IDAHO FALLS, ID 83415 USA

R. STIRN
GE NUCLEAR
PO BOX 780, MC F24
WILMINGTON, NC 28402 USA

J. STONE
MPR ASSOCIATES, INC.
320 KING ST.
ALEXANDRIA, VA 22314-3238 USA

P. STOREY
HSE/NSD
BROADLANE
SHEFFIELD, S37HQ UK

V. STRIZHOU
NSI RRS
B. TULSKAYA, 52
MOSCOW, RUSSIA, 113191 RUSSIA

E. STUBBE
TRACTEBEL INGENIERIE
AVE. ARIANE 7, BTE 1
BRUSSELS, 1200 BELGIUM

R. SUMMERS
SANDIA NATIONAL LABORATORIES
P.O. BOX 5800, MS 0745
ALBUQUERQUE, NM 87185-0745 USA

B. SUN
SUNUTECH, INC.
PO BOX 978
LOS ALTOS, CA 94023 USA

J. SUN
ARGONNE NATIONAL LABORATORY
9700 SOUTH CASS AVENUE
ARGONNE, IL 60439 USA

A. SUSLOV
RRC KURCHATOV INSTITUTE
KURCHATOV SQUARE 1
MOSCOW, RUSSIA, 123182 RUSSIA

E. SWANSON
B&W NUCLEAR TECHNOLOGIES
PO BOX 10935
LYNCHBURG, VA 24506-0935 USA

I. SZABO
COMMISSARIAT L'ENERGIE ATOMIQUE
C.E. CADARACHE
ST. PAUL LES DURANCE, 13108 FRANCE

K. TAKIGUCHI
2-12-1 OH-OKAYAMA, MEGURO-KU
TOKYO, TOKYO 152 JAPAN

P. TALARICO
GILBERT/COMMONWEALTH, INC.
PO BOX 1498
READING, PA 19603 USA

T. TANAKA
SANDIA NATIONAL LABORATORIES
MS/0737, PO BOX 5800
ALBUQUERQUE, NM 87185 USA

P. TANGUY
ELECTRICITE DE FRANCE
32 RUE DE MONCEAU
PARIS, 75008 FRANCE

Z. TECHY
VEIKI
ZRINYI U. 1.
BUDAPEST, 1051 HUNGARY

C. THIBAULT
WYLE LABORATORIES
PO BOX 077777
HUNTSVILLE, AL USA

H. THORNBURG
ABB ATOM
901 S. WARFIELD DR.
MT. AIRY, MD 21771 USA

J. TOLY
CEA-IPSN DES/SEPRI
BP 6
FONTENAY AUX ROSES, 92265 FRANCE

M. TORCIVIA
KNOLLS ATOMIC POWER LAB.
PO BOX 1072
SCHENECTADY, NY 12301-1072 USA

N. TRIKOUROS
GPU NUCLEAR CORP.
ONE UPPER POND RD.
PARSIPPANY, NJ 07054 USA

A. TURRIAN
HSK SWISS FEDERAL NUC.SAFETY INSPECTORATE
WURENLINGEN
VILLIGEN-HSK, CH 5232 SWITZERLAND

W. URKO
ABB/COMBUSTION ENGINEERING
1000 PROSPECT HILL RD., DEPT. 9341-0421
WINDSOR, CT 06095 USA

K. VALTONEN
FINNISH CENTRE FOR RADIATION & NUCLEAR SAFETY
P.O. BOX 14
FIN-00881-HELSINKI, FINLAND

R. VAN HOUTEN
JUPITER CORP.
2730 UNIVERSITY BLVD., STE 900
WHEATON, MD 20902 USA

L. VANDEN HEUVEL
OAK RIDGE NATIONAL LABORATORY
PO BOX 2009, BLDG. 9201-3
OAK RIDGE, TN 37831-8065 USA

O. VESCOVI
SOCIETA INFORMAZIONI EXPERIENZE TERMOIDRAULICHE
VIA N. BIXIO 27
PIACENZA, 29100 ITALY

W. VESELY
SCIENCE APPLICATIONS INT'L CORP.
655 METRO PLACE SOUTH
DUBLIN, OH 43017 USA

J. WADE
ARIZONA PUBLIC SERVICE
P.O. BOX 52034
PHOENIX, AZ 85072-2034 USA

J. WALKER
AECL RESEARCH
CHALK RIVER LAB
CHALK RIVER, ONTARIO K0J1J0 CANADA

D. WALTERS
NUCLEAR ENERGY INSTITUTE - NEI
1776 I ST., N.W., SUITE 400
WASHINGTON, DC 20006-3708 USA

S-F WANG
INSTITUTE OF NUCLEAR ENERGY RESEARCH
1000 WENHUA RD., CHIAAN VILLAGE
LUNG-TAN, TAIWAN 325 ROC

W. WANG
STONE & WEBSTER ENG. CO.
P.O. BOX 5200
CHERRY HILL, NJ 08034 USA

A. WARE
IDAHO NATIONAL ENGINEERING LABORATORY
PO BOX 1625
IDAHO FALLS, ID 83415-3750 USA

P. WEBSTER
ATOMIC ENERGYCONTROL BOARD, CANADA
280 SLATER ST.
OTTAWA, ONTARIO K1P 5S9 CANADA

J. WHITCRAFT
BECHTEL POWER CORP.
9801 WASHINGTONIAN BLVD.
GAITHERSBURG, MD 20878 USA

D. WHITEHEAD
SANDIA NATIONAL LABORATORIES
PO BOX 5800, MS 0747
ALBUQUERQUE, NM 87185-0747 USA

K. WHITT
SOUTHERN NUCLEAR
40 INVERNESS CENTER PARKWAY
BIRMINGHAM, AL 35201 USA

G. WILKOWSKI
BATTELLE PACIFIC NORTHWEST LABORATORY
505 KING AVE.
COLUMBUS, OH 43201 USA

V. WILLEMS
GILBERT/COMMONWEALTH, INC.
P.O. BOX 1498
READING, PA 19603 USA

M. WILLIS
WESTINGHOUSE ELECTRIC CORP.
PO BOX 353
PITTSBURGH, PA 15230 USA

L. WOLF
UNIV. OF MARYLAND, DEPT. MATERIALS & NUCLEAR ENG'G
2135 BLDG. 090
COLLEGE PARK, MD 20742-2115 USA

K. WOLFERT
GESELLSCHAFT FUR ANLAGEN & REAKTORSICHERHEIT MBH
FORSCHUNGSGELANDE, D-85748 GARCHING
DEUTSCHLAND, GARCHING D-85748 GERMANY

J. WREATHALL
JOHN WREATHALL & CO.
4157 MACDUFF WAY
DUBLIN, OH 43017 USA

S. WRIGHT
SANDIA NATIONAL LABORATORIES
PO BOX 5800, MS 1145
ALBUQUERQUE, NM 87185-1145 USA

G. WROBEL
ROCHESTER GAS & ELECTRIC CORP.
49 EAST AVE.
ROCHESTER, NY 14649 USA

G. WU
NUCLEAR ENERGY INSTITUTE - NEI
1776 I ST., N.W., SUITE 400
WASHINGTON, DC 20006-3708 USA

M. YAMAGISHI
MITSUBISHI ATOMIC POWER INDUSTRIES, INC.
3-1, MINATOMIRAI 3-CHOME, NISHI-KU
YOKOHAMA, KANAGAWA 220 JAPAN

L. YEGOZOVA
RRC KURCHATOV INSTITUTE
ROGOV ST. 16, AP. 35
MOSCOW, RUSSIA

K. YOO
KOREA ATOMIC ENERGY RESEARCH INSTITUTE
PO BOX 105, YUSONG
TAEJON, 305-600 KOREA

Y. YOSHIZAWA
TOKYO INSTITUTE OF TECHNOLOGY
2-12-1 OH-OKAYAMA, MEGURO-KU
TOKYO, TOKYO 152 JAPAN

D. YU
KOREA ATOMIC ENERGY RESEARCH INST.
PO BOX 105, YUSONG
TAEJON, 305-353 KOREA

Y. YUNE
KOREA INSTITUTE OF NUCLEAR SAFETY
PO BOX 114
YUSUNG, TAEJON, 305-600 KOREA

G. ZACHARIAS
CHARLES RIVER ANALYTICS, INC.
55 WHEELER ST.
CAMBRIDGE, MA 02138 USA

D. ZANOBETTI
UNIVERSITY OF BOLOGNA
VIALE RISORGIMENTO 2
BOLOGNA, 40136 ITALY

P. ZMOLA
C&P ENGINEERING
5409 NEWINGTON RD.
BETHESDA, MD 20816 USA

PROCEEDINGS OF THE
TWENTY-SECOND WATER REACTOR SAFETY INFORMATION MEETING
October 24-26, 1994

CONTENTS - VOLUME 3

CONTENTS - VOLUME 2 (Cont'd)

AGING RESEARCH, PRODUCTS & APPLICATIONS
J. Vora, Chair

KEY RESULTS FOR THE NRC'S SHORT CRACKS IN PIPING AND PIPING WELDS RESEARCH PROGRAM

by

G. Wilkowski, P. Krishnaswamy, F. Brust, R. Francini, N. Ghadiali,
T. Kilinski, C. Marschall, R. Mohan, S. Rahman, A. Rosenfield, D. Rudland, and P. Scott

BATTELLE
COLUMBUS, OHIO 43201

1. Introduction

The overall objective of the Short Cracks in Piping and Piping Welds Program is to verify and improve engineering analyses to predict the fracture behavior of circumferentially cracked pipe under quasi-static loading with particular attention to crack lengths typically used in LBB or flaw evaluation criteria. This USNRC program at Battelle was initiated in March 1990 and is scheduled to be completed in December 1994. This paper discusses key results from the overall program with particular emphasis on the efforts since the last WRSIM meeting.

The program consists of eight technical tasks as listed below.

Task 1 Short through-wall-cracked (TWC) pipe evaluations
Task 2 Short surface-cracked (SC) pipe evaluations
Task 3 Bi-metallic weld crack evaluations
Task 4 Dynamic strain aging and crack instabilities
Task 5 Fracture evaluations of anisotropic pipe
Task 6 Crack-opening-area evaluations
Task 7 NRCPIPE code improvements
Task 8 Additional efforts

Task 8 is a collection of new efforts initiated during the course of the program.

A list of the full-scale pipe experiments in this program is given in Table 1. All of the experiments have been completed. The most recent accomplishments in each of the tasks listed above are discussed below. The details of all the results in the eight tasks are published in the semiannual reports [Refs. 1-6] as well as topical reports from the program.

2. Task 1 - Short Through-Wall-Cracked Pipe Evaluations

There are five subtasks:

Subtask 1.1	Material characterization
Subtask 1.2	Through-wall-cracked pipe experiments
Subtask 1.3	Facility modifications
Subtask 1.4	Through-wall-cracked pipe analysis
Subtask 1.5	Topical report

All activities in Subtasks 1.1, 1.2, 1.3, and 1.4 are completed. Pipe experiments and analysis efforts have been completed. A topical report is being written covering the activities in this task and will be published by the USNRC as a NUREG/CR report.

Key accomplishments in this task were:

- four full-scale through-wall-cracked pipe experiments
- development of new GE/EPRI functions and corrections to existing functions for the J-estimation scheme
- the inclusion of weld metal strength into the existing analysis method LBB.ENG2
- development of the analysis method LBB.ENG3 for TWC in welds.

These results have been presented at previous WRSIM meetings and will be included in the topical report.

3. Task 2 - Short Surface-Cracked (SC) Pipe Evaluations

There are five subtasks in this task:

Subtask 2.1	Material characterization
Subtask 2.2	Small-diameter surface-cracked pipe experiments
Subtask 2.3	Large-Diameter surface-cracked pipe experiments
Subtask 2.4	Surface-cracked pipe analyses
Subtask 2.5	Topical report.

All material characterization, small- and large-diameter pipe experiments, and surface-cracked analysis developments and improvements have been completed. A topical report on this task is being prepared and will be published in 1995 by the USNRC.

Key results from this task are the following:

- six full-scale pipe experiments have been completed as shown in Table 1
- modifications to the existing SC.TNP and SC.TKP analyses methods to predict moment-rotation behavior of surface-cracked pipe
- development of a new SC.ENG J-estimation scheme analogous to the LBB.ENG method to analyze the behavior of surface-cracked pipe
- verification of SC.ENG methods with finite element analysis.

The pipe experiment results and analyses have been discussed in previous WRSIM papers and will be given in the future topical report.

4. Task 3 - Bi-Metallic Weld Crack Evaluations

The objective of this task is to conduct experiments and develop the necessary analytical engineering estimation schemes to assess the behavior of a through-wall crack along the fusion line of a bi-metallic welded pipe under bending. There are four subtasks in this task:

Subtask 3.1	Material characterization
Subtask 3.2	Pipe experiments
Subtask 3.3	Analysis of pipe experiments
Subtask 3.4	Topical report.

The material characterization efforts as well as the through-wall-cracked bi-metallic pipe experiment are completed. Preliminary analysis of the pipe experiment has also been done. The TWC pipe was loaded in four-point bending at 288 C (550 F) without any internal pressure beyond the maximum load-carrying capacity of the pipe. Figure 1 shows a view of the specimen after the experiment. The load-displacement curve for this experiment is shown in Figure 2. Also shown in this figure are the predictions based on two of the J-estimation schemes, LBB.ENG2 and the GE/EPRI method. The predictions used the carbon steel stress-strain properties and the J-R curve for the weld metal. The LBB.ENG2 analysis method predicted the maximum load very well while the predictions of the GE/EPRI scheme were lower. Also, both schemes underpredict the pipe displacement at maximum load significantly, perhaps because the ductility associated with the stainless steel stress-strain behavior is not accounted for in the analysis. The J-estimation scheme predictions using the stainless steel stress-strain data are also being done and will be included in the topical report on this task.

5. Task 4 - Dynamic Strain Aging and Crack Instabilities

The objective of this task is to predict the effects of crack instabilities, believed to be due to dynamic strain aging, on the fracture behavior of ferritic pipe. Dynamic strain aging, which results in unstable crack jumps, occurs at certain combinations of temperatures and strain rates in ferritic steels and is believed to be due to the interactions between dislocations and free nitrogen and/or carbon atoms during plastic straining. The task has been divided into four subtasks:

Subtask 4.1	Establish screening criterion to predict unstable crack jumps
Subtask 4.2	Evaluate procedures for characterizing fracture resistance during crack jumps in laboratory specimens
Subtask 4.3	Assess current procedures for predicting crack jump magnitudes in pipes
Subtask 4.4	Prepare topical reports.

All work in this task has been completed and a topical report [Ref. 1] has been published. The key accomplishments in this task included the development of a dynamic strain aging screening criteria based on the hot hardness test. These criteria can be used to assess the susceptibility of ferritic steels to crack jumps, which are caused by dynamic strain aging. Also, a complete finite element analysis of a C(T) specimen was conducted to assess the behavior of J during a crack jump. The finite element results provided insight into some of the necessary conditions under which crack jumps can occur. However, the set of necessary conditions sufficient to initiate the dynamic crack jumps were not determined.

6. Task 5 - Fracture Evaluations of Anisotropic Pipe

The objective of this task is to assess if anisotropic fracture properties together with high principal stresses in a helical direction can cause a lower failure stress than when using typical fracture analyses. Typical fracture analyses for circumferential cracked pipe use the toughness in the circumferential orientation and only the longitudinal stresses. The toughness is typically lower in the

helical or axial direction than in the circumferential direction for ferritic pipe. There are three subtasks:

Subtask 5.1 Assess effect of toughness anisotropy on pipe fracture under combined loads
Subtask 5.2 Determine magnitude of toughness anisotropy and establish a screening criterion to predict out-of-plane crack growth
Subtask 5.3 Prepare topical report on anisotropy and mixed-mode studies.

The material characterization efforts in Subtask 5.1 and 5.2 have been discussed and presented at previous WRSIM meetings. Key elements involving the analysis aspects are described below. A topical report on the task will be published in 1995.

The analysis efforts focused on the following: i) assess the ratio of torsion to bending loads in actual nuclear plant piping, ii) conduct finite element analysis for a straight circumferential crack in a pipe under pure bending, pure torsion, and combined bending and torsion loads, iii) repeat the previous analysis with a circumferential crack kinked (at an angle), iv) assess the effect of various ways of calculating and "equivalent moment" for combined loading, and v) assess the effect of combined loading on the crack-opening displacement.

To date, we have completed the survey on obtaining the ratio of torsional to bending moment on pipe. Frequently occurring ratios of torsion to bending are 1:1 and 1:3. Table 3 shows several possible ways of combining torque and bending moment to obtain an effective moment. Figure 3 shows a plot of J versus the effective moment for several cases involving pure bending, combined bending and tension, pure torsion, and one ratio of torsion to bending. As seen in this figure, J versus the effective moment is lowest for the pure bending case and highest for the combined bending and tension case. Also the pure torsion curve follows the same trend as the pure bending curve. For two of the ways of calculating the effective moment ($c = 1$ and $c = 0$) the combined bending and torsion curve are almost identical, indicating that the effect of torque can be ignored for this ratio of torsion to bending (1:3). Further analyses for the kinked crack are underway, as well as determining the effects on crack-opening displacement, and will be included in the topical report for this task.

7. Task 6 - Crack-Opening-Area Evaluations

The objective of this subtask is to make improvements in the crack-opening-area (COA) predictions for circumferentially cracked pipe, with particular attention to cracks in welds. The crack-opening-area analyses will be incorporated into the NRCPIPE code and then into the SQUIRT leak-rate code. There are six subtasks in this task:

Subtask 6.1 Create combined loading improvements
Subtask 6.2 Implement short through-wall-crack opening displacement analysis improvements
Subtask 6.3 Improve weld crack evaluations
Subtask 6.4 Modify SQUIRT code
Subtask 6.5 Prepare topical report on crack-opening-area improvements
Subtask 6.6 Leak-rate quantification analysis.

Key efforts in the COA analyses, Subtasks 6.1 - 6.5, involve the following:

- developing a new scheme to compute the COD and the COA

- comparing the analytical predictions to experimental data
- improving the SQUIRT code used to predict the leak rates
- determining the effect of pressure-induced bending in a pipe system as well as residual stresses on COA.

A topical report discussing the above analyses is being compiled and will be published at the end of the program.

Key results in Subtask 6.6, Leak Rate Quantification, have been presented in previous meetings. This effort involved determining failure probabilities versus leak rates for assessing leakage detection equipment requirements for both PWR and BWR piping. Some of the probabilistic calculations in this work were redone using additional data to determine the statistical variation of material properties. These results are included in the revised topical report on this subtask, which will be published by the NRC.

8. Task 7 - NRCPIPE Code Improvements

As part of the Degraded Piping Program-Phase II, a PC computer program, NRCPIPE, was developed to analyze TWC pipes under combined pressure and bending using various simplified estimation schemes. The objectives of this task are to improve the existing TWC code based on the results of the analyses in Task 1 and also to develop a similar code to analyze surface cracks. The various subtasks in this effort are:

Subtask 7.1	Improve efficiency of current NRCPIPE code
Subtask 7.2	Incorporate through-wall-cracked pipe analysis improvements in NRCPIPE
Subtask 7.3	Make surface-cracked pipe version of the code (NRCPIPES)
Subtask 7.4	Provide new users manuals.

Several improvements to the NRCPIPE code were made to make it more user friendly. A new version, 1.4g, has been released. The improvements in the analysis of TWC pipe from Task 1 have been incorporated into NRCPIPE. Version 2.0 of this code is currently being beta tested and will be released at the end of the program.

Based on the surface-cracked pipe analysis methods SC.TNP and SC.TKP a PC code, NRCPIPES, was developed. Version 1.0 of this code has been released to the NRC. Improvements to this code as well as the new J-estimation scheme SC.ENG, developed in Task 2, have been incorporated into NRCPIPES. ASME Section XI Appendices C and H as well as the Code Case N-494 approach involving the deformation plasticity failure assessment diagram (DPFAD) have been included in NRCPIPES. Version 2.0 of this code will also be released at the end of the program.

9. Task 8 - Additional Efforts

To date there are six additional efforts being undertaken:

Subtask 8.1	Validation of J_m resistance curves
Subtask 8.2	Evaluation of fusion-line toughness of stainless steel SAW
Subtask 8.3	Improvements and addition to the PIFRAC database
Subtask 8.4	Development and expansion of a pipe fracture database

Subtask 8.5	Archiving of past degraded piping program pipe fracture data
Subtask 8.6	Evaluation of ASME Section III proposed allowable stresses
Subtask 8.7	Conducting microbiologically induced corrosion (MIC) pipe test

Subtask 8.1 was conducted at Brown University by Professor C. F. Shih. The reports from this work have been submitted to the NRC for publication. The work on fusion-line toughness has been reported in previous meetings and will not be repeated here. The topical report on this work has also been submitted for publication. PIFRAC, the material property database on piping materials, has currently 871 J-R curves and 643 tensile curves from data generated at Battelle and elsewhere. Chemical analyses and Charpy data are also included in this database. This database will also be released at the end of the program. Another database of all circumferential pipe fracture experiments, CIRCUMCK.WK1, has been developed as a Lotus 1-2-3 spreadsheet. This database contains over 700 pipe fracture experiments conducted worldwide and will also be released at the end of the program. Subtask 8.6 has been presented at previous meetings and will not be discussed further.

Subtask 8.7 is a new addition to the program. This effort involves testing a girth-weld surface-cracked pipe (6-inch-diameter) removed from service that had extensive microbiologically induced corrosion (MIC) along a lack-of-penetration defect in the girth weld. The objectives of this effort are: i) to assess an actual girth weld defect and the validity of the various analyses methods developed in this program, and ii) to assess the ASME Section XI criteria with specific attention to brittle-to-ductile failure at ambient temperature and the effect of the variable depth surface flaw geometry on predicted failure loads.

Figure 4 shows a schematic of the MIC pipe geometry with the girth weld flaw in the section close to the elbow. Figure 5 shows a photograph of the specimen received from Northeast Utilities. The surface- flaw depth was assessed prior the test using ultrasonic testing. The elbow in the specimen was cut out and the flawed section was prepared for testing under pure bending as shown in Figure 6. The flaw geometry as determined by ultrasonic testing is shown in Figure 7. The moment-rotation curve from the experiment conducted under bending with an internal pressure of 0.69 MPa (100 psi) and at room temperature (20 C) is shown in Figure 8. As seen, just beyond maximum load the surface crack penetrated through the wall after which the crack grew in a ductile mode until an unstable failure occurred with a significant load drop. The analysis of this experiment is still underway and the results will be included in the seventh semiannual report.

10. Conclusions

This program will be concluded at the end of 1994. The deliverables from this program are seven semiannual reports, 11 topical reports, updates on three computer codes (NRCPIPE, NRCPIPES, and SQUIRT), an update of the nuclear piping material property database (PIFRAC), databases on circumferentially cracked and axially cracked pipe experiments, and the final program report.

11. References

1. Wilkowski, G.M. et al., " Short Cracks in Piping and Piping Welds" Semiannual Report, NUREG/CR-4599, BMI-2173, Vol. 1, No. 1, May 1991.

2. Wilkowski, G.M. et al., " Short Cracks in Piping and Piping Welds" Semiannual Report, NUREG/CR-4599, BMI-2173, Vol. 1, No. 2, April 1992.

3. Wilkowski, G.M. et al., " Short Cracks in Piping and Piping Welds" Semiannual Report, NUREG/CR-4599, BMI-2173, Vol. 2, No. 1, September 1992.

4. Wilkowski, G.M. et al., " Short Cracks in Piping and Piping Welds" Semiannual Report, NUREG/CR-4599, BMI-2173, Vol. 2, No. 2, May 1992.

5. Wilkowski, G.M. et al., " Short Cracks in Piping and Piping Welds" Semiannual Report, NUREG/CR-4599, BMI-2173, Vol. 3, No. 1, September 1992.

6. Wilkowski, G.M. et al., " Short Cracks in Piping and Piping Welds" Semiannual Report, NUREG/CR-4599, BMI-2173, Vol. 3, No. 2, March 1994.

7. Marschall, C. W., Mohan, R., Krishnaswamy, P., and Wilkowski, G. M., "Effect of Dynamic Strain Aging on the Strength and Toughness of Nuclear Ferritic Piping at LWR Temperatures", NUREG/CR-6226, October 1994.

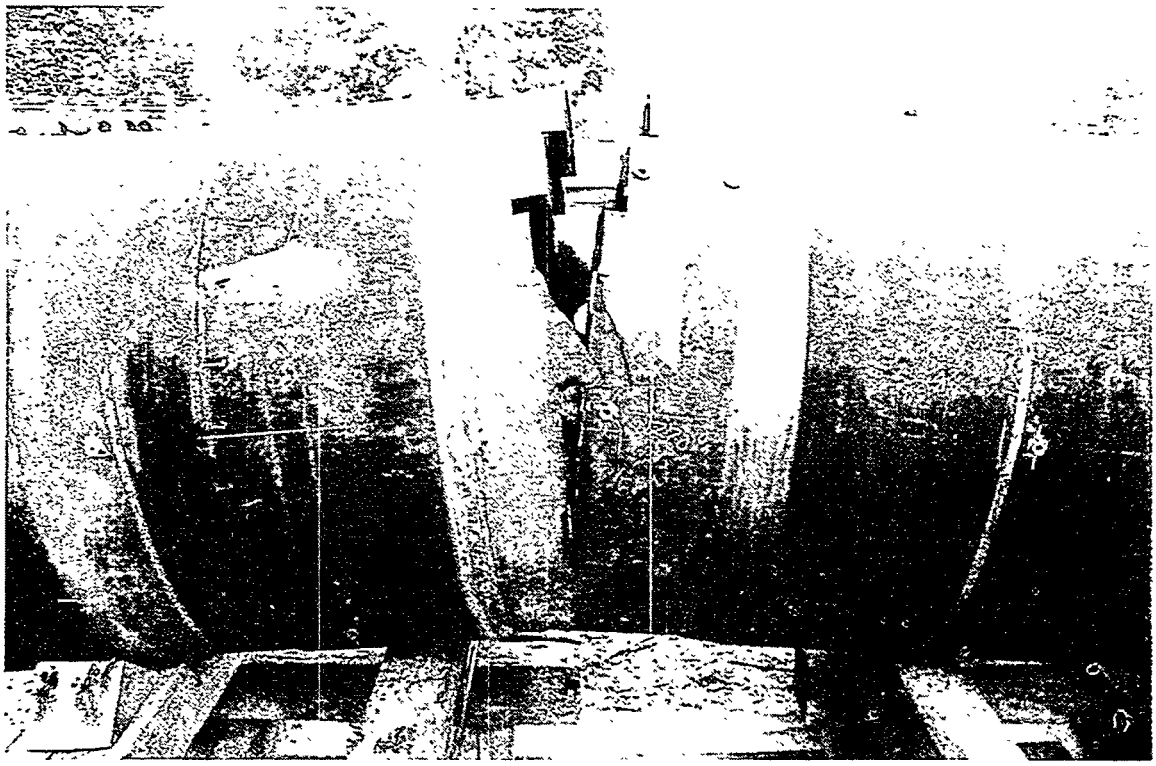

Figure 1. View of cracked pipe after experiment.

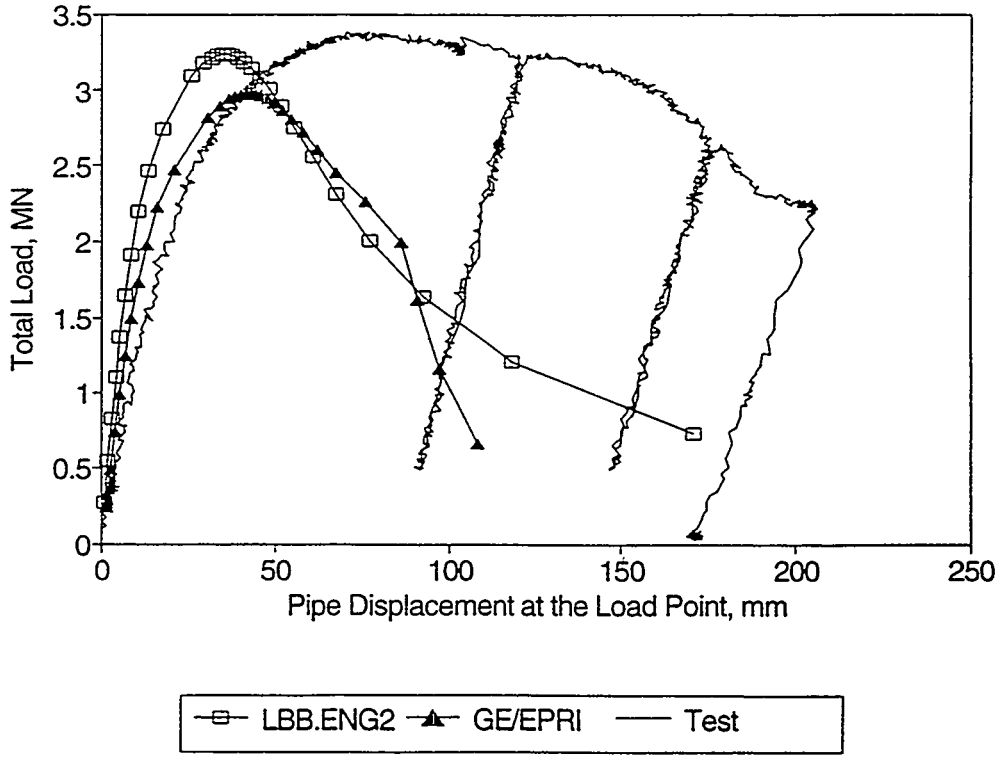

Figure 2. Comparison of estimation schemes with experiment for bi-metallic through-wall-cracked pipe test.

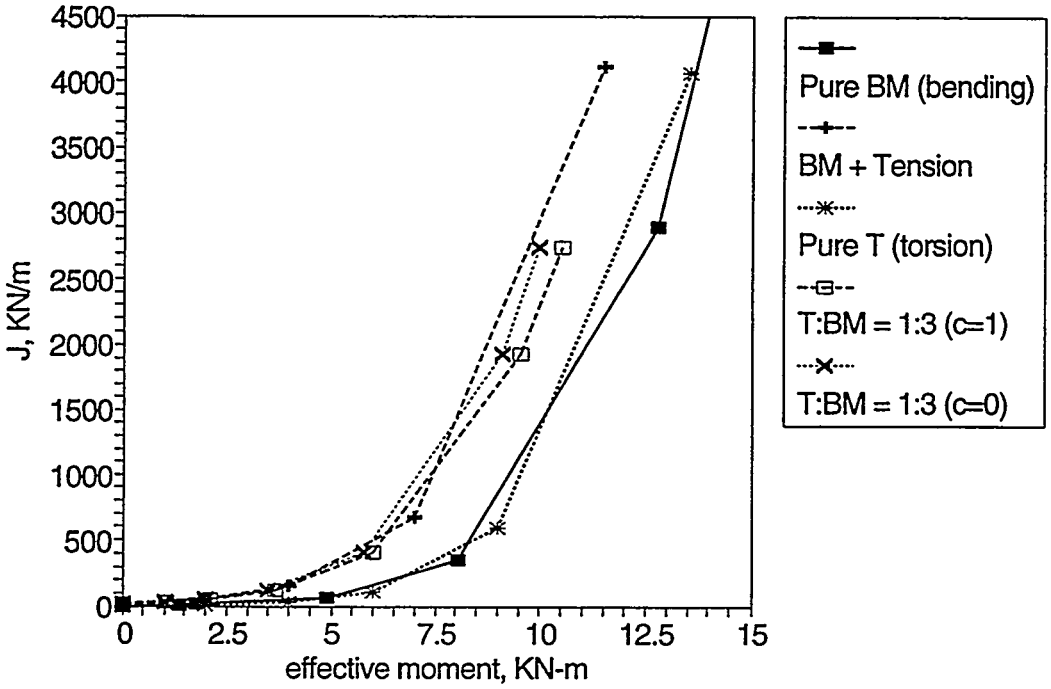

Figure 3. Effect of combined loading on J.

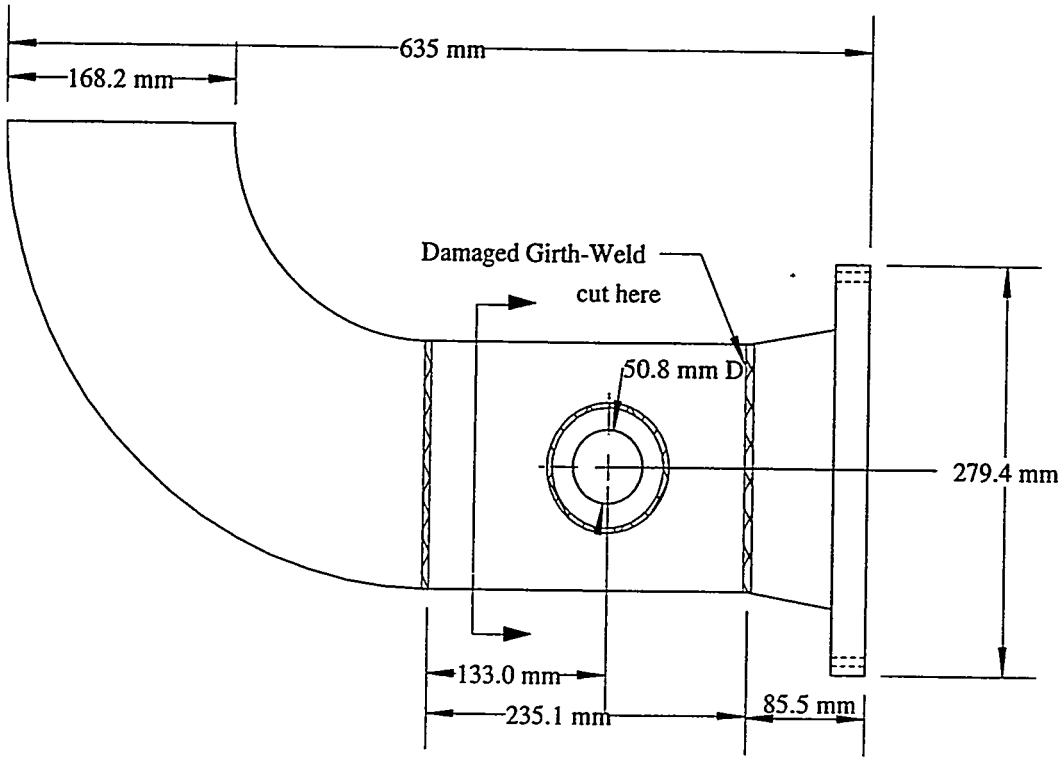

Figure 4. MIC pipe geometry.

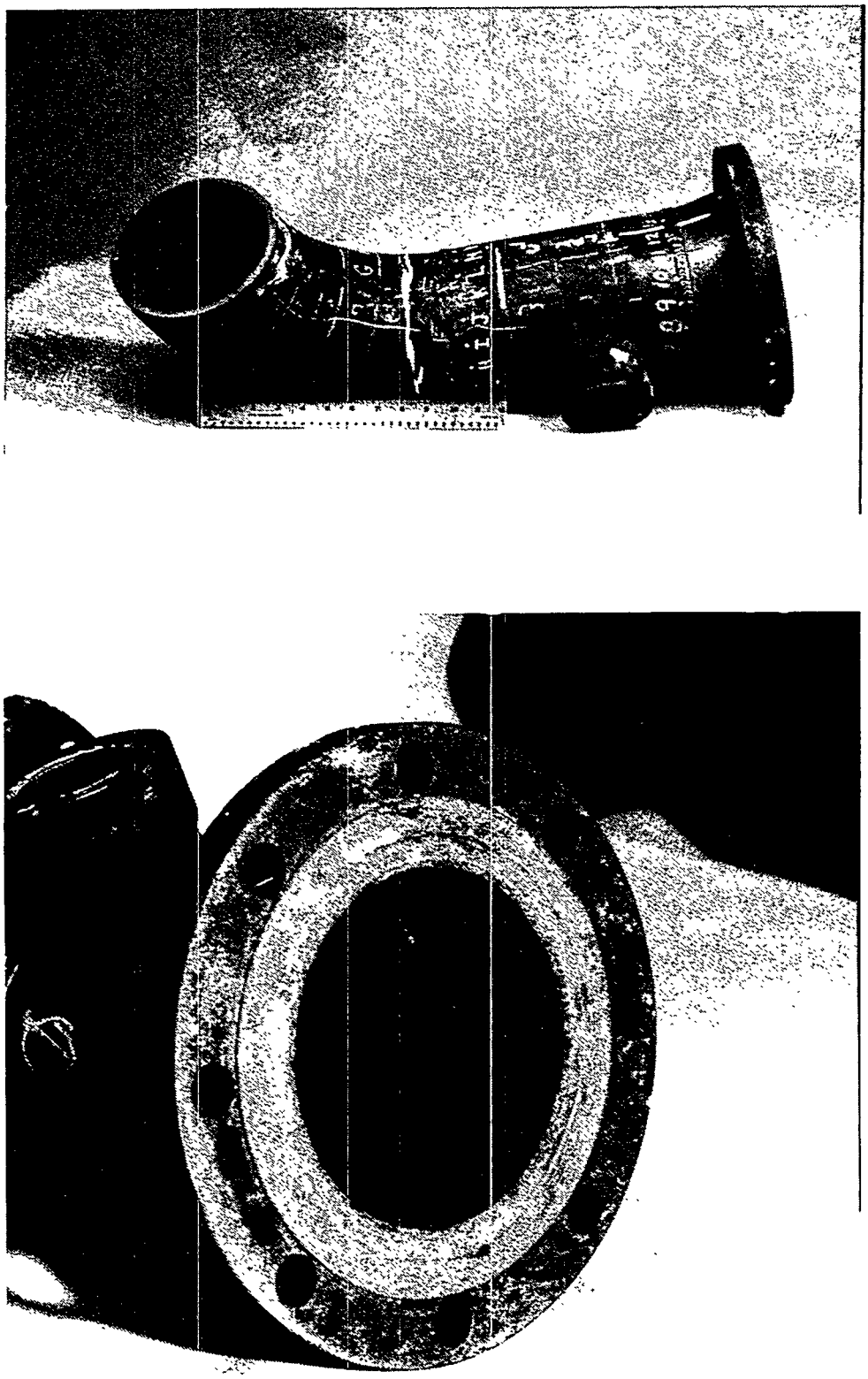

Figure 5. MIC pipe photographs

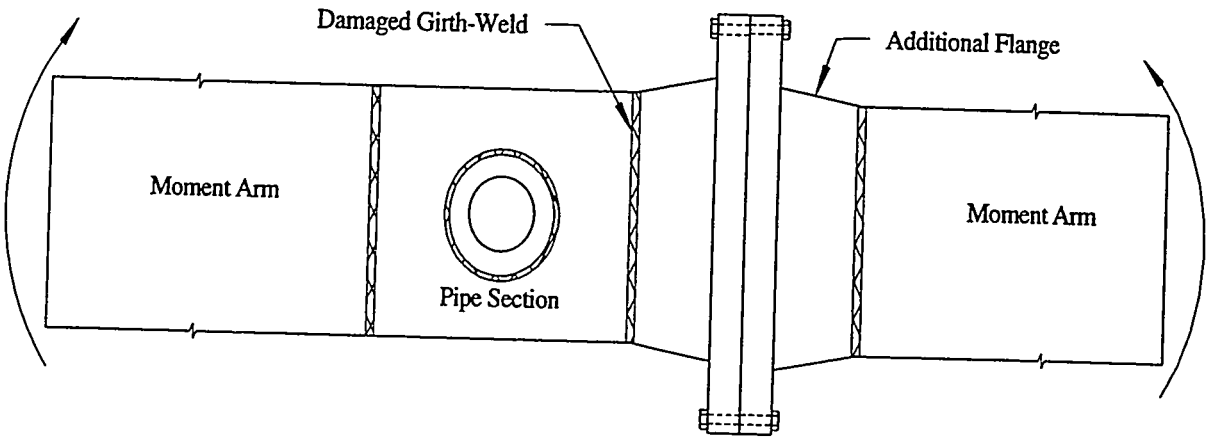

Figure 6. MIC specimen geometry.

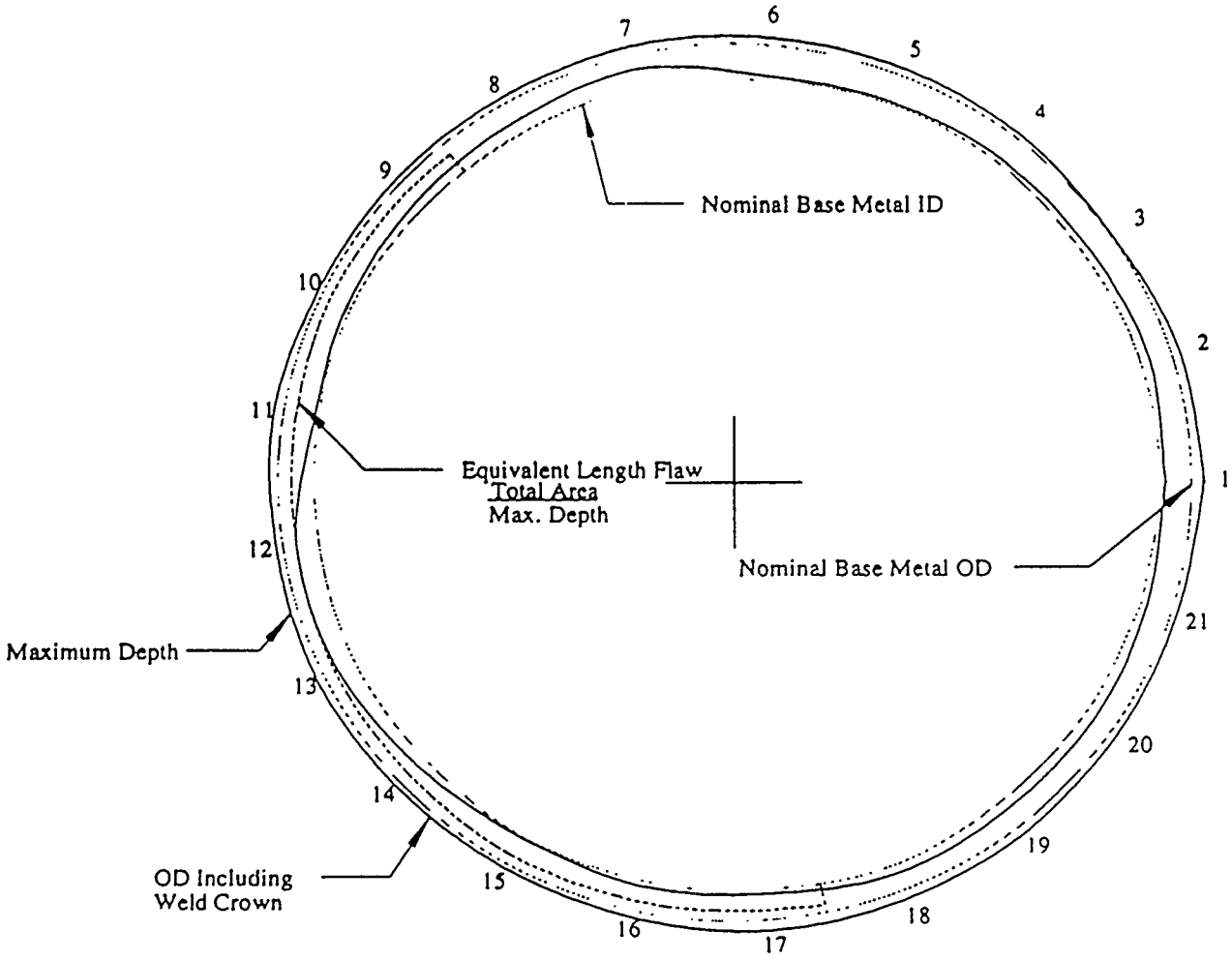

Figure 7. MIC flange-to-weld flaw geometry.

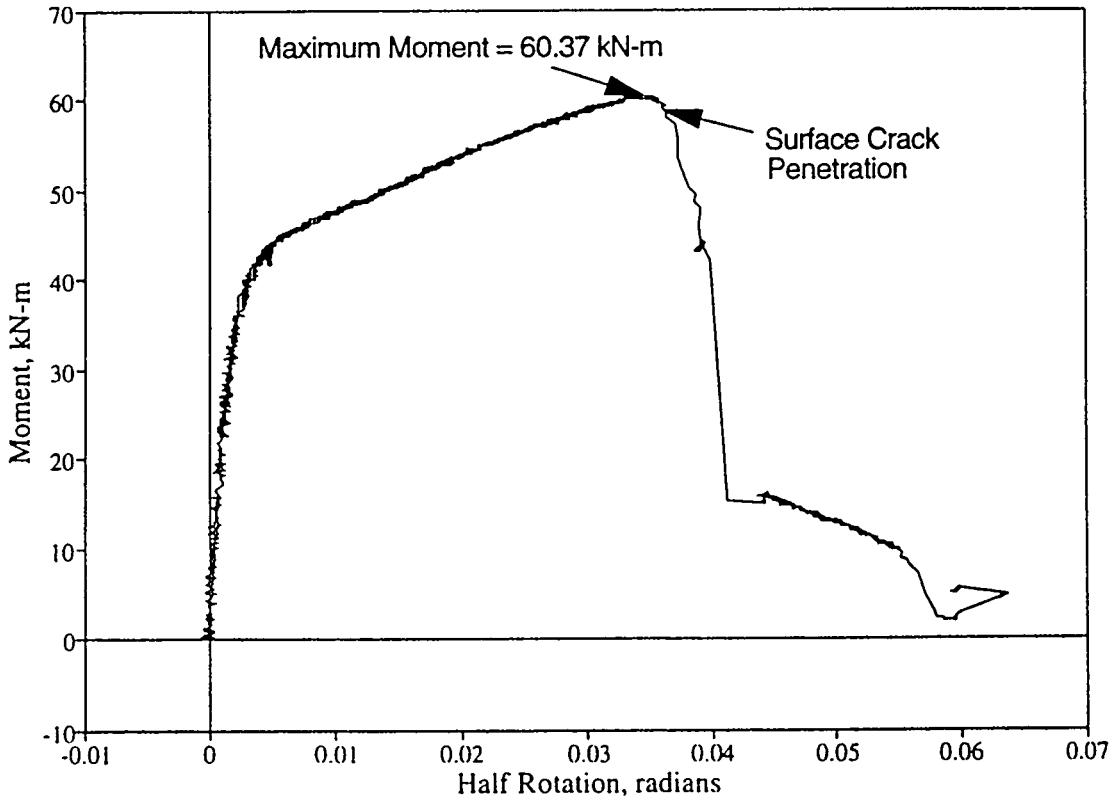

Figure 8. Experimental moment-rotation curve for MIC test.

Table 1. Current matrix of pipe experiments

Expt. No.	Diameter, in.	Schedule	Material	Temperature	Test Date
Unpressurized through-wall-cracked pipe experiments					
1.1.1.21	28	60	A515 Gr60	288C (550F)	10/25/90
1.1.1.23	28	80	TP316L SAW	288C (550F)	5/23/91
1.1.1.24	24	80	A333 Gr6 SAW	288C (550F)	3/13/92
1.1.1.26	4	80	TP316LN	22C (72F)	2/27/91
Unpressurized uncracked pipe experiment					
1.1.1.25	28	60	A515 Gr60	288C (550F)	2/07/92
Bimetallic weld fusion line experiments - TWC					
1.1.3.8	36	160	A516/SS-SAW	288C (550F)	9/93
Unpressurized surface-cracked pipe experiments					
1.2.1.20	16	30	TP316	99C (210F)	1/15/92
1.2.1.21	6	XXS	TP304	288C (550F)	4/16/91
1.2.1.22	6	40	TP304	288C (550F)	3/15/91
Pressurized surface-cracked pipe experiments					
1.2.3.15	28	60	A515 Gr60	288C (550F)	11/08/91
1.2.3.16	28	80	TP316L SAW	288C (550F)	9/05/91
1.2.3.17	24	100	A106B SAW	288C (550F)	12/93

Table 2. Bi-metallic weld through-wall crack test specimen
Pipe NUMBER DP2-F34 Piece E

Material	Outside Diameter	Wall Thickness	$2c/\pi D$
TP304 Stainless Steel	920.8 mm (36.25 inches)	82.6 mm (3.25 inches)	
A516 Grade 70 Carbon Steel with SA-240 TP 304L Stainless Steel Clad on Inside	927.1 mm (36.50 inches)	85.7 mm (3.38 inches)	0.33 (along Carbon Steel fusion line)

Bi-metal Weld - Inconel 182 buttered layers on A516 with stainless steel saw for balance of weld.

Table 3. Engineering approach for combined torsion and bending in piping systems

Effective Moment

M_B= Bending Moment
M_T = Torque

$$M_{eff} = \sqrt{M_B^2 + (cM_T)^2}$$

$c = 1 \Rightarrow$ Resultant of Bending Moment plus Torque

$c = \frac{\sqrt{3}}{2} \Rightarrow$ Effective Moment calculated from $\sigma_{eff} = \sqrt{\sigma_B^2 + 3\tau_T^2}$

$c = \frac{1}{2} \Rightarrow$ Effective Moment calculated from $\sigma_{eff} = \sqrt{\sigma_B^2 + \tau_T^2}$

$c = 0 \Rightarrow$ Ignore Torque

Reactor Pressure Vessel Structural Integrity Research

W. E. Pennell and W. R. Corwin
Oak Ridge National Laboratory*
Oak Ridge, TN 37831

Summary

Development continues on the technology used to assess the safety of irradiation-embrittled nuclear reactor pressure vessels (RPVs) containing flaws. Fracture mechanics tests on RPV steel, coupled with detailed elastic-plastic finite-element analyses of the crack-tip stress fields, have shown that (1) constraint relaxation at the crack tip of shallow surface flaws results in increased data scatter but no increase in the lower-bound fracture toughness, (2) the nil ductility temperature (NDT) performs better than the reference temperature for nil ductility transition (RT_{NDT}) as a normalizing parameter for shallow-flaw fracture toughness data, (3) biaxial loading can reduce the shallow-flaw fracture toughness, (4) stress-based dual-parameter fracture toughness correlations cannot predict the effect of biaxial loading on shallow-flaw fracture toughness because in-plane stresses at the crack tip are not influenced by biaxial loading, and (5) an implicit strain-based dual-parameter fracture toughness correlation can predict the effect of biaxial loading on shallow-flaw fracture toughness. Experimental irradiation investigations have shown that (1) the irradiation-induced shift in Charpy V-notch vs temperature behavior may not be adequate to conservatively assess fracture toughness shifts due to embrittlement, and (2) the wide global variations of initial chemistry and fracture properties of a nominally uniform material within a pressure vessel may confound accurate integrity assessments that require baseline properties.

1 Introduction

Regulatory requirements limit the permissible accumulation of irradiation damage in the material of a reactor pressure vessel (RPV). Irradiation damage limits are set such that required fracture prevention margins are maintained throughout the nuclear plant licensed operating period. Regulatory requirements are based on fracture mechanics technology and utilize materials aging data drawn from mandatory reactor vessel irradiation damage surveillance programs.

In recent years it has become evident that a number of nuclear plants will exceed the regulatory limits on irradiation damage to the reactor vessel material before the end of their current operating license period.[1] One result from this development is that several nuclear industry organizations have gained experience in the application of fracture margin assessment technology. This experience has resulted in the identification of a number of issues with the technology in its present form. Data from irradiation testing programs, operating plant surveillance programs, and large-scale fracture technology validation tests have identified additional issues. The Nuclear Regulatory Commission (NRC)-funded Heavy-Section Steel Technology (HSST) and Heavy-Section Steel Irradiation (HSSI) Programs at Oak Ridge National Laboratory (ORNL) are performing the research required to resolve these issues and further develop and refine the fracture margin assessment technology.

This paper presents a brief overview of some of the research programs implemented to resolve the issues just identified. Elements of the HSST Program concerned with shallow-flaw and biaxial loading effects on fracture toughness are described. Application of results from these program elements to the evaluation of stress-based dual-parameter fracture toughness correlations and the development of an implicit strain-based dual-parameter correlation are reviewed. The HSSI Program elements concerned with the experimental investigation of irradiation effects on materials are presented. Results are reviewed from a study in which data from these experimental investigations were used to assess the adequacy of Charpy V-notch (CVN) vs temperature behavior as an indicator of the effects of neutron-irradiation-embrittlement of RPV steels.

*Research sponsored by Office of Nuclear Regulatory Research, U.S. Nuclear Regulatory Commission under Interagency Agreements 1886-8011-9B and 1886-8109-8L with the U.S. Department of Energy under contract DE-AC05-84OR21400 with Martin Marietta Energy Systems, Inc.

2 HSST Program Research

Pressurized-thermal-shock (PTS) loading produces biaxial pressure and thermal stress fields in an RPV wall. Thermal stresses are highest adjacent to the inner surface of the vessel where the effects of irradiation embrittlement and transient temperatures combine to produce the maximum reduction in the material fracture toughness. The net result of this combination of conditions is that the majority of crack initiations predicted originate from shallow flaws located on the inner surface of the vessel. The dominant influence of shallow surface flaws generates a need for an experimental investigation of (1) the effect of reduced crack-tip constraint on the material fracture toughness associated with shallow flaws and (2) the effect of prototypical biaxial stress states on the material shallow-flaw fracture toughness, coupled with (3) development and validation of dual-parameter correlations that can be used to predict the material fracture toughness associated with shallow flaws in a biaxial stress field.

2.1 Shallow-Flaw Fracture Toughness

Fracture toughness tests have been performed on single-edge-notch-bending (SENB) test specimens using both deep (a/W = 0.5) and shallow (a/W = 0.1) flaws.[2,3] Beam specimens used in these tests are shown in Figs. 1 and 2. The beams tested by ORNL (Fig. 1) were fabricated from A 533 B material and were nominally 100 mm (4 in.) deep. Beams with a 230-mm-square (9-in.) cross section (Fig. 2) were cut from the RPV from a cancelled nuclear plant and tested, under an HSST Program subcontract, by the National Institute for Standards and Technology (NIST). The inner-surface stainless steel cladding remained in place on the large-scale test beams tested by NIST, and the flaws were located in the RPV longitudinal welds. Additional shallow-flaw fracture toughness data for A 533 B material were generated by the Fatigue and Fracture Branch of the Naval Surface Warfare Center (NSWC) in Annapolis, Maryland.[4] Material for the NSWC tests was heat treated to increase its yield stress. The NSWC tests were also conducted using large (B = 89 mm, W = 83 mm) SENB specimens. Use of large-scale beams permitted testing of shallow flaws with depths in the range identified as critical for PTS analysis. Data from Refs. 2–4 were all generated using large-scale SENB specimens fabricated from RPV steel. They can, therefore, be combined into deep- and shallow-flaw data sets.

Use of prototypical flaw depths reduced the uncertainties associated with extrapolation of shallow-flaw fracture toughness data for application to full-scale structures.

The reference temperature for nil-ductility transition (RT_{NDT}) is used as a normalizing parameter for fracture toughness data. The *American Society of Mechanical Engineers (ASME) Boiler and Pressure Vessel Code*[5] defines RT_{NDT} in terms of both the nil ductility temperature (NDT) and the temperature (T_{cv}) at which the lower-bound Charpy energy from three tests is not less than 68 J (50 ft·lb.). One of the temperatures (NDT or T_{cv}) will be the controlling temperature for RT_{NDT} in a given situation. Table 1 gives NDT, T_{cv}, and RT_{NDT} for each of the materials tested in the shallow-flaw program. Examination of the NDT and RT_{NDT} data in Table 1 reveals that a mix of governing conditions is contained within the data sets from NSWC, ORNL, and NIST. NDT and RT_{NDT} are identical, within a data set, in the NSWC tests, and in the ORNL tests on the Combustion Engineering (CE) material. RT_{NDT} is higher than NDT for the ORNL tests on material from HSST Plate 13B and for the NIST tests on weld metal, indicating that T_{cv} controlled RT_{NDT} in these cases.

Deep- and shallow-flaw fracture toughness data generated in these tests are plotted as a function of the normalizing temperature RT_{NDT} in Figs. 3 and 4, respectively. Open points and solid points in these plots represent data from material where RT_{NDT} was controlled by NDT and T_{cv}, respectively. The deep-flaw open and solid data points in Fig. 3 form a homogeneous group, indicating that RT_{NDT} is a satisfactory normalizing parameter for deep-flaw data. In contrast, the open- and solid-point shallow-flaw data in Fig. 4 appear to belong to two separate families, with quite separate lower-bound curves. The apparent existence of two separate families of data for a single material calls into question the adequacy of RT_{NDT} as a normalizing parameter for the shallow-flaw fracture toughness of A 533 B plate and weld material.

Tests used to determine NDT and T_{cv} are fundamentally different in character, and this difference could influence the interpretation, shown in Fig. 4, of the shallow-flaw fracture toughness data. This problem can be eliminated by adopting a common basis for the normalizing parameter used to compare the data sets. This has been done in Fig. 5, where NDT has been used as the normalizing parameter for all data points. Figure 5 shows that the shallow-flaw fracture toughness data from all sources form a homogeneous population when plotted as a function of T – NDT. A single curve defines the lower bound to the shallow-flaw fracture toughness data sets. A comparison of Figs. 3 and 5 shows that the lower-bound curves for the deep- and shallow-flaw data are similar, but the mean fracture toughness and scatter of data are significantly higher for shallow flaws than for deep flaws.

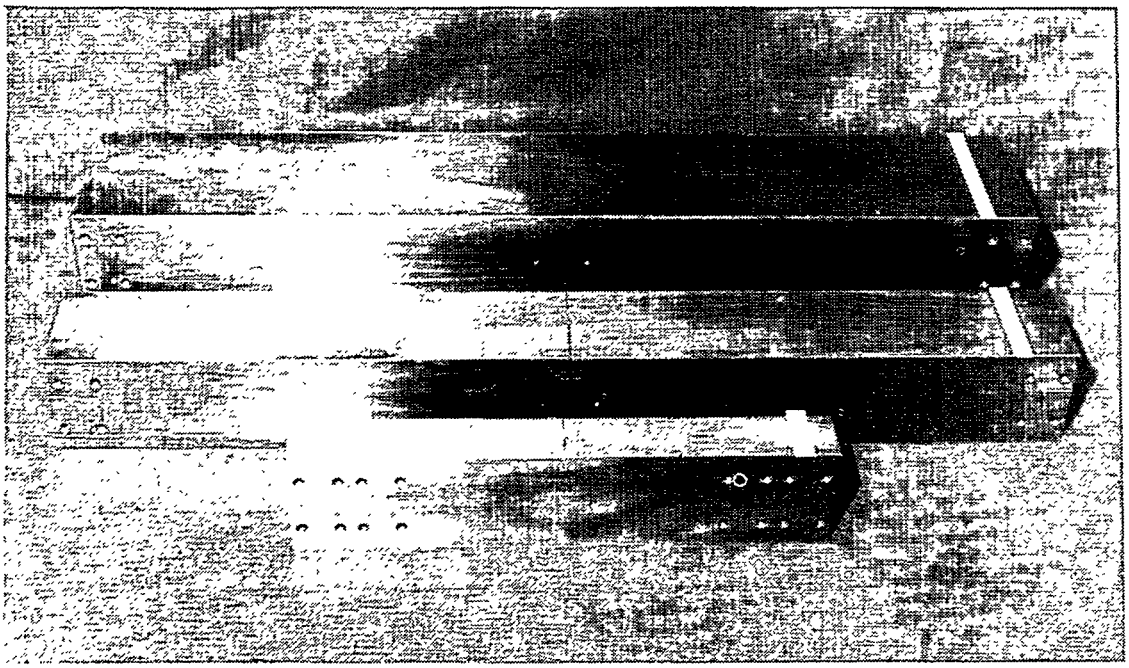

Figure 1 **The 100-mm deep beams were used in the shallow-flaw test program to permit full-scale testing of surface flaws having depths in the range that PTS analysis has shown to be the controlling range for crack initiation.**

Figure 2 **A limited number of full-scale beam specimens used in shallow-flaw test program were cut from the shell of an RPV from a cancelled nuclear plant.**

Table 1 Reference temperatures for material used in the shallow-flaw SENB and cruciform test specimens

Laboratory	Specimen type	Material	NDT [°C (°F)]	T_{cv} [°C (°F)]	RT_{NDT} [°C (°F)]
NSWC	SENB	Plate 11 (surface)	–7 (19)	24 (76)	–7 (19)
NSWC	SENB	Plate 11 (1/4 thickness)	4 (39)	31 (88)	4 (39)
ORNL	SENB	C-E plate	–35 (–31)	–17 (1)	–35 (–31)
ORNL	SENB	Plate 13B	–30 (–22)	18 (65)	–15 (5)
ORNL-NIST	SENB	V. weld	–50 (–58)	10 (50)	–23 (–10)
ORNL	BIAX	C-E plate	–35 (–31)	–17 (1)	–35 (–31)

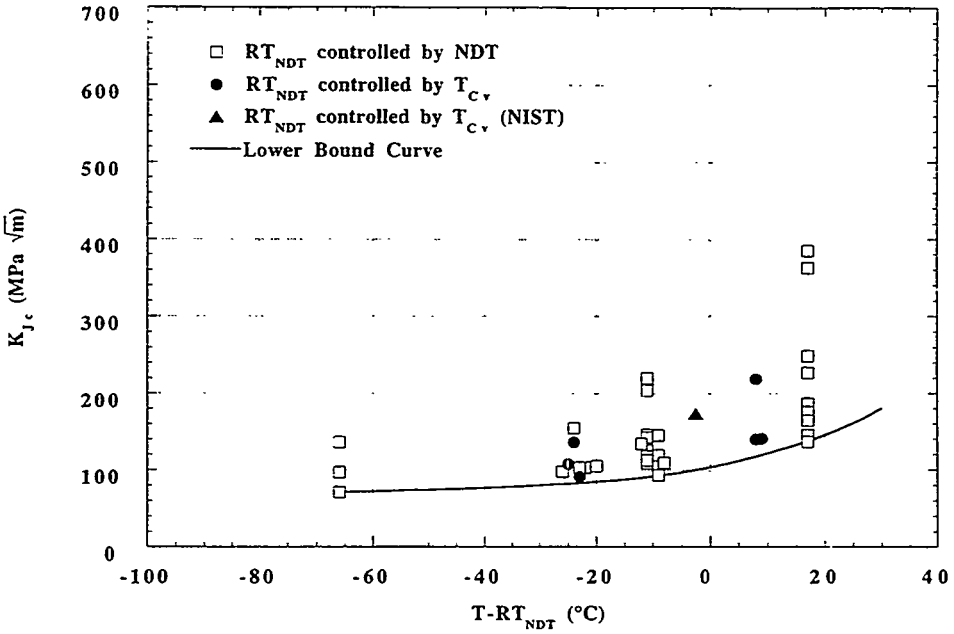

Figure 3 The parameter-controlling RT_{NDT} has no significant effect on the distribution of K_{Jc} vs $T - RT_{NDT}$ data points from the deep-crack SENB A 533 B specimens. A single curve adequately defines the lower bound for the combined data set.

2.2 Biaxial Loading Effects on Shallow-Flaw Fracture Toughness

A typical biaxial stress field produced by PTS transient loading is shown in Fig. 6, together with a constant-depth shallow surface flaw. One of the principal stresses is seen to be aligned parallel to the crack front. There is no counterpart of this far-field out-of-plane stress in the shallow-flaw fracture toughness tests previously described. The far-field out-of-plane stress has the potential to increase stress triaxiality (constraint) at the crack tip and thereby reduce some of the fracture toughness elevation associated with shallow flaws. The HSST biaxial test program was instituted to investigate this effect.

A cruciform test specimen was developed at ORNL to investigate the effects of biaxial loading on the shallow-flaw fracture toughness of pressure vessel steels.

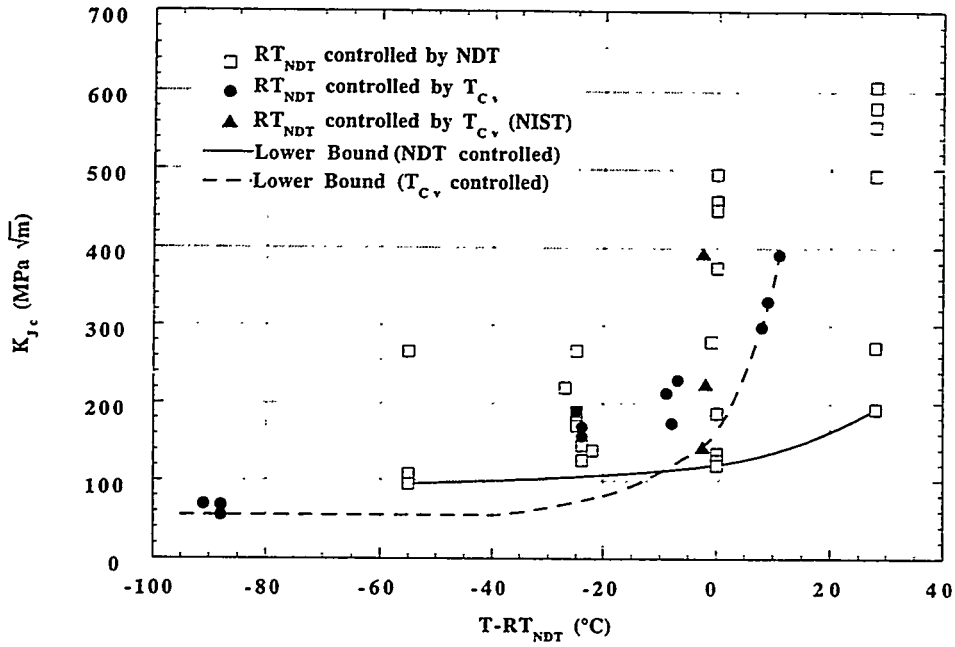

Figure 4 **Shallow-flaw fracture toughness data for A 533 B plate and weld material fall into two distinct groups when plotted as a function of the normalizing parameter T – RT_{NDT}. The groups are characterized by the parameter-controlling RT_{NDT} (NDT or T_{CV}).**

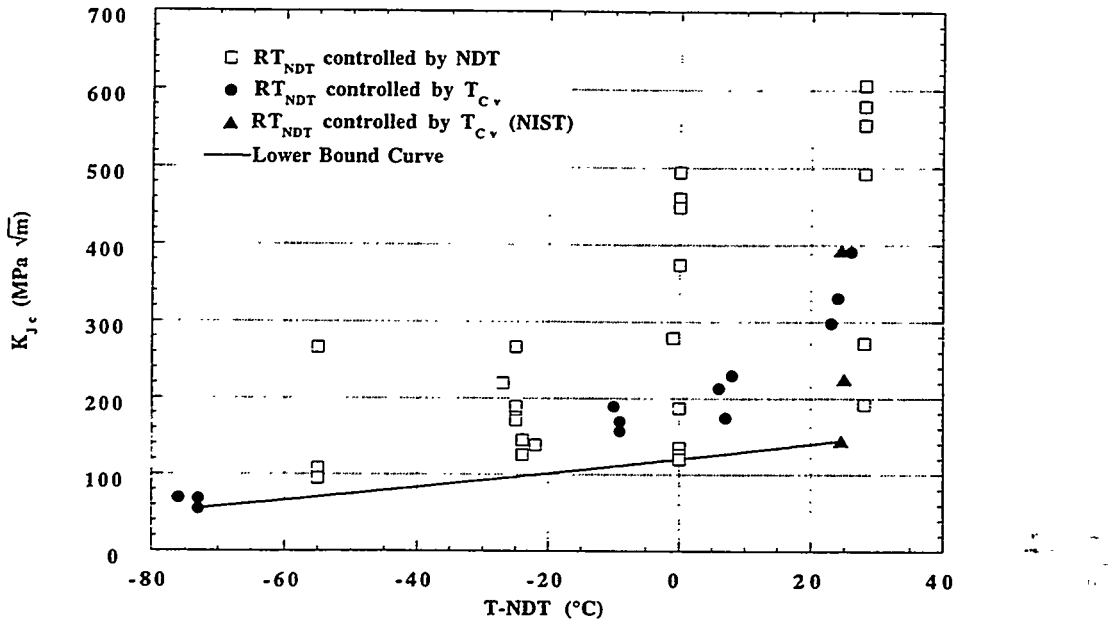

Figure 5 **Shallow-flaw fracture toughness data for A 533 B plate and weld material form a single homogeneous group when plotted as a function of the normalizing parameter T –NDT. The lower-bound curve of this data set is similar to that of the deep-flaw data set, but the shallow-flaw data set shows an increase in both mean toughness and data scatter.**

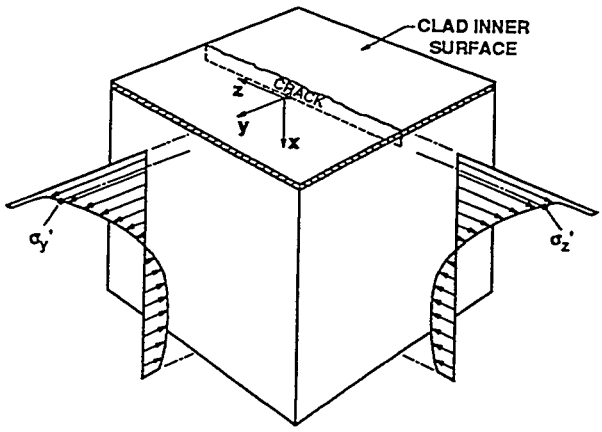

Figure 6 PTS loading produces biaxial stresses in an RPV wall with one of the principal stresses aligned parallel with the tip of a constant-depth shallow surface flaw.

Conceptual features of the specimen are shown in Fig. 7. The specimen design is capable of reproducing a linear approximation of the nonlinear biaxial stress distribution shown in Fig. 6. The cruciform design, coupled with a statically determinate load reaction system, permits the specimen to be loaded in either uniaxial (4-point bending) or biaxial (8-point bending) configurations. Tests of nominally identical specimens can thus be performed with the level of stress biaxiality as the only test variable.

An initial series of biaxial tests has been completed using test specimens fabricated from a single heat of A 533 B material. The biaxial load ratio is defined as P_T/P_L, where P_T is the total load applied to the transverse beam arms, and P_L is the total load applied to the longitudinal arms. Tests were run with P_T/P_L ratios of 0, 0.6, and 1. Details of those tests have been extensively reported[6,7] and will not be repeated here. K_{Jc} data from the biaxial tests are shown in Fig. 8, plotted as a function of the biaxiality ratio P_T/P_L. The plot shows a decrease in the lower-bound shallow-flaw fracture toughness with increasing biaxiality ratios. The data also indicate a trend of decreasing data scatter at a stress ratio of 0.6 when compared with the data scatter observed in both the uniaxial ($P_T/P_L = 0$) SENB shallow-flaw tests (see Fig. 5) and the biaxial shallow-flaw tests at a P_T/P_L loading biaxility ratio of 1.

2.3 Development of a Dual-Parameter Fracture Toughness Correlation

Dual-parameter fracture toughness corrections and correlations have been proposed to provide a quantitative assessment of effect of reduction of crack-tip constraint on fracture toughness. These include the J-A_{cr} fracture toughness correction proposed by Dodds, Anderson, and Kirk[8] and the J-Q dual-parameter fracture toughness correlation proposed by O'Dowd and Shih.[9,10] These dual-parameter fracture-toughness corrections and correlations share a common feature because they each utilize the effect of crack-tip constraint on in-plane stresses at the crack-tip to infer the effect of constraint on fracture toughness.

In the J-Q fracture toughness correlation, Q defines the departure of the stress-state-dependent opening-mode stress distribution on the crack plane from the opening-mode stress distribution derived by Hutchinson[11] and Rice and Rosengren[12] (HRR) for a highly constrained crack tip. Richie, Knott, and Rice (RKR) have proposed a criterion relating the critical value of the crack-tip opening-mode tensile stress at a critical distance from the crack tip for the onset of cleavage fracture in mild steel under plane-strain constraint conditions.[13] The J-Q fracture toughness correlation uses the RKR concept of a critical opening-mode tensile stress, together with the influence of constraint on opening-mode stresses represented by the parameter Q, to correlate the effect of crack-tip constraint on fracture toughness.

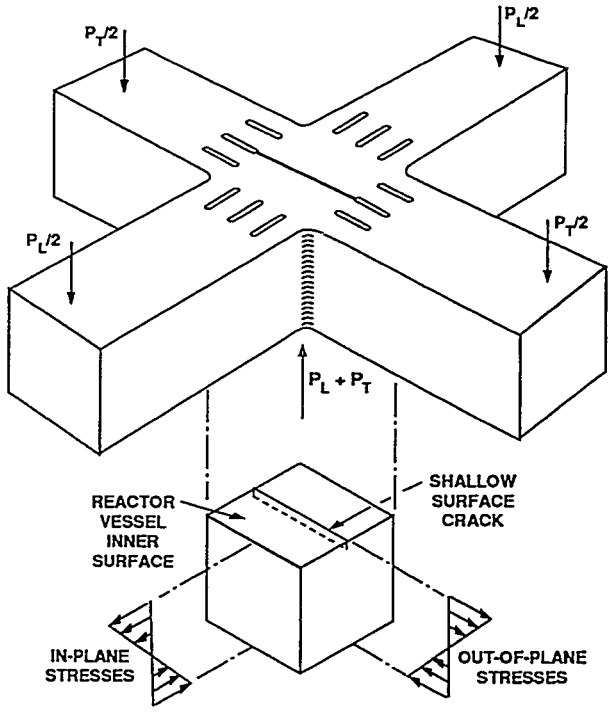

Figure 7 Conceptual features of the cruciform shallow-flaw biaxial fracture toughness test specimen.

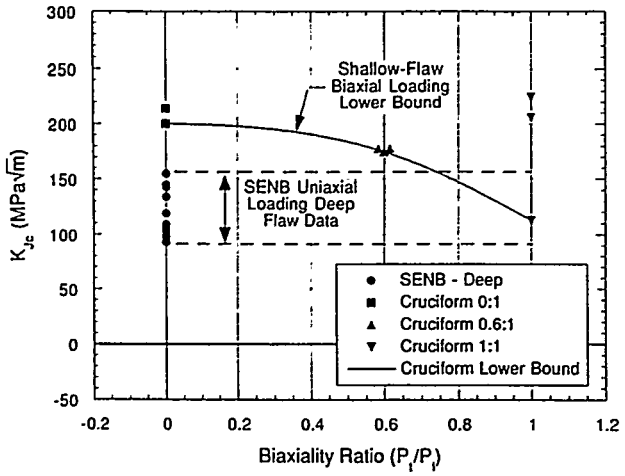

Figure 8 Data from a single heat of A 533 B steel tested at T – NDT = –10°C indicate that biaxial loading reduces the lower-bound transition-range shallow-flaw fracture toughness.

Prior investigations of biaxial loading effects have concluded that out-of-plane biaxial loading had no effect on in-plane stresses at the crack tip[14,15] but did influence the width of the crack-tip plastic zone in the direction of crack propagation. Recent elastic-plastic finite-element analyses of the ORNL biaxial specimen, performed by B. R. Bass and J. W. Bryson using a model with highly refined treatment of the crack-tip region (see Fig. 9), have confirmed these conclusions. The Bass-Bryson analyses have further confirmed that the stress-based J-A_{cr} constraint correction cannot predict the observed effects of biaxial loading on shallow-flaw fracture toughness. The HSST Program has, therefore, investigated the utility of strain-based constraint-effects technology.

A review of the facts supporting development of a strain-based dual-parameter correlation for transition range fracture toughness is appropriate at this point. Clausing[16] showed that the plane-strain ductility of structural steels increases rapidly over a relatively small temperature range, corresponding with the fracture toughness transition temperature range. Clausing related the decrease in toughness associated with increased strength to the associated decrease in plane-strain ductility. Barsom[17] and Merkle[18] developed expressions for K_{Ic} based upon plane-strain ductility. The expressions of Refs. 17 and 18 produced K_{Ic} predictions that matched the test data for temperatures in the transition range. Weiss[19] developed an equation for fracture toughness based upon the stress-state-dependent material fracture strain. An adaptation of the Weiss equation was used in the scoping analysis of Ref. 15 to determine the potential impact of biaxial loading on fracture toughness. The scoping analysis of Ref. 15 predicted a K_{JcB}/K_{JcU} ratio of 0.47 for equibiaxial loading, where K_{JcB} and K_{JcU} are values of K from J for biaxial and uniaxial loading conditions, respectively. This compares with the lower-bound K_{JcB}/K_{JcU} ratio of 0.56 obtained in tests (see Fig. 8) with equibiaxial and uniaxial loading. Similarity of the predicted and measured K_{JcB}/K_{JcU} values is supportive of a strain-based fracture toughness correlation. Fractographic data from examinations of broken fracture specimens[7,20] provide further support for a strain-based fracture toughness correlation. The fractographic data indicate that many crack initiation sites are located in the region of the crack-tip process zone where strain is increasing, but stress is decreasing, with increasing applied K_J.

Tetleman and McEvily (T&M)[21] postulate that plastically induced fracture initiates in a ligament immediately adjacent to the blunted crack tip when the ligament strain reaches the fracture strain (e_f) of the material. They approximate the ligament length as twice the root radius of the blunted crack tip. The T&M fracture criterion can be interpreted as a limiting condition for energy absorption by inelastic deformation of the crack-tip material. It should be possible, therefore, to determine the effects of constraint on fracture toughness by analyzing the response of the crack-tip material to increasing load and determining the radius of the blunted crack tip at which the crack-tip ligament strain reaches e_f. The blunted crack tip has a free surface. The fracture strain (e_f) for material immediately adjacent to the crack tip is, therefore, the plane-strain fracture strain determined by Clausing.[16]

Direct implementation of the strain-based constraint-effects methodology just described would require a computationally intensive, finite strain, elastic-plastic finite-element analysis. This analysis would be required to

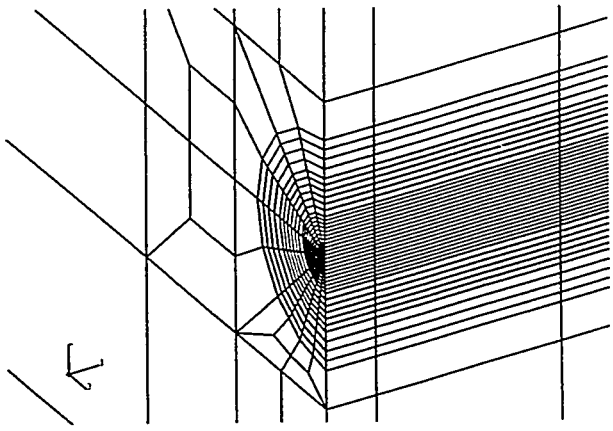

Figure 9 Detail of the crack-tip region of the cruciform specimen finite element model.

determine the crack-tip radius corresponding with the generation of strains equal to the fracture strain in material immediately adjacent to the blunted crack tip. Fortunately, the crack-tip plastic deformation is approximately equal to the plastic displacement $e_y \cdot R$, where e_y is the material yield strain and R is the width of the crack-tip plastic zone in the crack plane.[21] A strain-based constraint effects methodology can, therefore, be based on the effects of crack-tip constraint on R. The parameter R can be calculated accurately in a small strain analysis.

The influence of biaxial loading on the growth of the plastic zone width (R) in response to increasing load is shown in Fig. 10. Results plotted in Fig. 10 were taken from analyses performed by Bass and Bryson using the analysis model of Fig. 9, with the material stress-strain properties shown in Fig. 11. The curves of Fig. 10 show that biaxial loading has the effect of inhibiting the growth of the plastic zone width R. In the case of the $P_T/P_L = 0.6$ loading, the inhibiting effect is present over the entire loading range. In the case of the $P_T/P_L = 1.0$ loading, however, growth of the plastic zone width is inhibited up to an applied loading of ~1000 MPa (150 kips), where rapid growth occurs because of the onset of uncontained yielding of the specimen. The curve for $P_T/P_L = 1.0$ loading becomes similar to the curve for uniaxial loading at load levels beyond those shown in Fig. 10. This effect of uncontained yielding may explain why some researchers, using small test specimens in which uncontained yielding was unavoidable, have reported no effects of biaxial loading on fracture toughness. The influence of biaxial loading on R depicted in Fig. 10 would indicate that a strain-based constraint-effects model, using R as a second parameter, should predict an effect of biaxial loading on fracture toughness.

Biaxial fracture toughness (K_{Jc}) values from Fig. 8 are shown plotted as a function of the natural logarithm of the plastic zone width [ln(R)] in Fig. 12. The parameter ln(R) was used rather than R because the data conformed to a simple straight-line relationship when presented in this form. A $\pm$ 22-MPa$\sqrt{m}$ ($\pm$20-ksi$\sqrt{in.}$) uncertainty band accomodates scatter in the, admittedly small, data set. The uncertainty band in Fig. 12 represents the fracture toughness locus for the test material for a normalized temperature (T – NDT) of – 10°C. A series of fracture toughness loci would have to be generated to cover the range of normalized temperatures of interest in RPV safety evaluations.

K_{Jc} – ln(R) loading trajectories from the Bass-Bryson analyses are shown in Fig. 13, superimposed on the fracture toughness locus from Fig. 12. Note that each biaxial loading ratio produces a unique K_{Jc} – ln(R) trajectory. Intersection of the K_{Jc} – ln(R) loading trajectory for a particular loading biaxiality ratio with the fracture

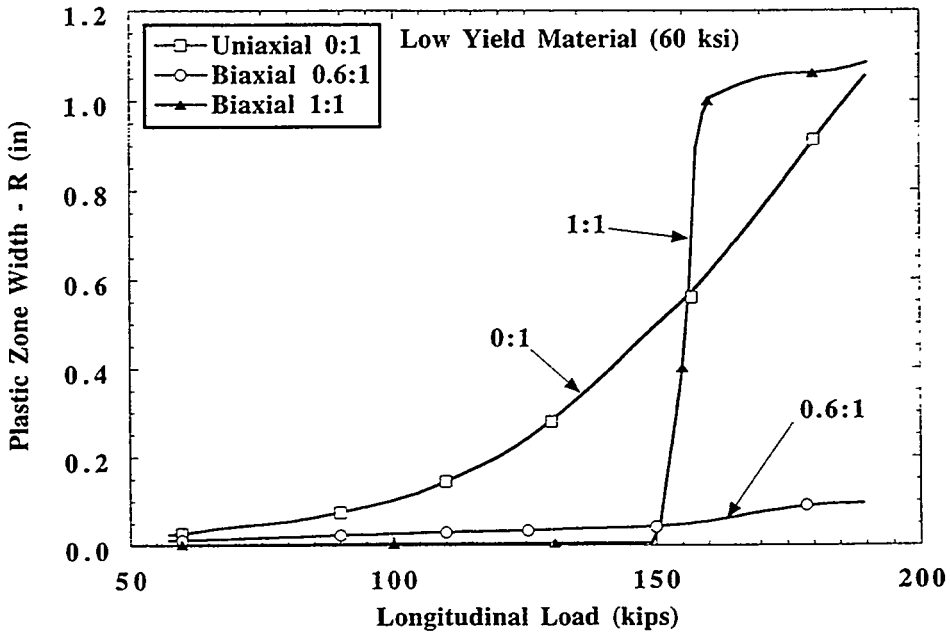

Figure 10 The rate of increase of the width (R) of the crack-tip plastic zone in the direction of crack propagation is directly related to the biaxial loading ratio P_T/P_L.

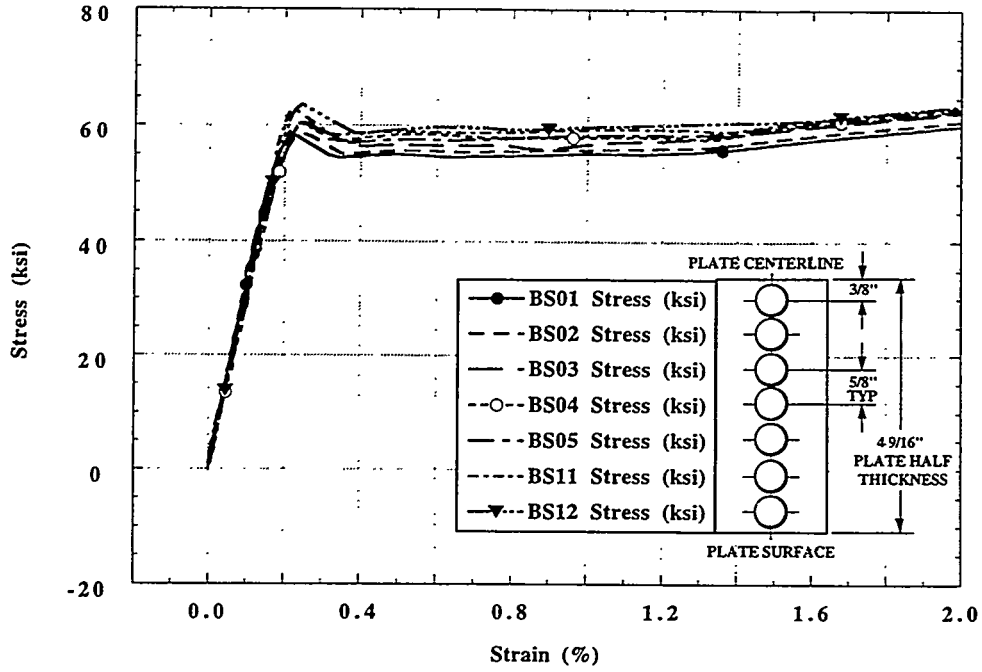

Figure 11 **The C-E A 533 B Grade 1 plate material used to fabricate the biaxial test specimens exhibits an abrupt transition from linear-elastic behavior followed by significant Lüders straining, before the onset of strain hardening.**

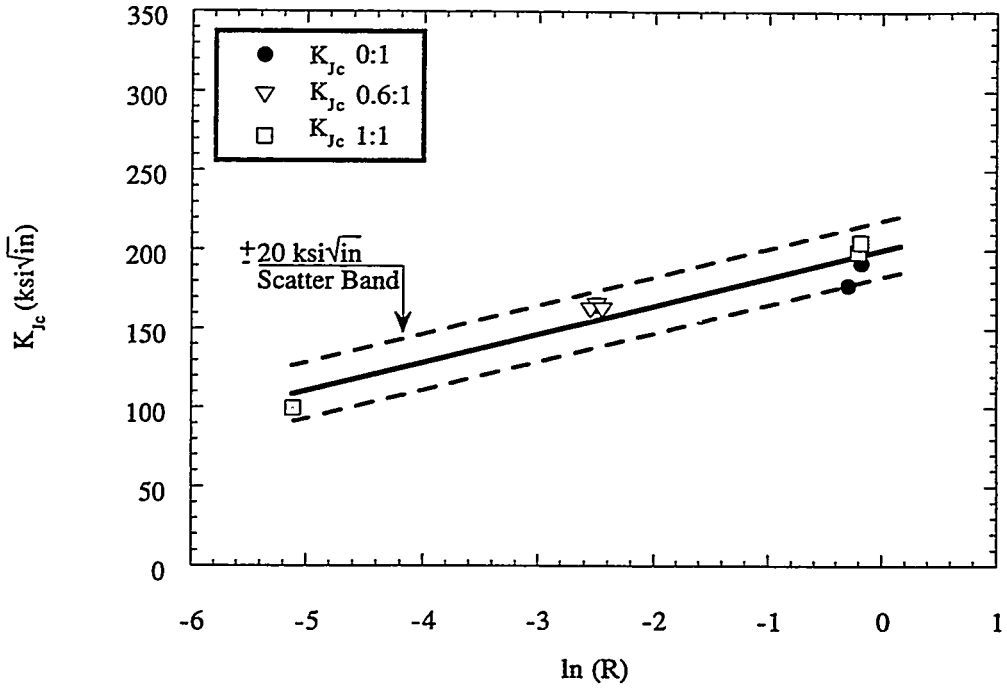

Figure 12 **Test data and analysis results for the biaxial specimen are combined to define a K_{Jc}-ln(R) shallow-flaw fracture toughness locus.**

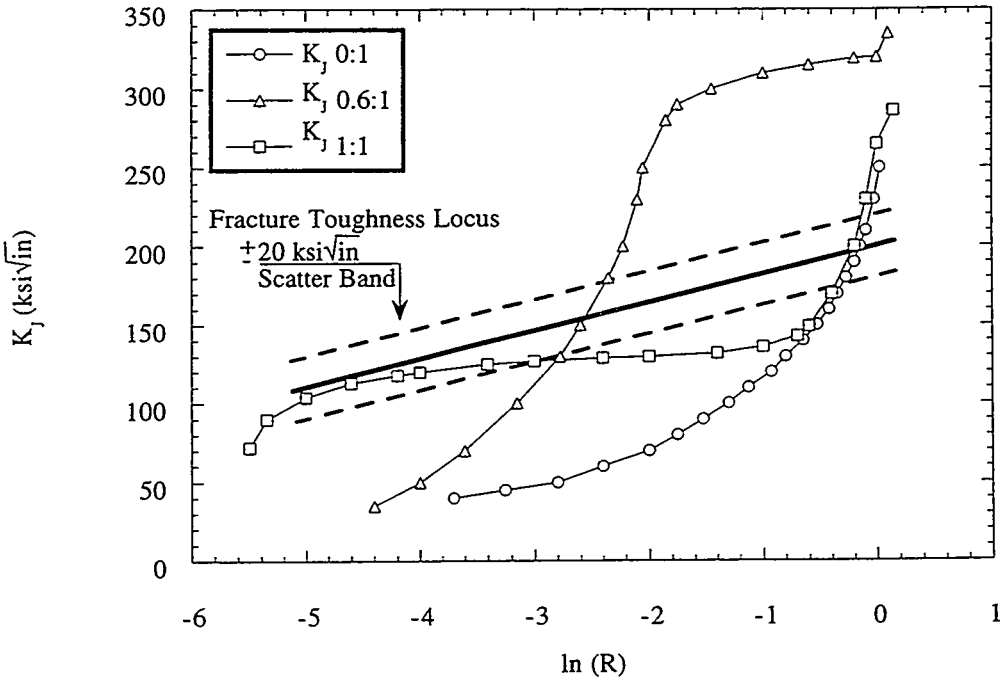

Figure 13 K_{Jc}-ln(R) trajectories for the biaxial specimen predict unique K_{Jc} values for uniaxial and $P_T/P_L = 0.6$ loading, but both high and low K_{Jc} values are possible for the $P_T/P_L = 1.0$ loading because of the low yield stress of the material used for these tests.

toughness locus predicts the range of fracture toughness values possible for that loading condition at a normalized temperature (T – NDT) of –10°C. The results summarized in Fig. 13 suggest that a strain-based K_{Jc} – ln(R) has the potential for development into a dual-parameter fracture toughness correlation capable of representing the effects of crack-tip constraint on the fracture toughness of RPV steels, including the effects of stress biaxiality.

Before leaving this topic, two important influences of the material stress-strain curve on the results presented above should be noted.

1. The onset of uncontained yielding has a pronounced effect on the loading trajectory for the $P_T/P_L = 1.0$ loading condition, causing it to intersect the fracture toughness locus at both low and high values of K_{Jc}. The low yield stress of the material used in this series of tests [σ_y = 414 MPa (60 ksi)] resulted in uncontained yielding in two of the $P_T/P_L = 1.0$ tests, giving biaxial test results that are similar to the uniaxial results. Analysis performed with a material yield stress of 621 MPa (90 ksi) did not show any effects of uncontained yielding with $P_T/P_L = 1.0$ over the loading range investigated.
2. Test data for A 533 B RPV steel, irradiated to fluences up to 5.5×10^{19} neutrons/cm^2 (E >1 MeV), showed that a sharply defined departure from linear-elastic behavior is present in both unirradiated and irradiated material tested at both very low and very high straining rates.[22] Inclusion of the sharply defined departure from linear-elastic behavior shown in Fig. 11 is essential to an accurate prediction of the effect of biaxial loading on the width R of the plastic zone. The effects of concern cannot be predicted using a power law approximation of the stress-strain curve.

3 HSSI Program Research

3.1 K_{Ic} Curve Shifts in High-Copper Welds

To account for the effects of neutron irradiation on toughness, the initiation and arrest fracture toughness curves as described in Sect. XI of the *ASME Boiler and*

Pressure Vessel Code are shifted upward in temperature without change in shape by an amount equal to the shift (plus a margin term) of the CVN impact energy curve at the 41-J (30-ft·lb) level. Such a procedure implies that the shifts in the fracture toughness curves are the same as those of the CVN 41-J energy level and that irradiation does not change the shapes of the fracture toughness curves.

The objectives of the HSSI Fifth and Sixth Irradiation Series are to determine the K_{Ic} and K_{Ia} curve shifts and shapes for two irradiated high-copper, 0.23 and 0.31 wt %, submerged-arc welds (72W and 73W, respectively). Irradiations were performed at 288°C (550°F) to average fluences of about 1.5×10^{19} neutrons/cm^2 (E > 1 MeV). Tests included tensile, CVN impact, drop-weight, and fracture toughness. Compact specimens up to 203 and 101 mm (8 and 4 in.) in thickness were tested in the unirradiated and irradiated conditions, respectively. The detailed results of testing have been presented previously.[23] For the CVN results, the 41-J (30-ft·lb) transition temperature shifts were 72 and 82°C (130 and 148°F), while the 68-J (50-ft·lb) shifts were 82 and 105°C (148 and 189°F) for welds 72W and 73W, respectively.

For those fracture specimens that met the American Society for Testing and Materials (ASTM) E399 criteria for a valid K_{Ic}, the K_{Ic} value is used in the analysis. For those specimens that exhibited curvature in the load-displacement record, indicative of plastic deformation and, perhaps, stable ductile tearing, the K_{Jc} value was used. To include both linear-elastic and elastic-plastic fracture mechanics calculations, data have been designated K_{cl} for cleavage fracture toughness. Figure 14 shows that an unexpectedly large number of cleavage pop-ins occurred in the irradiated data set. Of 156 unirradiated compact specimens, only 2 exhibited pop-ins, as compared to 36 pop-ins for the 110 irradiated specimens. To be conservative, only the initial pop-in is used here to determine cleavage fracture toughness for those specimens exhibiting pop-ins.

Linearized two- and three-parameter nonlinear regression analyses similar in form to the K_{Ic} curve in Sect. XI of the ASME Code gave fracture toughness temperature shifts, measured at the 100-MPa$\sqrt{m}$ (91- ksi$\sqrt{in.}$) level, of about 83 and 99°C (149 and 178°F) for 72W and 73W, respectively. The analyses show some decreases in slopes for the irradiated data for both welds. These decreases, however, are only about 4.1 and 6.9% for 72W and 73W, respectively, with large enough standard errors to imply a low statistical significance of the slope changes. For the combined data sets, with temperature normalized to RT_{NDT}, the differences are about 10, 15, and 17°C (18, 27, and 31°F) between the unirradiated and irradiated mean fracture toughness curves at K_{cl} values of 50, 100, and 200 MPa$\sqrt{m}$ (46, 91, and 182 ksi$\sqrt{in.}$), reflecting the average change in curve shape.

Figure 15 shows a plot of the irradiated fracture toughness data and various curves for 73W. The ASME K_{Ic} curve is shown for both the unirradiated and the irradiated conditions after shifting the curve upward. The dashed curves labeled 1–3 represent different methods for shifting the K_{Ic} curve. The curve labeled 4 represents the ASME K_{Ia} curve shifted upward in temperature equal to the Charpy 41-J (30-ft·lb) shift (TT41). The curve labeled 5 is the five- percentile curve produced using the method of Wallin.[24] For 72W, the data are bounded by the TT41 + margin curve and the K_{cl} curve, but neither of these curves quite bound all the data for 73W. The margin is 15.6°C (28°F) as defined in Regulatory Guide 1.99 (Rev. 2) assuming credible surveillance data. The K_{Ia} curve is shown to allow for comparison of that curve with the shifted K_{Ic} curves, especially regarding curve shape, in view of the observation that the irradiated K_{cl} curves for these two welds appear to have exhibited some shape change after irradiation. Figure 16 shows all the irradiated fracture toughness data for 72W and 73W plotted vs temperature normalized to the RT_{NDT}. As shown in the figure, a total of eight data points fall below the ASME K_{Ic} curve. To bound all data, the dashed K_{Ic} curve must be shifted upward in temperature 18°C (32°F).

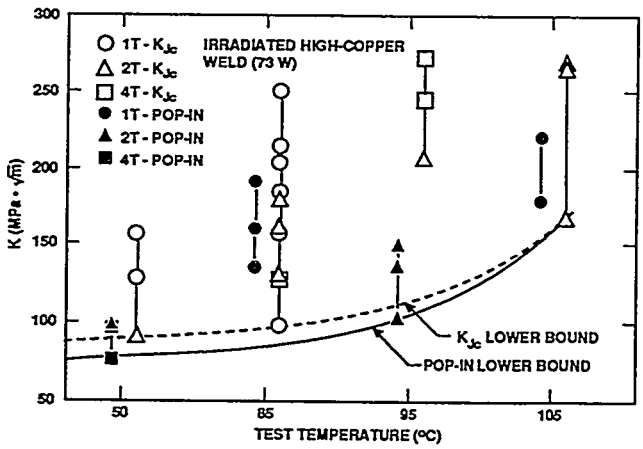

Figure 14 Test data for irradiated high-copper weld (73W) indicate that lower-bound fracture toughness curve reflecting pop-in test data differs very little from one derived from K_{Jc} data.

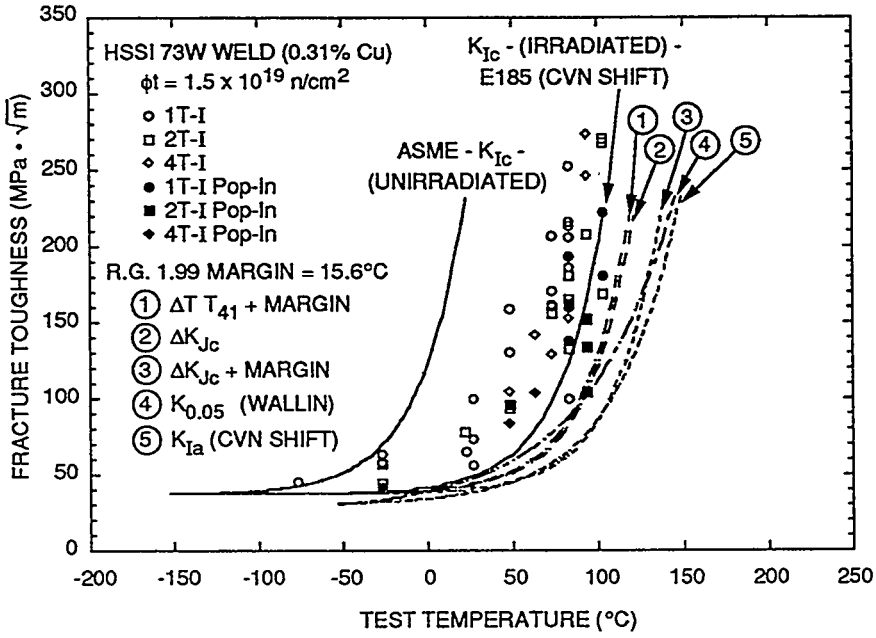

Figure 15 **Fracture toughness, K_{cl}, vs test temperature for irradiated HSSI weld 73W. The ASME K_{Ic} curve for the unirradiated data is shown, as is the same curve after shifting it upward in temperature equal to the Charpy 41-J shift. The curves labeled 1, 2, and 3 represent the ASME curve shifted by the indicated criterion, where margin is 15.6°C. The K_{Ia} curve represents the ASME K_{Ia} curve shifted by the Charpy 41-J shift. The $K_{0.05}$ curve is the five-percentile curve for all the HSSI 72W and 73W combined data using the Wallin procedure.**

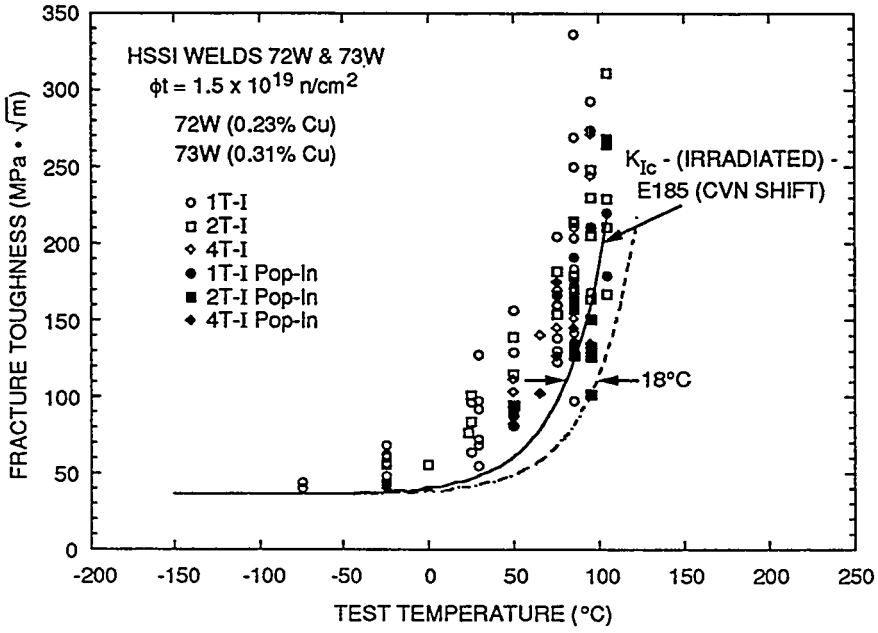

Figure 16 **Fracture toughness, K_{cl}, vs normalized temperature, $T - RT_{NDT}$, for irradiated welds 72W and 73W. The dashed curve is the ASME curve shifted upward in temperature to just bound the irradiated data.**

Observations from the HSSI Fifth and Sixth Irradiation Series included the irradiation-induced temperature shift. Statistical analyses and curve fitting showed that the temperature shifts at a fracture toughness of 100 MPa$\sqrt{m}$ (91 ksi$\sqrt{in.}$) were greater than those at a Charpy energy of 41 J (30 ft·lb) but were in good agreement with the Charpy 68-J (50-ft·lb) transition shifts. The 68-J temperature shifts were greater than the 41-J shifts, reflecting the change in the slope of the CVN curves following irradiation.

Results from the HSSI Sixth Irradiation Series on crack-arrest toughness indicate no irradiation-induced curve shape changes in the K_{Ia} curve. Similar shifts were measured at the 41-J (30-ft·lb) level for CVN specimens and the 100-MPa$\sqrt{m}$ (91-ksi$\sqrt{in.}$) level for K_{Ia} (Ref. 25). Figure 17 shows a comparison of the fracture toughness and crack- arrest toughness for the combined irradiated data for 72W and 73W normalized to the RT_{NDT}. The mean irradiated K_{cI} curve has been shifted much closer to the irradiated K_a curve than is the case for the unirradiated

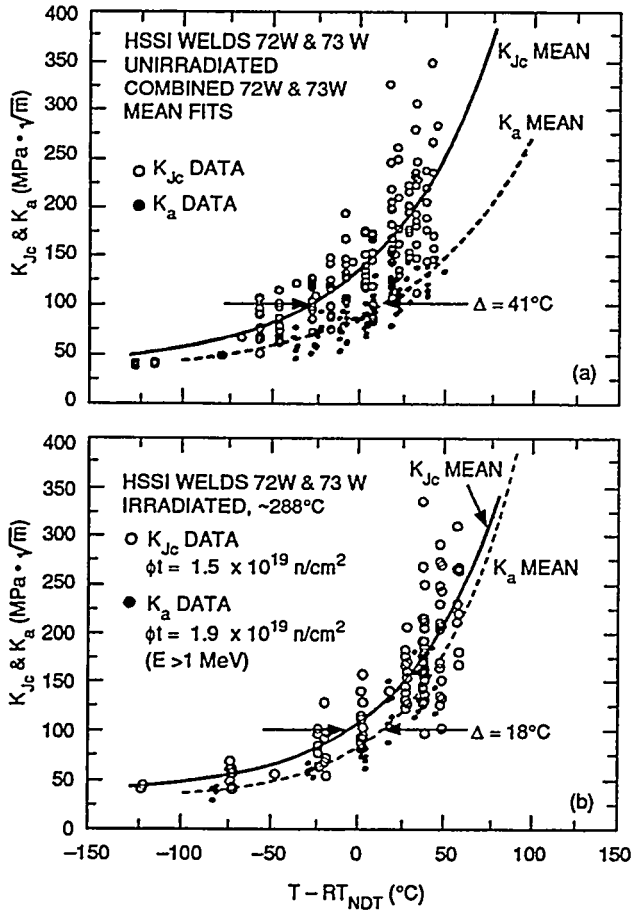

Figure 17 Comparison of mean fracture toughness and crack-arrest toughness vs normalized temperature for welds 72 and 72W in (*a*) unirradiated and (*b*) irradiated conditions.

conditions. The fact that the average separation in initiation and arrest toughness at any given temperature is reduced in the irradiated condition may help explain the enhanced propensity for pop-in events following irradiation.

3.2 Irradiation Embrittlement in a Commercial LUS Weld

The HSSI Program includes examination of the fracture resistance of low-upper-shelf (LUS) welds. This class of submerged-arc welds was produced using Linde 80 welding flux because it produced a very fine dispersion of inclusions within the weld and a resultant low number of reportable defects observed by radiography. Unfortunately, this fine dispersion of inclusions provided such a large number of microvoid initiation sites that the macroscopic resistance of these welds to ductile crack extension by the microvoid growth and coalescence process was significantly reduced. This fine inclusion dispersion, in combination with the common early practice of using copper-coated welding wire, has resulted in a significant number of pressure vessels in which major fabrication welds have both relatively low resistance to ductile fracture in the unirradiated condition and a high sensitivity to further degradation from neutron exposure.

The principal current activity within the HSSI Program to examine LUS welds is the Tenth Irradiation Series. The effects of irradiation on the fracture toughness of commercially fabricated LUS submerged-arc welds from the RPV of the canceled Midland Unit 1 nuclear plant are being investigated. The welds from the Midland plant carry the Babcock and Wilcox Company designation WF-70, a specific combination of weld wire and welding flux that exists in several commercial pressurized-water reactors. The initial part of this study involved the determination of variations in chemical composition, RT_{NDT}, tensile properties, and fracture toughness throughout the welds.[26] Four 1.17-m-long (46-in.) sections of beltline weld and two similar sections of nozzle course weld have been examined. NDT temperatures ranged from –40 to –60°C (–40 to –76°F). Because the Charpy impact energy did not achieve 68 J (50 ft-lb) at NDT + 33°C (59°F), the RT_{NDT} values are all controlled by the Charpy behavior. The RT_{NDT} values vary from –20 to 37°C (–4 to +99°F) with position in the vessel (Fig. 18); the upper-shelf energies (USEs) varied from 77 to 108 J (57 to 80 ft·lb). Analysis of the combined data revealed a mean 41-J (30-ft·lb) temperature of –8°C (18°F) with a mean USE of 88 J (65 ft·lb). Even though both welds carry the WF-70 designation, their bulk copper contents range widely from 0.21 to 0.34 wt % and 0.37 to 0.46 wt % in the beltline and nozzle course weld, respectively.

Tensile and fracture toughness properties were determined on nozzle and beltline weld metals at six temperatures ranging from -100 to 288°C (-148 to 550°F). The yield

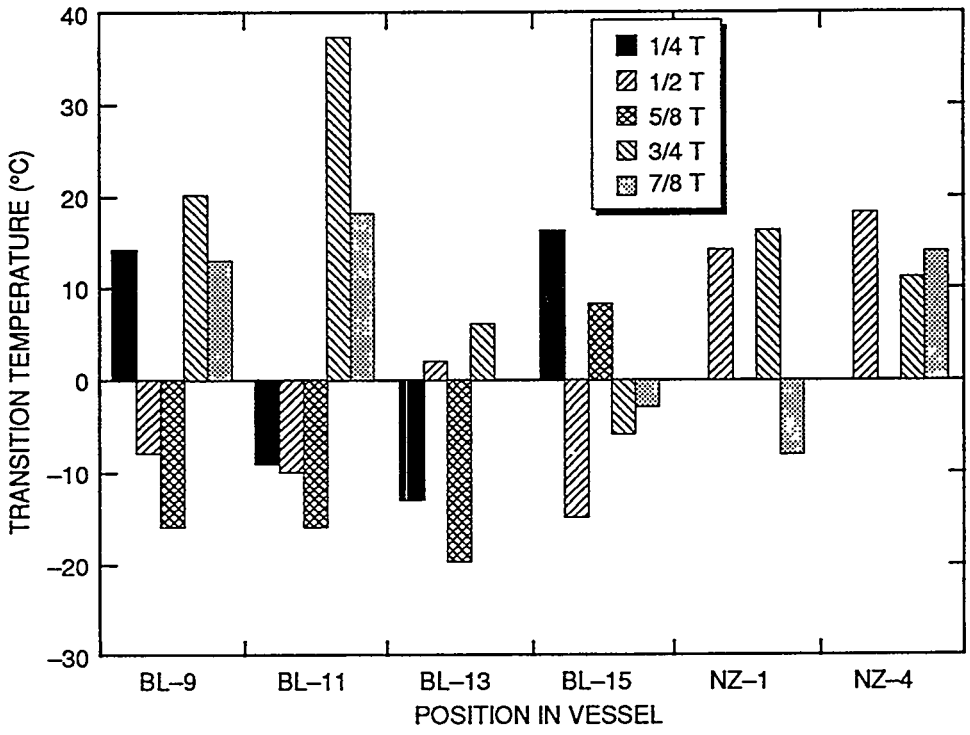

Figure 18 Distribution of RT_{NDT} values for different sections of Midland LUS beltline (BL) and nozzle (NZ) course welds as function of through-thickness position.

strength of the nozzle weld metal was significantly higher than that of the beltline weld, on the order of 100 MPa (14.5 ksi). All the fracture toughness tests to characterize the unirradiated material, using compact specimens ranging up to 101 mm (4 in.) in thickness, have been completed. Data to characterize ductile-to-brittle transition temperature were evaluated using a test standard currently under development by ASTM. This involves the determination of the position of a median fracture toughness transition curve (master curve), using only the data from six 12.5-mm-thick (0.5-in.) (1/2T) compact specimens, to compare with data from large specimens. The "reference temperature" for the master curve was found to be –60°C (–76°F) for the beltline weld and –43°C (–45°F) for the nozzle weld. This appears to agree well with the fact that the mean fracture toughness vs temperature behavior for the beltline weld is higher than for the nozzle weld (Fig. 19).

The irradiation of the Midland weld is in progress. The exposure of the first of the two large irradiation capsules, containing tensile, CVN, and fracture toughness specimens, to the primary target fluence of 1×10^{19} neutrons/cm^2 (E > 1 MeV) has been completed, and the second one has begun. Small fracture toughness and CVN specimens are also being exposed in low- and high-fluence scoping capsules to 5×10^{18} and 5×10^{19} neutrons/cm^2 to examine fluence effects over this range.

4 Interim Conclusions

- The lower-bound fracture toughness for A 533 B plate and weld metal is similar for both shallow- and deep-flaw data sets.
- Data scatter and mean values of fracture toughness are higher for shallow flaws than for deep flaws.
- NDT appears to be a better normalizing parameter than RT_{NDT} for shallow-flaw fracture toughness data.
- The ORNL biaxial specimen permits the effects of biaxial loading on shallow-flaw fracture toughness to be isolated and measured.
- Biaxial loading can produce reductions in the shallow-flaw fracture toughness that can be as high as 40% for equibiaxial loading.

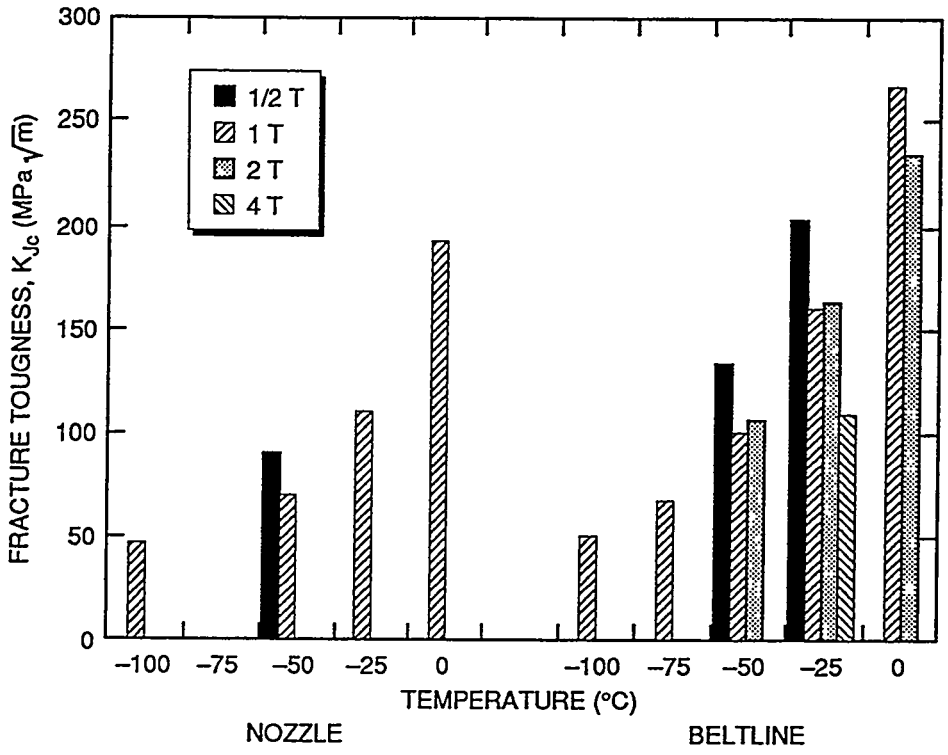

Figure 19 Mean values of unirradiated transition-temperature-range fracture toughness of Midland LUS beltline and nozzle course welds as function of test temperature and specimen size.

- Stress-based dual-parameter fracture toughness correlations cannot predict the observed effects of biaxial loading on shallow-flaw fracture toughness.
- An implicit strain-based dual-parameter fracture toughness correlation has been developed using K_{Jc} and ln(R) as the parameters.
- The K_{Jc}-ln(R) fracture toughness correlation performed acceptably when applied to the uniaxial and biaxial shallow-flaw fracture toughness data.
- Wide ranges in initial fracture properties are observed in some vessel materials, and the current method using CVN-based indices may not be adequately conservative to account for irradiation-induced shifts in fracture toughness.
- Wide ranges of initial chemistry and fracture properties are found in nominally uniform material within a pressure vessel.

References

1. U. S. Nuclear Regulatory Commission, Regulatory Guide 1.99, "Radiation Embrittlement of Reactor Vessel Materials, Enclosure 3, Regulatory Analysis," Rev. 2, November 1987.
2. T. H. Theiss and D. K. M. Shum, Martin Marietta Energy Systems, Inc., Oak Ridge National Laboratory, "Experimental and Analytical Investigation of the Shallow-Flaw Effect in Reactor Pressure Vessels," USNRC Report NUREG/CR-5886 (ORNL/TM-12115), July 1992.
3. J. A. Keeney, B. R. Bass, W. J. McAfee, and S. K. Iskander, Martin Marietta Energy Systems, Inc., Oak Ridge National Laboratory, "Preliminary Assessment of the Fracture Behavior of Weld Material in Full-Thickness Clad Beams," USNRC Report NUREG/CR-6228 (ORNL/TM-12735) (in process).
4. R. E. Link and J. A. Joyce, "Experimental Investigation of Fracture Toughness Scaling Models," *Constraint Effects in Fracture: Theory and Applications*, ASTM STP 1244, M. Kirk and A. Bakker, Eds., 1994.
5. *American Society of Mechanical Engineers Boiler and Pressure Vessel Code*, Sect. III, Div. 1, Paragraph NB-2331, July 1992.
6. T. J. Theiss et al., Martin Marietta Energy Systems, Inc., Oak Ridge National Laboratory, "Initial Results of the Influence of Biaxial Loading on Fracture Toughness," USNRC Report NUREG/CR-6036 (ORNL/TM-12349), June 1993.

7. B. R. Bass, J. W. Bryson, T. J. Theiss, and M. C. Rao, Martin Marietta Energy Systems, Inc., Oak Ridge National Laboratory, "Biaxial Loading and Shallow Flaw Effects on Crack-Tip Constraint and Fracture Toughness," NUREG/CR-6132 (ORNL/TM-12498), January 1994.

8. R. H. Dodds Jr., T. L. Anderson, and M. T. Kirk, "A Framework to Correlate a/W Ratio Effects on Elastic-Plastic Fracture Toughness (Jc)," *International Journal of Fracture,* 48, 1–22 (1991).

9. N. P. O'Dowd and C. F. Shih, "Family of Crack-Tip Fields Characterized by a Triaxiality Parameter: Part 1 – Structure of Fields," *J. Mech. Phys. Solids,* 39, 989–1015 (1991).

10. N. P. O'Dowd and C. F. Shih, "Two Parameter Fracture Mechanics: Theory and Applications," USNRC Report NUREG/CR-5958 (CDNSWC/SME-CR-16-92), Brown University, February 1993.

11. J. W. Hutchinson, "Singular Behavior at the End of a Tensile Crack in a Hardening Material," *J. Mech. Phys. Solids,* 16, 13–31 (1968).

12. J. R. Rice and G. F. Rosengren, "Plane Strain Deformation Near a Crack-Tip in a Power-Law Hardening Material," *J. Mech. Phys. Solids,* 16, 1–12 (1968).

13. R. O. Richie, J. F. Knott, and J. R. Rice, "On the Relationship Between Critical Tensile Stress and Fracture Toughness in Mild Steel," *J. Mech. Phys. Solids,* 21, 394-410 (1973).

14. D. Aurich, "The Influence of the Stress State on the Plastic Zone Size," *Eng. Frac. Mech.* 7, 761–765 (1975).

15. W. E. Pennell, "Heavy-Section Steel Technology Program: Recent Developments in Crack Initiation and Arrest Research," *Nucl. Eng. Des.* 255–266 (1993).

16. D. P. Clausing, "Effect of Plastic-Strain State on Ductility and Toughness," *International Journal of Fracture Mechanics* 6 (1), 71 (March 1970).

17. J. M. Barsom, "Relationship Between Plane-Strain Ductility and K_{Ic} for Various Steels," *Journal of Engineering for Industry* (November 1971).

18. J. G. Merkle, Union Carbide Corp. Nucl. Div., Oak Ridge National Laboratory, "An Elastic-Plastic Thick-Walled Hollow Cylinder Analogy for Analyzing the Strains in the Plastic Zone Just Ahead of a Notch Tip," ORNL-TM-4071, January 1973.

19. V. Weiss, "Material Ductility and Fracture Toughness of Metals," *Proceedings of the International Conference on Mechanical Behavior of Materials, Kyoto, Japan, August 15–20, 1971,* The Society of Materials Science, Japan, 1972.

20. G. P. Gibson, M. Capel, and S. G. Druce, "Effect of Heat Treatment on the Fracture Toughness Transition Properties of an A508 Class 3 Steel, Defect Assessment in Components—Fundamentals and Applications," ESIS/EGF9 (J. G. Blauel and K. H. Schwalbe, Eds.), Mechanical Engineering Publications, London, 1991, pp. 587–611.

21. A. S. Tetleman and A. J. McEvily Jr., *Fracture of Structural Materials,* John Wiley & Sons, Inc., New York, 1967.

22. J. M. Steichen and J. A. Williams, Hanford Engineering Development Laboratory, "High Strain Rate Tensile Properties of Irradiated ASTM A533 Grade B, Class 1, Pressure Vessel Steel," HEDL-TME 73–74, UC-78, July 1973.

23. R. K. Nanstad et al., Martin Marietta Energy Systems, Inc., Oak Ridge National Laboratory, "Irradiation Effects on Fracture Toughness of Two High-Copper Submerged-Arc Welds, HSSI Series 5," USNRC Report NUREG/CR-5913 Vol. 1 (ORNL/TM-12156/V1), October 1992.

24. K. Wallin, "The Scatter in K_{Ic} Results," *Eng. Frac. Mech.* 19(6), 1085–1093 (1984).

25. S. K. Iskander, W. R. Corwin, and R. K. Nanstad, Martin Marietta Energy Systems, Inc., Oak Ridge National Laboratory, "Results of Crack-Arrest Tests on Two Irradiated High-Copper Welds," USNRC Report NUREG/CR-5584 (ORNL/TM-11575), December 1990.

26. R. K. Nanstad et al., Martin Marietta Energy Systems, Inc., Oak Ridge National Laboratory, "Chemical Composition and RTNDT Determinations for Midland Weld WF-70," USNRC Report NUREG/CR-5914 (ORNL-6740), December 1992.

Development and Field Validation of Advanced Array Probes for Steam Generator Inspection

C. V. Dodd and J. R. Pate
Oak Ridge National Laboratory*
Oak Ridge, TN 37831-6158

Summary

The aging of the steam generators at the nation's nuclear power plants has led to the appearance of new forms of degradation in steam generator tubes and an increase in the frequency of forced outages due to major tube leak events. The eddy-current techniques currently being used for the inspection of steam generator tubing are no longer adequate to ensure that flaws will be detected before they lead to a shutdown of the plant. To meet the need for a fast and reliable method of inspection, ORNL has designed a 16-coil eddy-current array probe which combines an inspection speed similar to that of the bobbin coil with a sensitivity to cracks of any orientation similar to the rotating pancake coil. In addition, neural network and least squares methods have been developed for the automatic analysis of the data acquired with the new probes. The probes and analysis software have been tested at two working steam generators where we have found an increase in the signal-to-noise ratio of a factor of five and an increase in the inspection speed of a factor of 75 over the rotating pancake coil which maintaining similar detection and characterization capabilities.

Introduction

As the nation's steam generators have aged, new mechanisms for the degradation of steam generator tubes have appeared, and the frequency of forced outages due to major tube leak events has increased. To ensure that tube degradation is detected before it leads to a forced outage, it will be necessary to inspect during each outage a large number of the tubes in each steam generator using a technique which is sensitive to all forms of degradation. The primary method for the inspection of steam generator tubing is eddy-current testing, and while eddy-current testing can be used to perform a fast and reliable inspection, the eddy-current techniques currently being used for steam generator inspection are no longer adequate for the needs of the nuclear power industry.

The bobbin probe has traditionally been the primary method for the inspection of steam generator tubing. The probe consists of a pair of circumferentially-wound coils which are pulled through the tube at speeds of up to 40 inches per second, acquiring data as they travel. The probe's high speed and complete coverage of the tube circumference have made it a favorite of utilities with a tight outage schedule. However, since the probe induces eddy-currents in the tube wall with components only in the circumferential direction, the bobbin probe is not sensitive to circumferential cracks because these will not interrupt the flow of the induced currents. Furthermore, since the probe looks at the entire tube circumference at one

*Research sponsored by Office of Nuclear Regulatory Research, U. S. Nuclear Regulatory Commission under Interagency Agreements 1886-8011-9B and 1886-8109-8L with the U. S. Department of Energy under contract DE-AC05-84OR21400 with Martin Marietta Energy Systems, Inc.

time, the ability to use bobbin probe data to distinguish between cracks and volumetric flaws is limited.

To overcome the sensitivity limitations of the bobbin probe, the rotating pancake probe (RPC) was introduced. The RPC consists of one or more small coils pressed against the inner surface of the tube wall. In order to inspect the entire circumference of the tube, it is necessary to rotate the coil as it is pulled through the tube. Unfortunately, this means that the RPC is quite slow, with an inspection speed of only 0.2 in per second. This is clearly too slow to inspect the large numbers of tubes that should be inspected, and utilities avoid this type of inspection when at all possible. The result has been forced outages for tube leaks. Plants such as Palo Verde 2, have had outages lasting several months while long sections of tubes were inspected using the RPC.

Clearly a new probe design which combines the speed of the bobbin probe with the sensitivity of the RPC is needed to ensure the detection of all types of defects and to improve the ability to characterize defects. Toward this end, ORNL has developed a 16-coil eddy-current array probe. This probe consists of 16 small coils pressed against the inner surface of the tube and distributed about its circumference. The data obtained with this probe are similar in nature to those from the RPC, allowing detection of cracks of any orientation, but since it is not necessary to rotate the probe to achieve full coverage of the tube circumference, inspection speeds approaching those of the bobbin coil are possible.

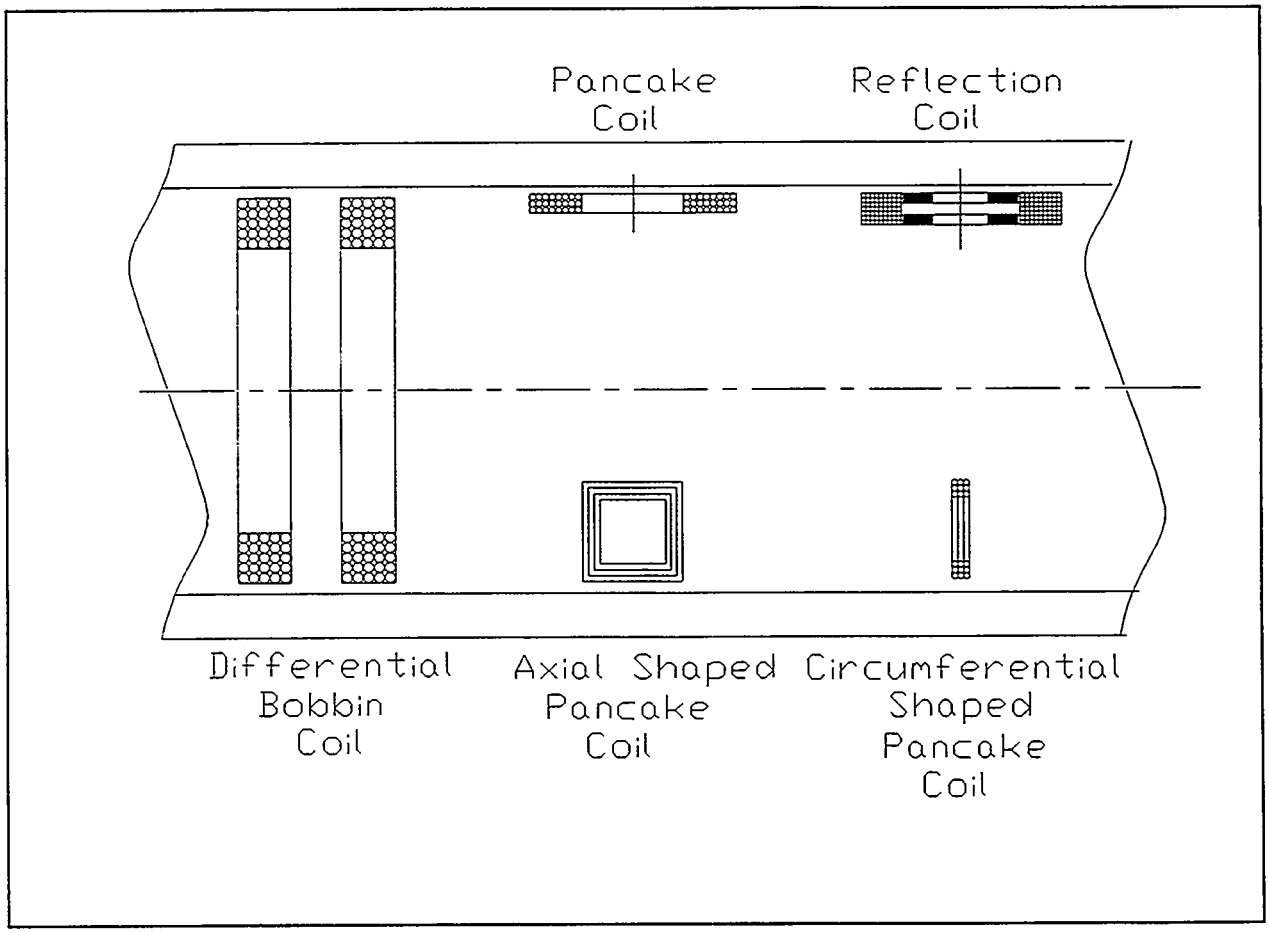

Figure 1 Types of eddy-current coils used for steam generator tube inspection

Array Probe Design

The eddy-current array probes developed by ORNL consist of 16 small coils pressed against the inner surface of the tube as shown in Figure 2. The coils are divided into two

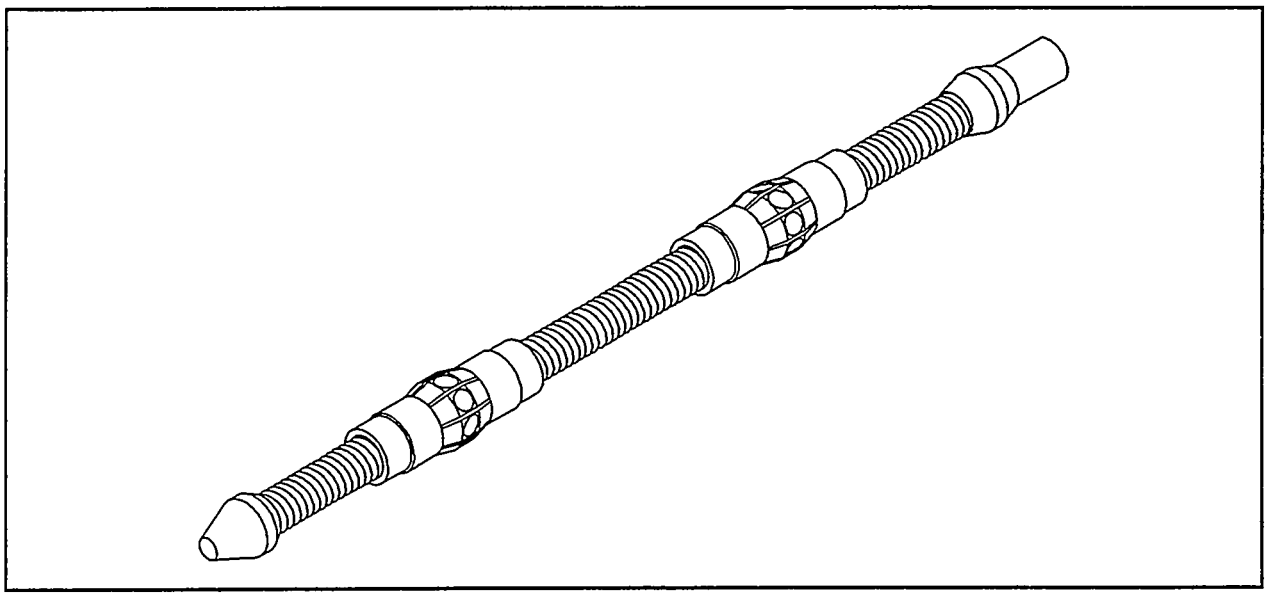

Figure 2 The 16-coil array probe

groups of eight coils each with the two groups being separated by a distance of approximately 4.5 inches in the axial direction. Each coil is mounted in an individual spring-loaded shoe to keep the coil pressed against the inner surface of the tube, which has a diameter of 0.775 inches, but if necessary the shoe will retract, allowing the probe to pass through a tube of diameter 0.720 inches. This makes it possible to inspect tubes with a significant amount of denting.

Figure 3 shows a cross section of one of the groups of eight coils. Neighboring coils in the same group are separated by 45 degrees in the circumferential direction. The coils in one group are centered in the regions between the coils in the other, resulting in there being 22.5 degrees between adjacent coils.

While the array probe has been designed for and tested in only straight sections of tubes with an outer diameter of 7/8 inches, Zetec, the company which

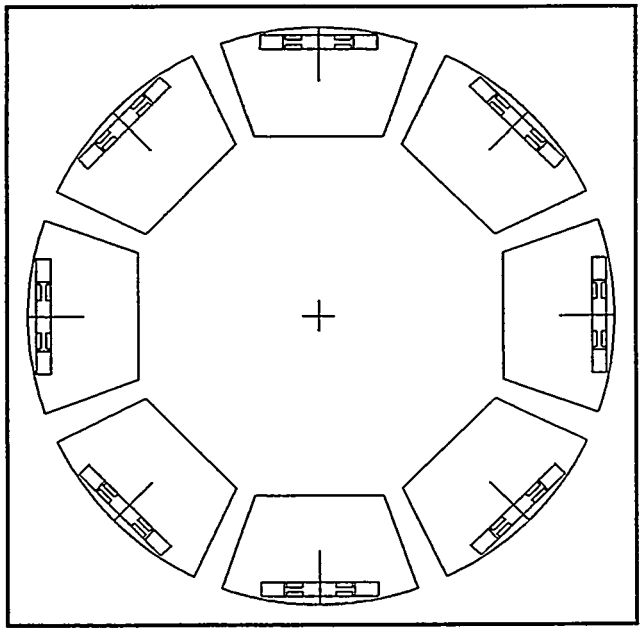

Figure 3 A cross section of the array probe

manufactured the probe, feels that the probe can be constructed to inspect the U-bends of the tubes and that it can be scaled to inspect tubes with an outer diameter of 3/4 inches.

Individual Coil Design

The individual coils which make up the 16-coil array probe were designed to maximize sensitivity to small defects on the outer diameter of the tube. Two array probes with different types of coils were designed and constructed; one probe contained the commonly used pancake coil, and the other contained reflection coils. Figure 4 shows a pancake coil and its electrical circuit. The pancake coil is used as the test coil in a typical bridge circuit, and a second identical coil placed is in a reference tube. The voltage measured is the difference between the test and reference signals, and since the probes will be nearly balanced, the signal can be amplified, increasing the sensitivity to small changes in the part being tested.

In Figure 5 we show a reflection coil and its electrical connections. The reflection coil consists of a driver coil which is used to induce eddy currents in the part being tested, and two smaller pickup coils in which a voltage is induced by the eddy currents in the part. The reflection coil can be designed in such a way to offer better discrimination to lift-off, the distance between the coil and the test part, than can be obtained with the pancake coil, and it therefore has a significant advantage over the pancake coil for steam generator inspection. The reflection coil circuit is similar to an induction bridge which is widely used for many types of highly accurate measurements.

Design studies were done for both of the types of coils in order to maximize their sensitivity to small defects on the far side of the tube wall and to minimize the effects of other variables. For the purpose of the design study, we considered the tube wall to be a flat plate. The

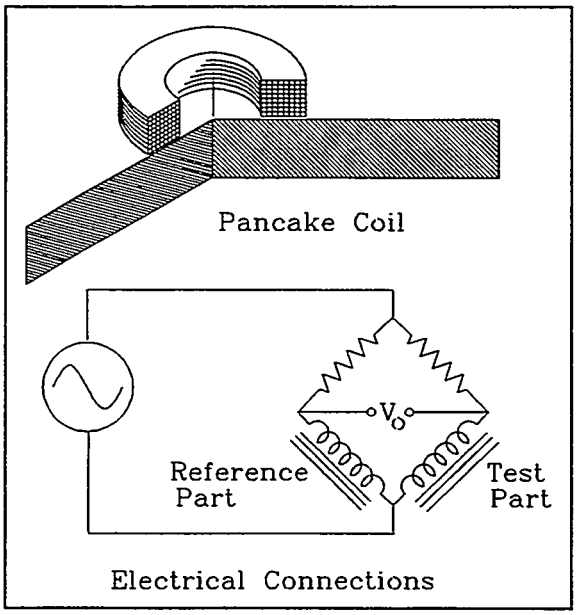

Figure 4 Pancake coil and electrical connections

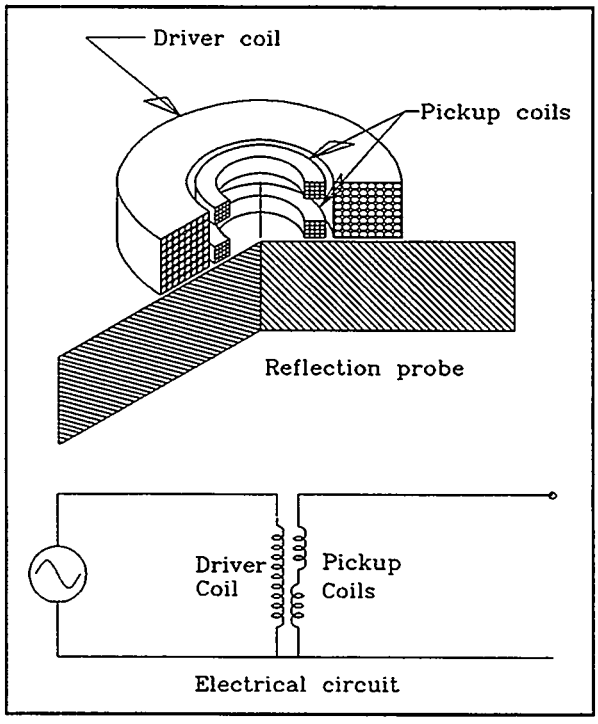

Figure 5 Reflection coil above a flat plate

first consideration was to make the coils as flat as was practical. Figure 6 illustrates how the normalized coil impedance depends on the shape of the coil cross section. From the figure it is evident that for a given value of the quantity $\omega\mu\sigma r^2$, the product of the inspection frequency, tube conductivity, tube permeability, and coil mean radius squared, increasing coil flatness increases the coil impedance change from its air value. Therefore, the coil is more sensitive to the properties of the part being tested when its turns are as close to the part as possible. There is a limit on the coil flatness, however, since if the coil is made too thin, its dc resistance becomes too high. In addition, the small defects that we wish to measure are usually on the far side of the conductor, so that the absolute flatness is not critical. It is recognized that as coils become flatter, the sensitivity to lift-off, conductivity variations, and other conductor property variations will also increase, but other methods will be used to reduce these effects.

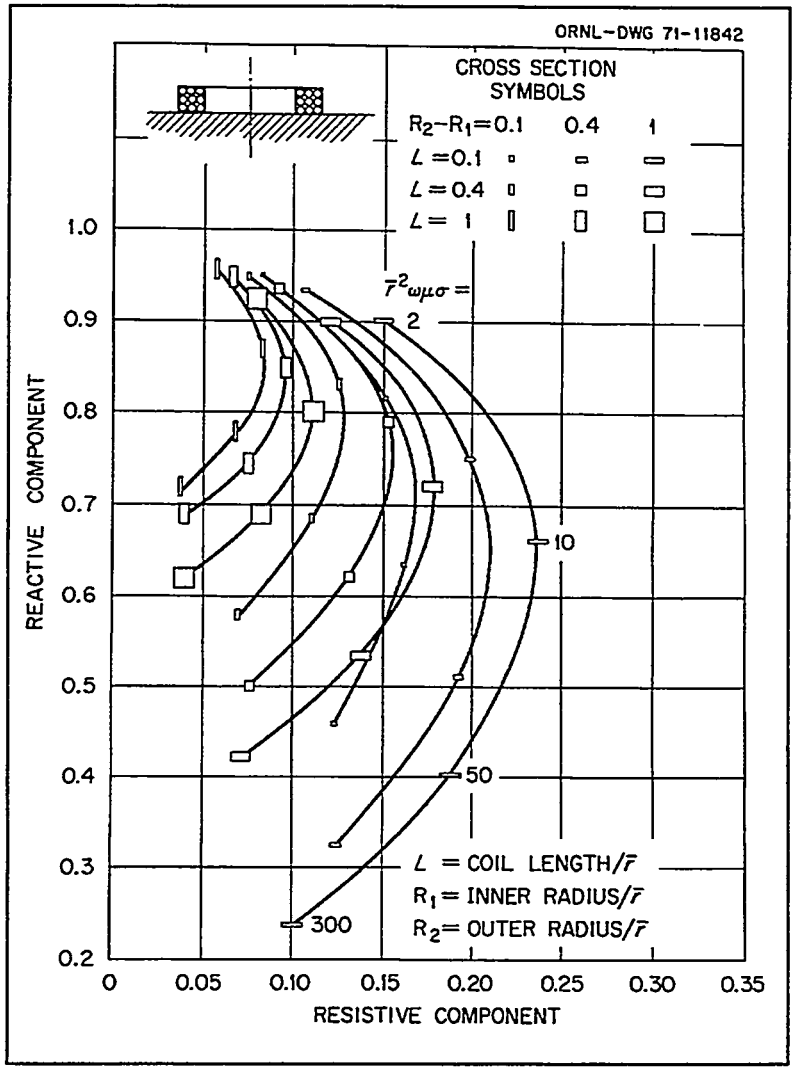

Figure 6 Variation in normalized coil impedance for different values of coil cross-section

A number of different pancake and reflection coil designs were tested using both analytical calculations and experimental measurements. The model used for most of the calculations was a point defect or a very small spherical defect. The reasoning was that if we could optimize for the smallest defects, detection of the larger ones would also be accomplished. Also, the mathematical model used for most of the calculations is only valid for small defects.

In Figure 7 we show the calculations of the impedance change for the P90 pancake coil due to a point defect on the far side of a conducting plate as a function of the defect radial location for several different test frequencies. Notice that there is an optimum frequency for maximum sensitivity and an optimum radius. This gives an indication of the field spread of the coil.

We show in Figure 8 a plot of the defect signal for different size coils as a function of the distance from the center of the coil. The outer diameter of the coils was fixed at 0.240 inches by the size of the shoe in which the coil was mounted, and the inner radius was varied from 0.0 to 0.16 inches, causing the mean radius of the coil to vary from 0.06 to 0.1 inches. Both the maximum sensitivity and the radial distance at which the maximum sensitivity occurs vary with coil size. The maximum sensitivity occurs for the P75 at a radius of 0.080 inches, and for the P90 it occurs at 0.0875 inches. While the maximum sensitivity of the P90 is slightly less than that of the P75, the greater field spread of the P90 means that it is to be preferred for use in the array coil. Both the P75 and P90 coils were built and tested, and the results were similar to those expected.

A comparison study was performed between the reflection and pancake coils to measure the defect depth in the presence of other property variations. The signals from the pancake and reflection coils were computed using the programs IMPTST and MULRFD, respectively. Property variations (in the file NRCPRO.DAT) include a lift-off variation of 0.010 inches, tube wall thickness values of 0.050 inches, 0.040 inches, and 0.030 inches, and defect depth values of 0.000 inches, 0.005 inches, 0.010 inches, and 0.015 inches, with copper deposits, tube supports, and magnetite deposits on the outside of the tube at various locations. The copper was placed at 15 locations, the tube support at 12 locations, and the magnetite at 12 locations, for a total of 39 OD artifact property values. For each of these artifact property values there are four defect depth values and five lift-off values, for a total of 780 property combinations. The frequencies were varied from 10 kHz to 1 MHz in a 1,2,5 sequence. The property variations for each of the three

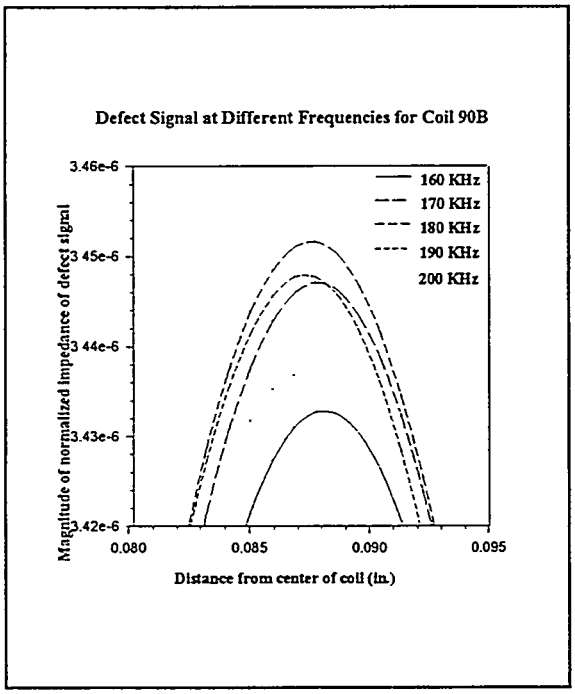

Figure 7 Defect signal for a far-side defect

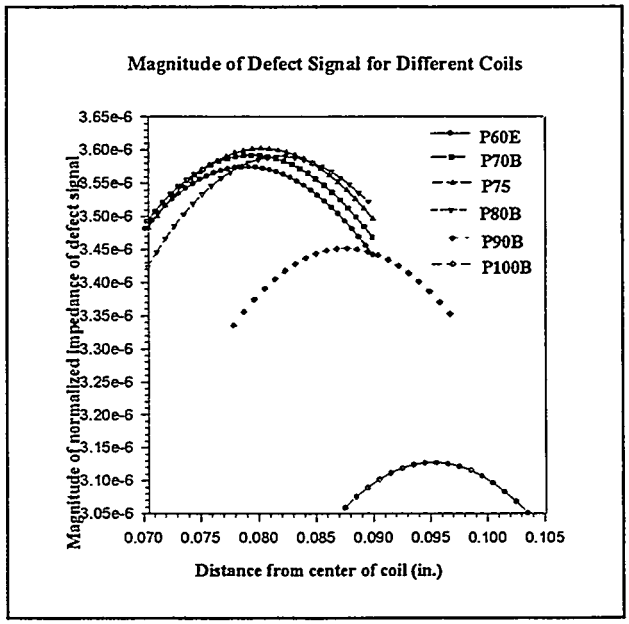

Figure 8 Magnitude of defect signals for coils of different sizes

types of OD artifacts are summarized below.

Region	Material	Thickness
1	Copper	Infinite
2	Air	0.5, 0.005, 0.003, 0.001
3	Inconel	0.050, 0.040, 0.030
4	Coil	

Region	Material	Thickness
1	Tube Support	Infinite
2	Air	0.005, 0.003, 0.0001
3	Inconel	0.050, 0.040, 0.030
4	Coil	

Region	Material	Thickness
1	Magnetite	Infinite
2	Air	0.005, 0.003, 0.0001
3	Inconel	0.050, 0.040, 0.030
4	Coil	

The best combination of three frequencies was chosen from the six frequencies used by running the program FINDFIT on the data for both coil types. Although this is only an approximation of the complexity of an actual problem, it does give an indication of how the multiple property fits can work without requiring an excessive amount of computer time. FINDFIT computes the best least squares fit of the property variations to the computed readings.

In Figure 9 we show the results of the error in the measurement of defect depth for both the pancake and reflection coils. The defect depth measurement error is the RMS of the fit error and the drift error, and it is measured in percent of wall thickness. For both types of coils, the fit error dominates. The neural net analysis techniques would probably give a better fit with no significant increase in the drift. From this comparison, the reflection coil seems to offer a significant advantage over the pancake coil.

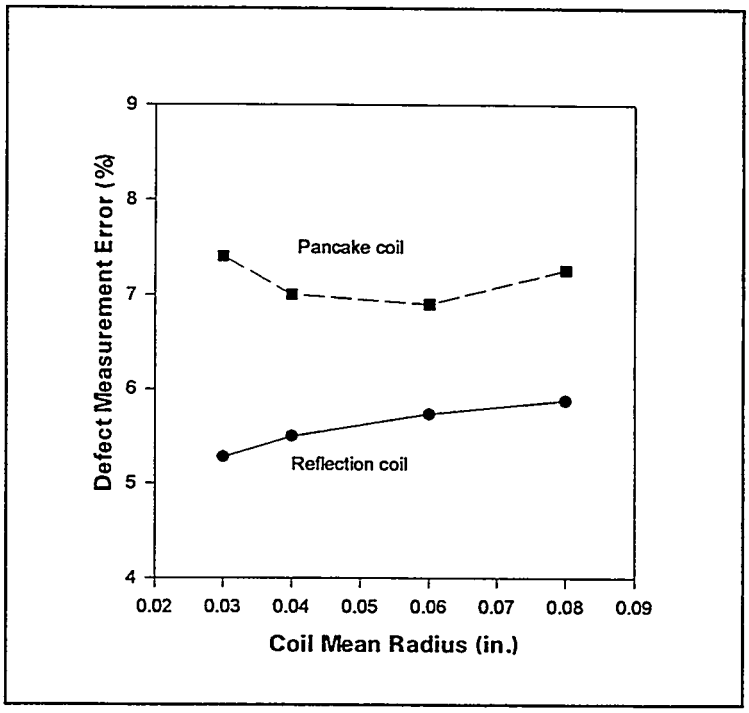

Another important factor is the ability of the coils to cover the entire circumference of the tube. To measure this ability the probes were used to scan an axial EDM notch of depth 40% of wall thickness and length 0.25 inches. The scan was conducted once with the center of the coil passing directly over the notch, and then it was repeated with an angle of 12 degrees between the center of the coil and the notch. The ratio of the response to the defect when the probe is at 12 degrees to the response when the probe is at 0 degrees is plotted in Figure 10. The figure shows that the sensitivity of the P90 is much more uniform than that of the P75 or the P60, and that the pancake coils have greater field uniformity than the reflection coils.

The zero lift-off, or the distance between the coil and the inner surface of tube, will also have an effect on the sensitivity to small defects on the far side of the tube wall. Both the sensitivity to and the resolution for small defects increases as the zero lift-off decreases. It is therefore best to get the coil as close to the tube wall as is practical. If the coil is flat, the curvature of the tube increases the distance between the coil and the tube wall. One method of reducing this distance

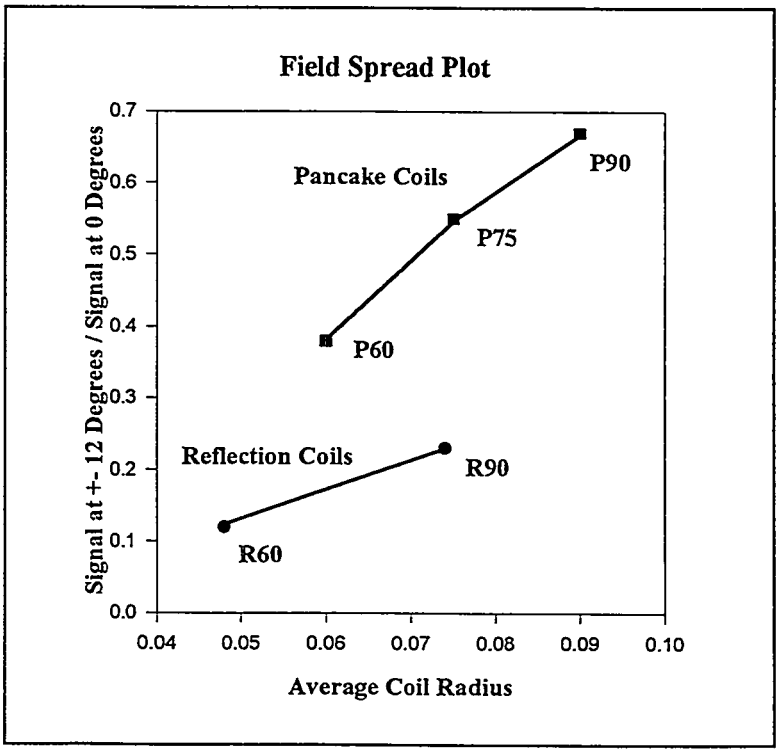

Figure 10 Field uniformity comparison

is to contour the coil to conform to the curvature of the tube, as shown in Figure 11. Coils of two different shapes were used, one with the coil cylindrically shaped to fit the tube wall, and another with the coil spherically shaped.
The cylindrically shaped coil has smaller zero lift-off, but it appears to be very slightly more susceptible to lift-off effects than the spherically shaped coil. The spherically shaped coil was also easier to fabricate. An attempt was made to build a cylindrically shaped reflection probe, but it was not successful.

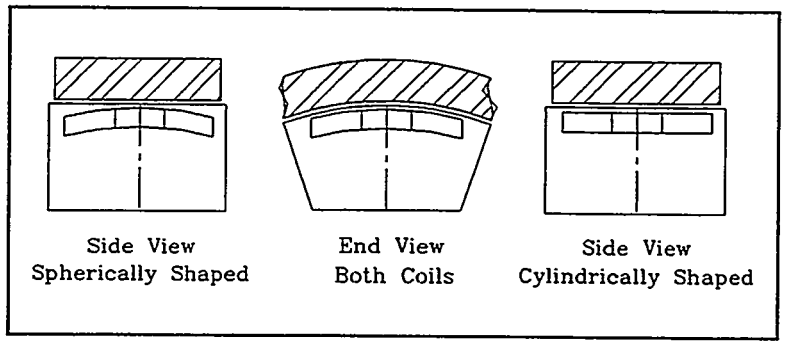

Figure 11 Shaped coils

As a final consideration the number of turns in the coil was determined. The number of turns is a compromise between the ratio of the dc coil impedance changes to the ac impedance changes and the effects of probe wire capacitance. It is desirable (but not always possible) to have a low cable capacitance between the instrument and the probe so that the probe operates well below its resonant frequency because near the coil resonance a 5 pF change in capacitance will lead to a signal change as large as that produced by a through-wall hole. For a 16-coil pancake array probe, 16 coaxial connections are needed, and for a 16-coil reflection array probe, 32 coaxial connections are needed. The initial reflection array probes were built using cable of capacitance 26 pF per foot. Since that time, cable with a capacitance of 20 pF per foot has been found for the reflection array, and cable with a capacitance of 17 pF per foot has been found for the pancake array probe. The inductance of the coils is about 50 to 90 microhenries so that with 110 feet of low-loss cable, the resonant frequency can be as high as 650 kHz, which is slightly above the highest test frequency we have used in the field validation of the probes. The number of layers in the coil, the number of turns per layer, and the wire gage are computed by the program AIRCO.

Instrumentation

The MIZ-30 eddy-current instrument was designed and constructed by Zetec specifically for array probe inspections. It is a high-speed multiple-frequency digital instrument that can drive 16 individual coils in either a bridge arrangement with a reference probe or in a transmit-receive mode for the reflection coils. It is capable of taking 500 readings per second for all 16 coils at four frequencies. The gain and hardware null are also software adjustable. A Hewlett Packard workstation is used to control the instrument over a local area network. The configuration of the instrument is set by the acquisition operator. The configuration can be entered manually or a data file containing the setup information can be transmitted over the LAN from any other workstation on the network and stored in the appropriate file. The configuration file can contain the setup information for up to 16 different types of inspections. The probe is positioned on the face of the tubesheet (a Zetec SM-22 was used for the Prairie Island tests), and the probe pushed into the tube and then the probe pulled as the data are acquired and recorded. Up to 16 channels can be displayed so that the acquisition operator can verify that all the channels of the probe are working and can tell where the probe is in the tube. However, with the amount of data to be processed

when all 16 channels were displayed, the computer lagged too far behind the actual probe motion so that it was much better to display only one channel most of the time. The acquisition computer also controlled the probe positioning and insertion, which lagged too far behind when the 16 channels were displayed. This problem is considerable when using a 700 series workstation.

Prairie Island test results for array probes - first test

The array probes were first tested at the Prairie Island Unit 2 steam generators on November 14, 1993. The system was assembled and tested on the Prairie Island mock-up the week before it was tested in the generators. The acquisition operators were not familiar with the MIZ-30, and some instructions were necessary before the acquisition programs could be successfully run. The probe pusher-pullers were designed to drive 3/8 inch diameter polyurethane cable into the tubing, and since the array probes use 1/2 inch diameter cable, a modification had to be made to the pusher-puller before it would drive the array probe cable. A special part had to be machined and another part had to be removed. One of the twister cables was discovered to be bad, and personnel from Conam, the company which performed the acquisition and primary analysis of the eddy-current data at Prairie Island, repaired it. Conam also suggested that we add enough extension cable (10 feet) to allow the MIZ-30 to be moved to an area with lower contamination, which we did.

The MIZ-30 and the cables were installed in the generator on Sunday morning, November 14. The pusher-puller in the steam generator had to be modified in the same manner as the one in the mock-up. Unfortunately, due to the contamination and other problems, it was much more difficult to modify, and the probe speed was limited to 15 inches per second by mechanical considerations.

A set of 48 tubes was selected for inspection based on the results of the regular eddy-current inspection which had been completed. The reflection array probe was tested first. The gain in the original design of the MIZ-30 was not as high as was needed to obtain the best results with this type of coil, and the signal-to-noise ratio for the reflection was thus about the same as that for the Zetec rotating pancake coil (RPC). The pancake array with spherically shaped P60 coils was then tested. The signal level for this probe was greater than that for the Zetec RPC by a factor of 5 to 10 for the same gain setting. The data from the various coils were reviewed by Gary Henry of EPRI, who determined that the signal-to-noise ratio of the pancake array probe was higher than that of the Zetec RPC by about a factor of 5.

In order to do improved signal analysis a circumferential groove standard had to be used to calibrate each coil in the probe. Figure 12 shows a drawing of the standard used. The grooves

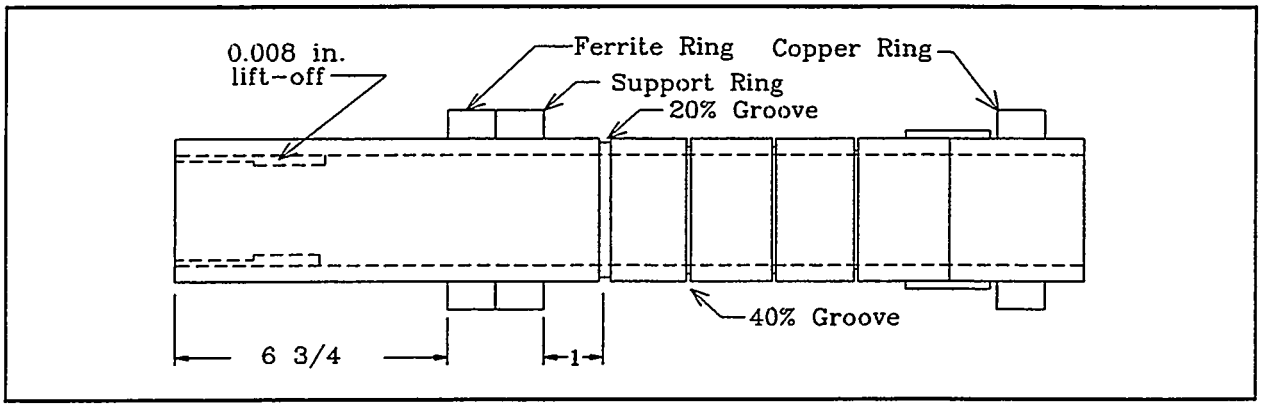

Figure 12 Circumferential groove standard

extend all the way around the circumference of the tube and have depths of 20%, 40%, 60%, 80% and 100% of wall thickness. In addition to the grooves the standard contained a ferrite ring (to simulate a magnetite deposit), a tube support ring, and a copper ring. Scanning the standard allowed us to perform mixes for the suppression of tube supports, magnetite, and copper. The data were analyzed at the site using the Zetec analysis software by analysts from Conam and Zetec. The data were also analyzed using the ORNL analysis software. Since the ORNL software was developed especially for array probe data, it is less cumbersome to use to perform mixes and other tasks. In general the array probes detected all indications that the bobbin coil detected. There were some calls made with the ORNL array probes that were not made with the bobbin coil, but these were all quite small and harmless. There were some indications at the tube supports, but none were judged to be serious. Figure 13 shows the bobbin coil scan of a section of tube R35C30 and Figure 14 shows a plot of the pancake array probe data from the same section of the tube. There appear to be three small defects just above the tubesheet.

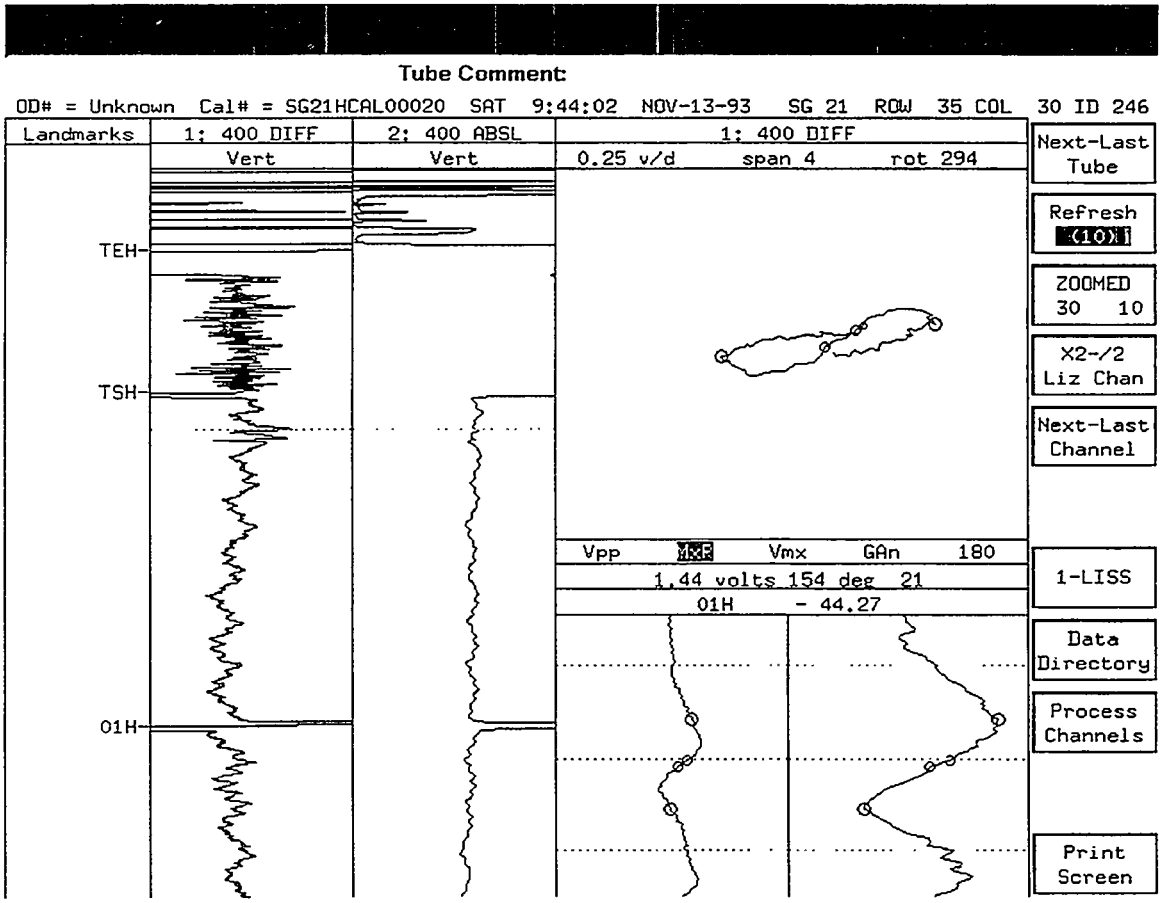

Figure 13 Bobbin probe scan of tube row 35 column 30 using Zetec Eddynet software

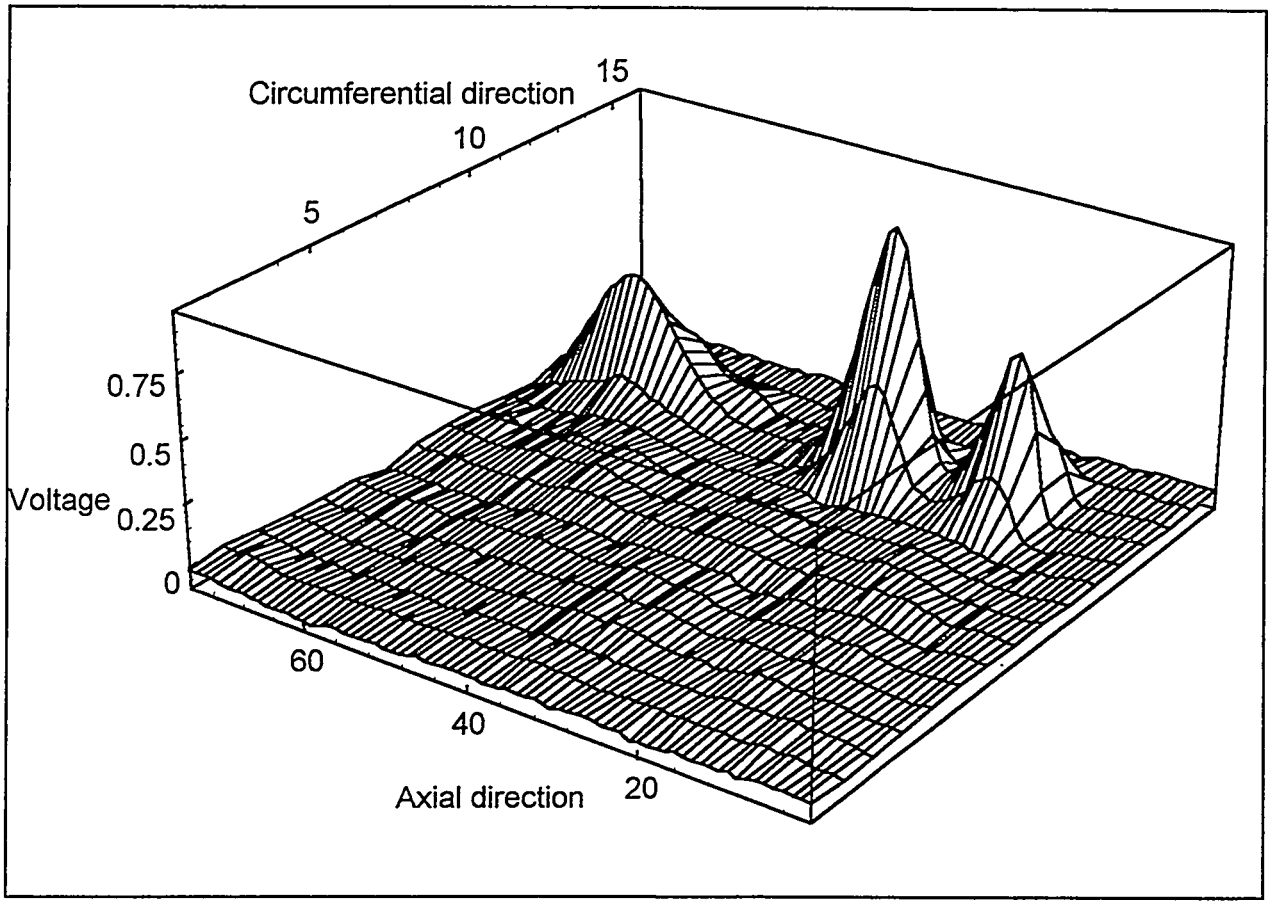

Figure 14 Pancake array scan of tube Row 35 Column 30 showing three indications

Speed trial studies

Near the end of the test, a special production test was run. In order to simulate the production inspection conditions, two adjacent tubes from the test group were selected. The probe was inserted in one tube after the other, alternating between the tubes. This simulated the conditions that would obtain if the tubes were being tested by going in a straight line down a row of tubes. A total of 17 inspections were performed at a rate of 68 seconds per tube or 53 tubes per hour for inspection of 30 feet of tubing. In these tests the insertion speed was limited to 15 inches per second due to mechanical problems. An insertion speed of 40 inches per second would improve the inspection rate by 20 percent to 68 tubes per hour. The array probes were tested at a pull speed of 15 inches per second, which is about 75 times faster then the pull speed (0.2 inches per second) of the RPC. At this pull speed there was more than adequate resolution.

Prairie Island test results for array probes - second test

The second test at Prairie Island was conducted on the steam generators of Unit 1 on Saturday, May 29, 1994. The plan was to perform an eddy-current test on selected tubes using the contaminated pancake and reflection array probes that had been stored at the plant since they were used in the inspection of Unit 2 in November 1993. Uncontaminated probes and cables were sent directly to Prairie Island from Zetec (where our MIZ-30 had been upgraded). Upon its arrival, the instrument was checked out with both types of array probes. The reflection probe exhibited a "touch effect", in which the signal changed if the connectors were touched. This had been noticed during development and checkout at Zetec, and it was found that if the connectors were wrapped in bubble padding, the effect disappeared.

One of the channels of the pancake array probe was not working. This probe had been tested at Zetec and all of the channels had been working properly then. The problem was traced to one of the extension cables (two are required for the pancake array probes) and this cable was repaired. A Conam technician examined the connectors and said that one of them was not wired well. He repaired the lead and broke two more in the process and then fixed those. The probes were then tested, and it was found that all channels were working. The data obtained on standard runs looked very good for both probes, and the signal-to-noise ratio appeared to be about the same for the reflection and pancake array probes.

There was a delay of several days due to problems in getting access to the generators, problems in setting up for the production eddy-current inspections, and problems in data acquisition over the network used for these tests. The problems were finally resolved, but only after a delay of several days. The ORNL inspection, which came at the end of the other eddy-current tests, was delayed from Monday until 3:00 a.m. Saturday.

During this time extensive testing and mixing with both types of array probes were performed. One important discovery was that a better mix was obtained if the ferrite ring was placed directly against the tube support ring, to simulate magnetite adjacent to the support. The mixes obtained using this showed very little residual and very little distortion of the 20% defect. Preliminary results using the Zetec mix showed that scans of the actual tube had very little residual, and that small defects at the tube supports could be easily detected. The ORNL analysis program would not run on the data due to an upgrade that Zetec had made in their software.

Fifty tubes were selected to be tested with both the reflection and pancake array probes.

Our acquisition window was only 12 hours, which included the time necessary to make modifications to the pusher-puller and the time required to run the cable. We used a ten foot twister cable and a 50 foot extension cable for both probes. The data were evaluated at Prairie Island by the Conam analysts. The data from Unit 1, which is older than Unit 2, showed many more magnetite deposits. The pancake array probe had one channel missing. It was not possible to tell if the missing channel was due to another broken connection in the extension cable or if the contaminated array probe used in the previous inspection had a broken coil. Due to the fact that we already had problems with the extension cable we decided not to contaminate our spare probe. Therefore, the test of the pancake array probe was run with only 15 of the 16 coils working. In spite of the high cost of extension cables, future inspections should be performed with at least one spare set of all cables and probes.

We did not experience as much difficulty in getting the pusher-puller to drive the cable as we had at the first inspection. In addition, the computer (a Hewlett Packard 700 series workstation) used was fast enough to take the data and send it to the analysis building in very near real time. While the program did abort twice at the start of the test, for the remainder of the test we had no problems. However, we experienced problems with the SM-22 positioner. It seemed to lose its location on the generator after about the first hour of testing. This required extensive time to locate plugs and other artifacts to verify the position of the tubes. It is possible that some of the tubes scanned were not the ones indicated, although the operators used every reasonable precaution.

Several valuable lessons were obtained from the tests at a small cost to our programs. The new MIZ-30 appears to give good, low-noise data. We were able to copy the setup file for the MIZ-30 acquisition which had been prepared earlier from an optical disk into the proper directory (named /miz30d) on the acquisition computer and rename it so that it was used for the acquisition. It would have been faster to do this over the LAN, but the operator who knew how to do it was not on duty at the time. Copying the setup file saved a great deal of time that would have been required to type in the proper settings and also reduced the chances of making an error. However, the setup for the individual coils in the array probe did not match since we used the old, contaminated probes that were used in the last outage rather than the similar but not identical ones that were used for testing before the inspection. The setup for the individual channels is obtained from the acquisition header, and if the correct individual values are used, that data analyst does not have to reset these. With 16 coils for each of the four frequencies, the setup time can be considerable using the Zetec software. Any mixes that are used require considerable time with the Zetec software. The scan of the tubing in the generator had a larger lift-off variation than we encountered in the scans of the standard, which made the data appear noisy at first. When the proper adjustments were made, the problem was corrected.

The ORNL analysis program was modified to match the new Zetec acquisition format and the data were analyzed at ORNL. In general, the array probes were able to detect all of the defects that the bobbin and RPC inspections showed. Figure 15 shows the vertical component of the reflection array probe data taken at 260 kHz at tube support 01H of tube R43C59 in steam generator 12. The dark horizontal band across the plot is the tube support, and the bright spot near the center of the graph appears to be a defect. Figure 16 shows the same data with the tube support suppression mix applied. Here we see that the dark band representing the tube support has been eliminated while the bright spot has been amplified, indicating that it is indeed a defect.

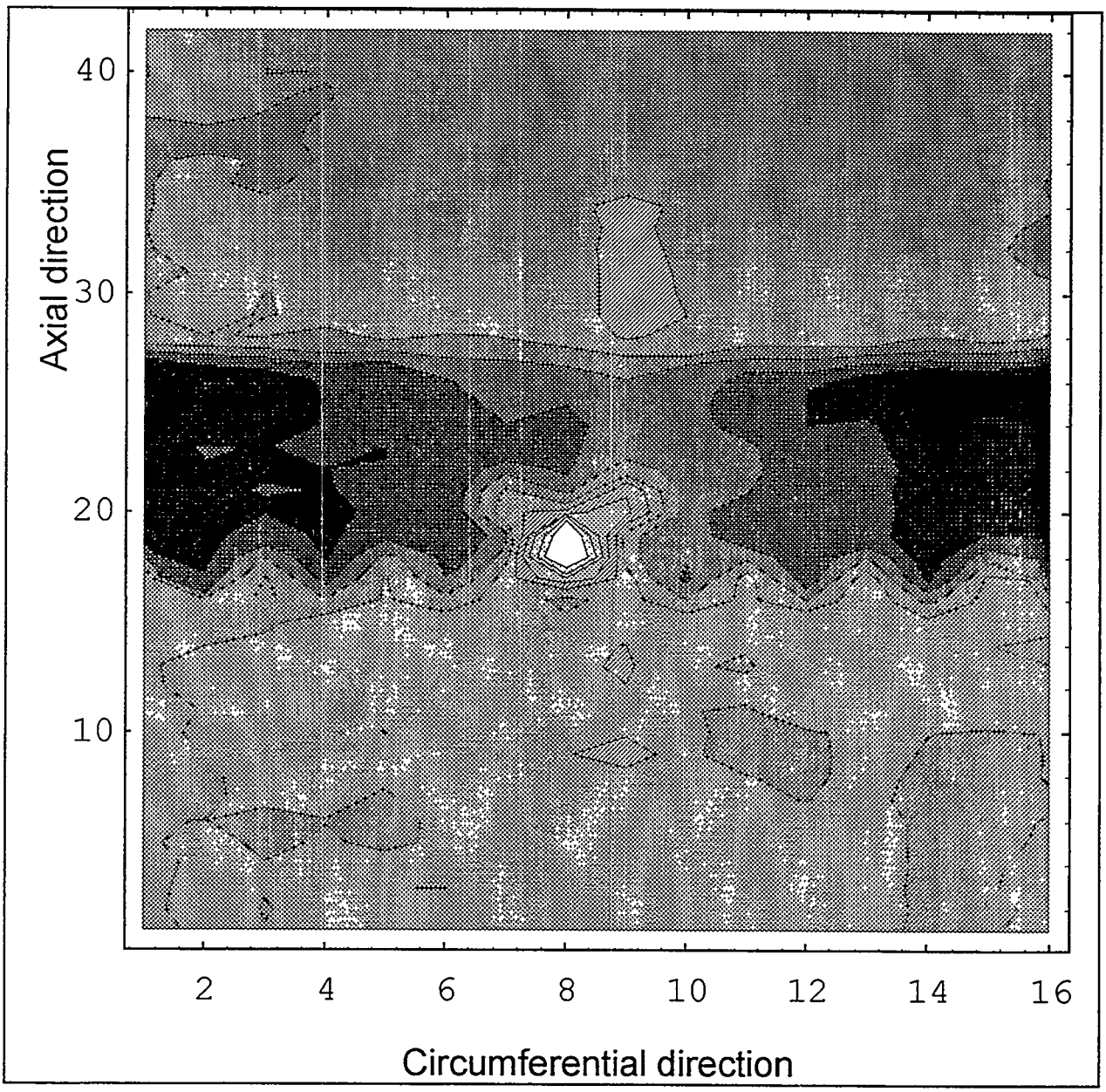

Figure 15 The vertical component of the 260 kHz data from the reflection array probe at tube support 01H in tube R43C59 in steam generator 12.

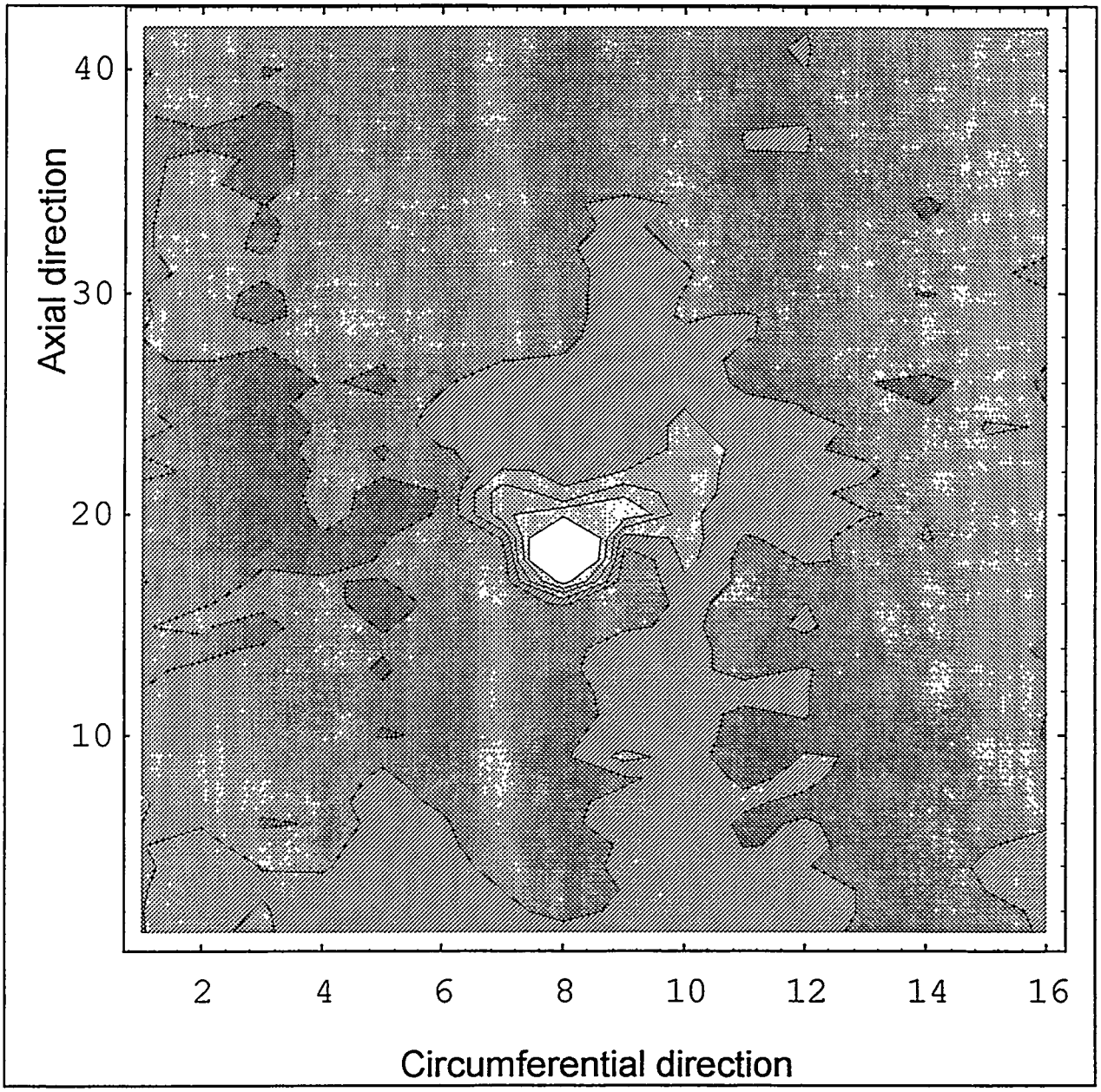

Figure 16 The vertical component of the 260 kHz reflection array probe data from tube support 01H in tube R43C59 of steam generator 12 with the tube support suppression mix applied.

LESSONS LEARNED FROM THE 1994 NORTHRIDGE EARTHQUAKE *

Mark W. Eli and Stanley C. Sommer
Lawrence Livermore National Laboratory
P.O. Box 808
7000 East Ave
Livermore, CA 94550

ABSTRACT

Southern California has a history of major earthquakes and also has one of the largest metropolitan areas in the United States. The 1994 Northridge Earthquake challenged the industrial facilities and lifeline infrastructure in the northern Los Angeles (LA) area. Lawrence Livermore National Laboratory (LLNL) sent a team of engineers to conduct an earthquake damage investigation in the Northridge area, on a project funded jointly by the United States Nuclear Regulatory Commission (USNRC) and the United States Department of Energy (USDOE). Many of the structures, systems, and components (SSCs) and lifelines that suffered damage are similar to those found in nuclear power plants and in USDOE facilities. Lessons learned from these experiences can have some applicability at commercial nuclear power plants.

INTRODUCTION

On January 17, 1994, at 4:31 AM (PST), an earthquake with moment magnitude (M_w) 6.7 struck the Northridge area of metropolitan Los Angeles, California. It was the largest earthquake to occur close to a heavily populated area in the United States since 1906. The 1994 Northridge Earthquake has caused roughly $15-30 billion in damage and has been estimated to have one of the highest amounts of insured losses due to a natural disaster in U.S. history. This high amount of losses is due to the considerable damage to the built environment such as industrial facilities, lifelines, commercial centers, and residential buildings. Damage included collapsed buildings, loss of electric power to large portions of the city of Los Angeles, closure of major freeways due to collapsed freeway bridges, and disrupted water and natural gas service. In addition, there was a substantial amount of nonstructural damage including closure of hospitals due to water damage and destroyed contents which overturned or fell from shelves or cabinets.

---

* This work was performed at Lawrence Livermore National Laboratory under the auspices of the United States Department of Energy, Contract No. W-7405-ENG-48.

Fortunately, the number of deaths and injuries during the earthquake were limited by its timing which was early in the morning and on a Federal holiday, the observance of Dr. Martin Luther King Jr.'s Birthday. Many nonresidential buildings were empty, and traffic on the Los Angeles freeways was relatively light. Over 55 deaths were attributed to the earthquake, and about 1500 people sustained major injuries during the event [ref 1]. In addition, about 16,000 people were treated and quickly released by hospitals while about 100,000 people were temporarily or permanently displaced from their dwellings.

The epicenter of the earthquake is located in the community of Northridge which is about 20 miles northwest of downtown Los Angeles as shown in Figure 1. Figure 1 also provides strong-motion acceleration values from selected California Strong-Motion Instrumentation Program (CSMIP) stations. Several recorded accelerations within 15 miles of the epicenter exceeded 1.0 g in the horizontal and vertical directions. Due to the large amount of strong-motion recordings and the vast diversity of engineered structures and systems which experienced the earthquake, it provides an unprecedented opportunity to learn about the effects of earthquakes.

Since the Northridge Earthquake occurred in a highly populated and industrialized area, numerous types of structures, systems, and components (SSCs) and lifelines experienced the event. Many of these SSCs and lifelines are similar to those found in nuclear power plants and in United States Department of Energy (DOE) facilities. To observe and document the effects of the earthquake on SSCs and lifelines, teams from Lawrence Livermore National Laboratory (LLNL) and from EQE Engineering Consultants traveled to the epicentral region immediately following the seismic event. On several other occasions, teams from LLNL and EQE were joined by members of the Nuclear Regulatory Commission (NRC), DOE, and the Electric Power Research Institute (EPRI) to conduct more detailed investigations of earthquake effects on SSCs and lifelines. The observations made during these investigations along with supplemental documentation are the bases of this paper.

This paper will provide a general overview of earthquake-caused damage to lifelines, bridges and highways, and commercial buildings. However, the emphasis of this paper will be on the performance of structures and equipment in industrial facilities similar to those found in nuclear power plants, in other electric power generation and transmission facilities, and at DOE facilities. While nuclear power plants, other electric power plants and substations, and DOE facilities may not have the identical SSCs as those discussed in this paper, the engineering trends discovered about the seismic performance of the SSCs can be directly applicable.

MITIGATING THE EFFECTS OF EARTHQUAKES

This paper provides a study of the effects of the Northridge Earthquake of January 1994 that interest the electric power industry, DOE, and NRC. The study is part of a series of post-earthquake investigations which have been conducted since the 1971 San Fernando Earthquake. The main purpose of this paper is to

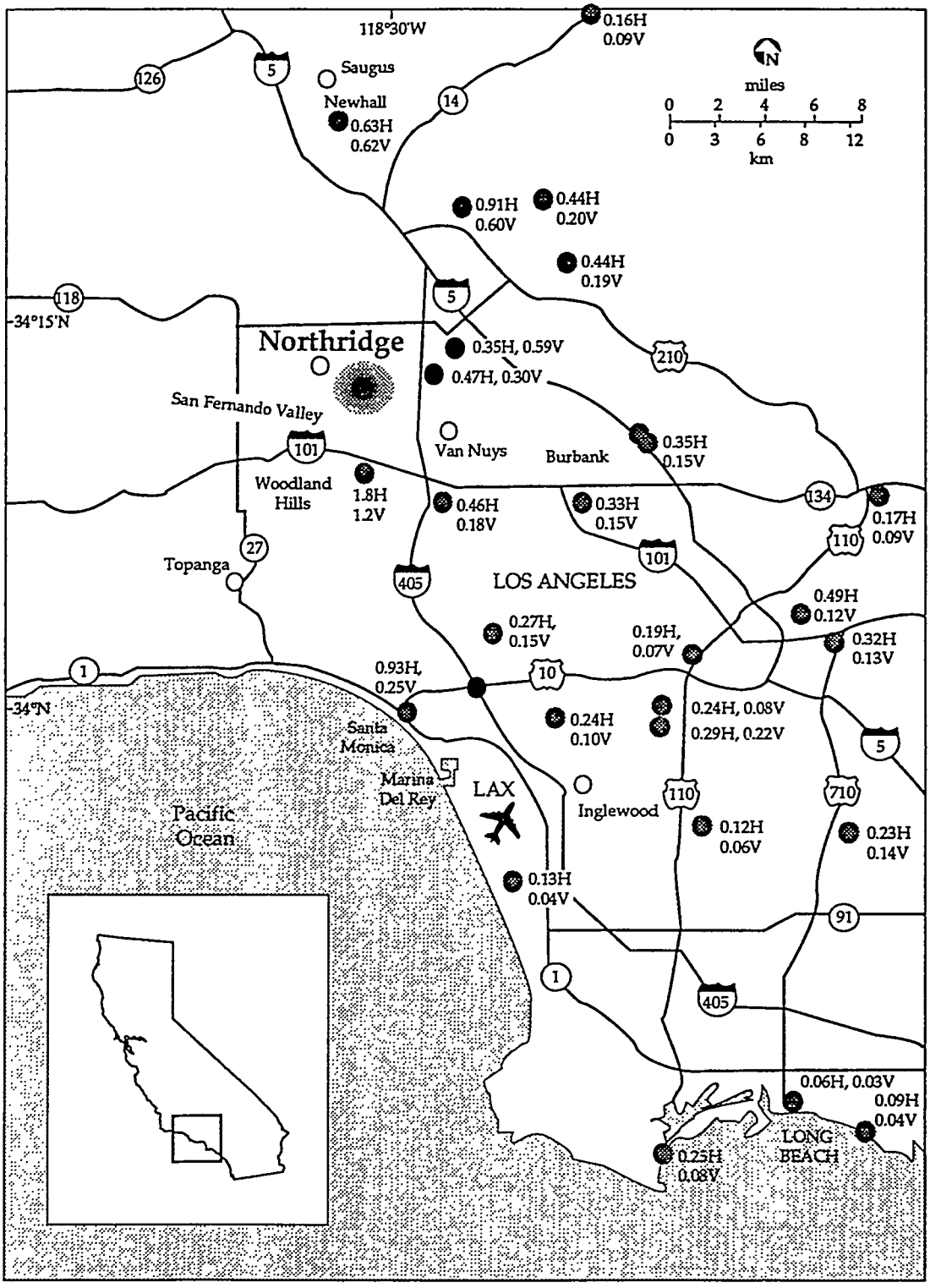

Figure 1. Based on the "Fifth Quick Report on CSMIP Strong-Motion Data from the Northridge/San Fernando Valley Earthquake of January 17, 1994," Report OSMS 94-05, California Strong Motion Instrumentation Program (CSMIP), January 25, 1994. Selected CSMIP stations that recorded the Northridge earthquake are shown as ● . The earthquake epicenter is denoted by ✹ , and peak horizontal and vertical acceleration values are shown.

disseminate information about the effects of the Northridge Earthquake on industrial facilities and lifelines in order to develop effective seismic mitigation methodologies. The study discussed in this paper focuses on electric power facilities, which were heavily shaken and damaged by the earthquake, and on industrial facilities and lifelines containing equipment and structures of relevance to DOE facilities and electric power systems. While most of the damage caused by the Northridge Earthquake is repairable, much of it could have been avoided with proper seismic design practices and implementation and with effective seismic planning. Many studies have shown that the costs of repairing or replacing earthquake-damaged SSCs exceed those associated with implementing appropriate seismic design and planning procedures before the earthquake.

As part of the Unresolved Safety Issue (USI) A-46 program (Verification of Seismic Adequacy of Equipment in Operating Plants), selected facilities provide earthquake experience data for the Seismic Qualification Utility Group (SQUG) 20 Classes of active electrical and mechanical equipment. Many of the selected facilities which experienced the 1971 San Fernando (Sylmar) Earthquake also were affected by the 1994 Northridge Earthquake. The data and observations from the Northridge Earthquake will provide valuable information to augment the SQUG database for potential resolution of A-46 issues. As new and replacement equipment (NARE) issues are explored, the 1994 Northridge Earthquake may help to yield useful data for future seismic evaluations.

Information gained from ongoing investigations of the 1994 Northridge Earthquake also has potential to benefit the development of criteria and procedures for seismic qualification of equipment that will be installed in Advanced Light Water Reactor (ALWR) plants. Performance of particular equipment classes and distribution systems in this earthquake can add to the database being assembled for the ALWR First-of-a-Kind Engineering (FOAKE) Project on Equipment Seismic Qualification.

TYPES OF DAMAGE CAUSED BY THE EARTHQUAKE

Two unique characteristics of the Northridge Earthquake are the vast number of strong-motion recordings and the significant amount of affected structures. The records indicate that the peak ground accelerations were much larger than the design values for many facilities. This effect had been previously noted in the literature, but now much more information is available. In addition, the vertical accelerations were equal to or greater than the horizontal accelerations in some cases *(see Figure 1)*. It is postulated that these high vertical accelerations may have contributed to some of the failures in the earthquake-affected region. Other seismological effects, also noticed in the 1992 Landers Earthquake, were directivity and fling.

The relatively large ground motions during the Northridge Earthquake caused several types of structural damage. In general, nonductile reinforced concrete frame structures did not perform well. A considerable amount of buildings with poor structural details such as soft first stories, inadequate connections in precast structures, tilt-up frames, or unreinforced masonry suffered significant damage including collapse. Surprisingly, there was also considerable damage to steel moment-frame buildings. Even though no steel moment-frame buildings

collapsed, observed connection failures were not expected by most of the structural engineering practitioners.

The types of damage to nonductile reinforced concrete frame structures are shown in Figures 2 to 5. An example of a concrete frame building which collapsed is the Kaiser Permanente Medical Office Building in Granada Hills. As shown in Figures 2 and 3, all of the columns failed just above the second floor. Located about 2 miles east of the epicenter, the Kaiser Permanente Building was a multistory frame with east-west reinforced brick shear walls on its north and south faces. Poor beam-to-column details and lack of north-south shear walls on the east and west faces contributed to the collapse. The massive east-west shear walls at each end of the building contributed little strength for resistance to the dominant north-south component of the lateral load on the structure. Another nonductile reinforced concrete frame which collapsed was the Bullock's Department Store at the Northridge Fashion Center. It appeared that the concrete waffle slab on the second floor was not securely tied to the columns which allowed the floor to collapse as shown in Figures 4 and 5.

There were many severely damaged apartment buildings, especially those with parking garages on the first floor. These buildings were constructed as dwellings-over-garages (DOGs). This building type does not usually perform well during earthquakes due to the inadequate horizontal shear capacity in the first floor. Minimal seismic design details and poor construction practices contributed to the collapse of the first story at the Northridge Meadows Apartments in Northridge as shown in Figure 6. Fifteen people were killed at this one apartment complex due to the earthquake.

The Northridge Earthquake caused seven parking garages to have partial or total collapse and caused damage to numerous other parking garages. Most of these parking garages are precast structures which can have poor construction details and inadequate lateral-load resisting systems. One example was the collapsed parking garage at the Northridge Fashion Center. Even though this parking garage was constructed in the early 1990s, it lacked adequate connection details to withstand the strong motion of the Northridge Earthquake. Another modern parking structure which collapsed during the earthquake is the parking structure at the California State University at Northridge (CSUN) shown in Figure 7. Both the structures at the Northridge Fashion Center and CSUN were located within 2 miles of the epicenter. The CSUN structure had been designed as an exterior ductile frame with a nonductile interior structure. The short, interior columns (between the ramps and adjacent floors) failed because they attracted high loads beyond their design capacities. Also, the short development length of rebar between each column and floor diaphragm did not resist the seismic motion.

As is common in other earthquakes, unreinforced masonry (URM) buildings did not perform well. Figure 8 shows damage to a URM building in Santa Monica, which experienced excessive diagonal cracking. Throughout the epicentral region, there were widespread occurrences of typical earthquake damage including broken glass, fallen chimneys, and fallen poorly reinforced block walls as shown in Figure 9.

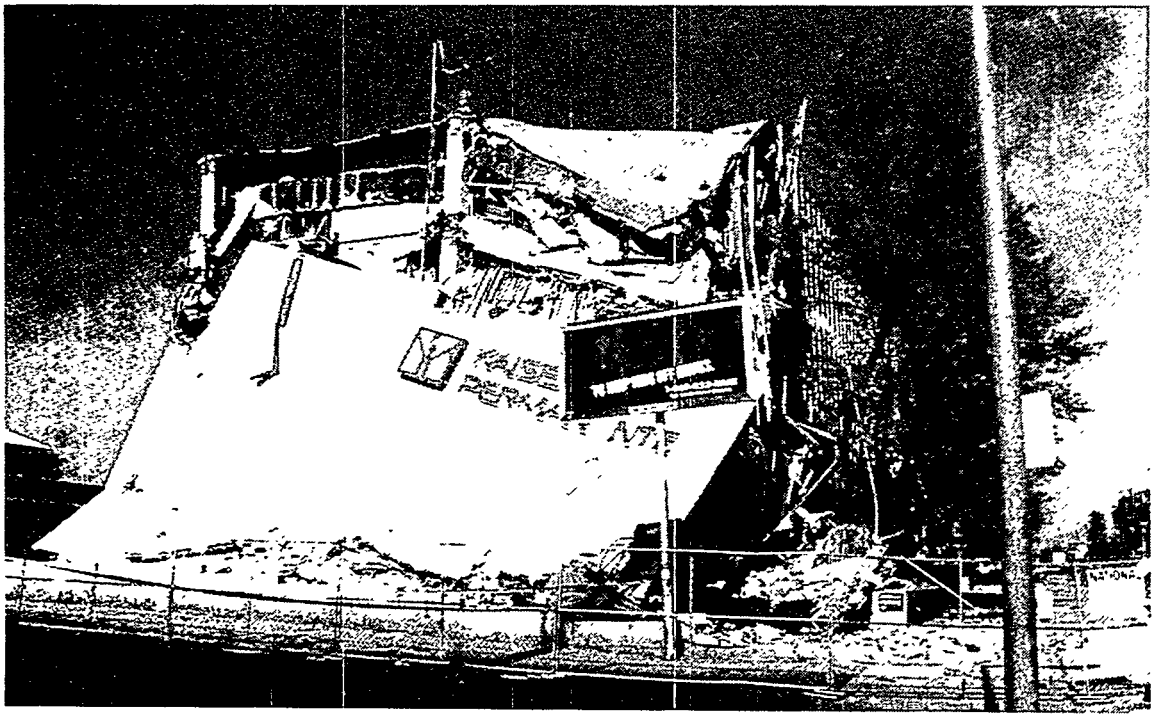

Figure 2. An example of a nonductile reinforced concrete frame building which collapsed is the Kaiser Permanente Medical Office Building in Granada Hills.

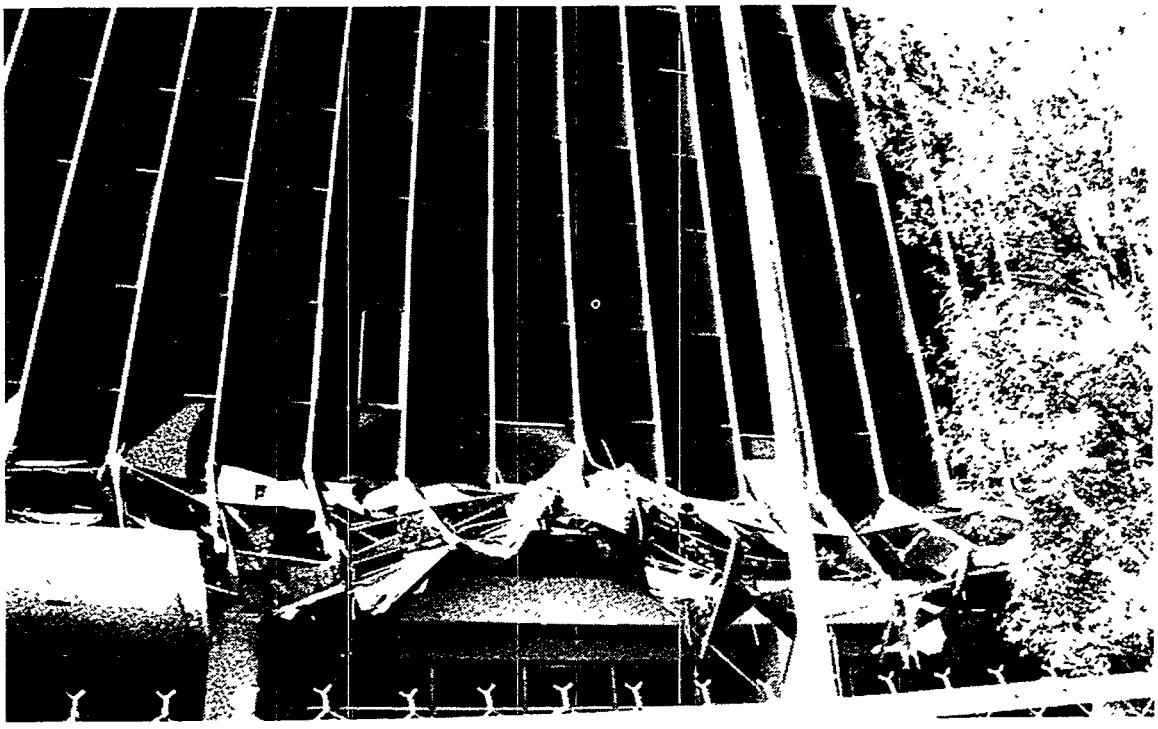

Figure 3. Close-up view of the collapsed second story of the Kaiser Permanente Medical Office Building. All of the columns had failed just above the second floor.

Figure 4. Bullock's Department Store at Northridge Fashion Center was another nonductile reinforced concrete frame structure that performed poorly.

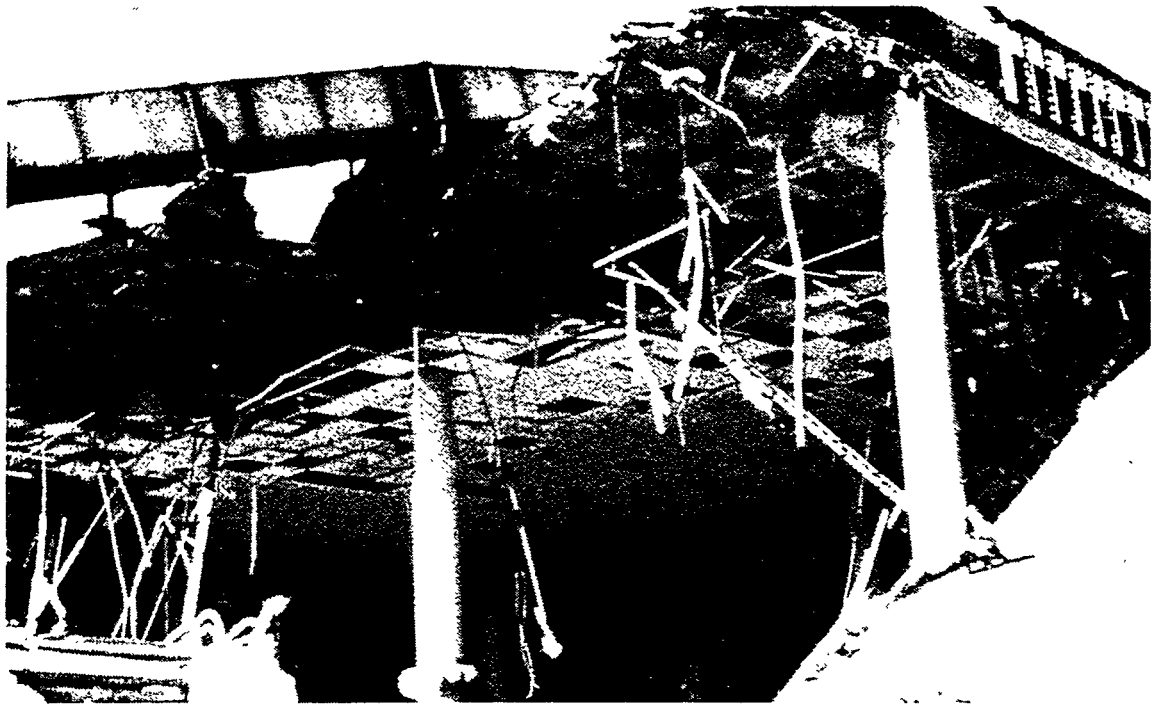

Figure 5. Close-up view of Bullock's Department Store at Northridge Fashion Center. The concrete slab on the second floor was apparently not securely tied to the columns, allowing the second floor to collapse.

Figure 6. Northridge Meadows Apartments was an example of multi-story apartment buildings built with minimal seismic design details and poor construction practices. Due to collapse of the first story, 15 people were killed at this one apartment complex.

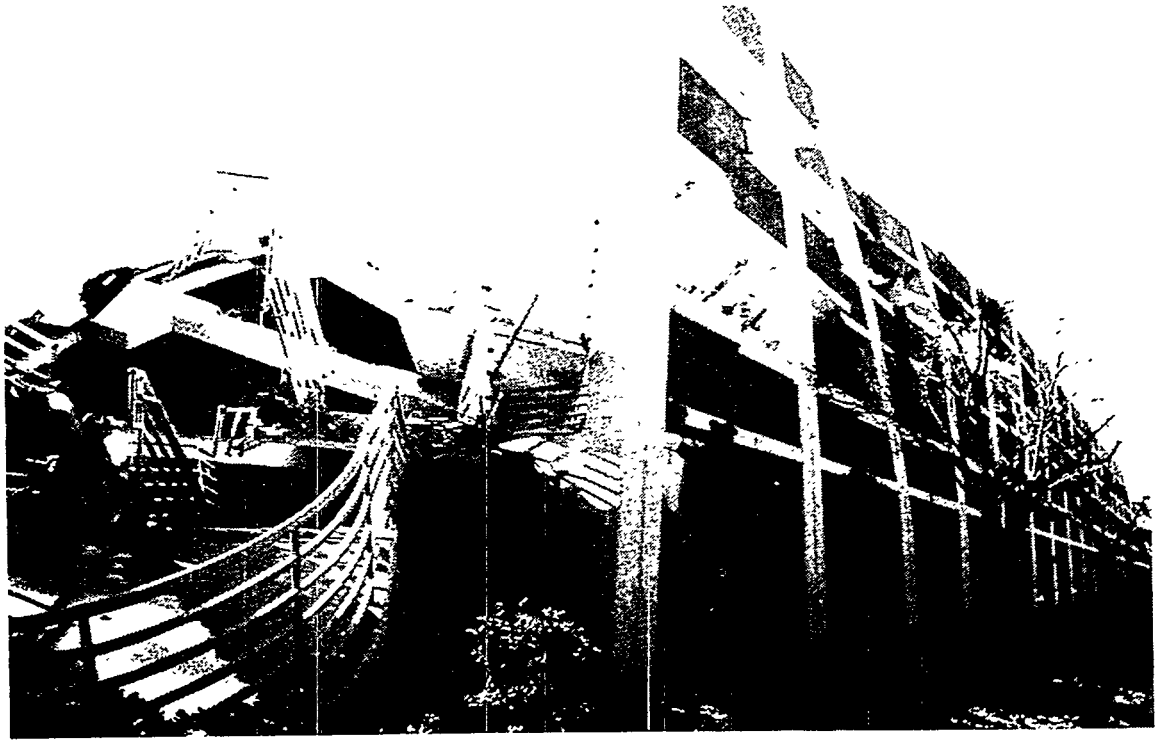

Figure 7. Collapsed parking structure at CSU Northridge.

Figure 8. Excessive diagonal cracking of unreinforced masonry cladding (one-wythe thickness) over a reinforced concrete frame in an L-shaped apartment building in Santa Monica [ref 5].

Figure 9. Typical poorly reinforced concrete block wall that collapsed in the San Fernando Valley area. Note that there was no grout in the cells that had rebar, and that any rebar used did not have adequate overlapping splices.

An area which is generating a lot of research currently is the damage to steel moment-frame buildings. In particular, the welded-flange, bolted-web connections of steel beams to steel columns have experienced failures in several modes *(see Figures 10 and 11)*. The most common fracture resulted in the severing of a beam flange from a column flange and passed through the weld or through the adjacent heat-affected material *(see Figure 12)*. Lack of fusion between the backup bar (under the beam flange) and the column created a crack which may have initiated the fracture. The bolts shown in the figure were replaced after being sheared off when the beam flange connection broke [ref 6]. In the aftermath, about 60 buildings are being repaired and many other welded steel-frame structures are being inspected in more detail. This topic could have a widespread impact on design details and welding procedures and applications for both steel moment-frame and steel braced-frame structures.

Another characteristic associated with the Northridge earthquake is the large number of lifelines that were affected. On the morning of the earthquake, approximately 2 million customers in the Los Angeles area lost electric power. In addition, 600,000 customers in nearby cities were without power and power was disrupted along interconnected power grids such that 150,000 customers in Idaho lost power for three hours [ref 2]. Pipeline distribution systems, carrying water, gas, and liquid fuels all suffered failures, much of which was attributed to permanent ground deformations. Transportation was disrupted by the failure of bridges along four major highways, Interstate (I) 5, State Route (SR) 14, I-10, and SR-118.

The freeway bridges for SR-118 over San Fernando Mission and Gothic Streets located within 5 miles of the epicenter were severely damaged by the earthquake. Figures 13 & 14 show the partially collapsed bridges in which the bridge columns lost core confinement of the concrete and thereby lost their capacity to support the bridge deck. Another location of damage to freeway bridges included some interchanges at I-5 and SR-14. Connection bridges for SR-14 to I-5 had short column effects and abutment damage which led to failed columns and collapse of some bridge spans. Near these collapsed bridges along SR-118 and I-5/SR-14, several other lifeline systems suffered damage. At an electric power substation, the earthquake caused the bushing in a 500 kV transformer to rock and become damaged. Figure 15 shows the repair efforts to the transformer in order to return it to service. Figures 16 to 19 show other types of problems experienced at electrical substations.

In many cases during the Northridge earthquake, the emergency power systems at industrial facilities started up immediately and provided the necessary power to the critical systems and components throughout the buildings involved. However, individual components or seismic weak links inhibited or curtailed successful operations for days to weeks. These items include: failure of automatic transfer switches from normal offsite power to the emergency power circuit; failure of controls to properly switch from the empty fuel (day) tank to the auxiliary fuel tank; failure of piping on subsystems attached to the cooling tower which lost capacity to provide cooling water to the emergency power generators; failure of relays in some of the emergency power distribution cabinets; failure of piping connections in fire protection systems and other water lines that resulted in extensive water leaks -- these leaks caused electrical shorts in the emergency

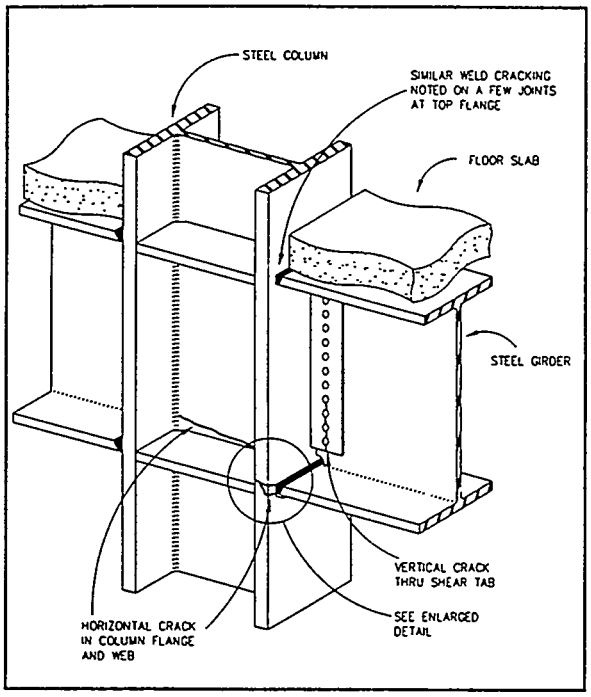

Figure 10. Typical damage to Welded-flange, bolted-web connections of steel beams to steel columns in moment-frame buildings [ref 3].

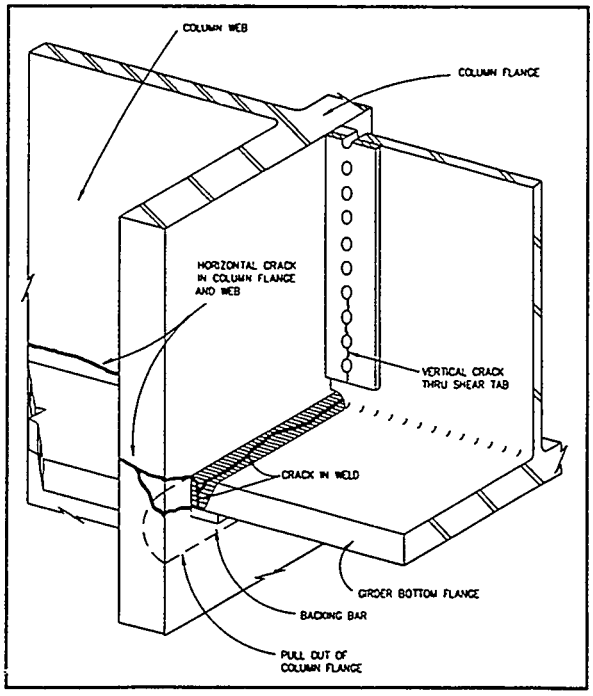

Figure 11. Enlarged detail of Welded-flange, bolted-web connection damage [ref 3].

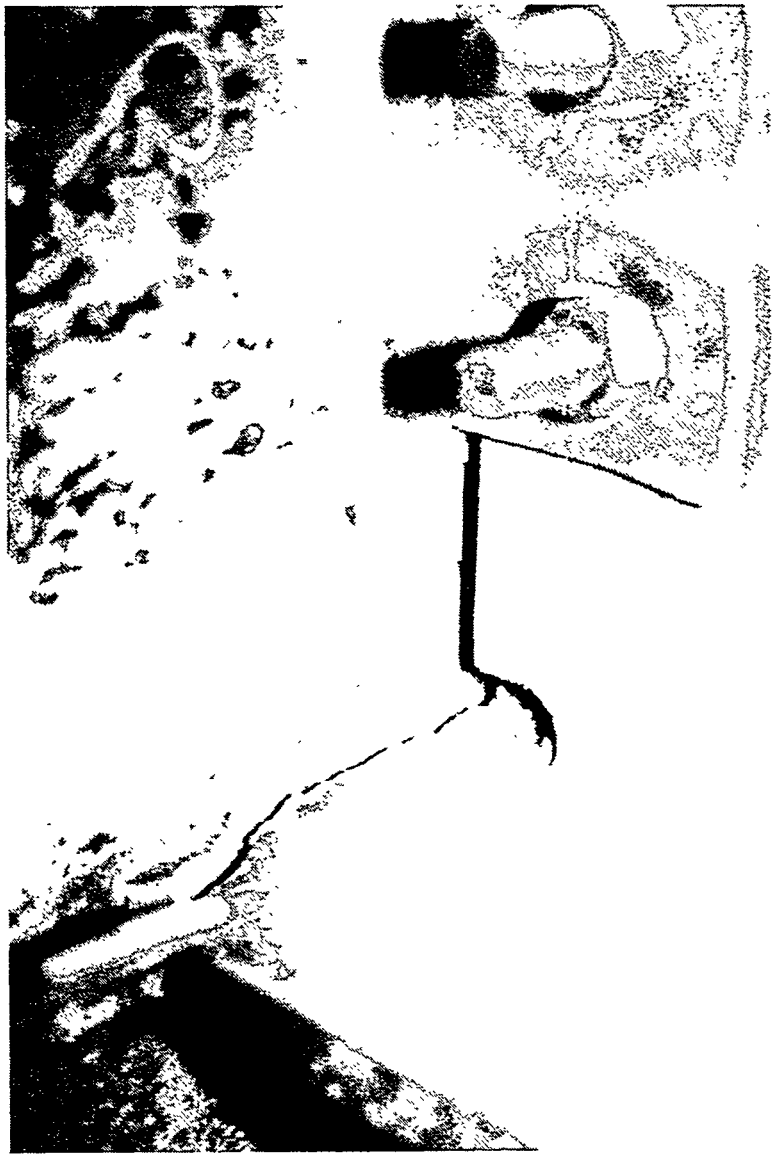

Figure 12. Close-up photo of typical failure of welded-flange, bolted-web connection of steel beams to steel columns in moment-frame buildings. The most common fracture resulted in the severing of a beam flange from a column flange and passed through the weld or through the adjacent heat-affected material. Note that the bolts were replaced after being sheared off when the beam flange connection broke [ref 6].

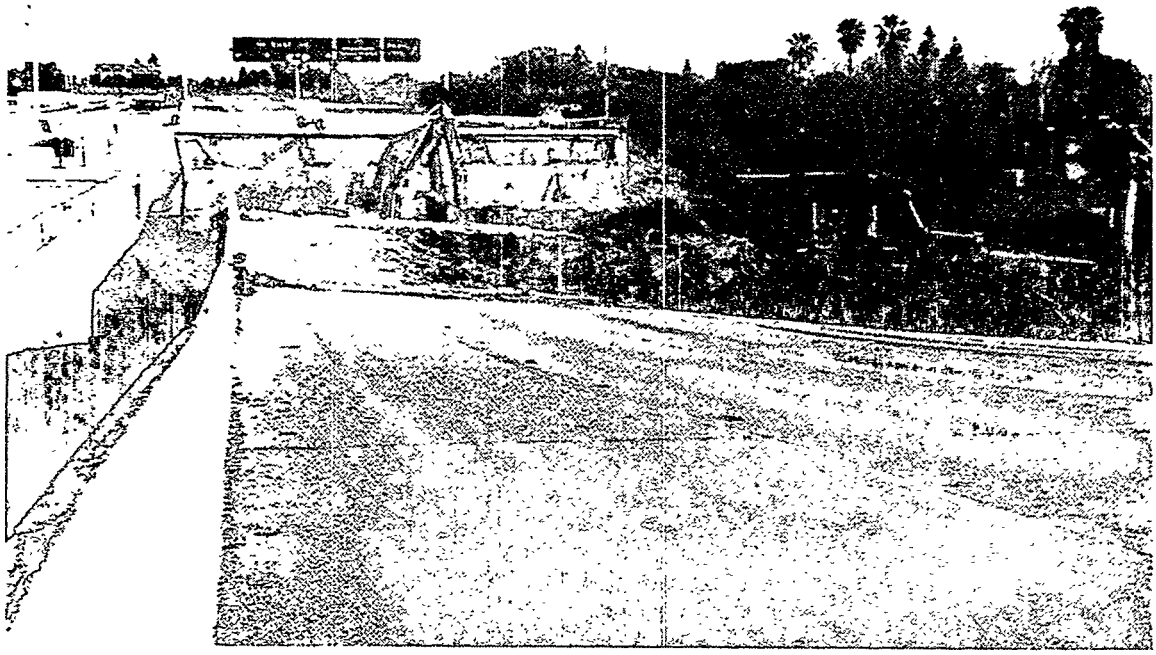

Figure 13. Partially collapsed span at SR-118 at Mission-Gothic Undercrossing.

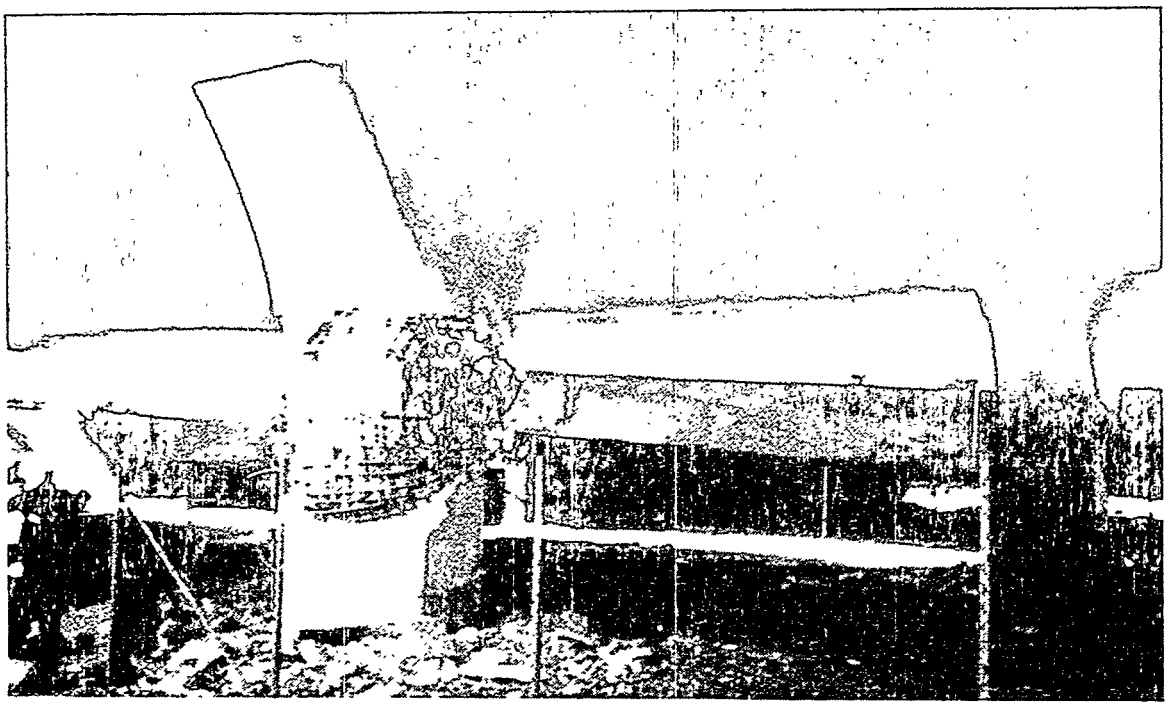

Figure 14. SR-118 at Mission-Gothic Undercrossing. Close-up of damaged columns with partially collapsed span in background.

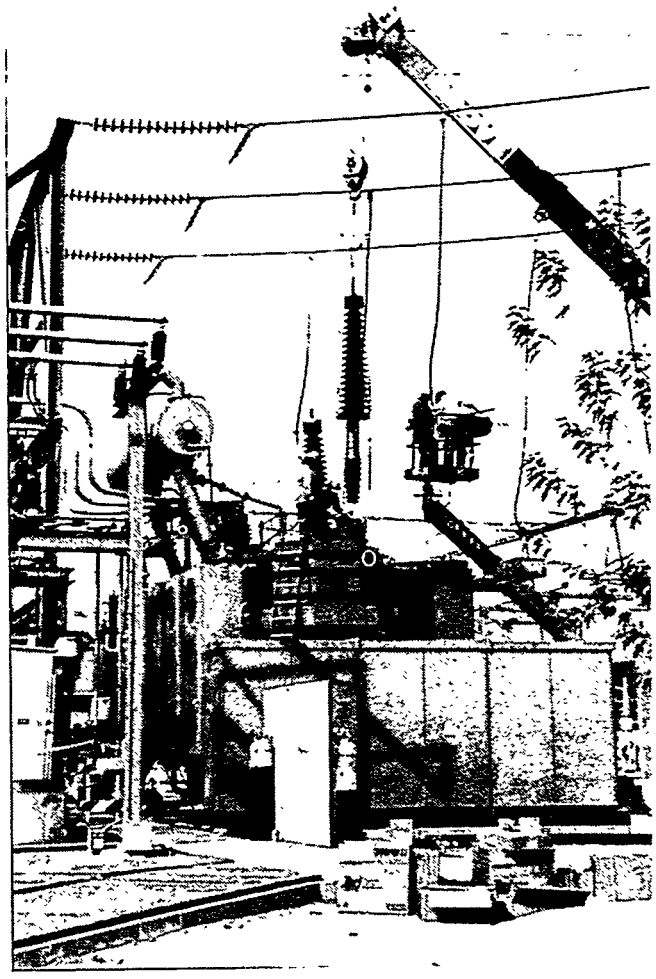

Figure 15. Replacement of a 500 kV transformer bushing at a substation about 6 miles from the epicenter.

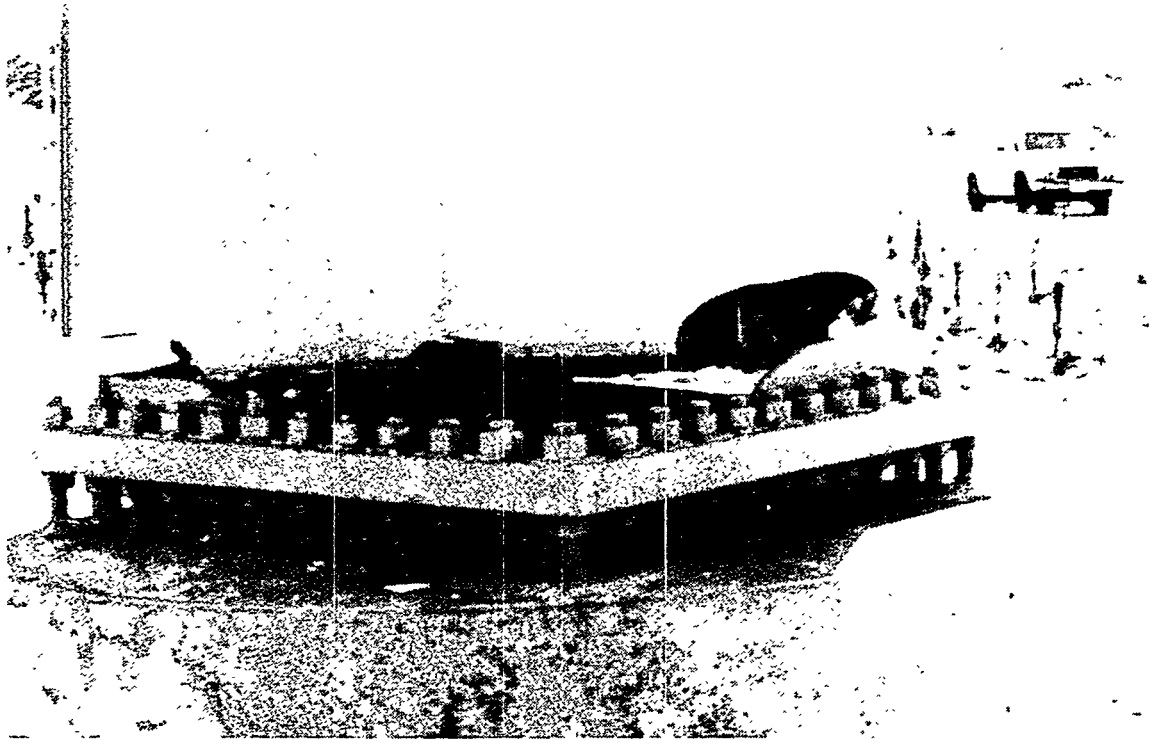

Figure 16. Weld failure and base metal fracture occurred in the heat-affected zone at this steel column base.

Figure 17. Rigid buswork was suspended by short chains. The chains became the seismic weak link, and the rigid bus fell and damaged the nearby disconnect switches.

Figure 18. Close-up of typical rigid buswork suspended by short chains. This photo was taken after temporary repairs were made.

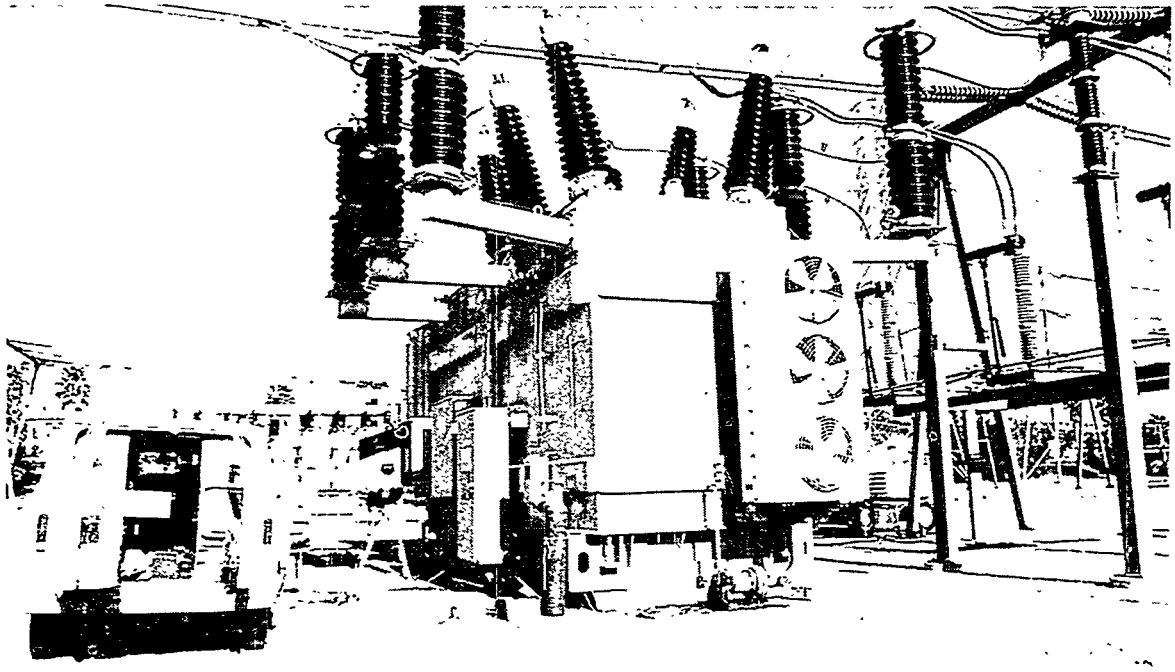

Figure 19. This 230 kV transformer shifted about 12 inches north on its concrete pad during the Northridge Earthquake. Temporary tack welds had been made (between the transformer and the embedded steel in the foundation) after the 1971 San Fernando Earthquake, but were not replaced with adequate welds before the Northridge Earthquake.

Figure 20. Fire protection lines with threaded connections on elbows at branch lines experienced leaks due to interaction with suspended ceiling systems.

power distribution cabinets.

At several hospitals in the earthquake-affected area, the main structures performed fairly well. However, the chilled water lines and fire protection lines suffered breaks or leaks in many of the connections *(see Figure 20)* or at building separations. In some cases, the water lines were attached to unreinforced masonry (URM) walls. The water leaks caused the following types of problems as examples: (1) loss of availability or of distribution of emergency power due to shorts in electrical cabinets; (2) loss of cooling to major critical components and electronics equipment; (3) lack of water and/or water pressure in fire protection systems; and (4) evacuation of occupants due to life safety or lack of support systems availability.

In one hospital complex, the main electrical transfer switch (from normal offsite power to onsite emergency power) failed to function properly immediately after the quake; even though the emergency diesel was running and was available to handle the electrical load. One example of an electrical relay problem was on an emergency power subsystem. The relay had intermittent problems prior to the Northridge quake and malfunctioned again during the quake. In a penthouse on the roof of a hospital, the acceleration levels were so high that the inertial forces caused failure of a 3-inch diameter valve body on a 4-inch diameter chilled water line *(see Figure 21)*.

Vibration isolators worked well in those cases where there were also adequate seismic bumpers to limit the displacements. Emergency diesel generators, chillers, air handling units, and compressors experienced problems with attached lines when vibration isolators were not seismically designed properly. On the roof of one hospital, an air handler unit's (AHU) anchorage configuration was good except for the inadequate length of the connecting bolts between the AHU and its vibration isolators. Due to failure of these connections, the AHU came off its supports and broke the attached lines.

Within the Santa Clarita Valley, there was damage to both welded- and bolted-seam water storage tanks. Several internal roof trusses collapsed inside welded steel tanks due to the sloshing motion of the water. In Valencia, an 800,000-gallon water tank was damaged due to rupture of its inlet and outlet piping which lacked sufficient flexibility to accommodate the motion of the tank. As the piping failed, the escaping water produced a vacuum effect which buckled the roof. Proper ventilation at the top of this tank may have prevented its roof damage by relieving the suction caused by the escaping water.

In addition to damage to water tanks in the Santa Clarita Valley, there were examples of good and poor performance of water tanks in the Calleguas Water District which serves the Simi Valley. Two welded-seam steel tanks located about 10 miles northwest of the epicenter lost their contents when inlet and outlet piping ruptured. The tanks were each holding about one million gallons of water and this water flooded several homes in a nearby neighborhood. A rigid tee connection in the piping between the two tanks was severely cracked due to differential motion between the adjacent tanks during the earthquake. In addition, a 12-inch diameter, cast iron, valve body ruptured when there was differential movement at the rigid connection between the attached piping and the tank

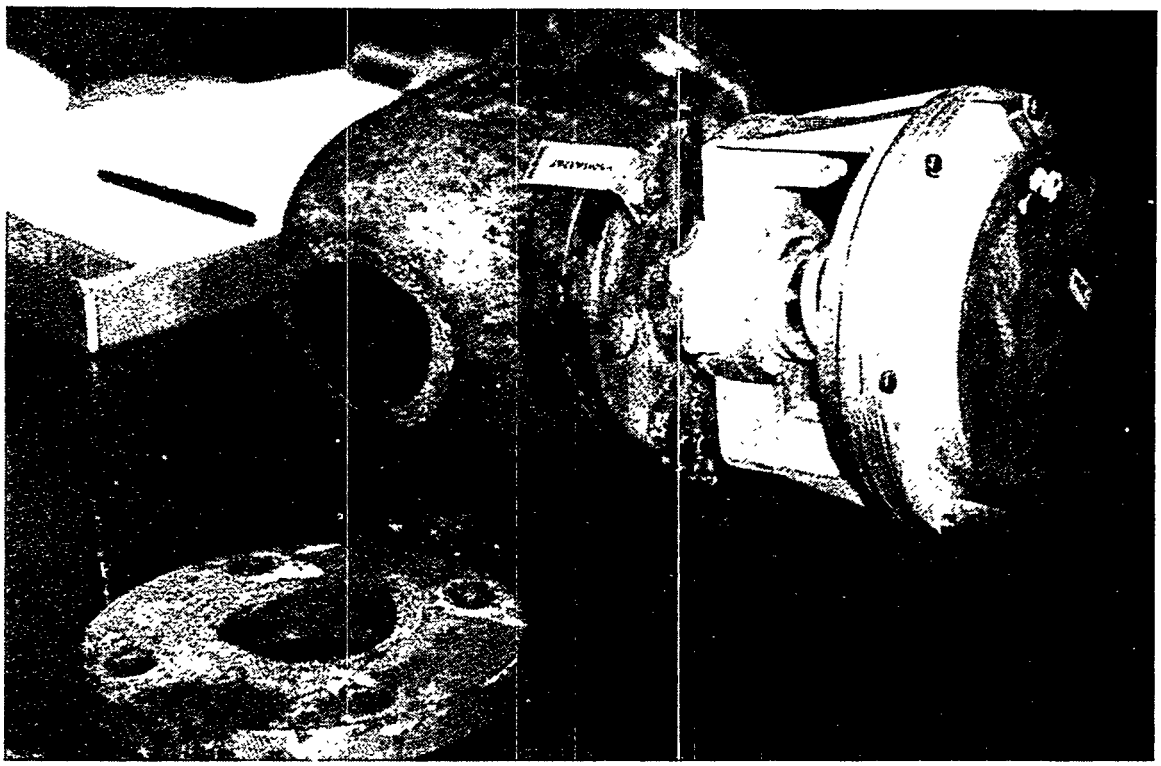

Figure 21. In a penthouse on the roof of a hospital, the acceleration levels were so high that the inertial forces caused failure of a 3-inch diameter valve body on a 4-inch diameter chilled water line.

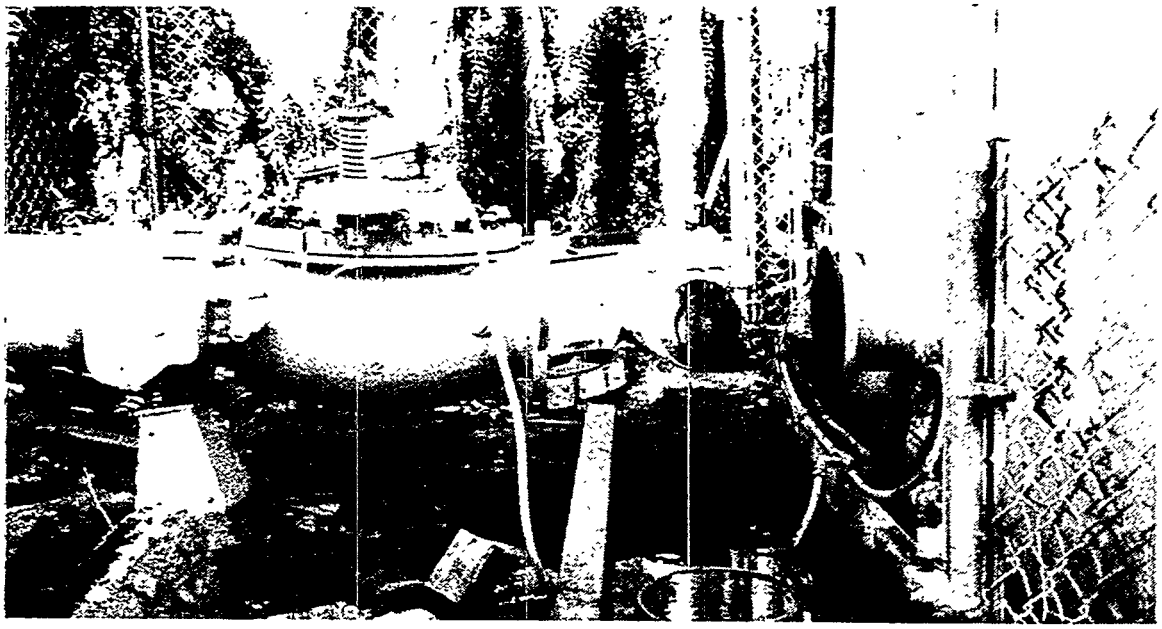

Figure 22. A 12-inch diameter, cast iron, valve body ruptured when there was differential movement at the rigid connection between the attached piping and the tank during the earthquake

during the earthquake *(see Figure 22)*. Cast-iron components, such as the valve body shown in Figure 23, typically do not have sufficient ductility to accommodate large displacements. Fortunately, there was adequate ventilation at the top of the tanks which allowed the evacuated tanks to appear salvageable. In contrast to the performance of those two tanks, several other tanks closer to the epicenter appeared fully functional. Located about 5 miles northwest of the epicenter, a 300,000-gallon and a one million-gallon welded-seam steel tank showed no evidence of structural damage. As shown in Figure 24, the tanks had flexible, elastomeric couplings between the tank valves and their inlet and outlet pipes entering the ground. The flexible couplings permitted relative motion between the tanks and the rigidly anchored piping.

Balboa Boulevard is a utility corridor with several lifeline systems including water, natural gas, electric power, telecommunications, oil, and sewer. There are six major pipelines underneath Balboa Boulevard between Lorillard and Rinaldi Streets. These pipelines include the 22-inch diameter Line 120 for natural gas, the 49-inch diameter Granada Trunk Line for water, the 68-inch diameter Rinaldi Trunk Line for water, and the 16-inch diameter Mobil Oil pipeline. In addition to the already mentioned oil, water, and gas pipelines, there are also two 30-inch diameter gas transmission pipelines and several smaller diameter sewer, water distribution, and gas distribution pipelines. The earthquake caused ground displacements which created a tensile zone near Lorillard Street and a compression zone near Rinaldi Street. A water main and a natural gas main experienced tensile failures near Lorillard Street. The water line rupture caused extensive flooding and hampered repairs. The natural gas that escaped from the failed line was later ignited by the starter on a pickup truck. As a result, about six nearby homes were destroyed by the fire.

In addition to damage to structures and lifelines, there was considerable nonstructural damage throughout the epicentral region. Building inventory loss and contents damage was a common problem throughout the region. The large seismically induced motions caused contents to fall off shelves, nonstructural items to fall on contents, and support racks for the contents to fail because of inadequate design details. Typical nonstructural interior damage included overturned cabinets and fallen lights and ceiling tiles. At some locations, the interior damage caused the facilities to close. Mechanical systems within structures were also damaged.

With all the damage and problems associated with the Northridge Earthquake, the local, state, and Federal agencies moved quickly to aid people affected by the event. The Los Angeles metropolitan area was extremely fortunate that the event occurred early in the morning on a holiday. As many have stated, this earthquake was another "wake-up call" reminding us of the importance of preparing for earthquakes and for retrofitting SSCs that are not seismically safe. The lessons learned from this and previous earthquakes greatly aid efforts by DOE, NRC, and EPRI to mitigate the effects of earthquakes on industrial facilities and lifelines.

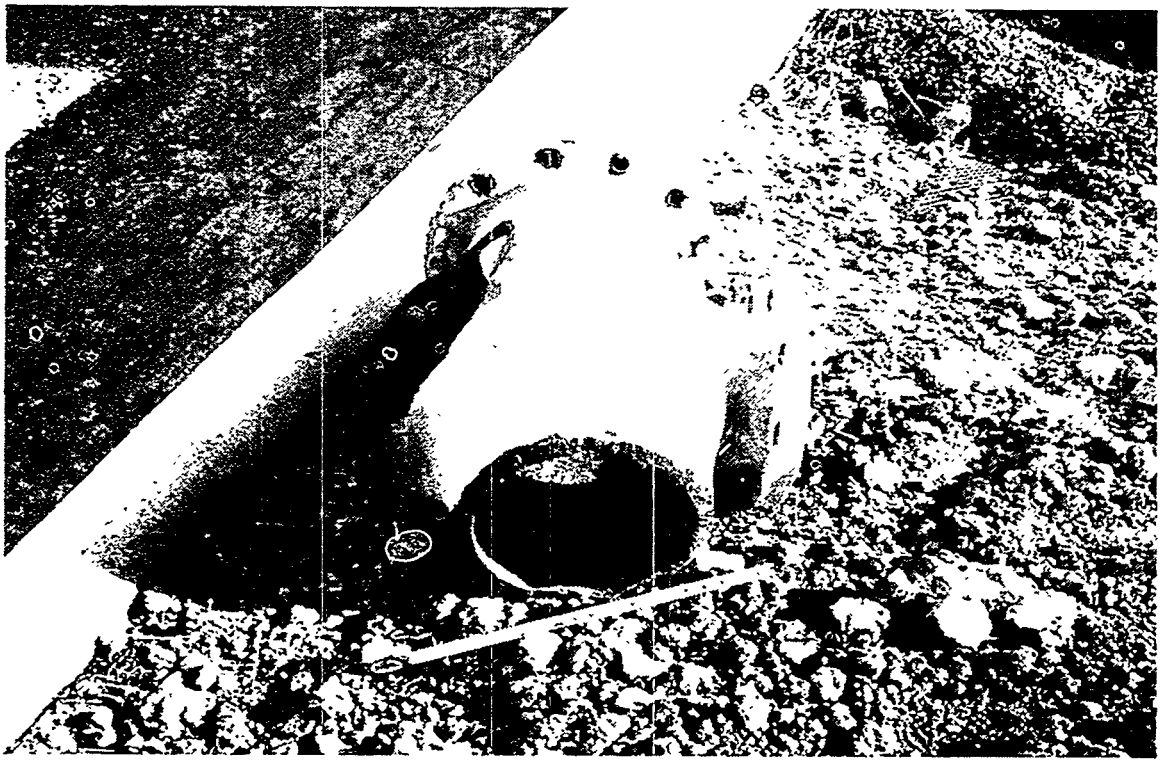

Figure 23. Cast-iron components such as this valve body typically do not have sufficient ductility to accommodate large displacements.

Figure 24. Large tanks and attached piping performed well when there was an elastomeric flex connection between the tank and the rigidly anchored piping

SUMMARY OF LESSONS LEARNED

Following are some of the lessons either learned or re-learned from the 1994 Northridge Earthquake which have some applicability at nuclear power plants:

- accommodate differential movement of piping at building separations -- especially where adjacent buildings have a significant difference in natural frequency or where one building is on a spread footing and the adjacent building is on deep pile foundations

- fire protection lines with threaded connections on elbows at branch lines experienced leaks due to interaction with suspended ceiling systems

- large tanks and attached piping performed well when there was an elastomeric flex connection between the tank and the rigidly anchored piping

- vibration isolators on equipment performed well when used along with adequate seismic bumpers

- welded connections on steel moment-frame buildings (such as some of the turbine buildings, auxiliary buildings, fuel handling buildings, and office buildings) -- need to have a redundant structural system to allow load redistribution upon damage to critical beam-to-column joints

- emergency generators may be able to start on demand, but if one of the supporting systems fails to function properly during the earthquake there may be no capability to distribute the emergency power to the critical SSCs -- examples include:

  - automatic transfer switch (from normal offsite power to emergency power) fails to function properly

  - electrical shorts in distribution cabinets and switchgear due to water leaks

  - failure of controls to switch from empty fuel (day) tank to auxiliary tank

- damage to turbine bearings can occur when there is no back-up power (e.g., batteries) to the lube oil pump

- vulnerability of lifelines need to be reviewed for impact on continued operations or ability to re-start after a major seismic event

- vulnerability of a lifeline that shares right-of-way with other lifelines is determined by the most fragile member; which may not necessarily be the lifeline under study

- potential seismic-induced relay chatter should be evaluated on electromechanical protective relays for critical electrical circuits

- porcelain-supported power components (e.g., transformer bushings, rigid buswork, live-tank circuit breakers, capacitor banks, disconnect switches, and lightning arrestors) are vulnerable in earthquakes

- live-tank circuit breakers and components with tall, slender porcelain insulators (such as disconnect switches and lightning arrestors) are vulnerable to seismic accelerations as low as 0.15g

- seismic interaction issues: rigid buswork fell and damaged the adjacent disconnect switches

REFERENCES

1. Todd, D., et al, 1994 Northridge Earthquake - Performance of Structures, Lifelines, and Fire Protection Systems, NIST Special Publication 862, ICSSC TR14, United States Department of Commerce Technology Administration, National Institute of Standards and Technology, May 1994.

2. Earthquake Engineering Research Institute (EERI), *"Northridge Earthquake January 17, 1994 Preliminary Reconnaissance Report"*.

3. H.J.Degenkolb Associates, Engineers, June 1994.

4. UCRL-CR-106554, *Structural Concepts and Details for Seismic Design*, Figure 4-27, Lawrence Livermore National Laboratory, 9/91.

5. Earthquake Engineering Research Center (EERC), *"Seismological and Engineering Aspects of the January 17, 1994 Northridge Earthquake: Abridged Slide Set"*, University of California at Berkeley, 1994.

6. Earthquake Engineering Research Institute (EERI), *"Slides on the January 17, 1994, Northridge Earthquake"*.

7. Eli, M. and Sommer, S., "1994 Northridge Earthquake Damage Investigation", *Phenomenal News - Natural Phenomena Hazards Newsletter*, prepared by Lawrence Livermore National Laboratory for United States Department of Energy, April 1994.

8. Eli, M. and Sommer, S., "Update on 1994 Northridge Earthquake Damage Investigation", *Phenomenal News - Natural Phenomena Hazards Newsletter*, prepared by LLNL for DOE, August 1994.

STRUCTURAL AGING PROGRAM STATUS REPORT

Dan J. Naus and C. Barry Oland
Oak Ridge National Laboratory (ORNL)
Oak Ridge, Tennessee 37831-8056

Bruce Ellingwood
The Johns Hopkins University
Baltimore, Maryland 21218-2686

H. L. Graves, III
United States Nuclear Regulatory Commission (USNRC)
Washington, DC 20555-0001

ABSTRACT

Research is being conducted at the Oak Ridge National Laboratory (ORNL) under U.S. Nuclear Regulatory Commission (USNRC) sponsorship to address aging management of safety-related concrete structures. Documentation is being prepared to provide the USNRC with potential structural safety issues and acceptance criteria for use in continued service evaluations of nuclear power plants. Program accomplishments have included development of the Structural Materials Information Center containing data and information on the time variation of 144 material properties under the influence of pertinent environmental stressors or aging factors, performance assessments of reinforced concrete structures in several United Kingdom nuclear power facilities, evaluation of European and North American repair practices for concrete, an evaluation of factors affecting the corrosion of metals embedded in concrete, and application of the time-dependent reliability methodology to reinforced concrete flexure and shear structural elements to investigate the role of in-service inspection and repair on their probability of failure.

1. INTRODUCTION

By the end of this decade, 63 of the 111 commercial nuclear power plants in the United States will be more than 20 years old, with some nearing the end of their 40-year operating license. Faced with the prospect of having to replace the lost generating capacity from other sources and the potential for substantial shutdown and decommissioning costs, many utilities are expected to seek extensions to their plant operating licenses. A major concern in evaluating such applications is ensuring that the capacity of the safety-related systems to mitigate extreme events has not deteriorated unacceptably due to either aging or environmental stressor effects during their previous service history. Although major mechanical and electrical equipment items in a plant could be replaced, if necessary, replacement of the containment and many other safety-related concrete structural components would be economically

*Research sponsored by the Office of Nuclear Regulatory Research, U.S. Nuclear Regulatory Commission under interagency Agreement 1886-8084-5B with the U.S. Department of Energy under Contract DE-AC05-840R21400 with Martin Marietta Energy Systems, Inc.

unfeasible. Approval for service life extension must be supported by evidence that these structures will continue to be capable of withstanding potential future extreme events.

2. BACKGROUND

In general, the performance of nuclear power plant concrete structures has been good. However, there have been some instances where the capacity of the containment and other safety-related structures to meet future functional and performance requirements has been challenged. Degradation mechanisms that can potentially impact the performance of nuclear power plant reinforced concrete structures include corrosion of steel reinforcing systems, chemical attack, alkali-aggregate reactions, sulfate attack, frost attack, leaching, salt crystallization, and microbiological attack. Some of the aging concerns identified to date include inaccessibility of reinforced concrete basemat for inspection to detect potential degradation resulting from mechanisms such as leaching or sulfate attack, corrosion of steel reinforcement contained in water-intake structures, and corrosion of embedded portion of steel pressure boundary (liner) due to a breakdown of the seal at the concrete floor-to-liner interface. Where degradation incidences have occurred, they have generally done so early in the life of the particular structure and have been corrected. Causes were primarily related to improper material selection, construction/design deficiencies, or environmental effects. Examples of some of the more serious instances are described elsewhere [1-4].

3. STRUCTURAL AGING PROGRAM

Incidences of structural degradation related to the concrete components in nuclear power plants indicate a potential need for improved surveillance, inspection/testing, and maintenance to enhance the technical bases for assurances of continued safe operation. The Structural Aging (SAG) Program was initiated in 1988 and has the overall objective of preparing documentation that will provide USNRC license reviewers with (1) identification and evaluation of the potential structural degradation processes; (2) issues to be addressed under nuclear power plant continued service reviews, as well as criteria, and their bases, for resolution of these issues; (3) identification and evaluation of relevant in-service inspection, structural assessment or remedial measures programs; and (4) methodologies to perform current assessments and reliability-based life predictions of safety-related concrete structures. To meet this objective, SAG Program activities are conducted under four task areas: (1) program management, (2) materials property data base, (3) structural component assessment/repair technologies, and (4) quantitative methodology for continued service determinations.

3.1 PROGRAM MANAGEMENT

3.1.1 Objective and Scope

The overall objective of the program management task is to effectively manage the technical tasks undertaken to address priority structural safety issues related to nuclear power plant continued service assessments. Management duties include planning, integrating, monitoring, reporting, and technology transfer. A key part of the management function is integration of the technical objectives and efforts of program participants. In addition, efforts are continuously made to maintain effective technology transfer and to maintain liaison with peer groups, technical committees, and programs in foreign countries.

3.1.2 Summary of Recent Accomplishments

Recent activities under this task have included administration of four subcontracts, and preparation of a technical progress report [5] and two foreign trip reports [6,7]. Program overview presentations were made at the *Workshop on Concrete Performance and Modeling of Low-Level and Radioactive Waste Disposal* [8], the National Institute of Standards and Technology *Symposium on Integrated Knowledge Systems for High-Performance Construction Materials and Systems* [9], British Nuclear Energy Society-sponsored *International Conference on Thermal Reactor Safety Assessment* [10], Nuclear Electric [11], and Electricité de France [12]. Program personnel participated in technical committees of the American Concrete Institute (Service Life Prediction, Concrete Materials Property Data Base, and Radioactive and Hazardous Waste Management) and American Society of Mechanical Engineers (Section XI Working Group on Concrete Pressure Components, Subgroup on Containments, and Special Working Group on Plant Life Extension). In addition, program personnel participated in an International Atomic Energy Agency Coordinated Research Program on Aging of Concrete Containment Buildings, and in development of an International Union of Testing and Research Laboratories for Materials and Structures Technical Committee, *Methodology for Life Prediction of Concrete Structures in Nuclear Power Plants*.

3.2 MATERIALS PROPERTY DATA BASE

3.2.1 Objective and Scope

The objective of the materials property data base task is to develop a reference source that contains data and information on the time variation of material properties under the influence of pertinent environmental stressors and aging factors. This source will be used to assist in the prediction of potential long-term deterioration of critical structural components in nuclear power plants and to establish limits on hostile environmental exposure for

these structures. Primary activities under this task have involved the development of the Structural Materials Information Center and assemblage of materials property data. In addition, survey data and a durability assessment review of several reinforced concrete structures contained in several nuclear power stations located in England were assembled.

3.2.2 Summary of Recent Accomplishments

Structural Materials Information Center. Initial development of the *Structural Materials Information Center* (SMIC) has been completed [13]. Contained in this report are detailed descriptions of the *Structural Materials Handbook* and *Structural Materials Electronic Data Base* that comprise the SMIC. In addition, a reassessment of software tools for building customized data bases was performed.

The *Structural Materials Handbook* is an expandable, four volume, hard-copy reference document containing complete sets of data and information for each material. Volume 1 contains performance and analysis information (i.e., mechanical, physical, and other properties) useful for structural assessments and safety margins evaluations. Volume 2 provides the data used to develop the performance curves in Volume 1. Volume 3 contains material data sheets (e.g., constituent materials, general information, and material composition). Volume 4 contains appendices describing the handbook organization and revision procedures.

The *Structural Materials Electronic Data Base* is an electronically-accessible version of the handbook that provides an efficient means for searching the data base files. It has been developed on an IBM-compatible personal computer and employs two software programs — Mat.DB [14] and EnPlot [15]. Mat.DB is a menu-driven program for data base management that was developed for metallic materials. It employs window overlays to access data searching and editing features. Textual, tabular, and graphical information and data can be maintained, searched, and displayed. EnPlot is a program that incorporates pop-up menus for creating and editing engineering graphs. This software includes curve-fitting and scale-conversion features for preparing engineering graphs and utility features for generating output files. The engineering graphs can be entered directly into the Mat.DB data base files. A new version of Mat.DB (Version 2.0) based on Microsoft Windows [16] is being developed by ASM International (Materials Park, Ohio).

Based on experience gained during development of SMIC, advances in personal computer hardware capabilities, and corresponding developments in software tools for building customized data bases, a reassessment of candidate systems was conducted [17]. It was concluded that custom software provides enough flexibility to meet SMIC requirements for a data base management system (Table 3.6 of Ref. 5) and also permits entry of existing data and information files. Existing object-oriented relational data base software provides a foundation for a new data base management system that could be designed and built locally.

Data Collection. In parallel with efforts to develop the SMIC, activities have been conducted to establish materials property data for input into the SMIC. Two primary approaches have been utilized — open-literature information and testing of prototypical samples. To date, 132 material data bases have been developed based on open-literature sources (i.e., 116 concrete, 12 metallic reinforcement, 1 prestressing tendon, 2 structural steel, and 1 rubber). Twelve data bases have been prepared based on testing of prototypical samples associated with nuclear power plant facilities. Reference [18] presents summary descriptions of the material property data base files contained in SMIC.

Material Behavior Modeling. Activities related to an evaluation of models for predicting performance of concrete materials, collection of survey data and durability assessments of reinforced concrete structures contained in United Kingdom (UK) nuclear power stations, and evaluations of the performance of post-tensioning systems in UK prestressed concrete reactor vessels were described previously [19].

3.3 STRUCTURAL COMPONENT ASSESSMENT/REPAIR TECHNOLOGY

3.3.1 Objective and Scope

The objectives of this task are to: (1) develop a systematic methodology that can be used to make quantitative assessments of the presence, magnitude, and significance of any environmental stressors or aging factors that adversely impact the durability of safety-related concrete structures in nuclear power plants; and (2) provide recommended in-service inspection or sampling procedures that can be utilized to develop the data required both for evaluating the current condition of concrete structures and for trending the performance of these components. Associated activities include an assessment of techniques for repair of concrete components that have experienced an unacceptable degree of deterioration, and the identification and evaluation of techniques for mitigation of any environmental stressors or aging factors that may act on critical concrete components.

Assessment of the ability of concrete components to meet their functional and performance characteristics is an important consideration in continuing the service life of nuclear facilities. Given the complex nature of the various environmental stressors and aging factors that potentially can exert deteriorating influences on the concrete components, a systems approach is probably best in addressing an evaluation of a structure for continued service. Basic components of such an approach would encompass the development of (1) a classification scheme for structures, elements, and deterioration causes and effects; (2) a methodology for conducting a quantitative assessment of the presence of active deteriorating influences; and (3) remedial measure considerations to reestablish the capability of degraded structures or components to meet potential future requirements, such as a loss-of-coolant accident (LOCA).

LWR Critical Concrete Component Classification. An aging assessment methodology for identifying structural components of most importance to aging and the degradation factors that can potentially impact the performance of these components was described previously [19].

NDE Sampling/Inspection Technology. Detection of age- or environmental stressor-related degradation, as well as its magnitude and rate of occurrence, is a key factor in maintaining the readiness of safety-related concrete components to continue their functions in the unlikely event as accident situation could develop. Basic activities under this subtask have addressed evaluation of destructive and nondestructive testing techniques, development of statistical data for selected nondestructive testing techniques, identification of potential aging concerns associated with post-tensioning systems used in prestressed concrete containments, and preparation of guidelines for in-service inspection of nuclear power plant concrete structures [19].

The ability of a prestressed concrete nuclear power plant containment to withstand the loadings that could develop as a result of a loss-of-coolant accident depends on the continued integrity of the prestressing tendons. In the U.S., the condition and functional capability of unbonded post-tensioning systems must be periodically assessed. This is accomplished, in part, through an in-service inspection program that must be developed and implemented for each containment. Requirements for containment tendon surveillance programs are provided in documents such as Regulatory Guide 1.35, Regulatory Guide 1.35.1, ASME Section XI Subsection IWL, and the U.S. Standard Technical Specification for Tendon Surveillance. Although the overall performance of the post-tensioning systems has been very good, there have been several instances of degradation. Examples include voids under tendon bearing plates resulting from improper concrete placement, cracking of anchorheads due to stress-corrosion cracking or embrittlement, containment dome delaminations due to low quality coarse aggregate material and absence of radial reinforcement or unbalanced prestressing forces, and low prestressing forces. A report is being prepared in which potential structural issues related to aging of post-tensioning systems in nuclear power plant containments are discussed. An overview of current requirements associated with in-service inspection of the post-tensioning systems will be used as the basis for development of a life management program for these systems. Potential aging- and environmental-stressor related items that can impact the performance of these systems are being identified (e.g., corrosion; loss of prestressing force due to relaxation, concrete creep, concrete shrinkage; etc.). The effectiveness of current life management programs in identifying problem areas is being assessed and recommendations are being prepared on how post-tensioning system-aging issues can be addressed in the future. For example, can post-tensioning tendons with prestressing force levels approaching the lower bound of acceptable performance merely be retensioned? What are the long-term effects on the mechanical performance of the post-tensioning system of being under

load? That is, does the tendon ultimate tensile strength and elongation capacity decrease with age under load? This activity is scheduled for completion in December 1994.

In-service inspection requirements are imposed on nuclear plants through documents such as the following: 10CFR50, NRC Regulatory Guides, Plant Technical Specifications, Inspection and Enforcement Bulletins, NRC letters, and the American Society of Mechanical Engineers *Boiler and Pressure Vessel Code* [20]. However, because each nuclear plant has unique construction permit and operating license issue dates, each plant could potentially have a different set of minimum in-service inspection requirements. Therefore, to simplify continued service evaluations, it would be advantageous to have a standardized in-service inspection program that could be used to identify and also to quantify any deteriorating influences. The availability of such a standardized inspection program would also help ensure that a uniform set of evaluation criteria is applied to each plant. Limited information on criteria, inspection, and testing requirements for development of such a procedure is available (e.g., Refs. [21-22]). However, the application requirements presented in these documents to nuclear safety-related concrete structures requires evaluation with respect to items such as accessibility, service history, functional requirements, construction materials, etc. A report is being prepared that has the overall objective of providing a suggested in-service inspection approach for reinforced and prestressed concrete structures in nuclear power plants. Criteria are being established to assess the current structural reliability of the safety-related concrete structures and to develop data for use in assessments of future performance. Specific activities include (1) a review and assessment of current NRC and industry-related in-service inspection requirements for reinforced concrete structures; (2) an evaluation of the applicability of available information on criteria, inspection, and testing requirements for general civil engineering concrete structures provided through organizations such as the American Concrete Institute and American Society for Testing and Materials; and (3) development of a structural component condition assessment methodology that establishes criteria for relating damage state and environmental exposure in terms of a "three tiered hierarchy" (e.g., acceptance "as-is," acceptance after review, and acceptance after additional evaluations). Visual acceptance criteria, per this hierarchy, are being developed to parallel the effort of American Concrete Institute Committee 349 [23]. Basic criteria for acceptance without further evaluation and acceptance after review based on visual inspections have been developed for (1) exposed concrete surfaces; (2) lined concrete surfaces; (3) areas around embedments in concrete; (4) joints, coatings, and non-structural components; and (5) prestressing steel systems. Any condition outside the criteria for these two conditions is considered unacceptable and requires additional nondestructive testing, destructive testing, analytical assessment, or a combination of the three. Degradation-based acceptance criteria are being established for concrete cracking, loss of concrete section, conventional and prestressing steel corrosion, and loss of

prestressing force. When completed in December 1994, the structural component condition assessment methodology will provide guidance for dispositioning of conditions or findings from in-service inspections.

Remedial/Preventative Measures Considerations. The life of reinforced concrete components in nuclear power plants is expected to be greater than any likely period for which the plant would operate, provided neither environmental factors, applied load, nor a combination of load and environmental factors compromise its integrity [24]. When concrete structures have been fabricated with close attention to the details related to fabrication of good quality concrete, the concrete should exhibit extended durability. A breakdown in any of these factors or occurrence of an extreme environmental stressor or adverse aging factor can result in distress. Basic activities under this subtask have included reviews of European and North American repair practices for degraded reinforced concrete, and an assessment of corrosion of metals embedded in concrete [19].

3.4 QUANTITATIVE METHODOLOGY FOR CONTINUED SERVICE DETERMINATIONS

3.4.1 Objective and Scope

The goal of this task is to develop a methodology that will facilitate quantitative assessments of current and future structural reliability and performance of concrete structures in nuclear plants. Specific objectives associated with accomplishing this goal include (1) identification of models to evaluate changes in strength of concrete structures over time in terms of initial conditions, service load history, and aggressive environmental factors; and (2) formulation of a methodology to predict structural reliability of existing concrete structures during future operating periods from a knowledge of initial conditions of the structure, service history, aging, nondestructive condition assessment techniques, and inspection-maintenance strategies.

Prior activities have developed a probability-based methodology to estimate strength degradation of a component and to evaluate the effect of periodic maintenance from a reliability point of view [25]. This methodology has been extended to consider cases where several defects or zones of damage may contribute to a reduction in strength of a structural member.

Time-Dependent Reliability Analysis. Structural loads, engineering material properties, and strength degradation mechanisms are random in nature. Time-dependent reliability analysis methods provide a framework for performing condition assessments of existing structures and for determining whether in-service inspection and maintenance are required to maintain reliability and performance at the desired regulatory level.

The strength, $R(t)$, of the component and the applied loads, $S(t)$, both are random (or stochastic) functions of time. At any time, t, the margin of safety , $M(t)$, is

$$M(t) = R(t) - S(t). \qquad (1)$$

Making the customary assumption that R and S are statistically independent random variables, the (instantaneous) probability of failure is,

$$P_f(t) = P\left[M(t) < 0\right] = \int_0^\infty F_R(x)\, f_S(x)\, dx. \tag{2}$$

in which $F_R(x)$ and $f_S(x)$ are the probability distribution function of R and density function of S. Equation 2 provides one quantitative measure of structural reliability and performance, provided that P_f can be estimated and validated. The numerical evaluation of Eqn. 2 and the development of supporting statistical data remain research challenges. However, significant progress has been made in this regard during the past several years.

For service life prediction and reliability assessment, one is more interested in the probability of satisfactory performance over some period of time, say (0,t), than in the snapshot of the reliability of the structure at a particular time provided by Eqn. 2. Indeed, it is difficult to use reliability analysis for engineering decision analysis without having some time period (say, an in-service maintenance interval) in mind. The probability that a structure survives during interval of time (0,t) is defined by a reliability function, L(0,t). If, for example, n discrete loads S_1, S_2,..., S_n occur at times t_1, t_2,..., t_n during (0,t), the reliability function becomes,

$$L(0,t) = P\left[R(t_1) > S_1, \ldots, R(t_n) > S_n\right]. \tag{3}$$

If the load process is continuous rather than discrete, there is an analogous but more complex expression.

The conditional probability of failure within time interval (t,t+dt), given that the component has survived during (0,t), is defined by the hazard function:

$$h(t) = -d \ln L(0,t)/dt. \tag{4}$$

Solving for L(0,t) yields,

$$L(0,t) = \exp\left[-\int_0^t h(x)dx\right]. \tag{5}$$

The hazard function is especially useful in analyzing structural failures due to aging or deterioration. For example, the probability that time to structural failure, T_f, occurs prior to a future maintenance operation scheduled at $t+\Delta t$, given that the structure has survived to t, can be evaluated as,

$$P\left[T_f \le t + \Delta t \mid T_f > t\right) = 1 - \exp\left[-\int_t^{t+\Delta t} h(x)dx\right]. \quad (6)$$

The hazard function for pure chance failures (case 1 in next section) is constant. When structural aging occurs and strength deteriorates, h(t) characteristically increases with time. In-service inspection and maintenance impact the hazard function, causing it to change discontinuously at the time an inspection is performed. The main difference between time-dependent reliability of undegrading and degrading structural components can be characterized by their hazard functions. Much of the challenge in structural reliability analysis involving deteriorating structures lies in relating the hazard function to specific degradation mechanisms, such as corrosion.

It is assumed that significant structural loads can be modeled as a sequence of load pulses, the occurrence of which is described by a Poisson process with mean rate of occurrence λ, random intensity S_j, and duration τ. Such a simple load process has been shown to be an effective model for extreme loads on structures, since normal service loads challenge the structure to only a small fraction of its strength. With this assumption, the reliability function becomes

$$L(0,t) = \int_0^\infty \exp\left(-\lambda t\left[1 - t^{-1}\int_0^t F_S(rg)\,dt\right]\right) f_R(r)\,dr. \quad (7)$$

in which $f_R(r)$ is the probability density function of initial strength, R(0), and g(t) equals the mean of R(t)/R(0), a function describing the degradation of strength in time (see Fig. 1). The limit state probability, or probability of failure during (0,t), can be determined as F(t) = 1 - L(0,t); F(t) is not the same as $P_f(t)$ in Eqn. 2.

Service Life Predictions for Reinforced Concrete Slab. Time-dependent reliability concepts are illustrated with a simple example of a concrete slab drawn from recent research on aging of concrete structures in nuclear plants [26-27]. This slab was design using the requirements for flexure strength found in ACI Standard 318 [28]:

$$0.9\ R_n = 1.4\ D_n + 1.7\ L_n. \quad (8)$$

in which R_n is the nominal or code resistance, and D_n and L_n are the code-specified dead and live loads, respectively. The strength of the slab changes in time, initially increasing as the concrete matures and then decreasing due to (unspecified) environmental attack. This situation is illustrated conceptually by the sample functions r(t) and s(t) for strength and load in Fig. 1. The behavior of the resistance over time must be obtained from mathematical models describing the degradation mechanism(s) present.

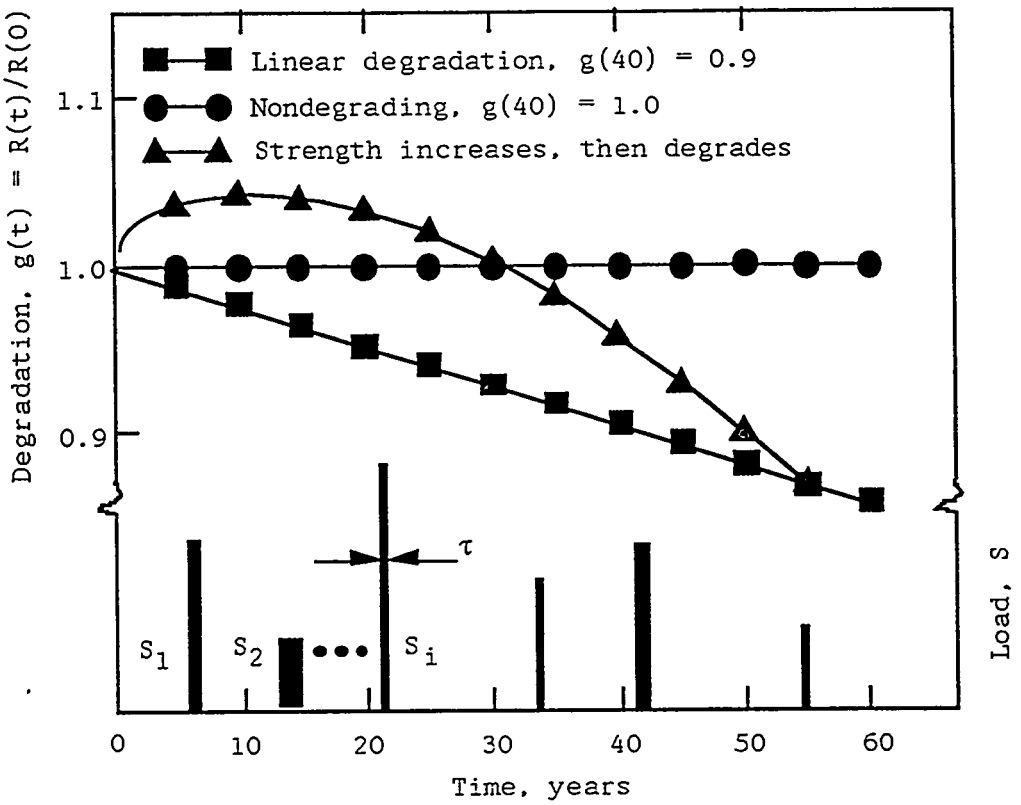

Fig. 1 Mean degradation functions of one-way slab.

Figure 2 presents a comparison of limit state probabilities for intervals (0,t) for t ranging up to 60 years. Three cases are presented (see Fig. 1): (1) no degradation in strength, i.e., R(t) = R(0), a random variable (this case is analogous to what has been done in probability-based code work to date [29]); (2) R(t) initially increasing with concrete maturity and then degrading; and (3) R(t) degrading linearly over time to 90% of its initial strength at 40 years. The statistics used in the illustrations that follow are summarized in Table 1. The basis for these statistics is given elsewhere [30]. Neglecting strength degradation entirely in a time-dependent reliability assessment can be quite unconservative, depending on the time-dependent characteristics of strength.

Service Life Predictions for Reinforced Concrete Shear Wall. As shown above, the failure probability of a structural component or system under stationary random loading can be evaluated as a function of time if the strength degradation and the probabilistic characteristics of the initial strength are known. In previous papers, a probability-based method to estimate the strength degradation of a component and to evaluate the effect of periodic maintenance from a reliability point of view was provided [26,27]. In the method developed, it was assumed that strength degradation at any section is caused by one randomly occurring defect of random intensity. Such a model is reasonable when the degradation is such that at most one defect or

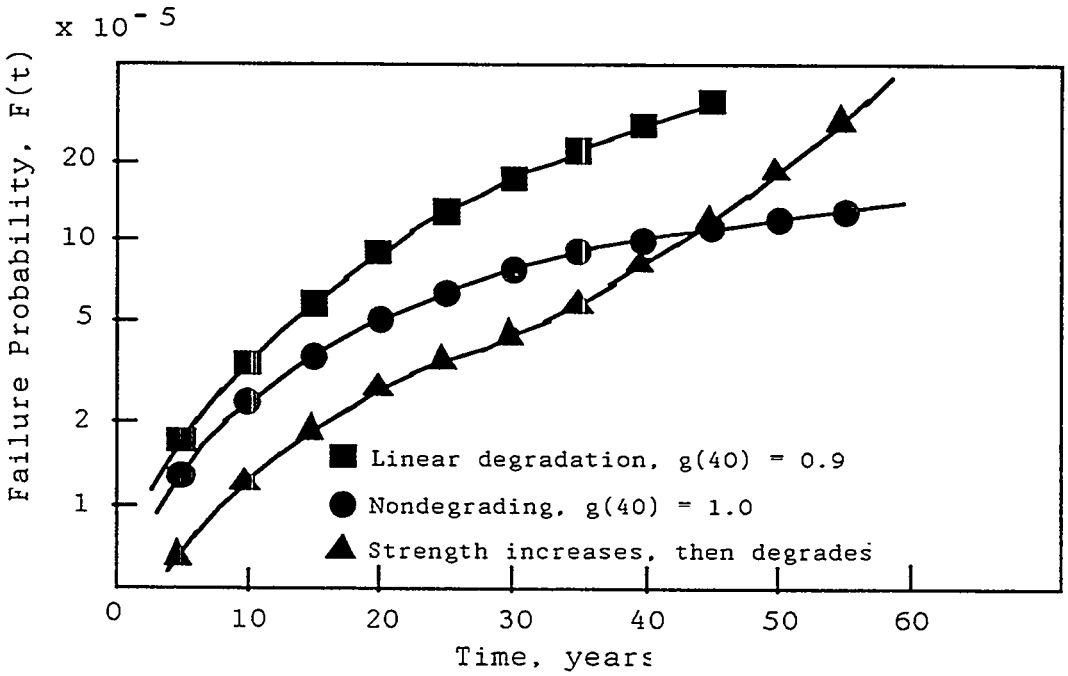

Fig. 2 Failure probability of one-way slab.

Table 1 Statistical properties of strength and load.

Parameter	Rate of Occurrence	Duration	Main	C.O.V.	Pdf
Flexure Strength	—	—	1.12Mn	0.14	Lognormal
Shear Strength	—	—	$1.7V_n$	0.18	Lognormal
Dead Load	—	—	$1.0D_n$	0.07	Normal
Live Load	0.5/yr	3 mo.	$0.4L_n$	0.50	Type I
Earthquake Load	0.05/yr	30 sec.	$0.08E_{sse}$	0.85	Type II

zone of damage is likely to occur within a given cross section. The strength degradation of a reinforced concrete beam or column due to corrosion of reinforcement can be estimated by such modeling. However, there are cases where several defects or zones of damage may contribute in reducing strength. For example, the strength of a reinforced concrete wall in flexure and/or shear might degrade due to the combined effects of expansive aggregate reactions at several points along a given cross section of the wall. The

evaluation of the (random) residual strength of the wall requires that the cumulative effect of defects in a cross section be considered. Recent research has provided a method whereby the impact of randomly occurring multiple defects on structural capacity can be considered [33]. Some results are summarized in the following.

The wall considered is a low-rise wall with a height-to-width ratio equal one, and is subjected to vertical load, D, which is uniformly distributed on the top of the wall, and in-plane lateral load, V, which is concentrated at the top of the wall. The shear strength of concrete walls can be estimated from empirical models [28,34]. These models are not sufficient to analyze the strength of deteriorating low-rise shear walls. Although finite-element analysis is versatile and able to provide detailed information on the shear resistance mechanisms, it requires lengthy computational effort, especially when adapted to reliability analysis. A recent theoretical approach for evaluating shear strength of reinforced concrete components [35-37] determines the ultimate shear strength as the sum of the forces sustained by a truss mechanism, V_t, and by an arch mechanism, V_a. It is assumed that the wall fails if all the reinforcing bars yield in tension and the concrete arch crushes in compression. According to the lower bound theorem of plasticity [38], this approach provides a conservative estimate of the shear strength. These models have been modified for the reliability analysis of a degrading low-rise concrete shear wall [33]. Figure 3 shows that the strength predicted by this method compares well to experimental tests of low-rise shear walls.

Wall in Shear

A wall subjected to expansive aggregate reaction or chemical attack suffers a loss of concrete section. If the wall is not heavily reinforced in the transverse direction, the contribution of the truss mechanism is small. Thus, it can be assumed that only the strength of the arch mechanism decreases due to the loss of concrete section while the strength attributed to the truss mechanism is independent of the degradation. If the wall is reinforced in the longitudinal direction, the vertical reaction is sustained by the longitudinal reinforcement and degradation of concrete outside the concrete strut in the arch mechanism can be neglected. Assume that the stress in the concrete strut is uniform. Then the degradation function of the shear wall can be given by

$$G(t) = \frac{V_t + V_a(t)}{V_{u0}} = \frac{V_t + G_a(t) \cdot V_a(0)}{V_{u0}} \tag{9}$$

in which V_{u0} is the initial shear strength of the wall, $V_a(t)$ is the shear strength of the arch mechanism at time t, and $G_a(t)$ is the degradation function of the shear strength of the arch mechanism.

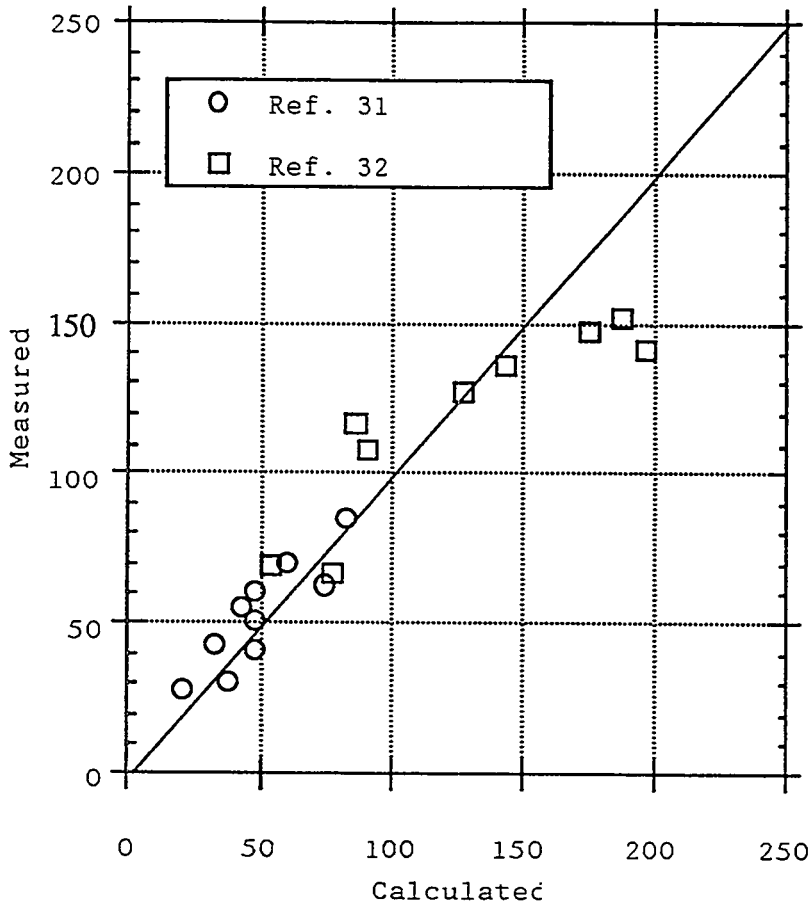

Fig. 3 Comparison of measured and calculated shear strength.

Wall in Flexure and Compression

The ultimate flexural capacity of a cross section is expressed as

$$M_u = T_s\left(\frac{b}{2} - d_c\right) + C_c\left(\frac{b}{2} - k_2 c_u\right) + C_s\left(\frac{b}{2} - d_c\right) \tag{10}$$

in which T_s and C_s are the total force transferred to reinforcement in the tension and compression zone, respectively, d_c is the concrete cover, c_u is the distance from the compressive face to the neutral axis, and $k_2 c_u$ locates the compressive resultant, C_c.

For illustration, assume that

- The wall is subjected to time-invariant dead load, D, which is uniformly distributed on the wall, and intermittent lateral load V, which is concentrated at the top of the wall and may act either in-plane or out-of-plane.

- The wall is designed for in-plane shear based on the current design requirement [39].

$$0.9R_n = E_{ss} \tag{11}$$

in which R_n is the nominal shear strength and E_{ss} is the structural action due to safe-shutdown earthquake. The statistical characteristics of the shear strength and the earthquake load are shown in Table 1. It is assumed that $E_{ss} = 3D = 3.21$MN.

- The mean initiation rate of local damage per unit surface area, ν_u, due to expansive aggregate reaction is time invariant and is $0.1/m^2/year$.

- The defect intensity is modeled as,

$$Y(t) = C(t - T_I)^2 \tag{12}$$

in which C is a time-invariant random variable described by a lognormal distribution with mean value, m_C, of 2.22×10^{-6}/year and coefficient of variation, V_C, of 0.5. This value results in an average defect size that is large enough after several years following its initiation to be found by visual inspection.

- The 28-day specified compressive strength of concrete equals 27.6 MPa. The corresponding mean compressive strength at 28 days is 28.7 MPa [40]. The specified yield strength of the reinforcement is 414 MPa and the mean is 465 MPa.

- Compressive strength of the concrete increases during the first 10 years but does not change thereafter. The mean compressive strength (in units of MPa) at time t is evaluated by [41]

$$E[f_c(t)] = \begin{cases} 15.51 + 3.95\ln t, & t < 10 \text{ years} \\ 47.91, & t \geq 10 \text{ years} \end{cases} \tag{13}$$

in which t is in days. The concrete section area decreases with time as damage accumulates. Other engineering properties of the wall are assumed to be time-invariant.

The mean degradation in shear strength of the wall in which expansive aggregate reactions occur in the concrete is illustrated in Fig. 4, assuming $\nu_u = 0.1/m^2/year$. The mean degradation in shear strength evaluated ignoring the cumulative effect of multiple defects in a section on the strength degradation of the wall is also illustrated in the figure. The gain in shear strength due to the continuous hydration of concrete more than compensates for

the strength degradation due to the loss of section area up to about 50 years. Ignoring the cumulative effect of defects provides an overly optimistic degradation function.

The failure probabilities and the hazard functions associated with the strength degradation illustrated in Fig. 4 are presented in Figs. 5 and 6, respectively. The increase in failure probability due to the strength degradation is small because of the large variability in earthquake load intensity [42]. However, the hazard function increases rapidly after about 50 years when the cumulative effect of defects is considered.

The mean degradation in flexure/compression strength of the wall is more sensitive to the loss of the outer part of the cross section area than is the shear strength, as shown in Fig. 7. Since the loss of the outer part of the wall leads to a reduction in the internal moment arm, the flexural strength degrades more rapidly than the shear strength, which decreases linearly as a function of the loss of cross-section area. Thus, if the governing limit state of the wall is flexure, special attention should be given to the potential for degradation when performing a condition assessment.

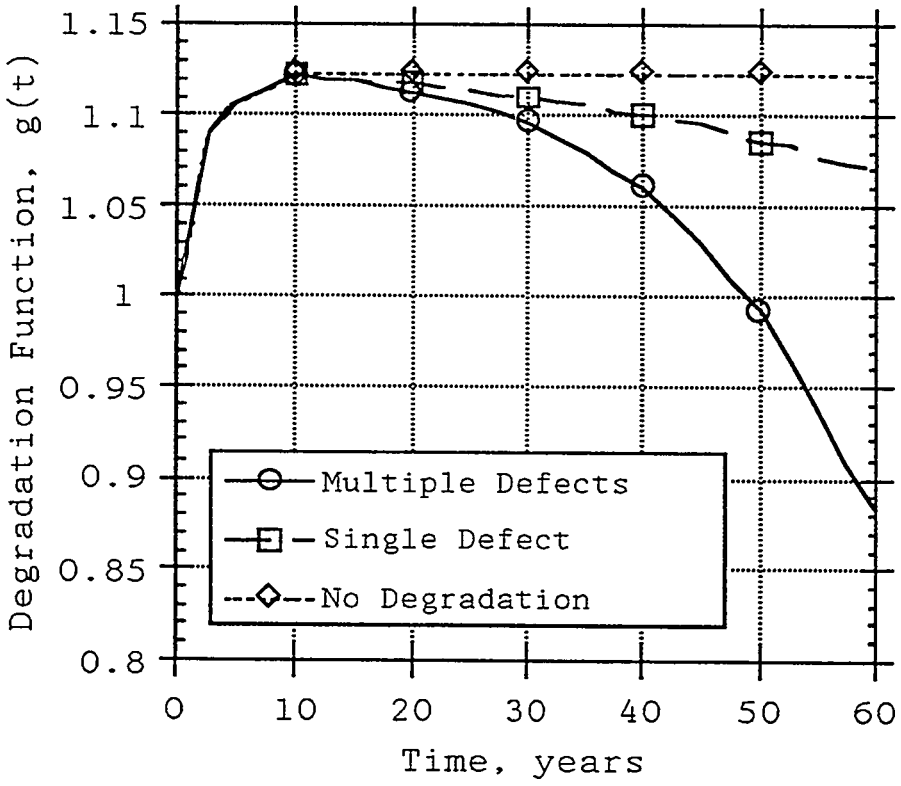

Fig. 4 Mean degradation function of wall in shear without repair.

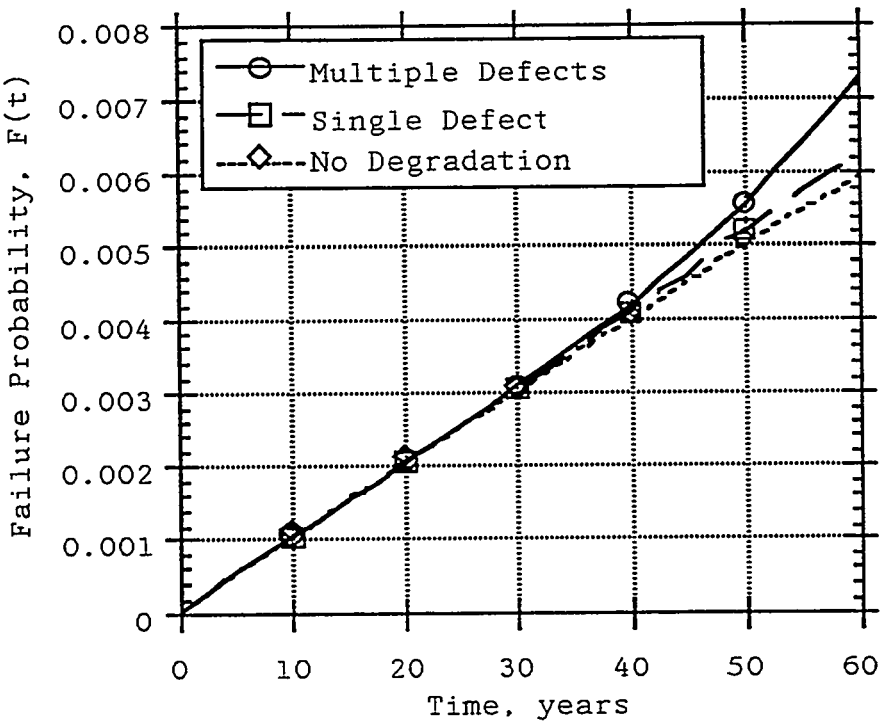

Fig. 5 Failure probability of wall in shear without repair.

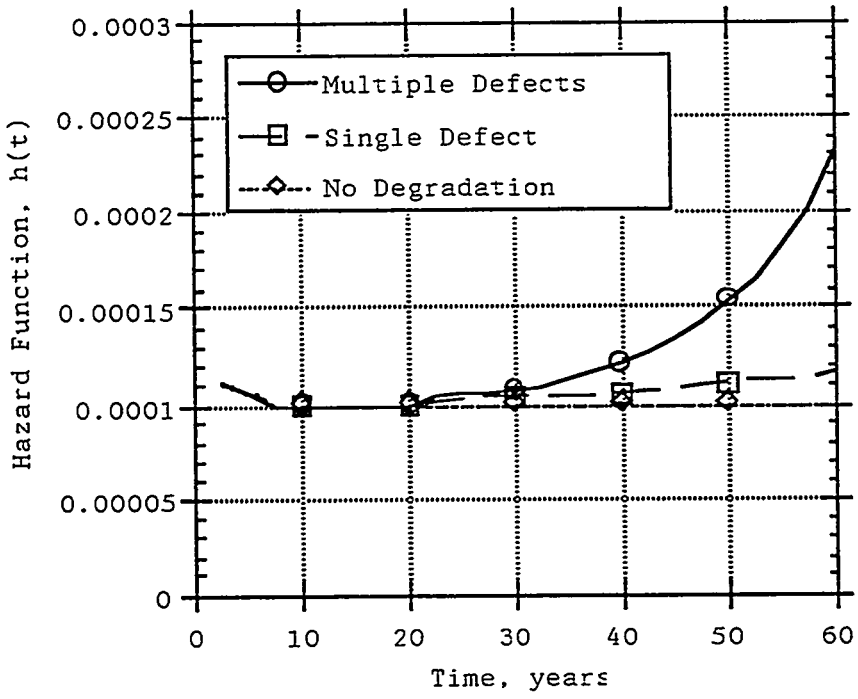

Fig. 6 Hazard function of wall in shear without repair.

Condition Assessment and In-Service Inspection Forecasts of reliability of the type illustrated in Fig. 2 enable the analyst to determine the time period beyond which the desired reliability of the structure cannot be ensured. At such a time, the structure should be inspected. Intervals of inspection and maintenance that may be required as a condition for continued operation can be determined from the time-dependent reliability analysis. In-service inspection and maintenance are a routine part of managing aging and deterioration in many engineered facilities; work already has been initiated to develop policies for offshore platforms [43] and aircraft [44] using probabilistic methods.

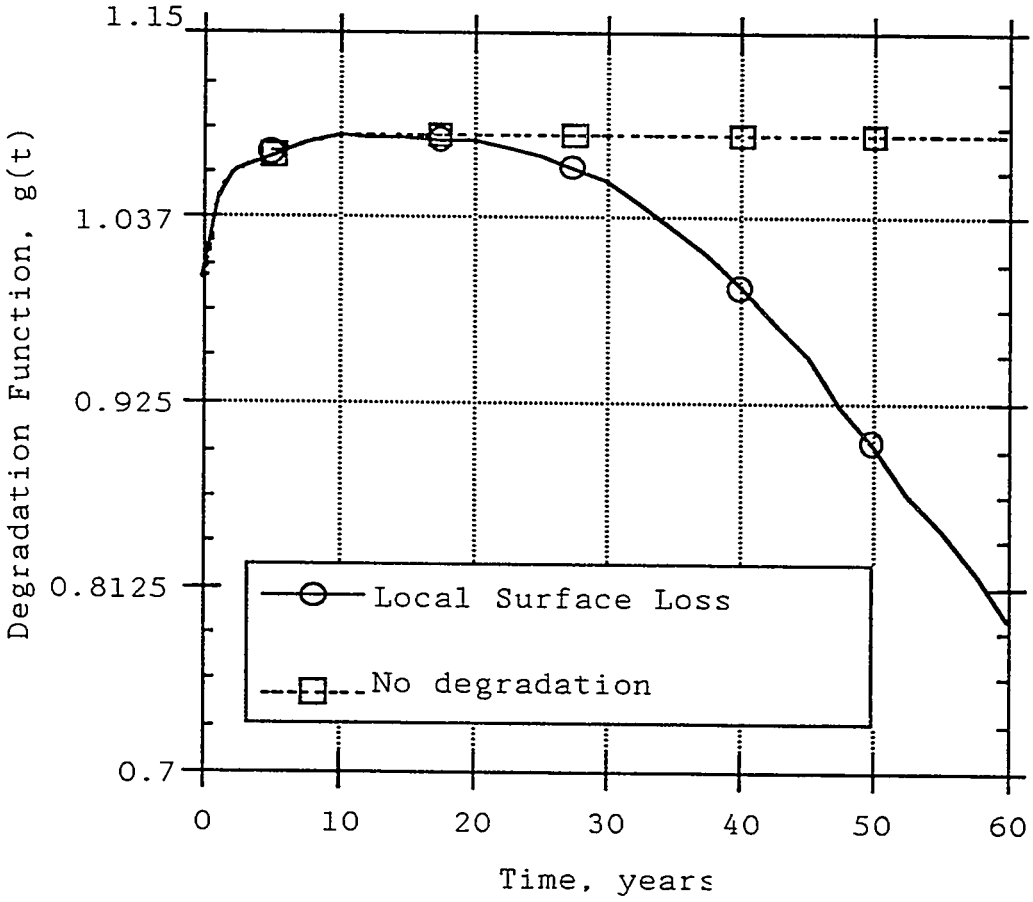

Fig. 7 Mean degradation function of wall in flexure/compression.

When a structure is inspected and/or repaired, something is learned about its in-service condition that enables the probability distribution of strength to be updated. The density function of strength, based on prior knowledge of the materials in the structure, construction and standard methods of analysis, is indicated by $f_R(r)$. Scheduled inspection, maintenance and repair cause the characteristics of strength to change; this is denoted by the (conditional)

density $f_R(r|B)$, in which B is an event dependent on in-service inspection. The information gained from inspection usually involves several structural variables including dimensions, defects, and perhaps an indirect measure of strength or stiffness. If these variables can be related through event B, then the updated density of R following in-service inspection is,

$$f_R(r|B) = P[r < R \leq r + dr, B]/P[B] = c\,K(r)\,f_R(r), \tag{14}$$

in which $f_R(r)$ is termed the prior density of strength, K(r) is denoted the likelihood function, and c is a normalizing constant. The time-dependent reliability analysis then is re-initialized following in-service inspection/repair using the updated $f_R(r|B)$ in place of $f_R(r)$. The updating causes the hazard function (e.g., Fig. 6) to be discontinuous.

Uncertainties in methods of in-service inspection/repair affect the density $f_R(r|B)$. Using a combination of methods usually is more effective from a reliability point of view than using one method. When there are limited resources, it often is most effective to select a few safety-critical elements and concentrate on them [30,45]. Optimal intervals of inspection and repair for maintaining a desired level of reliability can be determined based on minimum life cycle expected cost considerations. Preliminary investigations of such policies have found that they are sensitive to relative costs of inspection, maintenance, and failure [42]. If the cost of failure is an order (or more) of magnitude larger than inspection and maintenance costs, the optimal policy is to inspect at nearly uniform intervals of time. However, additional research is required before such policies can be finalized as part of an aging management plan.

4. APPLICATION OF PROGRAM RESULTS

Potential regulatory applications of this research include: (1) improved predictions of long-term material and structural performance and available safety margins at future times, (2) establishment of limits on exposure to environmental stressors, (3) reduction in total reliance by licensing on inspection and surveillance through development of a methodology that will enable the integrity of structures to be assessed either pre- or post-accident), and (4) improvements in damage inspection methodology through potential incorporation of results into national standards that could be referenced by standard review plans.

5. REFERENCES

1. D. J. Naus, *Concrete Component Aging and Its Significance Relative to Life Extension of Nuclear Power Plants*, NUREG/CR-4652 (ORNL/TM-10059), Martin Marietta Energy Systems, Inc., Oak Ridge National Laboratory, Oak Ridge, Tennessee, September 1986.

2. H. Ashar, D. J. Naus, and C. P. Tan, Prestressed Concrete in U.S. Nuclear Power Plants (Part 1)," pp. 30-34 in *Concrete International*, **16(5)**, American Concrete Institute, Detroit, Michigan, May 1994.

3. H. Ashar, C. P. Tan, and D. J. Naus, "Prestressed Concrete in U.S. Nuclear Power Plants (Part 2)," pp. 58-61 in *Concrete International*, **16(6)**, American Concrete Institute, Detroit, Michigan, June 1994.

4. H. Ashar and D. Jeng, "Effectiveness of In-Service Inspection Requirements of Prestressed Concrete Containments – U.S. Experience," *Proceedings of Second International Conference on Containment Design and Operation*, Toronto, Ontario, Canada, October 1990.

5. D. J. Naus and C. B. Oland, *Structural Aging Program Sesquiannual Technical Progress Report for Period January 1, 1993, to June 30, 1994*, ORNL/NRC/LTR-94/21, Martin Marietta Energy Systems, Inc., Oak Ridge National Laboratory, Oak Ridge, Tennessee, September 1994 (draft).

6. D. J. Naus, *Report of Foreign Travel of D. J. Naus, March 8-15, 1994, Engineering Technology Division*, ORNL/FTR-4924, Martin Marietta Energy Systems, Inc., Oak Ridge National Laboratory, Oak Ridge, Tennessee, March 25, 1994.

7. D. J. Naus, *Report of Foreign Travel of D. J. Naus, May 23-28, 1994, Engineering Technology Division*, ORNL/FTR-4987, Martin Marietta Energy Systems, Inc., Oak Ridge National Laboratory, Oak Ridge, Tennessee, June 8, 1994.

8. D. J. Naus, "Overview of ORNL/NRC Programs Addressing Durability of Concrete Structures," *Workshop on Concrete Performance and Modeling for Low-Level Radioactive Waste Disposal*, National Institute of Standards and Technology, Gaithersburg, Maryland, February 2, 1994.

9. C. B. Oland, "Data and Information in a Concrete Materials Data Base," *Symposium on Integrated Knowledge Systems for High-Performance Construction Materials and Systems*, held at National Institute of Standards and Technology, Gaithersburg, Maryland, May 2, 1994.

10. D. J. Naus, "Structural Aging Program to Evaluate Continued Performance of Safety-Related Concrete Structures in Nuclear Power Plants," *BNES/ENS International Conference on Thermal Reactor Safety Assessment held at the Ramada Hotel*, Manchester, United Kingdom, May 23, 1994.

11. D. J. Naus, "The Structural Aging Program at Oak Ridge National Laboratory," presentation to Nuclear Electric Personnel and Associated Organizations, Berkeley Technology Center, Berkeley, Gloucestershire, United Kingdom, May 26, 1994.

12. D. J. Naus, "ORNL Structural Aging Program," Service Etudes et Projects Thermiques et Nuclaires, Electricité de France, Lyon, France, March 15, 1994.

13. C. B. Oland, *The Structural Materials Information Center and Its Potential Applications*, ORNL/NRC/LTR-92/8, Martin Marietta Energy Systems, Inc., Oak Ridge National Laboratory, Oak Ridge, Tennessee, May 1992.

14. *Mat.DB*, **Version 1.0**, ASM International, ASM/Center for Materials Data, Materials Park, Ohio, 1990.

15. *EnPlot*, **Version 2.0**, ASM International, ASM/Center for Materials Data, Materials Park, Ohio, 1989.

16. *Microsoft Windows*, Microsoft Corporation, One Microsoft Way, Redmond, Washington.

17. M. F. Marchbanks and C. B. Oland, *Considerations in the Formulation of a Customized Data Base for Structural Materials*, ORNL/NRC/LTR-94/20, Martin Marietta Energy Systems, Inc., Oak Ridge National Laboratory, Oak Ridge, Tennessee, July 1994 (draft).

18. C. B. Oland and D. J. Naus, *Summary of Materials contained in the Structural Materials Information Center*, ORNL/NRC/LTR-94/22, Martin Marietta Energy Systems, Inc., Oak Ridge National Laboratory, Oak Ridge, Tennessee, July 1994 (draft).

19. D. J. Naus, C. B. Oland, and B. R. Ellingwood, "Structural Aging Program Approach to Providing an Improved Basis for Aging Management of Safety-Related Concrete Structures," *Proceedings of United States Nuclear Regulatory Commission Twenty-First Water Reactor Safety Information Meeting held at Marriott Hotel*, Bethesda, Maryland, October 25-27, 1993.

20. *Section XI Rules for Inservice Inspection of Nuclear Power Plant Components*, American Society for Mechanical Engineers, New York, New York, 1983.

21. ACI Committee 201, "Guide for Making a Condition Survey of Concrete In-Service," pp. 905-918 in *Proceedings of Journal of American Concrete Institute*, 655(11), November 1968.

22. ACI Committee 207, "Practices for Evaluation of Concrete in Existing Massive Structures for Service Conditions," pp. 47-61 in *Concrete International*, 1(3), 1979.

23. ACI Committee 349, "Evaluation of Existing Nuclear Safety-Related Concrete Structures," *ACI 349.2R-93*, American Concrete Institute, Detroit, Michigan, 1993 (draft).

24. R. E. Weyers et al., "Concrete Deterioration Inspection System for Extending the Operating Life of Nuclear Power Plants Applied to Surry One," Charles E. via Department of Civil Engineering, Virginia Polytechnic Institute and State University, Blacksburg, Virginia, February 1988.

25. D. J. Naus, C. B. Oland, E. G. Arndt, B. Ellingwood, and Y. Mori, "An Overview of the ORNL/NRC Program to Address Aging of Concrete Structures in Nuclear Power Plants," pp. 327-329 in *Nuclear Engineering and Design*, 142, 1993.

26. Y. Mori and B. Ellingwood, "Maintaining Reliability of Concrete Structures I: Role of Inspection/Repair," pp. 824-845 in *Journal of Structural Engineering*, 120(3) American Society of Civil Engineers, New York, 1994.

27. Y. Mori and B. Ellingwood, "Maintaining Reliability of Concrete Structures II: Optimum Inspection/Repair Strategies," pp. 846-862 in *Journal of Structural Engineering*, 120(3) American Society of Civil Engineers, New York, 1994.

28. ACI Committee 318, *Building Code Requirements for Reinforced Concrete*, ACI Standard 318-71, American Concrete Institute, Detroit, Michigan, November 1971.

29. B. Ellingwood and T. V. Galambos, "Probability-Based Criteria for Structural Design," pp. 15-26 in *Structural Safety* 1(1), 1982.

30. B. Ellingwood and Y. Mori, "Probabilistic Methods for Condition Assessment and Life Prediction of Concrete Structures in Nuclear Power Plants," pp. 155-166 in *Nuclear Engineering and Design* 142, 1993.

31. F. P. Vecchio and M. P. Collins, "The Modified Compression-Field Theory for Reinforced Concrete Elements Subjected to Shear," Journal American Concrete Institute 83(2), pp. 219-231, March - April 1986.

32. A. E. Cardenas et al., "Design Provisions for Shear Walls," Journal American Concrete Institute 70(3), pp. 221-230, March 1973.

33. Y. Mori and B. Ellingwood, *Reliability Assessment of Degrading Concrete Shear Walls*, ORNL/NRC/LTR-94/6, (ORNL/Sub/93-SD684V), Subcontract 19X-SD684V with The Johns Hopkins University, Baltimore, Maryland), Martin Marietta Energy Systems, Inc., Oak Ridge National Laboratory, Oak Ridge, Tennessee, April 1994.

34. F. Barda, J. M. Hanson, and W. G. Corley, "Shear Strength of Low-Rise Walls with Boundary Element," in *Reinforced Concrete Structures in Seismic Zones*, ACI SP-53, American Concrete Institute, Detroit, Michigan, 1977.

35. I. Shiraishi, N. Shirai, T. Murakami, and K. Minami, "Macroscopic Models for R/C Shear Walls," pp. 271-280 in *Proceedings of Structural Congress*, Structural Design, Analysis, and Testing, ASCE, New York, 1989.

36. R. Shohara, N. Shirai, and H. Noguchi, "Verification of Macroscopic Models for R/C Walls," pp. 281-290 in *Proceedings of Structural Congress*, Structural Design, Analysis, and Testing, ASCE, 1989.

37. F. Watanabe and T. Ichinose, "Strength and Ductility Design of RC Members Subjected to Combined Bending and Shear," pp. 429-438 in *Concrete Shear in Earthquake*, Eds. T. C. C. Hsu and S. T. Mau, Elsevier Applied Science, New York, New York, 1992.

38. W. F. Chen and D. J. Han, *Plasticity for Structural Engineers*, Spring-Vartag, New York, 1988.

39. ACI Committee 349, *Code Requirements for Nuclear Safety Related Concrete Structures*, ACI Standard 349-76, American Concrete Institute, Detroit, Michigan, June 1976.

40. J. G. MacGregor, A. Mirza, and B. Ellingwood, "Statistical Analysis of Resistance of Reinforced and Prestressed Concrete Members," pp. 167-176 in *Journal of American Concrete Institute* 80(3), 1983.

41. G. W. Washa, J. C. Saemann, and S. M. Cramer, "Fifty-Year Properties of Concrete Made in 1937," pp. 367-371 in *ACI Matls Journal* 86(4), 1989.

42. Y. Mori, "Reliability-Based Condition Assessment and Life Prediction of Concrete Structures," thesis presented to The Johns Hopkins University, Baltimore, Maryland, in partial fulfillment of the requirements for the degree of Doctor of Philosophy, 1992.

43. H. Madsen, J. D. Sorenson, and R. Olesen, "Optimal Inspection Planning for Fatigue Damage of Offshore Structures," pp. 2099-2106 in *Proceedings of ICOSSAR '89*, Vol. III, ASCE, New York, 1989.

44. J. Yang, "Application of Reliability Methods to Fatigue, Quality Assurance, and Maintenance," pp. 3-18 in *Proceedings of ICOSSAR '93*, Vol. I, A. A. Balkema, Rotterdam, The Netherlands, 1994.

45. C. J. Hookham, *Structural Aging Assessment Methodology for Concrete Structures in Nuclear Power Plants*, ORNL/NRC/LTR-90/17, Martin Marietta Energy Systems, Inc., Oak Ridge National Laboratory, Oak Ridge, Tennessee, March 1991.

DYNAMIC BEHAVIOR OF ANCHORS IN CRACKED AND UNCRACKED CONCRETE: A PROGRESS REPORT

Milton Rodriguez[1], Yong-gang Zhang[1], Dieter Lotze[2],
Herman L. Graves III[3], and Richard E. Klingner[4]

ABSTRACT

In early 1993, the US Nuclear Regulatory Commission began a research program at The University of Texas at Austin, dealing with the dynamic behavior of anchors in cracked and uncracked concrete. In this paper, the progress of that research program is reviewed. The test program is summarized, and work performed to date is reviewed, with emphasis on the dynamic and static behavior of single tensile anchors in uncracked concrete. General conclusions from that work are discussed, and future plans are presented.

OBJECTIVES AND SCOPE OF THIS PAPER

The objectives of this paper are to describe the overall organization of this research program; to summarize the test program; and to review work performed to date, with emphasis on the dynamic and static behavior of single tensile anchors in uncracked concrete. General conclusions from that work will be discussed; and future plans will be presented.

BACKGROUND

As stated in the US Nuclear Regulatory Commission's original Request for Proposal, the overall objective of the research described in this paper is to verify, by testing, the adequacy of the assumption used in US nuclear power plant designs that the behavior and strength of anchor bolts

---

[1] Graduate Research Assistant, Department of Civil Engineering, The University of Texas, Austin, TX 78712

[2] Visiting Scholar, Department of Civil Engineering, The University of Texas, Austin, TX 78712

[3] Structural Engineer, US Nuclear Regulatory Commission, Washington, DC 20555

[4] Phil M. Ferguson Professor in Civil Engineering, The University of Texas, Austin, TX 78712

(cast-in-place, expansion and undercut) and their supporting concrete under seismic loads do not differ significantly from those for static conditions. That objective determined many of the research decisions that will be discussed in this paper.

At the start of the project, the researchers and the US Nuclear Regulatory Commission (NRC) agreed that the research should concentrate on the behavior, under dynamic loads, of anchors generally used in existing nuclear plants, particularly for equipment mounting. Based on information furnished by the NRC, it was agreed to test a particular wedge-type expansion anchor ("Expansion Anchor" and "Expansion Anchor II"), a particular undercut anchor ("Undercut Anchor 1"), and also some anchors placed in cored holes using cementitious grout ("Grouted Anchor"). Later in the testing program, other anchors were added ("Undercut Anchor 2" and "Sleeve Anchor").

OVERALL ORGANIZATION OF RESEARCH PROGRAM

The research program, with a scheduled duration of 3 years, comprises 5 tasks:

Task 1: Static and Dynamic Behavior of Single Tensile Anchors
Task 2: Static and Dynamic Behavior of Multiple Tensile Anchors
Task 3: Static and Dynamic Behavior of Near-Edge Anchors
Task 4: Static and Dynamic Behavior of Multiple-Anchor Connections
Task 5: Submission of Final Report

At the end of each task, an interim report is to be submitted to the NRC. At the present time, work is essentially complete on the first and second tasks, and is beginning on the third task. Each task is divided into sub-tasks. The sub-tasks comprising Tasks 1 and 2 are discussed in more detail in later sections of this paper.

MATERIALS, EQUIPMENT, AND TEST METHODS

Concrete Strength and Characteristics

Preliminary NRC data indicated that most concrete found in existing nuclear plants has a compressive strength between 4000 and 5500 psi. Some may be as weak as 3000 psi. The testing program therefore emphasizes concrete with compressive strengths between 4000 and 5500 psi, and includes some tests in 3000-psi concrete. Analytical research (studies with nonlinear fracture-type finite elements) will be verified using test results and then used to extend the test results to other concrete strengths. Concrete with soft limestone aggregate generally

represents the most conservative case. However, some concrete with river gravel aggregate of medium hardness is also being used.

Anchors

Based on surveys of existing anchors in nuclear applications, the NRC was primarily interested in documenting the behavior of selected wedge-type expansion anchors, of selected undercut anchors, and also of anchors in cementitious grout. The testing program for Tasks 1 and 2 originally emphasized one wedge-type expansion anchor (referred to here as "Expansion Anchor"), with some tests on one undercut anchor ("U/C Anchor 1"), and other tests on anchors in one type of cementitious grout. As described later in this paper, several anchors were added: a variant on the expansion anchor ("Expansion Anchor II"); another undercut anchor ("U/C Anchor 2"); and a heavy-duty sleeve-type expansion anchor ("Sleeve Anchor 1"). Based on current use in nuclear applications, it was decided to test anchors ranging in diameter from 3/8 to 1 inch, with emphasis on 3/4-inch diameter. In September 1993, the technical community on anchorage to concrete was advised in general terms of the research plans by means of a letter disseminated to ACI Committees 349 (Nuclear Structures) and 355 (Anchorage to Concrete).

Embedment Depths

For nuclear applications, the overall anchor design objective is to have failure governed by yield and fracture of anchor steel. Because the dynamic behavior of the anchor steel itself is relatively well understood, in Tasks 1 and 2 of this testing program the embedments were shallow enough so that behavior would be governed by pull-through (anchor through sleeve), pullout (anchor through concrete), or concrete cone breakout. Information on dynamic capacity as governed by those failure modes can be used to ensure ductile behavior in later phases of the testing program, and also in practice.

Anchor Installation

All anchors were installed according to manufacturer's instructions. To duplicate the effects of loss of prestress due to concrete relaxation, anchors were torqued to manufacturer's specifications, and then loosened and re-torqued to half the specified value.

Loading

Most static loads in Tasks 1 and 2 were applied using a hand-controlled electrical pump, applying displacement at a constant rate. For dynamic loads, two quite distinct loading patterns were used. For the initial dynamic testing covered in Tasks 1 and 2, it was desired to find the effect of earthquake-type dynamic loading on anchor capacity as governed by factors other than steel failure. Equipment response to strong earthquake depends on the earthquake, and also on the dynamic characteristics of the equipment. Unlike fatigue loading, earthquake response usually consists of relatively few reversed cycles of load, at frequencies of 3 Hz or less. It was initially considered appropriate to subject anchors to such pulses. However, for purposes of this test program, it was necessary to load the anchors dynamically to failure, as governed by mechanisms other than steel yield and fracture.

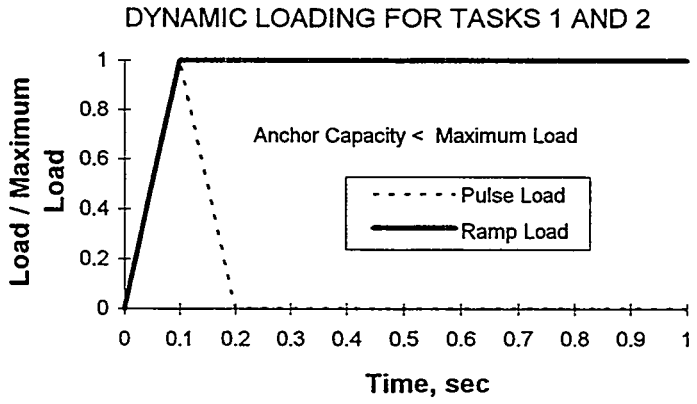

Figure 1 Ramp-Type Dynamic Loading Used in Tasks 1 and 2

Previous research (Collins, 1989) had shown that anchors loaded by triangular pulses would not fail under low-cycle fatigue unless the load level exceeded the static failure load. It would therefore be necessary to subject the anchors to a dynamic, triangular load pulse whose magnitude would need to exceed the anchor capacity (which would not be known in advance). Under these circumstances, it was reasoned that it would make no difference whether the pulse were a triangle or simply an increasing ramp load, since the test would be ended in any event by anchor failure. As a result, the dynamic load selected for Tasks 1 and 2 was a ramp load to failure. As shown in Figure 1, the rise time of this load (about 0.1 seconds) was set to correspond to that of typical earthquake response. For subsequent phases of the testing program, a reversed cyclic loading history representing earthquake response will be used.

Reinforcement

Most specimens were designed without reinforcement in the area that would be affected by the concrete breakout cone. Specimens in series labeled "reinforced concrete" had a curtain of #8 bars spaced at 8 inches in each direction, placed with 1-1/2 inch cover, and intended to simulate reinforcement in a heavily reinforced wall.

Procedures Used for Cracked Concrete Testing

Because this investigation is concerned with seismic behavior, it was necessary to investigate the effects of concrete cracking on anchor behavior under dynamic loads. For this purpose, the (UEAtc, 1992) criterion of a crack with a surface width of 0.3 mm was selected. Several procedures are now accepted for imposing this type of crack:

1) A large block of concrete can be subjected to tension, producing cracks. This procedure requires a reaction frame, and the resulting cracks are not uniform in width.

2) A block of concrete can be cast with metal plates in it. These act as crack formers when the block is placed in tension. This procedure is relatively complex, and only permits cracks to form where the plates are placed.

3) Cracks can be formed using split tubes placed on both sides of the planned anchor location. The split tubes are expanded by wedges to open the crack to the desired width. This procedure is relatively simple, and has the additional advantage of permitting cracks to be located anywhere on the surface of the concrete.

It was decided to use third method, with the following test sequence:

- The crack was started using wedges, and was reduced to hairline width.
- The anchor was installed at the location of the crack.
- The crack was widened to 0.3 mm at the surface.
- The anchor was tested. The crack width was monitored, but was not controlled.

DETAILED INFORMATION ON TASK 1 TESTING

Original Outline for Task 1 Testing (August 1993)

The original outline for Task 1 testing (August 1993) was as follows:

1) Static and Dynamic Behavior of Single Tensile Anchors
   a) Static tensile tests of single anchors in unreinforced concrete
   b) Dynamic tensile tests of single anchors in unreinforced concrete
   c) Static tensile tests of single anchors in reinforced concrete
   d) Dynamic tensile tests of single anchors in reinforced concrete
   e) Static tensile tests of single anchors in unreinforced, cracked concrete
   f) Dynamic tensile tests of single anchors in unreinforced, cracked concrete
   g) Static tensile tests of single anchors in reinforced, cracked concrete

h) Dynamic tensile tests of single anchors in reinforced, cracked concrete

Because the original outline for Task 1 was superseded in several respects (as explained in the next sections), the original test matrix is not given here. The final test matrix is given in Table 1.

Comparison of Original and Current Expansion Anchors

It had been known from the beginning of the test program that the wedge-type Expansion Anchor emphasized in the original Task 1 testing program was no longer commercially available in its original form (that found in many nuclear power plants). The current version of the anchor (identified here as Expansion Anchor II) was thought to behave quite differently from the previous version.

As a result, the static and dynamic performance of the original Expansion Anchor was compared with that of the current Expansion Anchor II. Efforts were made to select embedment depths such that all anchors would experience cone breakout failure.

Results obtained from comparison testing showed that 3/4-inch diameter original Expansion Anchors, installed at embedments equal to or greater than the manufacturer's standard embedment of 4-3/4 inches, failed by pull-through of the anchor rather than by concrete cone break-out. Because the Expansion Anchor II has improved performance in this regard, it was concluded that test results with the Expansion Anchor II at those embedments should not be assumed to apply to the original Expansion Anchor.

According to NRC estimates, more than three-quarters of the original Expansion Anchors were installed at embedments equal to or greater than the manufacturer's standard embedment. Therefore, in order to satisfy the specific objectives of this research project, it was believed necessary to conduct at least some static and dynamic tests on original Expansion Anchors, installed at the manufacturer's standard embedment. If those tests indicated that the pull-through capacity of the original Expansion Anchors was not decreased under dynamic loading conditions, then subsequent tests would be conducted at the smaller embedment depths associated with concrete cone breakout, down to the manufacturer's minimum embedment of 3-1/2 inches. At those embedment depths, the behavior of the Expansion Anchor II was expected to be the same as that of the original Expansion Anchor. This would also be verified by test.

Verification of Behavioral Differences between Original Expansion Anchor and Expansion Anchor II (December 1993)

As part of Series 0 of Task 1 (see Table 1 below), 20 static comparison tests were carried out using the original Expansion Anchor and the Expansion Anchor II, both 3/4-inch diameter, and embedded in 4700-psi limestone aggregate concrete. In each case, two embedment depths

were used: the manufacturer's standard embedment of 4-3/4 inches, and the minimum embedment of 3-1/2 inches. All measured capacities were normalized by the square root of the measured compressive strength of the concrete used.

Results showed that under static load, and using the standard embedment, Expansion Anchor II does not fail in the same way as the original Expansion Anchor. At the minimum embedment, the Expansion Anchor II does fail in the same way as the original Expansion Anchor, but at a higher load and a much smaller displacement. The reason for this increased capacity is probably the improvement in the wedge mechanism of the Expansion Anchor II, which significantly reduces pull-through.

Based on these results, it was clear that subsequent test results with Expansion Anchor II could not be assumed to apply to the original Expansion Anchor. It was expected that this would be particularly true in cracked concrete. Given the availability of original Expansion Anchors, it was proposed to conduct 20 additional dynamic comparison tests in cracked concrete, and then to conduct no further tests with the original Expansion Anchor.

Results would then be available from about 60 tests involving direct comparison of the two anchor types, including 30 tests with the original Expansion Anchor. Using those tests, limited conclusions could be derived regarding the performance of the original Expansion Anchor under dynamic loads, including the effects of cracked concrete. Those results would satisfy the minimum objectives of this project with respect to that type of existing anchor. However, it would not be possible to include the original Expansion Anchor in the other phases of the testing program, due to the lack of anchors. As a result, the rest of the test program would apply only to the Expansion Anchor II and to undercut and grouted anchors.

Extension of Task 1 Testing to Include Other Anchor Types

Because of the above findings, and because of some of the results obtained with wedge-type expansion anchors in the Task 1 testing, it was decided to expand the research objectives to include the performance of modern anchors designed specifically to function in cracked concrete. A torque-controlled sleeve anchor with follow-up expansion capability ("Sleeve Anchor") was added to the testing program, as was another undercut anchor ("Undercut Anchor 2").

Final Task 1 Test Matrix (250 Tests)

The final Task 1 test matrix, modified as discussed above, and comprising about 250 tests, is shown in Table 1:

Table 1: Final Test Matrix for Task 1

SERIES	DESCRIPTION	CONCRETE STRENGTH	ANCHORS TESTED	NO. OF ANCHORS	NO. OF TESTS
1-0	static comparison tests of Exp Anch and Exp Anch II at standard embedment	4700 psi limestone	Exp Anch, 3/4	5	5
			Exp Anch II, 3/4	5	5
	dynamic comparison tests of Exp Anch and Exp Anch II at standard embedment	4700 psi limestone	Exp Anch, 3/4	5	5
			Exp Anch II, 3/4	5	5
	static comparison tests of Exp Anch and Exp Anch II at minimum embedment	4700 psi limestone	Exp Anch, 3/4	5	5
			Exp Anch II, 3/4	5	5
	dynamic comparison tests of Exp Anch and Exp Anch II at minimum embedment	4700 psi limestone	Exp Anch, 3/4	5	5
			Exp Anch II, 3/4	5	5
1-1	Static tensile tests of single anchors in unreinforced concrete	4700 psi limestone	Exp Anch II 3/8, 3/4	10	10
		3000 psi limestone	Exp Anch II 3/4	5	5
		4700 psi river gravel	Exp Anch II 3/4	5	5
		3000 psi river gravel	Exp Anch II 3/4	5	5
		4700 psi limestone	U/C Anch 1 3/4	5	5
		4700 psi limestone	grouted 3/4	5	5
1-2	Dynamic tensile tests of single anchors in	4700 psi limestone	Exp Anch II 3/8, 3/4	10	10

	unreinforced concrete				
		3000 psi limestone	Exp Anch II 3/4	5	5
		4700 psi river gravel	Exp Anch II 3/4	5	5
		3000 psi river gravel	Exp Anch II 3/4	5	5
		4700 psi limestone	U/C Anch 1 3/4	5	5
		4700 psi limestone	grouted 3/4	5	5
1-3	Static tensile tests of single anchors in reinforced concrete	4700 psi limestone	Exp Anch II 3/4	5	5
1-4	Dynamic tensile tests of single anchors in reinforced concrete	4700 psi limestone	Exp Anch II 3/4	5	5
1-5	Additional static tensile tests of single anchors in unreinforced concrete	4700 psi limestone	U/C Anch 1 3/8	5	5
		4700 psi limestone	U/C Anch 2 3/4	5	5
		4700 psi limestone	Sleeve Anch M10, M20	10	10
		4700 psi river gravel	U/C Anch 1 3/4	5	5
		3000 psi limestone	U/C Anch 1 3/4	5	5
1-6	Additional dynamic tensile tests of single anchors in unreinforced concrete	4700 psi limestone	U/C Anch 1 3/8	5	5
		4700 psi limestone	U/C Anch 2 3/4	5	5
		4700 psi limestone	Sleeve Anch M10, M20	10	10

		4700 psi river gravel	U/C Anch 1 3/4	5	5
		3000 psi limestone	U/C Anch 1 3/4	5	5
1-7	Static tensile tests of single anchors in unreinforced, cracked concrete	4700 psi limestone	Exp Anch II 3/4	5	5
		4700 psi limestone	U/C Anch 1 3/8, 3/4	10	10
		4700 psi limestone	U/C Anch 2 3/4	5	5
		4700 psi limestone	Sleeve Anch M10, M20	10	10
		4700 psi limestone	Grouted 3/4	5	5
1-8	Dynamic tensile tests of single anchors in unreinforced, cracked concrete	4700 psi limestone	Exp Anch II 3/4	5	5
		4700 psi limestone	U/C Anch 1 3/8, 3/4	10	10
		4700 psi limestone	U/C Anch 2 3/4	5	5
		4700 psi limestone	Sleeve Anch M10, M20	10	10
		4700 psi limestone	Grouted 3/4	5	5

TYPICAL RESULTS FROM STATIC AND DYNAMIC TENSILE TESTS ON WEDGE-TYPE EXPANSION ANCHORS IN UNCRACKED CONCRETE (JANUARY 1994)

Effect of Embedment Depth, Concrete Strength, and Aggregate Type on Tensile Capacity of Expansion Anchors in Uncracked Concrete

Figure 2 shows the tensile capacities (normalized by $\sqrt{f_c}\ h_e^{1.5}$), for Expansion Anchor II, for different concrete strengths and aggregate types. Each bar represents the average of 5 tests. The figure shows that as embedment depth decreases, normalized capacity increases. The reason for this is that at deeper embedments, anchor capacity (not normalized) increases, and the anchor is more prone to pull-through and pull-out. Such anchors slip until the embedment depth is small enough to produce a cone breakout, at an embedment depth considerably smaller than the original value. Because capacity is normalized using the original embedment, the normalized capacity is artificially small. The graph also suggests that normalized tensile capacity is not significantly affected by concrete compressive strength or aggregate type. These points are discussed in more detail below.

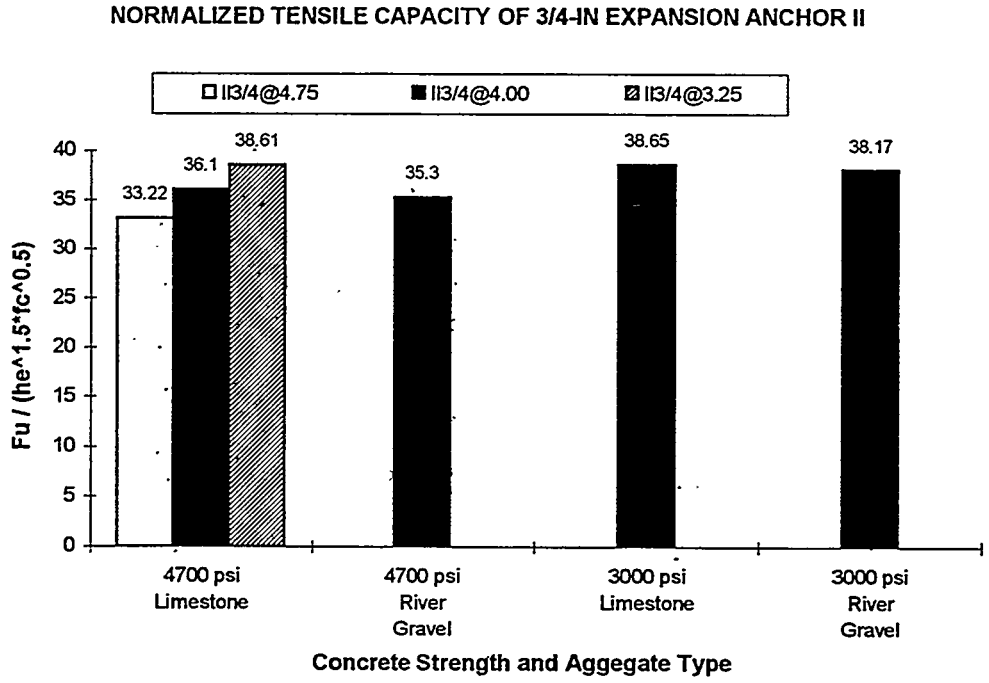

Figure 2 Effect of Embedment Depth, Concrete Strength, and Aggregate Type on Cone Breakout Capacity of Expansion Anchor II

Effect of Loading Rate (Static versus Dynamic) on Tensile Capacity of Wedge-Type Expansion Anchors

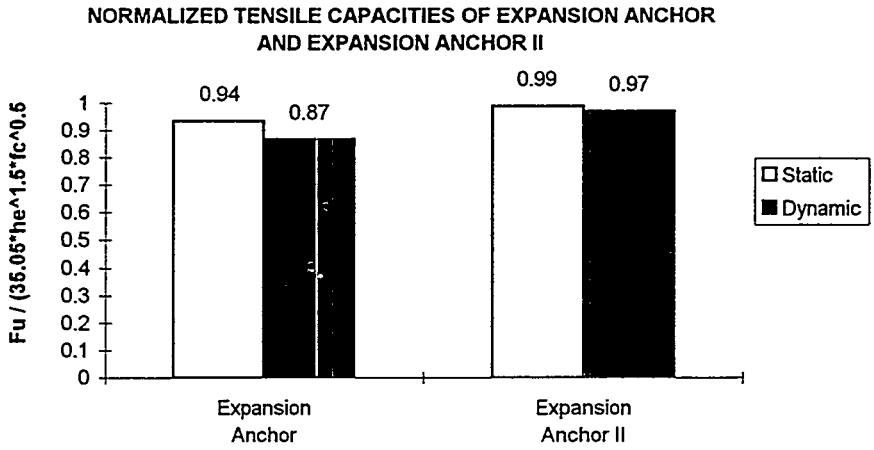

Figure 3 Effect of Loading Rate (Static versus Dynamic) on Tensile Capacity of Original Expansion Anchor and Expansion Anchor II

Figure 3 shows the tensile capacity, normalized by ($35.05\ \sqrt{f_c}\ h_e^{1.5}$), for the original Expansion Anchors and for Expansion Anchor II. The figure shows that the tensile capacity of the original Expansion Anchor is reduced by about 10% under dynamic loading. The tensile capacity of the Expansion Anchor II is about the same. Results are obtained from all concrete strengths, aggregate types, anchor diameters, and embedment depths.

Effect of Loading Rate (Static versus Dynamic) on Failure Mode of Wedge-Type Expansion Anchors

Figure 4 shows the tensile capacity (normalized by $\sqrt{f_c}\ h_e^{1.5}$), for Expansion Anchor and Expansion Anchor II, all 3/4-inch diameter, as a function of embedment depth. Nominal concrete strength was constant at 4700 psi, and limestone aggregate was used.

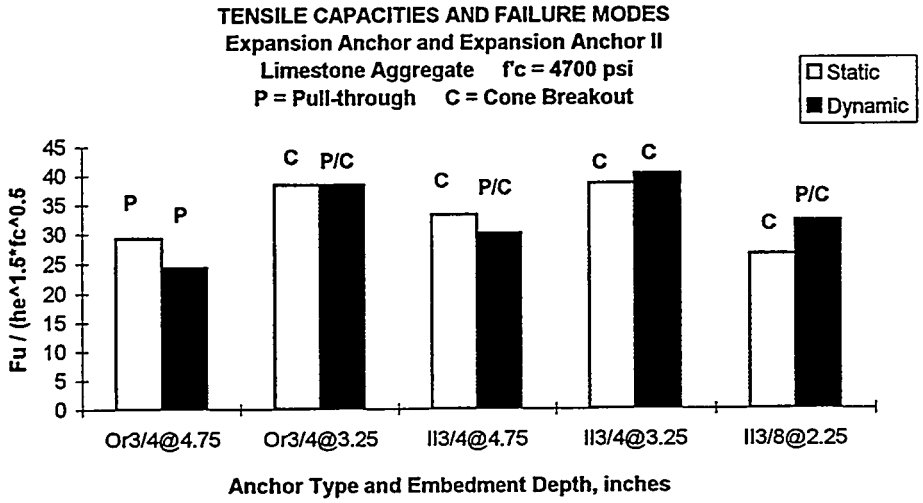

Figure 4 Effect of Loading Rate (Static versus Dynamic) on Failure Mode of Wedge-Type Expansion Anchors

The graph shows that at an embedment depth of 4.75 inches, the original Expansion Anchor fails by pull-through under static and dynamic loads. Dynamic capacity is less than static capacity. As the embedment depth is decreased to 3.25 inches, the statically loaded anchor fails by cone breakout. While the capacity of the dynamically loaded anchor is about the same, the failure mode for some of the 5 replicates is pull-through. Expansion Anchor II has a greater tendency toward cone failure rather than pull-through. In general, the capacity of both Expansion Anchors is slightly less under dynamic load than under static load.

Effect of Loading Rate (Static versus Dynamic) on Tensile Cone Breakout Capacity of Undercut and Grouted Anchors

Figure 5 shows the effect of loading rate on the tensile capacity, as governed by concrete cone breakout, of the Undercut 1 and the Grouted Anchor. All capacities are normalized by $\sqrt{f_c}\, h_e^{1.5}$. Results show an increase in normalized capacity of about 30%.

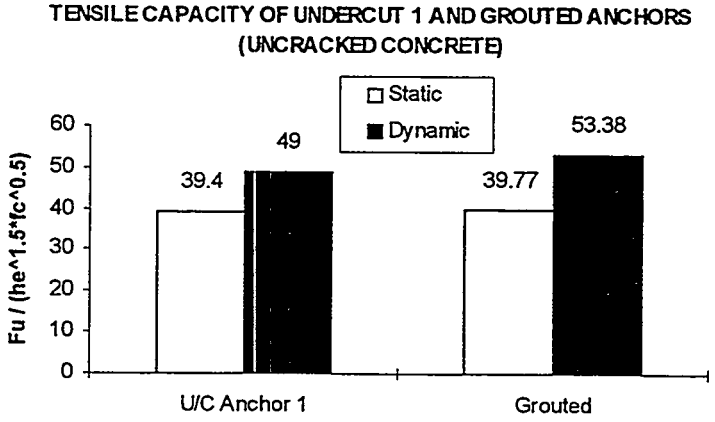

Figure 5 Effect of Loading Rate (Static versus Dynamic) on Tensile Cone Breakout Capacity of Undercut 1 and Grouted Anchors

Effect of Reinforcement on Tensile Capacity

Figure 6 shows the effect of reinforcement on the normalized tensile capacity of anchors loaded statically. All capacities are normalized by $\sqrt{f_c}\, h_e^{1.5}$. All anchors and all concrete strengths are included. Effects of reinforcement are seen to be negligible. This observation applies to reinforcement placed parallel to the free surface of the specimen, perpendicular to the axis of the anchor.

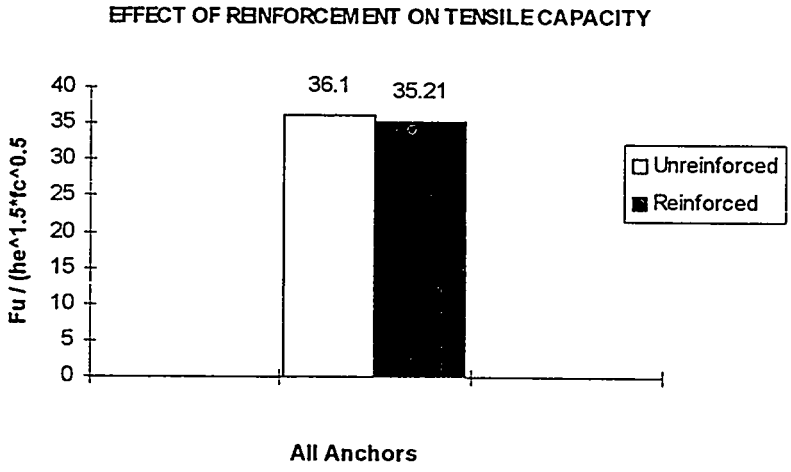

Figure 6 Effect of Reinforcement on Tensile Cone Breakout Resistance of All Anchors

Effect of Aggregate Type on Tensile Capacity

Figure 7 shows the effect of aggregate type on the normalized tensile capacity of all anchors. For both concrete strengths, changing from soft limestone aggregate to medium-hard river gravel aggregate has no significant effect on tensile capacity.

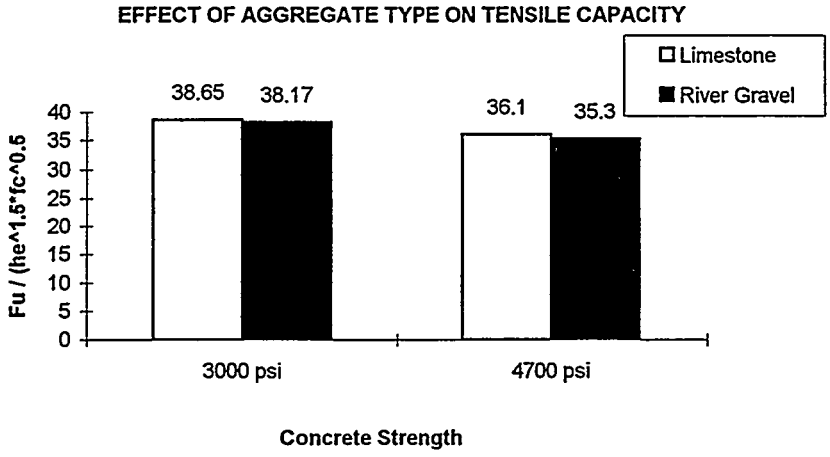

Figure 7 Effect of Aggregate Type on Normalized Tensile Capacity of All Anchors

PRELIMINARY CONCLUSIONS FROM STATIC AND DYNAMIC TESTS ON WEDGE ANCHORS IN UNCRACKED CONCRETE (JANUARY 1994)

The following conclusions were presented in general form at meetings of ACI Committees 349 (Nuclear Structures) and 355 (Anchorage to Concrete) in March 1994:

1) Wedge-type expansion anchors have approximately the same capacity under dynamic load, as under static load. However, this average is deceptive, because it is results from combining two distinct failure modes.

   a) For wedge-type expansion anchors, if failure is by concrete cone breakout, dynamic capacity exceeds static capacity. Concrete cone breakout capacity under static loads is predicted with a coefficient of variation of about 10%, by the CC Method (formerly known as the Kappa Method) (CEB, 1991) ($P = 35 \sqrt{f_c}\, h_e^{1.5}$). The multiplicative constant (ideally, 35) increases as the effective depth decreases. For wedge anchors, the effective embedment h_e is measured from the free surface of the concrete to the point of the clip in contact with the concrete. Because of pull-through of the mandrel, estimation of the effective embedment when the cone is produced is difficult for wedge anchors.

   b) For wedge-type expansion anchors, if failure is by pull-through, dynamic capacity is less than static capacity.

2) Dynamic loading worsens the performance of wedge-type expansion anchors. It increases the tendency for failure by pull-through and pull-out, rather than by concrete cone breakout. Evidently, dynamic loading decreases the coefficient of friction between the cone and the clip (steel to steel), and between the clip and the concrete (steel to concrete).

3) At embedments less than those required to produce steel failure, grouted anchors and undercut anchors fail by concrete cone breakout, without pullout. The concrete cone breakout capacity of grouted anchors and of undercut anchors is predicted with a coefficient of variation of less than 10%, by the CC Method (CEB, 1991) ($P= 42 \sqrt{f_c}\, h_e^{1.5}$).

4) Dynamic loading increases the capacity of grouted anchors and undercut anchors. Under dynamic loads, the concrete cone breakout capacity of grouted anchors and undercut anchors is about 30% greater than the capacity under static loads.

5) For all anchors tested so far, performance in concrete with limestone aggregate is not much different from performance in concrete with river gravel aggregate.

6) For all anchors tested so far, heavy reinforcement (#8 bars @ 8 inches, 1-1/2 inch cover) placed parallel to the surface of the concrete has no appreciable effect on performance.

SUCCESSFUL START OF CRACKED CONCRETE TESTING (MARCH 1994)

In March 1994, cracked-concrete testing was successfully begun, using the procedure discussed above. Implementation of this testing was facilitated through the loan of equipment and experienced technicians from the Hilti Corporation. Results from cracked concrete testing will be presented in the near future.

DETAILED INFORMATION ON TASK 2 TESTING

Original Outline for Task 2 Testing (August 1993)

The original outline for Task 2 testing (August 1993) was as follows:

1) Static and Dynamic Behavior of Multiple Anchors
   a) Static Tensile Tests on Multiple Anchors
   b) Dynamic Tensile Tests on Multiple Anchors

c) Overlapping Cone versus Linear Interpolation Approach
d) Static Tensile Tests of Multiple Anchors in Reinforced Concrete
e) Dynamic Tensile Tests of Multiple Anchors in Reinforced Concrete
f) Submission of Preliminary Task 2 Report to NRC

Modifications to Original Task 2 Testing

The above Task 2 testing program had been based on the original project proposal, prepared in 1992. Since that time, the overlapping cone versus linear interpolation issue has been significantly clarified. It was believed possible to use the linear interpolation procedure with little additional technical justification. It was also proposed to eliminate the reinforced concrete tests, since Task 1 testing had shown no significant influence of reinforcement.

It was proposed that in addition to a reduced number of multiple-anchor tests, the rest of Task 2 could be used to conduct a series of single-anchor tests aimed at filling in the gaps in our knowledge of the basic load-deflection behavior of ductile anchors loaded in pure tension (already almost done), pure shear (already almost done), and combined tension and shear (not well known). This information would be useful to calibrate engineering models of load-deflection behavior of single anchors. Those models are necessary to predict the behavior of complex connections, and to estimate the design requirements for ductile behavior in such connections.

Based on the above information, in March 1994 the following revised test matrix was approved for Task 2:

Table 2: Final Test Matrix for Task 2 (223 Anchors)

SERIES	DESCRIPTION	CONCRETE STRENGTH	ANCHORS TESTED	NO. OF ANCHORS	NO. OF TESTS
2-1	Static tensile tests on sets of two anchors in unreinforced, uncracked concrete, spaced at 1.5 and 2.5 times the embedment	4700 psi limestone	U/C Anch 1 3/4	20	10
		4700 psi limestone	Sleeve Anch 3/4	20	10
2-2	Dynamic tensile tests on sets of two anchors in unreinforced, uncracked	4700 psi limestone	U/C Anch 1 3/4	20	20

	concrete, spaced at 1.5 and 2.5 times the embedment				
		4700 psi limestone	Sleeve Anch 3/4	20	20
2-3	Basic load displacement behavior of single anchors under tensile, shear and oblique loading, failure mode: steel	4700 psi limestone	U/C Anch 1 5/8	15	15
		3000 psi limestone	U/C Anch 1 5/8	20	20
		4700 psi limestone	Sleeve Anch 5/8	20	20
		4700 psi limestone	U/C Anch 1 3/8	20	20
2-4	Basic load displacement behavior of single anchors under tensile, shear and oblique loading, failure mode: concrete	4700 psi limestone	U/C Anch 1 5/8	20	20
2-5	Static shear tests sets of two anchors in unreinforced, uncracked concrete, 6 in and 12 in eccentricity of the shear load, failure mode: steel	4700 psi limestone	Sleeve Anch 5/8	12	6
		4700 psi limestone	U/C Anch 1 5/8	12	6
		4700 psi limestone	U/C Anch 1 3/8	12	6
2-6	Static shear tests sets of two anchors in unreinforced, uncracked concrete, 6 in and 12 in eccentricity of the shear load, failure mode: concrete	4700 psi limestone	U/C Anch 1 5/8	12	6

The above test matrix included two series (Series 2-1 and 2-2) intended to fulfill the original objective of resolving the cone-versus-CC Method controversy, but now with emphasis on dynamic loads only. It also contained several test series (Series 2-3, 2-4, and 2-5) intended to investigate the basic load-deflection behavior of deeply embedded anchors for use in developing computer programs for predicting the response of multiple-anchor connections. Finally, it contained one test series at shallower embedments (Series 2-6), intended to help in estimating the behavior of existing anchors designed under previous assumptions, such as the 45-degree cone. The revised Task 2 test matrix involves 223 anchors.

Results from Task 2 Testing

At the present time, results from Task 2 testing are being reviewed by the researchers and by the Nuclear Regulatory Commission. They will be discussed in generic form at technical committee meetings associated with anchorage, and will be released in detailed form as soon as possible.

ANALYTICAL WORK TO DATE

At the present time, analytical work is proceeding from three different viewpoints:

- Work is continuing on smeared-cracking models to predict the load-displacement behavior of single anchors far from free edges. Reasonable correspondence has been obtained between analytical load-displacement predictions, and experimental results.

- Work has begun on discrete-cracking models. Results will be compared with those from smeared-cracking models.

- Work has begun on models intended to predict the overall load-displacement behavior of anchors loaded in combinations of axial force and shear. These will be used to predict the behavior of multiple-anchor connections with complex loading conditions.

Analytical results will be presented in the near future.

ACKNOWLEDGMENTS

The work described here is sponsored by the US Nuclear Regulatory Commission under Contract No. NRC-03-92-025 ("Anchor Bolt Behavior and Strength during Earthquakes"). The

Contract is administered by the Commission's Office of Research, and the Technical Contact is Herman L. Graves III.

REFERENCES

(CEB, 1989): "Fastenings to Reinforced Concrete and Masonry Structures: State-of-the-Art Report," Comite Euro-International du Beton, Bulletin D'Information Nos. 206 and 207, August 1991.

(Collins, 1989): Collins, D. M., Cook, R. A., Klingner, R. E. and Polyzois, D., "Load-Deflection Behavior of Cast-in-Place and Retrofit Concrete Anchors Subjected to Static, Fatigue, and Impact Tensile Loads," Research Report CTR 1126-1, Center for Transportation Research, The University of Texas at Austin, February 1989.

(UEAtc, 1992); European Union of Agrément, UEAtc Technical Guide on Anchors for Use in Cracked and Non-cracked Concrete, M.O.A.T. No. 49, London, 1992.

UNDERSTANDING SEISMIC DESIGN CRITERIA FOR JAPANESE NUCLEAR POWER PLANTS

Y.J. Park and C.H. Hofmayer
Brookhaven National Laboratory
Upton, Long Island, New York 11973

J.F. Costello
U.S. Nuclear Regulatory Commission
Washington, D.C. 20555

ABSTRACT

This paper summarizes the results of recent survey studies on the seismic design practice for nuclear power plants in Japan. The seismic design codes and standards for both nuclear as well as non-nuclear structures have been reviewed and summarized. Some key documents for understanding Japanese seismic design criteria are also listed with brief descriptions. The paper highlights the design criteria to determine the seismic demand and component capacity in comparison with U.S. criteria, the background studies which have led to the current Japanese design criteria, and a survey of current research activities. More detailed technical descriptions are presented on the development of Japanese shear wall equations, design requirements for containment structures, and ductility requirements.

INTRODUCTION

As part of the USNRC efforts to understand Japanese earthquake engineering practice, a publication by the Japan Electric Association entitled JEAG 4601-1987 (Ref. [1]), "Technical Guidelines for Aseismic Design of Nuclear Power Plants", was translated and recently published as NUREG/CR-6241 (Ref. [2]). The guidelines, which contain approximately 900 pages of technical material, provide a detailed description of the current Japanese seismic design methods, and can be considered to be a key document in understanding the seismic design criteria and practice for Japanese nuclear power plants.

In addition to the JEAG document, a large number of related documents published by the Ministry of International Trade and Industry (MITI) and the Architectural Institute of Japan (AIJ) have been reviewed to understand the seismic design criteria for various parts of nuclear power plants in Japan.

As a result of the survey studies, it was found that the Japanese design practice generally follows the ASME codes in designing components made of metallic materials, e.g., piping and vessels. However, differences between U.S. and Japanese practices have been found regarding the seismic design of concrete structures, particularly in shear wall design criteria.

This paper is intended to provide U.S. engineers with an overview of the current seismic design practice of nuclear power plants in Japan in some detail. The background studies for key design criteria for reactor buildings and containment structures are described based on the information collected in a recent survey.

CODES AND STANDARDS

Many of the design formulas for reactor buildings and containment structures have been adopted from non-nuclear standards with or without modifications. In the following, both non-nuclear and nuclear design codes and standards related to the seismic design of nuclear power plants are outlined.

The basic design requirements for non-nuclear building structures are defined in orders by the Ministry of Construction (MOC) (Ref [3]). The detailed design requirements, similar to the ASME and ACI codes, are provided by the following series of AIJ standards:

- Standard for Structural Calculation of Reinforced Concrete Structures, 1991.....also known as "RC-Standard" (Ref. [4]).
- Design Standard for Steel Structures, 1973.....also known as "Steel-Standard" (Ref. [5]).
- Standard for Structural Calculation of Steel Reinforced Concrete Structures, 1987 .....also known as "SRC-Standard" (Ref. [6]).
- Design Guidelines for Foundation Structures, 1988.....also known as "Foundation Guidelines" (Ref. [7]).

The above AIJ standards are used primarily for the traditional allowable stress design required for the seismic design against moderate earthquakes. For the ultimate strength design, or for relatively new design approaches, such as base isolation systems, a series of AIJ "Guidelines" and "Recommendations" are available, e.g.,

- Design Guidelines for Earthquake Resistant Reinforced Concrete Buildings Based on Ultimate Strength Concept, 1990 (Ref. [8]).
- Design Guidelines for Base-Isolated Buildings, 1989 (Ref. [9]).

For the design/construction standards of nuclear facilities, the Ministry of International Trade and Industry (MITI) is the responsible governmental body. The design of nuclear facilities/equipment is based on the following MITI Orders and Notifications:

- MITI Order No. 62, "Technical Standards for Nuclear Power Plant Facilities", 1989 (Ref. [10]).
- MITI Notification No. 501, "Technical Standards for Structural Design of Nuclear Power Plant Equipment", 1992 (Ref. [11]).
- MITI Notification No. 452, "Technical Standards for Structural Design of Concrete Containment Structures of Nuclear Power Plant Facilities", 1990 (Ref. [12]).

In addition, the basic design requirements for the seismic design of nuclear facilities are defined in the following guide:

- "Regulatory Guide for Aseismic Design of Nuclear Power Reactor Facilities", 1981, Japan Atomic Energy Commission (Ref. [13]).

The AIJ has also prepared the following recommendations:

- Recommendations for Structural Design of Reactor Buildings, 1988 (Ref. [14]).
- Recommendations for Structural Design of Nuclear Reactor Containment Structures, 1978 (Ref. [15]).

SEISMIC REQUIREMENTS BY MOC

One significant feature of the Japanese seismic codes by the MOC is the dual requirement that buildings should be evaluated both for moderate and severe earthquakes, as summarized below. For a moderate earthquake (basic seismic coefficient is C=0.2), conventional allowable stress design is performed, which is similar to the UBC design requirements. However, for a severe earthquake (seismic force is 1.0g in terms of 5% damped linear response), ultimate strength design should be performed which requires some type of nonlinear analysis to identify the failure mechanism of a building and the ductility requirements of components.

Earthquake	Base Coefficient	Analysis	Component Evaluation
Moderate	C = 0.2	Linear	Short-Term Allowable*
Severe	C = 1.0	Nonlinear	Ultimate Strength

* 2/3 f'_c for concrete, and yielding for steel.

In addition to the above basic seismic load requirements, limitations on the eccentricity and story drift (less than 1/200 for C=0.20) are imposed on each story. The lateral seismic force, Q_i, is defined as,

$$Q_i = D_s \cdot F_{es} \cdot R_t \cdot A_i \cdot Z \cdot C \cdot W_i \qquad (1)$$

where

- D_s = reduction factor due to ductility ($\approx 1/\sqrt{2\mu - 1}$; 0.3 for ductile frame, 0.5 for shear wall construction).
- F_{es} = penalty factor due to eccentricity (1.0 for no eccentricity).
- R_t = spectral shape (function of building vibration frequency).
- A_i = lateral shear distribution factor (function of story number, i).
- Z = Zone coefficient.
- C = 0.2 for moderate earthquake, = 1.0 for severe earthquake.
- W_i = weight of building above the i-th story.

OVERVIEW OF DESIGN CRITERIA FOR NPP

The seismic requirements of nuclear power facilities are determined according to the importance classification, As, A, B and C, as listed in Table 1 (Ref. [2]).

Table 1. Seismic Requirements

	Aseismic Importance Classification	Required Analysis	Design Earthquake	
			Horizontal	Vertical
Building & Structures	As	Dynamic	S_2	1/2 S_2
	As, A	Dynamic Static	S_1 3.0 C_I	1/2 S_1 C_v
	B	Static	1.5 C_I	---
	C	Static	C_I	---
Equipment & Piping	As	Dynamic	S_2	1/2 S_2
	As, A	Dynamic Static	S_1 3.6 C_I	1/2 S_1 1.2 C_v
	B	Static	1.8 C_I	---
	C	Static	1.2 C_I	---

Note: S_2 = extreme design earthquake
S_1 = maximum design earthquake
C_I = static seismic coefficient (=0.2)

Table 2 compares U.S. and Japanese design allowable stresses for reactor vessels and Class 1 piping. The Japanese S_1 design earthquake, which represents a moderate earthquake, is somewhat higher than the OBE of U.S. practice, and the S_2 earthquake, which represents a severe earthquake, is roughly equivalent to the SSE.

Table 3 lists some design damping values used in both countries. In general, the damping values used in Japan are lower than those used in the U.S. It should be noted that, since nonlinear analyses are required for the S_2 earthquake, an additional hysteretic damping is also accounted for in the Japanese seismic design.

Table 2. Comparison of Allowable Stresses Under Seismic Loads

(a) ASME Section III

LOADING CONDITIONS	REACTOR VESSEL	CLASS 1 PIPING
Level B Limit, Upset (OBE)	1.5 S_m	1.8 S_m, 1.5 S_y
Level C Limit, Emergency	1.8 S_m, 1.5 S_y	2.25 S_m, 1.8 S_y
Level D Limit, Faulted (SSE)	3.6 S_m, S_u	3 S_m, 2 S_y

(b) JEAG 4601

LOADING CONDITIONS	REACTOR VESSEL	PRIMARY PIPING
S_1 Earthquake	1.5 S_y, S_u	2.25 S_m
S_2 Earthquake	S_u	3 S_m

Table 3. Comparison of Damping (%) Values

	JAPAN	U.S.	
	S_1, S_2	OBE	SSE
Concrete Structures:			
(a) Reinforced	5.0	4.0	7.0
(b) Prestressed (PCCV)	3.0	2.0	5.0
Welded Steel Structures	1.0	2.0	4.0
Bolted Structures	2.0	4.0	7.0
Piping			
Regulatory Guide 1.61			
(a) Large Diameter > 12.0 in D_o.		2.0	3.0
(b) Small Diameter < 12.0 in D_o.		1.0	2.0
ASME Code Case N-411			
(c) Function of frequency for response spectrum analysis.		5.0 (≤ 10 Hz) 2.0 (≥ 20 Hz)	
JEAG 4601			
(d) Function of type and number of supports, with and without thermal insulation.	0.5 to 2.5		

DESIGN REQUIREMENTS FOR SHEAR WALL STRUCTURES

The AIJ standard for RC structures (Ref. [4]), which can be considered as the equivalent of ACI-318, defines the allowable stresses for concrete structures as listed in Table 4. Figure 1 compares the short-term allowable shear stress from Table 4 with available test data. The upper and lower limits of ACI-318 ($3.5\sqrt{f_c'}$ *and* $1.9\sqrt{f_c'}$), are also shown in the figure.

Table 4. Allowable Stresses for Concrete (unit: kg/cm^2)

Long-term allowable (D.L. & L.L.)		**Short-term allowable (Seismic Load)**	
Compression	Shear, v_c	Compression	Shear, v_c
$\frac{1}{3}F_c'$	$\min\left(\frac{F_c'}{30}, 5 + \frac{F_c'}{100}\right)$	$\frac{2}{3}F_c'$	$\min\left(\frac{F_c'}{20}, 7.5 + 0.015\ F_c'\right)$

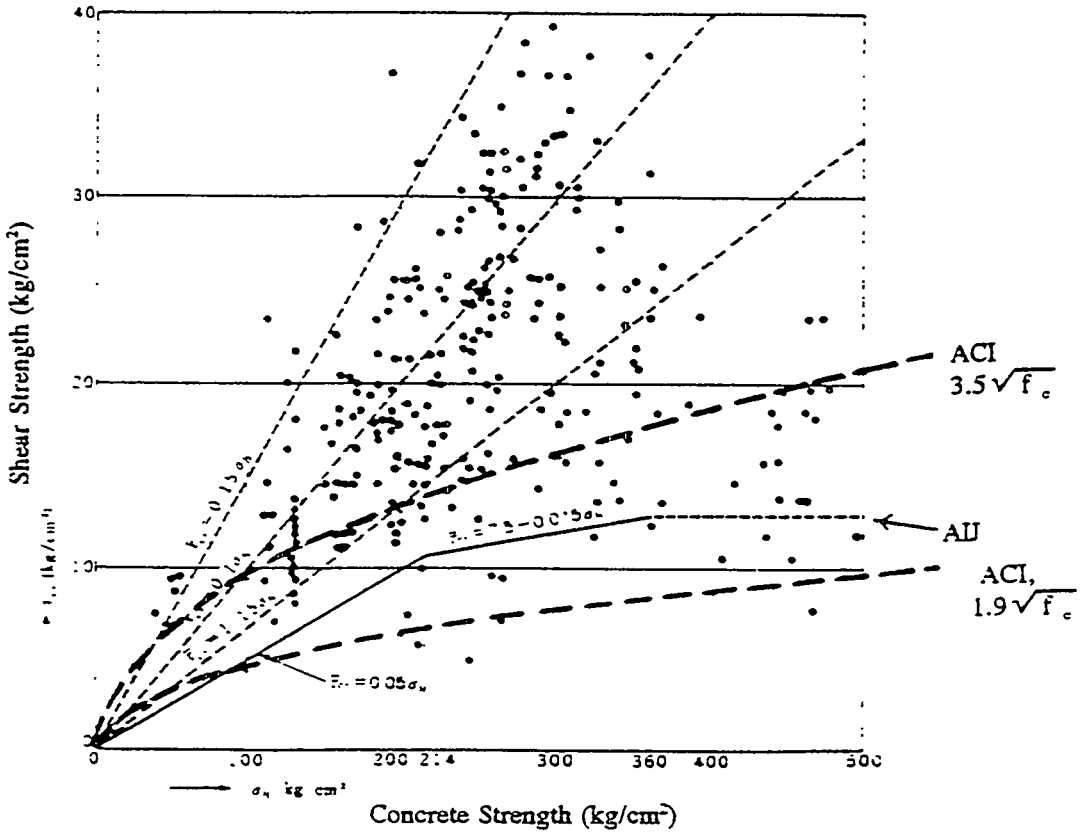

Figure 1. Shear Cracking Stress of Shear Walls Under Lateral Loads (Ref. [4]).

The AIJ recommendations for the design of reactor buildings, which are also described in JEAG4601-1987 (Ref. [1], [2]), are based largely on the foregoing AIJ RC-Standard (Ref. [4]). In the recommendations, the concept of "allowable state" has been introduced, which is similar to the classification of levels A, B, C and D (i.e., normal, upset, emergency and faulted) in the ASME code.

DEVELOPMENT OF SHEAR WALL EQUATIONS

In the seismic design of reactor buildings, nonlinear dynamic analyses are generally required when considering the response to the S_2 earthquake. Therefore, the shear wall equations are used not only for the component strength evaluation, but also to determine the restoring force characteristics of the nonlinear structural models. The latter requirement necessitates the development of shear wall equations which can predict the ultimate capacity and the nonlinear deformation properties without bias or excessive conservatism. Currently, Hirosawa's equation is extensively used in the seismic design of reactor buildings. Hirosawa's equation, which is also extensively used for non-nuclear buildings, is also called the modified Arakawa's equation, as it was developed by modifying the shear strength equation for beams and columns by Arakawa (Ref. [4]). Some benchmark studies, which led to the current Japanese shear wall equations, are described below.

Arakawa's Study (1960) The current Japanese design criteria on the shear capacity of R.C. components are based on the studies by Arakawa (Ref. [16], [17]). Figure 2 shows a part of the correlation study to develop the following shear strength equation for reinforced concrete beams, which now is called the original Arakawa's equation:

$$v_u(kg/cm^2) = K_u \cdot K_p \frac{0.12\,(180 + F_c)}{M/Vd + 0.12} + 2.7\sqrt{p_w \cdot f_y} \qquad (2)$$

in which
- K_u = reduction factor for scale effect (=0.72 when d>40 cm)
- K_p = $0.82\ p_t^{0.23}$
- p_t = tension steel ratio in percent
- M/Vd = shear span ratio (replaced by 3 when larger than 3)
- p_w = stirrup ratio

The contribution of the reinforcement to the shear strength, v_s or the second term of Eq. 2, was obtained empirically as illustrated in Figure 3. A total of 219 pairs of specimens, for which the shear reinforcement was the only parameter (i.e., one beam is shear reinforced and the other is not), were used to directly determine the contribution by the shear reinforcement as follows:

(Contribution by Shear Reinforcement) =(Shear Strength of Reinforced Beam) - (Shear Strength of Unreinforced Beam).

The results presented in Figure 3 indicate that the truss theory approximation, on which the current ACI equations are based, largely overestimates the shear contribution by steel. The data shown in Figures 2 and 3, in fact, had a major impact on the subsequent design code development in Japan.

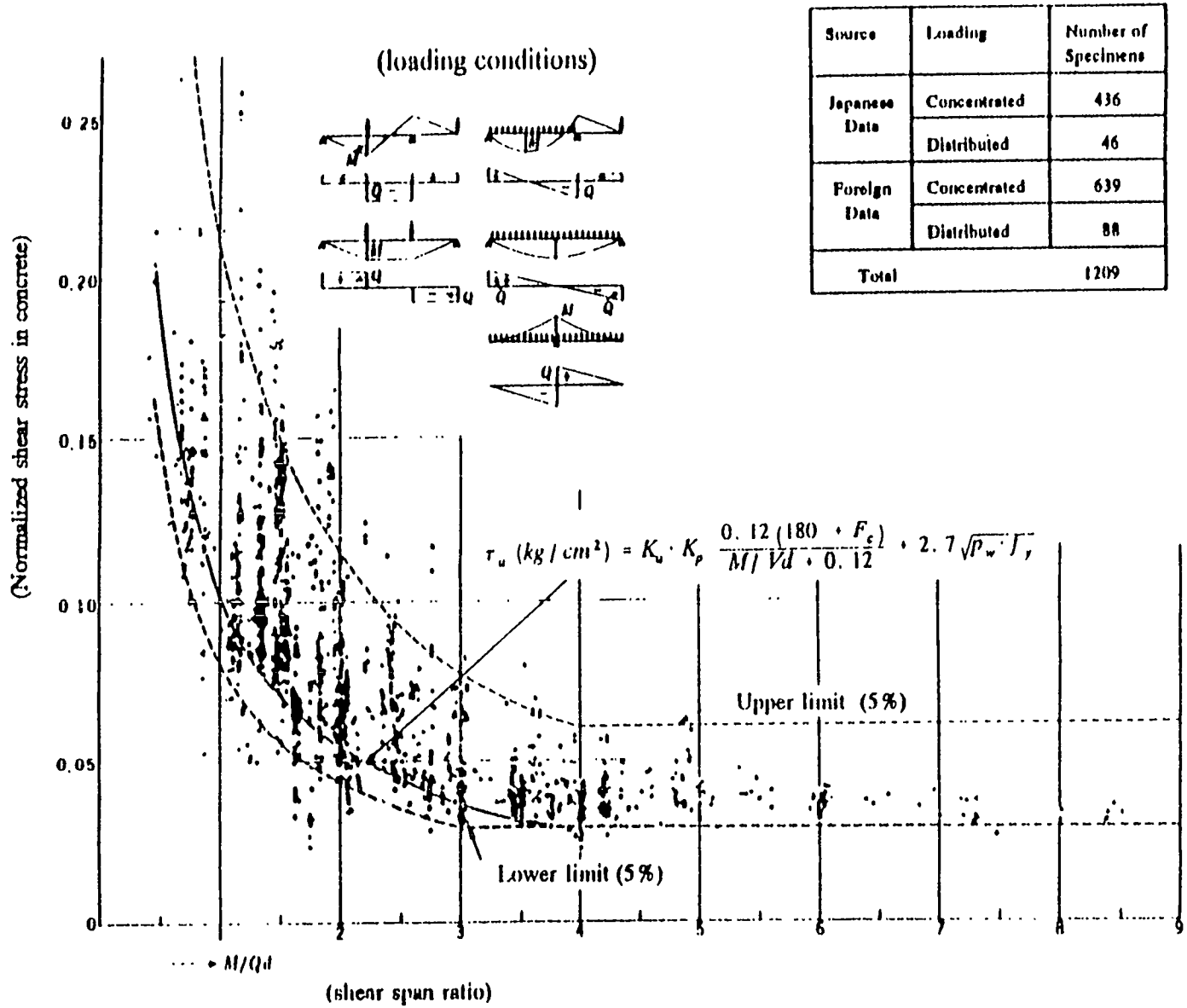

Source	Loading	Number of Specimens
Japanese Data	Concentrated	436
	Distributed	46
Foreign Data	Concentrated	639
	Distributed	88
Total		1209

Fig. 2 Correlation of Shear Strength by Arakawa (Ref. [4]).

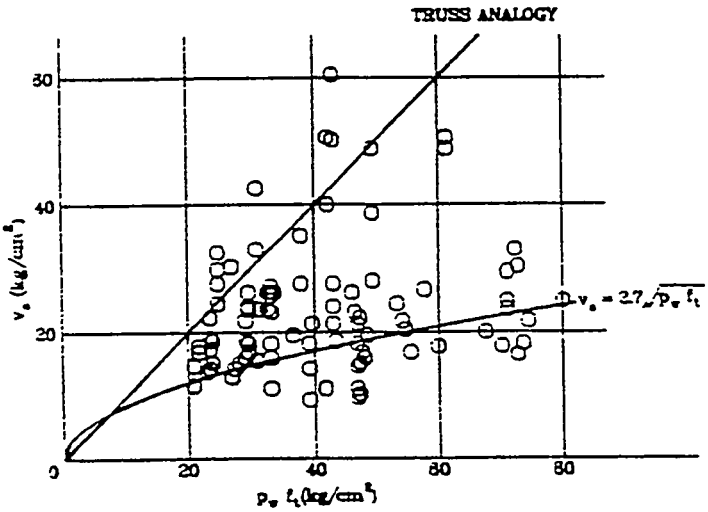

Figure 3. Contribution by Rebars to Shear Capacity (replotted based on the data in Ref. [16], components with $p_w f_t < 20$ are excluded).

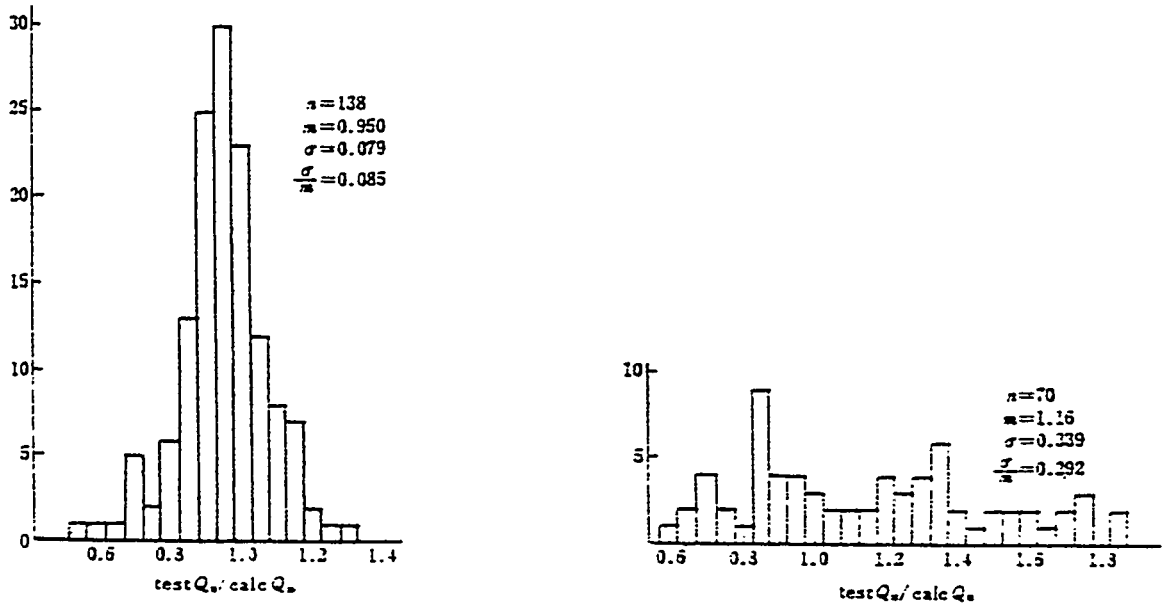

(a) AIJ equation (Eq. 1)

(b) ACI equation (Eq. 2)

Fig. 4. Histograms for the Ratios of Tests to Calculated Ultimate Shear Strength of R.C. Beams (Ref. [18]).

The corresponding ACI equation is,

$$V_u(lbs) = V_c + \phi p_w \cdot f_y \cdot bd$$

$$V_c(lbs) = \phi\left(1.9\sqrt{f_c'} + 2500\ p_w \frac{Vd}{M} \right) bd \le 3.5\sqrt{f_c' bd} \qquad (3)$$

Figure 4 shows the results for correlation studies of the above shear strength equations (Ref. [18]). The ACI equations show a much larger scatter compared with the AIJ equation.

Hirosawa's Study on Shear Walls (1975) Hirosawa's equation is extensively used in Japan to calculate the ultimate shear strength of shear walls both for non-nuclear and nuclear power structures. The empirical equation was obtained by modifying the above Arakawa's equation (Ref. [19]):

$$V_u(Kg) = \left\{ \frac{0.0679\ p_t^{0.23}\ (F_c + 180)}{\sqrt{M/VD + 0.12}} + 2.7\sqrt{f_{yw} \cdot p_w} + 0.1\sigma_o \right\} b_e j \qquad (4)$$

where b_e = effective thickness of wall (when a wall has flanges, 'b_e' is calculated from a uniform-thickness cross-section with equal area);

j = 0.83 D (D = total length of wall)

p_t (%) = 100 $A_t/(b_e \cdot j)$, tension axial steel ratio considering a wall as a column (A_t = total axial steel area in a flange);

M/VD = shear span ratio;

p_w = horizontal steel ratio using the effective thickness b_e;

F_c = concrete strength (kg/cm^2)

f_{yw} = steel yield stress (kg/cm^2)

σ_o = average axial stress (kg/cm^2)

Table 5 shows part of the correlation studies on this equation.

DESIGN REQUIREMENTS FOR CONTAINMENT STRUCTURES

The seismic design of concrete containment structures is performed based on MITI Notification No. 452 (Ref. [12]). This document, and in particular the background information upon which this standard is based, may be useful as the test results of large-scale containment structures are extensively utilized. Some unique features are highlighted herein, in the light of the U.S. practice for the seismic design of containment structures.

Loading State According to Notification No. 452, the structural design of containment structures is performed based on the "Loading States" shown in Table 6.

Table 5. Correlation of Hirosawa's Equation (Ref. [19]).

Range of Parameters	Number of Shear Walls	Range Vtest/Vcal	Mean Vtest/Vcal	Standard Deviation
$0<M/VD\leq 0.75$	52	0.44~1.59	0.90	0.23
$0.75<M/VD\leq 1.0$	79	0.35~1.52	0.92	0.21
$1.0<M/VD$	37	0.54~1.24	0.91	0.17
$0<t/L<0.3$	47	0.35~1.24	0.81	0.18
$0.3\leq t/L<1.0$	84	0.54~1.59	0.97	0.21
$t/L=1.0$	37	0.64~1.19	0.95	0.13
$p_w=0$	15	0.35~1.59	0.99	0.39
$0<p_w<0.4$	46	0.44~1.32	0.89	0.23
$0.4\leq p_w<0.8$	50	0.53~1.50	0.91	0.18
$0.8\leq p_w<1.2$	26	0.72~1.08	0.94	0.11
$1.2\leq p_w$	31	0.70~1.22	0.90	0.12
Total	168	0.35~1.59	0.92	0.21

M/VD = shear span ratio
b_e/D = thickness ratio
p_w = horizontal shear reinforcement ratio

Table 6. Loading State for Containment Structures

Loading States	Plant Condition	Allowable Concrete Compressive Stress	Other Allowable Stresses	Thermal Stiffness Reduction Factor
I	Normal	⅓ F_c	Long-term allowable (RC standard)	½
II	Relief valve/test			
III	S_1 EQ	⅔ F_c	Short-term allowable (RC standard)	⅓
IV	S_2 EQ/accident	Strain limit	0.3% for concrete 0.5% for steel	Neglect

Thermal Stress The evaluation of the thermal stresses is performed according to the following procedure.

- Reduce the elastic stiffness (i.e., Young's modulus) by a factor of ½ for Loading States - I and II, and ⅓ for Loading State - III, and calculate the thermal stresses.
- Calculate stresses for other loads using the original elastic stiffness.
- Combine the above stresses.
- For the Loading State - IV (S_2 earthquake and accident), the thermal stress is neglected.

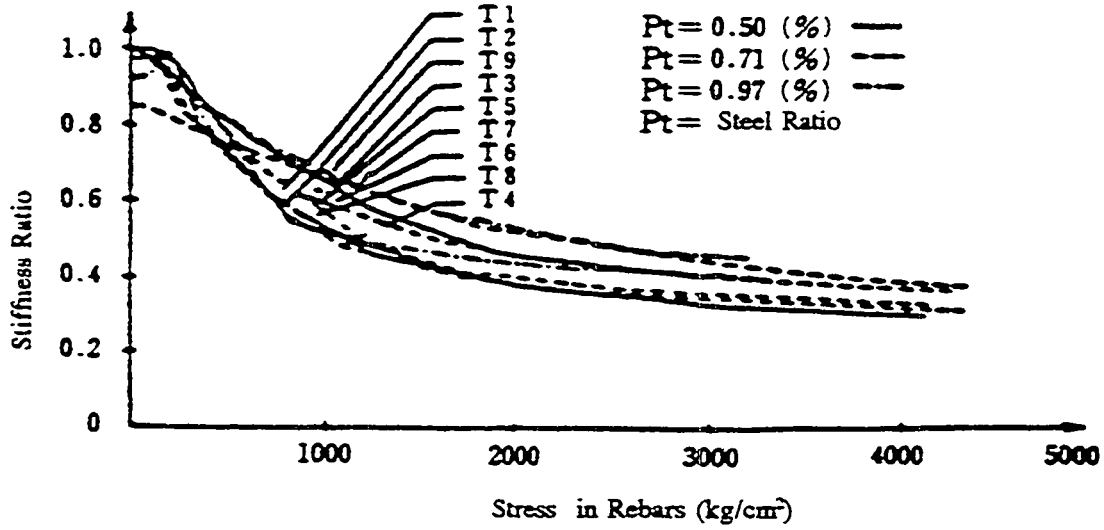

Figure 5. Reduction of Stiffness and Stress Level in Rebars (Ref. [14]).

Figure 5 shows the basis for the stiffness reduction factors of ½ and ⅓ shown in Table 6. This figure is based on the results of tests of reinforced concrete components subjected to lateral loading under elevated temperature conditions. The stress level of the component is represented by the stress in rebars and the stiffness ratio is the secant stiffness at each stress level divided by the initial stiffness. The allowable stress for Loading States I & II roughly corresponds to a stress of 2,000 kg/cm^2 (28.5 ksi), and for Loading State III, it is about 3,500 kg/cm^2 (49.8 ksi). Table 6 also indicates that the effects of thermal stresses can be neglected for the S_2 earthquake and accidental loadings both for containment structures and reactor buildings. This is based on the observation that the thermal stresses do not alter the ultimate strength of shear wall structures (Ref. [12]).

DUCTILITY CAPACITY/REQUIREMENTS

The allowable shear deformation for both reactor buildings and containment structures are defined to be 0.2% in radians (Ref. [1], [2], [12]). Based on a statistical analysis of available box-shaped and cylindrical shear wall structures, the minimum shear deformation capacity was estimated to be 0.4% in radians (Ref. [20]). Therefore, a safety factor of 2.0 is used to account for the large scatter associated with the shear deformation capacity.

Figure 6 shows the results of a study of available data on box-shaped and cylindrical shear walls by the authors. In the figure, the ultimate shear deformation capacity is plotted against the maximum shear stress. For high strength shear walls, the deformation capacity tends to decrease to about 0.4% in radians. However, for shear walls with less shear strength, a much higher ductility can be expected. The results of a similar study on shear deformation capacity are presented for both RCCV and PCCV structures in Ref. [12], in which the ultimate shear deformation capacity was plotted against the normalized steel ratio. According to this study, the ductility of containment structures tends to decrease as the steel ratio (therefore shear strength) increases. The minimum shear deformation

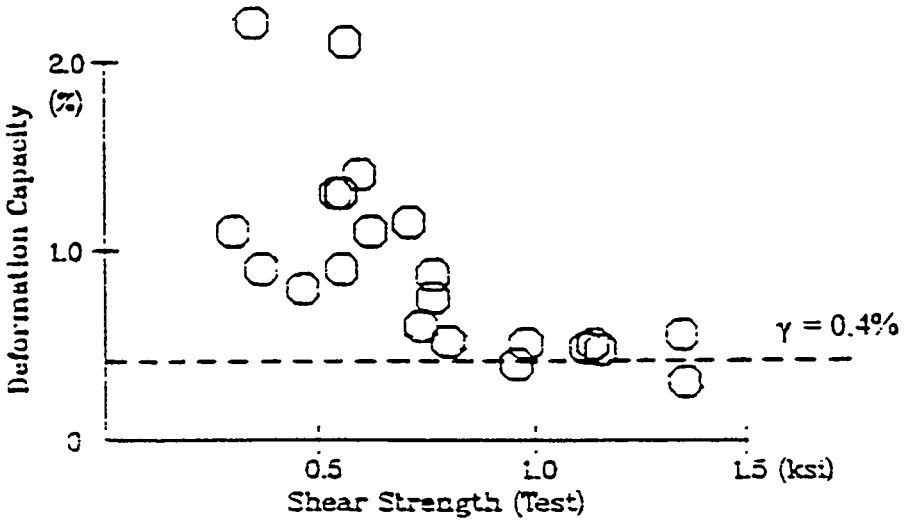

Figure 6. Shear Deformation Capacity of Box-Shaped and Cylindrical Shear Walls.

capacity for heavily reinforced containment structures converges to about 0.4% in radian. A more detailed statistical study on the shear deformation capacity of ordinary RC shear walls is also described in Ref. [18].

SUMMARY AND CONCLUSIONS

The current Japanese practice for seismic design, particularly that related to the seismic design of reactor buildings and containment structures, was reviewed in some detail as well as related research activities. There have been three decades of extensive experimental work, and judging from publications such as the transactions of the Annual Meeting of AIJ the experimental studies on components are continuing as the emphasis is being shifted more to newer design approaches, such as base isolation devices and pre-fabricated components.

The value of the wealth of accumulated information in Japan has been recognized by many prominent U.S. engineers. In fact, the test results of large-scale shear wall structures and pre-stressed components have been utilized in the fragility evaluation of nuclear reactor facilities, as they are the only available source of test data for these types of structures. The extent to which Japanese test data have been used by U.S. engineers, however, has been seriously limited due to the language barrier. Further efforts should be made to utilize the available information. The critical evaluation of existing nuclear facilities and the development of new design concepts require much more than structural analysis codes. The accumulated test results, mostly performed using modern testing facilities and earthquake-like loading conditions, should also be reviewed and evaluated in detail.

ACKNOWLEDGEMENTS

The authors wish to thank K. Akino, S. Kawakami, T. Taira and N. Tanaka of NUPEC, S. Yoshizaki of Taisei Co., M. Kanechika of Kajima Co., and R. Shohara and Y. Takeuchi of Shimizu Co. for the information and cooperation in this survey study. The permission by the Architectural Institute of Japan to use the figures and tables from AIJ's publications is greatly appreciated.

The work presented in this paper was performed under the auspices of the U.S. Nuclear Regulatory Commission. The findings and opinions expressed in this paper are those of the authors, and do not necessarily reflect the views of the U.S. Nuclear Regulatory Commission or Brookhaven National Laboratory.

REFERENCES

[1] "Technical Guidelines for Aseismic Design of Nuclear Power Plants, JEAG 4601-1987, Japan Electric Association, 1987.

[2] Y.J. Park and C.H. Hofmayer, "Technical Guidelines for Aseismic Design of Nuclear Power Plants - Translation of JEAG 4601-1987, "NUREG/CR-6241, June 1994.

[3] "Guidelines and Commentary on Structural Design Calculations," Japan Architectural Center, 1981.

[4] "Standard for Structural Calculation of Reinforced Concrete Structures," AIJ, 1991.

[5] "Design Standard for Steel Structures," AIJ, 1973.

[6] "Standard for Structural Calculation of Steel Reinforced Concrete Structures," AIJ, 1987.

[7] "Design Guidelines for Foundation Structures,"AIJ, 1988.

[8] "Design Guidelines for Earthquake Resistant Reinforced Concrete Buildings Based on Ultimate Strength Concept," AIJ, 1990.

[9] "Design Guidelines for Base-Isolated Buildings," AIJ, 1989.

[10] "Technical Standards for Nuclear Power Plant Facilities," MITI Order No. 62, ANRE/MITI, 1989.

[11] "Technical Standards for Structural Design of Nuclear Power Plant Equipment," MITI Notification No. 501, ANRE/MITI, 1992.

[12] "Technical Standards for Structural Design of Concrete Containment Structures of Nuclear Power Plant Facilities," MITI Notification No. 452, ANRE/MITI, 1990.

[13] "Regulatory Guide for Aseismic Design of Nuclear Power Reactor Facilities," Japan Atomic Energy Commission, 1981.

[14] "Recommendations for Structural Design of Reactor Buildings," AIJ, 1988.

[15] "Recommendations for Structural Design of Nuclear Reactor Containment Structures," AIJ, 1978.

[16] T. Arakawa, "Allowable Shear Stress and Shear Reinforcement of RC Beams," Concrete Journal, Japan, Vol. 8, No. 7, July 1970.

[17] K. Ohno and T. Arakawa, "Study on Shear Resistance of Reinforced Concrete Beams," Transaction of AIJ, No. 66, October 1960.

[18] "Data for Ultimate Strength Design of Reinforced Concrete Structures," AIJ, 1987.
[19] M. Hirosawa, "Past Experimental Results on Reinforced Concrete Shear Walls and Analysis on Them," Building Research Institute, Ministry of Construction of Japan, March 1975.
[20] T. Setogawa, "Allowable Limit of Shear Walls in Reactor Buildings," Annual Meeting of AIJ, pp. 2091-2092, Oct. 1987.

NPAR- Products, Applications and Closure

J. P. VORA

Office of Nuclear Regulatory Research, NRC

Abstract

Almost a decade ago the Office of Nuclear Regulatory Research (RES) developed and implemented a comprehensive research program (NUREG-1144)[1] widely known as NPAR or Nuclear Plant Aging Research. The NPAR program is a structured research program specifically oriented to understanding significant age-related degradation mechanisms and their long term effects on properties and performance of important components and systems and ways to mitigate detrimental effects of aging. It provided a road map and a phased approach to research that is applicable to any structure, system, or component of interest.

This hardware-oriented engineering research program led the industry worldwide and communicated a need to understand and manage age-related degradation effects in selected but important structures and components. At the conclusion (1995) of the NPAR program, 22 electrical and mechanical components, 13 safety-related systems, and 10 special topics will have been studied and results summarized in 160 technical reports. NPAR studies on special topics included Risk Evaluation of Significant Aging Effects, Recommendations for Aging-Related Data Needs and Recordkeeping, Reviews of Selected Segments of Standard Technical Specifications, and Reviews and Compilation of Technical Information Useful for Residual Life Assessment of Major Light-Water Reactor Components and Structures. This reference library of information listed and summarized in NUREG-1377, Rev. #4)[2] provides a foundation upon which individual programs can be built for the specific needs of a utility, a regulator, or equipment manufacturers. During the life of the NPAR program, it has provided technical bases and support for license renewal, codes and standards, resolution of generic safety issues, information notices, regulatory guides and the standard Review Plan, as well as the Office of Nuclear Reactor Regulation and the NRC Regions.

All ongoing NPAR activities will either be completed or terminated by the end of 1995. No new initiative will be undertaken. This paper summarizes NPAR products and accomplishments, application of the research results, and its status and closure.

INTRODUCTION

Commercial nuclear power plants are composed of many systems, structures, and components and must meet different functional requirements. They involve a wide spectrum of materials and operating and environmental stressors. Their interactions over time result, if unchecked, in degradation of physical and chemical properties of materials, and they may impact performance of structures and components. The good news is that age-related degradation effects can be controlled with effective inspection, surveillance, condition monitoring, and time trending of parameters/indicators, refurbishment, replacement, and maintenance. For materials with applications in a known environment, proper control of environmental stressors has also resulted in diminishing rates of degradation effects. Although aging is universal, its deleterious effects are controllable when understood.

Overall, the nuclear community in the U.S. has done a remarkable job in operating the commercial nuclear power plants (NPPs) and ensuring the public health and safety. Advancing age of the NPPs in the U.S. has resulted in maturity backed by experience. Regulatory requirements have been enforced effectively and decisively, guidelines have been provided for uniformity of operation and maintenance, codes and standards have been developed providing industry guidelines, and inspection and maintenance strategies have been formulated and implemented, implicitly to date, but they will be formally implemented in 1996.

This remarkable performance of U.S. operating plants is attributable, among other things, to the ability to anticipate and react decisively to overcome any emerging and deleterious effects of aging. Programs, regulations, requirements, and ongoing processes are effective in overcoming significant age-related degradation effects that may impact plant safety.

During the early 1980s, the NRC's emphasis shifted from the design and construction aspects of commercial nuclear power plants to the continued safe operation and maintenance of the existing facilities. Realizing a need for a research program to address emerging issues related to plant aging, and at the recommendation of the Advisory Committee on Reactor Safeguards (ACRS), the Office of Nuclear Regulatory Research developed and implemented a comprehensive research program commonly known as NPAR or Nuclear Plant Aging Research.

Over the last decade, the NPAR program provided a systematic and structured approach to understanding and managing aging in systems, structures, and components (SSCs), conducted well defined research and disseminated results, and provided technical bases for the utilization of results in the regulatory process. The NPAR program has achieved its overall programmatic goals and is nearing its closure in 1995.

NPAR APPROACH TO UNDERSTANDING AND MANAGING AGING

Realizing that "aging" occurs in all engineered complexes and in searching for ways to put arms around this complex issue at the plant level, a common sense and practical approach was adopted for NPAR. The following major factors contributed to the early formulation of the NPAR program:

- Learning from designs.
- Learning from experts' opinions.
- Focusing on important and risk significant components.
- Focusing on representative samples of electrical and mechanical components.
- Developing a road map that is useful for any structure, system, or component under study and of interest.
- Recognizing that systems aspects of aging studies were important, in addition to individual components and systems studies. Identifying the need for some generic studies.
- Recognizing the need for adopting a phased approach to research.
- Walking through some practical examples demonstrating the effectiveness of the NPAR approach.
- Recognizing the need for motivating the industry to do the bulk of the follow-on effort.
- Coordinating and integrating research activities to minimize duplication and maximize resources.
- Considering the utilization of research results.

The NPAR approach to understanding aging was to:

- Define the component's boundary and all interfaces of interest, identify materials used in the design and fabrication of component parts.
- Identify applicable stressors and environment during the lifetime of the component, including those expected during and post design basis events.
- Identify aging mechanisms and where they could be operative.
- Determine age-related degradation effects and their significance on operability or performance (performing, when necessary, in situ testing and testing under controlled laboratory conditions; performing testing on naturally aged components and samples of materials for correlation and validation).

The NPAR approach to managing aging was to:

- Identify detection and condition monitoring methods for evaluating age-related degradation effects.
- Identify and review ongoing programs with respect to their effectiveness in detecting and managing age-related degradation effects.
- Develop appropriate recommendations to overcome deficiencies.

PRODUCTS AND APPLICATIONS OF NPAR RESULTS

As stated earlier, the NPAR program has provided a lead for the industry worldwide by developing a road map to understanding and managing aging in operating nuclear power plants. An important contribution of the NPAR has been the development of national and international awareness of the need for an integrated approach to plan for and address significant age-related degradation effects in nuclear power plant systems, structures, and components. NPAR products include the publication of over 160 technical reports and numerous journal articles and conference papers published in the U.S. and abroad; the research results have been used in many facets of the regulatory process.

At the closure of the NPAR program, 22 electrical and mechanical components, 13 safety-related systems, and support systems will have been assessed for aging. Also noteworthy is the completion of 10 special topics. Major elements of the completed NPAR program include:

- Aging assessment of electrical components
  - Batteries, battery-chargers and inverters, circuit-breakers and relays, electrical cables and penetrations, motors, connectors, bistables/switches, resistance temperature detectors, transformers, surge arrestors, diesel generators
- Aging assessment of mechanical components
  - Pumps, motor-operated valves, check valves, power-operated relief valves, safety relief valves, main steam isolation valves, snubbers, heat exchangers, compressors, fans/chillers, air-operated valves.
- Aging assessment of electrical and I&C Systems
  - Reactor protection system, class IE distribution systems, motor control centers, control rod drives
- Aging assessment of fluid mechanical systems
  - High-pressure coolant injection system, low-pressure residual heat removal systems, component cooling water system, auxiliary feedwater system, reactor core isolation cooling system, service water system, standby liquid control system, chemical and volume control, containment isolation
- Elements covered under special topics:
  - Data needs and recordkeeping
  - Treatment of aging in passive structures
  - Risk evaluation of aging phenomena
  - Residual life evaluation of major LWR components[3]
  - Degradation modeling

- Insights gained from aging research--helpful hints for inspection and maintenance
- Treatment of aging in Standard Technical Specifications
- Reviews of regulatory instruments from an aging perspective
- Support for license renewal rulemaking and developing a draft format and content regulatory guide on technical information for applications to renew nuclear power plant operating licenses
- An evaluation of accident precursors from an aging perspective

In addition to the aforementioned products and applications, NPAR provided technical bases and support for:

- National consensus codes and standards (ASME - O&M, IEEE)
- Resolution of generic safety issues
- Development of information notices
- Development of regulatory guides
- Field cases involving electrical and mechanical components and electrical and fluid-mechanical systems

- License renewal rulemaking

In the early days of license renewal rulemaking, NPAR played a significant role in developing the basic principles upon which 10 CFR 50.54 was formulated. NPAR provided inputs and bases for integrated plant assessment to manage aging during the renewed license term, regulatory analysis, and a statement of consideration. A draft regulatory guide was developed on the standard format and content of technical information for applications to renew nuclear power plant operating licenses. Technical support was provided to NRR for the development of the Standard Renew Plan for License Renewal and for the reviews of the NUMARC-generated industry reports (IRs).

- National Consensus Codes and Standards

Technical bases were provided for the formulation and development of a number of national consensus codes and standards associated with IEEE and ASME-O&M. Examples of IEEE standards and guides include:

- Std. 338-1987, "Criteria for the Periodic Surveillance Testing of Nuclear Power Generating Station Safety Systems"
- Guide (89-TH9248-5-PWE), "Good Practices for Maintenance." NPAR results involving motors, solenoid operated valves, motor-operated valves, and battery-chargers and inverters.
- Guide, IEEE-1205, "A Methodology for Assessing and Mitigating the Effects of Class 1E Distribution System"
- Std. 387, "Criteria for Diesel Generator Units Applied as Standby Power Supplies for NPP Generating Stations"
- Std. 650-90, "Qualification of Class 1E Static Battery Chargers and Inverters for NPP Generating Station"
- Std. 334-91, "Standards for Type Tests of Continuous Duty Class 1E Motors for NPP Generating Stations"

- NPAR contributions to ASME-O&M committees include:

  - O&M 4, Examination and Performance of Nuclear Power Plant Dynamic Restraints
  - O&M 6, Requirements for Performance Testing of Pumps in Light Water Cooled Nuclear Power Plants
  - O&M 8, Requirements for Preoperational and Periodic Testing of Motor Operated Valve Assemblies
  - O&M 10, Requirements for Inservice Testing of Valves in Light Water Cooled Nuclear Power Plants
  - O&M 21, Requirements for Design and Performance Testing of Heat Exchangers

- Resolutions of Generic Safety Issues, Technical Bases for Implementation of Generic Letters, and Information Notices to which the NPAR program provided inputs include:

  - II.E.6.1, Insitu Testing of Valves
  - 70, PORV/BV Reliability
  - 87, Failure of HPCI Steam Line Without Isolation
  - GL 89-13, Service Water System Problems Affecting Safety-Related Equipment
  - GL 89-10, Safety-Related Motor-Operated Valve Testing and Surveillance
  - GL 89-04, Guidance on Developing Acceptable Inservice Testing Program
  - GL 88-04, Potential Safety-Related Pump Loss
  - IN 92-51, Misapplication and Inadequate Testing of Molded-Case Circuit Breakers

NPAR results were utilized to meet specific user needs of the Office of Nuclear Reactor Regulation and the Regions on service water systems, chlorine release from cables, pumps, valves, emergency diesel generators, battery-chargers/inverters, resistance-temperature-detectors, circuit-breakers, and relays.

CLOSURE OF THE NPAR PROGRAM

Since the major objectives of the NPAR program have been achieved, it is time to bring this research program to a systematic closure. During numerous discussions with researchers, equipment manufacturers, utilities operation and maintenance personnel, and members of codes and standards groups, the author perceived mixed feelings about the NPAR program and its coming to a closure. Some said NPAR was ahead of its time while others said it was timely because "aging" is not going to go away. Other comments were that when the time comes, results of the NPAR program will be appropriately recognized and be useful; NPAR provides a good road map for the future; People have characterized the NPAR approach as a "common sense" approach and nothing is new; aging is addressed routinely and ongoing programs take care of its deleterious effects.

The NPAR program was scrutinized and reviewed extensively within NRC and by the institutions and organizations outside the agency, both domestic and

foreign. Many elements of the NPAR program received high recognition and praise while others received mediocre or no appreciation and sometimes criticisms as well. Nevertheless, important contributions of the NPAR program include an awareness of the technical and regulatory issues related to plant aging, the need for an integrated approach to understanding and managing aging, and ways to mitigate significant age-related degradation effects.

Good or bad, only history will tell. Future performances and events will be the judge of the NPAR program. NPAR comes to a "closure" in 1995. After that, no new programs are contemplated under the NPAR program. In the future, should a need arise and on a case-by-case basis if aging-related research is supported by the user office, specific programs may be implemented depending on the availability of resources. In the spirit of the closure of the NPAR program, please allow me to state the following:

- Goals and objectives of the NPAR program have been met.
- Results of the NPAR program, directly or indirectly, are being utilized by the utilities.
- Results of the NPAR program are being utilized for developing national consensus codes and standards.
- Many countries around the world either have developed aging management programs or are in the midst of contemplating new programs based on the NPAR program.
- Some countries are considering aging management as part of their maintenance strategy.

NPAR expertise has influenced other programs requiring aging management, including DOE facilities, older jet aircraft and surface ships, defense facilities, and the nation's infrastructure. NPAR provided a foundation upon which aging management programs can be built to suit individual needs and requirements.

REFERENCES

1. "Nuclear Plant Aging Research (NPAR) Program Plan - Status and Accomplishments, "NUREG-1144, Rev. 2.

2. "NRC Research Program on Plant Aging: Listing and Summaries of Reports Issued Through September 1993, J.P. Vora, "NUREG-1377, Rev. 4, USNRC, December 1993.

3. V.N. Shah and P.E. MacDonald, "Aging and Life Extension of Major Light Water Reactor Components"

STUDY ON LONG-TERM IRRADIATION AGING OF ELECTRICAL CABLES

(THE VEILLE PROGRAM)

F. CARLIN - M. ATTAL - G. GAUSSENS - P. LE TUTOUR (CIS bio international)
J.F. CALMET - G. GAUTHIER (CEA-IPSN-DES)

ABSTRACT

The VEILLE program (French acronym for study on long-term irradiation aging of electrical cables) was implemented in 1988 by the Institute of Protection and Nuclear Safety (IPSN) in collaboration with the US Nuclear Regulatory Commission (NRC) for a period of six years. It is intended to validate the assumptions put forward as regards aging of electrical cables and to develop criteria for early detection of degradation likely to lead to functional failures.

The tests were carried out partly at the Sandia National Laboratories in the United States, partly in France in the CIS bio international Laboratories at the Saclay Nuclear Research Centre.

The study focused on the radiation effects from cobalt 60 on electrical cables made up of various polymers for two temperatures and at various dose rates. Other tests were also performed using a device laid under water in the OSIRIS reactor pool at Saclay to test cables under irradiation and temperature conditions close to those found in nuclear power plant operation.

Subsequently the aged cables were subjected to containment accident conditions (irradiation and thermodynamic profile) in order to show any degradation due to aging.

The study showed the significant effect of radiation doses on EPR and EPDM cable insulations as well as synergy between radiation dose rates and temperature on the mechanical properties of the Hypalon sheath.

Correlation between the mechanical properties and the function of cables is difficult to establish as electrical characteristics are preserved whatever the type of mechanical degradation observed.

Finally, the performance of electrical cables after an accident remains a key criterion to define the materials likely to be used when manufacturing cables intended to ensure safety functions.

I. INTRODUCTION

The research for criteria permitting the early detection of degradation of equipment considered to be important for safety, installed in the containment enclosure of nuclear power stations has always been a delicate matter with elastomers, because behavior can vary according to ambient conditions, and the formulations of the materials derived from the same family.

Electrical cables fall into this behavior pattern. Their long-term behavior under normal and accidental ambient conditions in pressurized water reactors (PWR) needs greater research, and is arousing among the Safety Organizations and supporting laboratories, programs designed to improve knowledge in the field.

The VEILLE program, a partnership project between CEA/IPSN and US/NRC, is aimed at studying the properties of electrical cables affected by low dose-rate irradiation to define the early aging-detection criteria of materials submitted to normal and accidental conditions in PWRs, and that can lead to functional failures. It is part of the constant endeavor being made in the field of electrical-equipment qualification by the US/NRC and IPSN teams through a number of successive cooperation ventures (1) (2) (3).

The text proposed in this communication describes the program followed at the present time, and is confined to the main results of the study, the integral publication of which will appear in the Nureg collection of Sandia National Laboratories.

II. CABLES PUT THROUGH TESTING

4 cables were put through testing :

- 3 control and instrumentation cables, of which 2 were of American origin and 1 of French origin.
- 1 coaxial cable of French origin, qualified solely for normal PWR-reactor operating conditions.

The cables were tested either in the form of complete 25-meters (82-feet) long cables supplied with electric power and irradiated at the middle over an effective length of 1.2 meters (0.37 foot), either, in the form of 40-cm (16-inch) sections covered at the ends with heat-shrink caps. The references of each cable were as follows :

1. U.S. ethylene propylene rubber (EPR) (Samuel Moore Dekoron. 2 conductors plus shield, flame-retarded ethylene propylene diene monometer (FR-EPDM) insulation. Hypalon jacket). The cable jacket has the following markings :
DEKORON 2/C 16 AWG 600 V SAMUEL MOORE GROUP, AURORA, OHIO.

2. U.S. cross-linked polyolefin (XLPO) (Rockbestos Firewall III. 3 conductors, cross-linked polyethylene (XLPE) insulation, Hypalon jacket). The cable jacket has the following markings :
12 AWG 3/C ROCKBESTOS 600V FIREWALL III XHHW NEC TYPE TC (UL) K-2 COLORCODE 1987-7C 1309 COPPER FAXLPE CSPE

3. French multiconductor (3 conductors manufactured by FILERGIE, EPR insulation, Hypalon jacket). The cable jacket has the following markings :
CGF-3x1, 5 CU-EPR-PCS-4-209-220.

4. French coaxial (polyethylene (PE) insulation, PL jacket). The cable jacket has no labelling; however, this cable has been identified by the French as FILECA F1203-Pro. They also indicated that the cable's insulation and jacket are constructed from different PE formulations.

III. TEST PROGRAM

3.1 General

The test program included aging at low dose-rate irradiation (2, 5, 10, 20 Gy/h), extending over a period of 6 years, combined with two temperature values (40 and 70°C) on cables and cable sections. It also included irradiation and thermodynamic shock, representative of accidental conditions, applied to samples taken at various stages of aging.
Throughout the testing, measurements were made on the samples and cables to verify their mechanical, physical-chemical and electrical characteristics.
Within the framework of collaboration between IPSN and US-NRC, an equivalent study was carried out in parallel at the Sandia National Laboratories using the same cables, put through aging at 90 Gy/h and 40°C in order to complete the spectrum of dose rates tested during the study work.

3.2 Equipment

Aging irradiation was carried out in the KRONOS installation, consisting of 6 rectangular box-shaped structures immersed at the bottom of the POSEIDON pool (Cobalt-60 irradiator) and in the EVOCABLE installation installed near the cooling circuit of the OSIRIS experimental reactor at the Saclay Study Center.
In EVOCABLE, the cable-aging conditions were close to the real aging conditions encountered in the PWR reactor buildings.
Thermodynamic shocks of LOCA were applied in the CESAR installation. In this installation, it is possible to obtain French and American thermodynamic profiles, whether irradiation is present or not.

3.3 Aging under irradiation

In KRONOS :

Dose rates :	5, 10 and 20 Gy/h.
Temperature :	40 and 70°C.
Total dose :	for cable sections : 210 kGy.
	for cables : 84 kGy.

In EVOCABLE :

Dose rate :	2 Gy/h.
Temperature :	40°C.
Total dose :	for cable sections and cables : 56 kGy.

The doses at which the cable sections were picked up in order to make mechanical and physical-chemical measurements were as follows :

- In KRONOS : 14, 28, 42, 56, 70, 84, 100, 150, 210 kGy.
- In EVOCABLE : 14, 28, 42 and 56 kGy.

During aging under irradiation, the cables were supplied with electric power in the following manner :

- control and instrumentation cables: 48 V DC, 300 mA
- coaxial cable: 600 V DC, 0 mA.

In parallel to aging under irradiation, thermal aging at 70°C was carried out on cable sections in order to compare the behavior of the cables with and without irradiation.

3.4 Accidental irradiation and thermodynamic shocks of LOCA

The LOCA (Loss of Coolant Accident) tests were carried out using cables and cable sections sampled :

From KRONOS, at the following doses :

- Cable sections : 28, 56, 70, 84, 100, 150 and 210 kGy.
- Complete cables : 84 kGy.

From EVOCABLE, at the following doses :

- Cable sections : 28, 56 kGy.
- Complete cables : 56 kGy.

The LOCA irradiation was performed with following conditions :

Total dose :	600 kGy.
Dose rate :	800 Gy/h.
Temperature :	70°C.

After irradiation, cables and cables sections were introduced inside CESAR facility. The steam water exposure was carried out in accordance with the accidental thermodynamic profile defined in french standard (figure 13) : the initial steam temperature increase up to 156°C in less than 30 seconds and decrease during 4 days. A chemical spray is carried out with boric acid solution after 200 seconds.

IV. MEASUREMENTS MADE ON THE SAMPLES

4.1 Mechanical measurements

The tensile strength and elongation at break were measured on standardized H3 dumbbells cut out of the jackets and insulator sections, 10 cm in length, cleared of their conducting wires.
If it was impossible to cut the samples from the cable jackets after LOCA (US-EPR cable), the mechanical characteristics were estimated by a winding test on forms.

4.2 Physical-chemical measurements

The gel fractions were measured on the basis of small chips cut into the jackets and insulators. This factor, calculated from the insoluble fraction of the elastomer in a solvent, basically represents the reticulation of the elastomer in question.

The density was measured by conventional picnometers for the jackets and using gas for the insulators. This facility makes it possible to make density measurements while doing away with problems of air adsorption on the samples.

4.3 Electrical measurements

The measurement of the insulation resistance at 500 V DC after a 1-minute stabilization time was carried out :

- On the control and instrumentation cables between each conducting wires and the other wires connected together.
- On the coaxial cable between the central conductor and the metal sheath.

The dielectric strength at 2000 V AC was tested for 1 minute while maintaining the voltage on the control and instrumentation cables. The voltage was applied between each conducting wire and the other wires connected together.

The measurement of electrostatic micro-discharges was made on the coaxial cable by gradually increasing the AC voltage from 0 to 1500 volts for 1.5 minutes, stabilizing the voltage for 3 minutes, then making measurements for the 3 minutes subsequent to the stabilization period. During the test, the voltage was applied between the central conductor wires and the metal sheath.
The characteristic impedance of the coaxial cable was measured by a comparison reflectometer with the impedance of a standard cable.

V. RESULTS

5.1 Results from mechanical measurements

The jackets of the 3 Hypalon control and instrumentation cables (CSPE) have similar behavior : the different formulations are still sensitive to irradiation and temperature during aging under irradiation(Figure 1). A dose/temperature synergy was observed for elongation at break values on irradiated sections of 5 Gy/h (Figure 3). After LOCA, the jackets are considerably degraded, but are still flexible enough to allow the cables to be manipulated (Figure 2).
The insulation on EPDM and EPR wires behaves similarly, indicating the sensitivity of the elastomers to the integrated dose during aging (Figures 4 and 5). However, the dose-rate effect is sometimes to be observed on EPDM for irradiation at 2 Gy/h with respect to irradiation at higher dose rates (Figure 6). On materials irradiated at 20 Gy/h, degradation is higher at 40°C than at 70°C. This phenomenon can be explained by the fact that a transition point was observed by Differential Scanning Calorimetry (DSC) between the 2 temperatures.
The CLPE insulator has irregular mechanical properties which will not facilitate the study of the variation of these properties during aging under irradiation.
After LOCA, only the EPR insulator of the French cable was suitable for cutting away; the CLPE insulator remained bonded into the filler of cables, which melted, and the EPDM insulator was firmly stuck to the copper wires. On the EPR, considerable degradation was observed after LOCA. This degradation is a little higher with prior aging dose (Figure 7).

The PE/PE coaxial cable has a specific behavior: the jacket and insulator degraded quickly during aging under irradiation. Contrary to what is usualy observed on polymers, degradation increased in proportion to the amount of dose rate (Figure 8). The cable which was not qualified under accidental conditions was effectively destroyed during the LOCA irradiation sequence.

The degradation of the mechanical properties (elongation at break), obtained for integrated doses of around 200 kGy, is higher for low dose rates (5 - 10 Gy/h) than for a higher dose rate of 90 Gy/h.
Similarly, after LOCA, it is observed that the degradation on previously-aged cables at lower dose rates was higher.

5.2 Results on the basis of physical-chemical measurements

5.2.1 Density

The densities of the jackets and the insulators of the conductors did not vary much during aging.
After LOCA, only virgin specimens that had not previously been aged had lower densities.

5.2.2 Gel fraction

For the Hypalon jackets on the 3 control and instrumentation cables, there is a regular increase in the gel fraction during aging under irradiation, independent of the irradiation dose-rate value. The increase represents approximately 10% of the initial value (Figure 9).
After LOCA, the gel fraction increases more to reach values in excess of 20% of the initial value, explicable by the strong reticulation of the elastomer, or by the extraction of part of the product during LOCA steam exposure (Figure 10).
The EPDM, EPR and CLPE insulators do not have any significant variation in the gel fraction during aging under irradiation and after the LOCA accident.

5.3 Results on the basis of electrical measurements

The electrical properties of the control and instrumentation cables remain generally satisfactory during aging under irradiation and after LOCA : insulation resistances were still above 5 10^5 MΩ (Figures 11 and 12). No breakdown occurred, except for one US-CLPE cable at a voltage of 2 kV after LOCA.
The coaxial cable preserves good electrical properties throughout aging under irradiation. A few micro-breaks were recorded on the irradiated cable in EVOCABLE. These occurred in a random manner, and were attributed to problems of connectors.

COMMENTS AND CONCLUSIONS

The design program, of which the procedure and results are outlined here, was aimed at :

- simulating realistically and measuring the effects of cable aging in a laboratory, limited to two important parameters, temperature and dose rate.
- comparing the results obtained during simulations with those of an identical cable put under conditions very similar to those found in PWRs.
- on the basis of the measurements made at different stages of aging, defining the criteria for early detection of aging which could cause functional failure.

This program, developed specifically for control and instrumentation cables, to ensure safety functions under normal and accidental ambient conditions, was also applied to a test to investigate a coaxial cable whose operation is required under normal PWR operating conditions.

Among the mechanical and physical-chemical measurements made on cables during aging under irradiation, and after the accidental tests of the LOCA, elongation at break and the gel fraction were found to be sufficiently sensitive to give precious information about the state of reticulation or degradation of the cables. Accordingly, it was possible to measure the influence of temperature and dose rate of irradiation upon the aging of the Hypalon jackets. The synergy between the irradiation and the temperature maintenance of the Hypalon jackets was revealed at a dose rate of 5 Gy/h and 70°C, confirming the results of an

earlier study (4), in which the same type of synergy had been demonstrated from the radio-chemical oxygen-absorption yields.
The EPR insulator of the French cable is not sensitive to irradiation dose-rate variations applied during the study. These materials, like FR-EPDM, remain extremely sensitive to an irradiation dose which, even at the lowest levels, causes a considerable drop in elongation at break.
The CLPE insulator of the American cable has irregular mechanical properties which did not allow the same measurements to be made as on the other cables.

The coaxial cable has a particular behavior, in that the higher the dose rate, the greater the degradation for a given dose. This is very probably due to a highly-ramified structure of the mononucleic chains.
No major electrical breakdown was measured on the control and instrumentation cables during aging and after the accident. This indicates that the residual mechanical characteristics of the cables remain satisfactory for them to be manipulated up to dose of 84 kGy.

The conclusions of this study are numerous: first, if we compare the state of the control and instrumentation cables aged at up to 56 kGy and 2 Gy/h in the EVOCABLE setup, with the state of the cables aged respectively at 5, 10, 20 and 90 Gy/h at the same temperature and total dose, there is no evidence of any major variations of the mechanical properties of these cables changing as a function of the irradiation dose rates. Conversely, for higher doses irradiation, at around 200 kGy, we observe the effect of the dose rate, even at 40°C, between irradiations at lower dose rates (5, 10 Gy/h) and irradiations at 90 Gy/h. The effect of the dose rate is emphasized by the temperature to the point that it is clearly visible for irradiations at 5, 10 and 20 Gy/h at 70°C.
Finally, it can be confirmed that the aging before the LOCA tests have an influence upon the residual properties measured after the accident.

- The higher the aging irradiation dose, the greater the degradation after LOCA.
- For an equal aging irradiation dose, degradation after LOCA is higher for aged materials at lower dose rates.

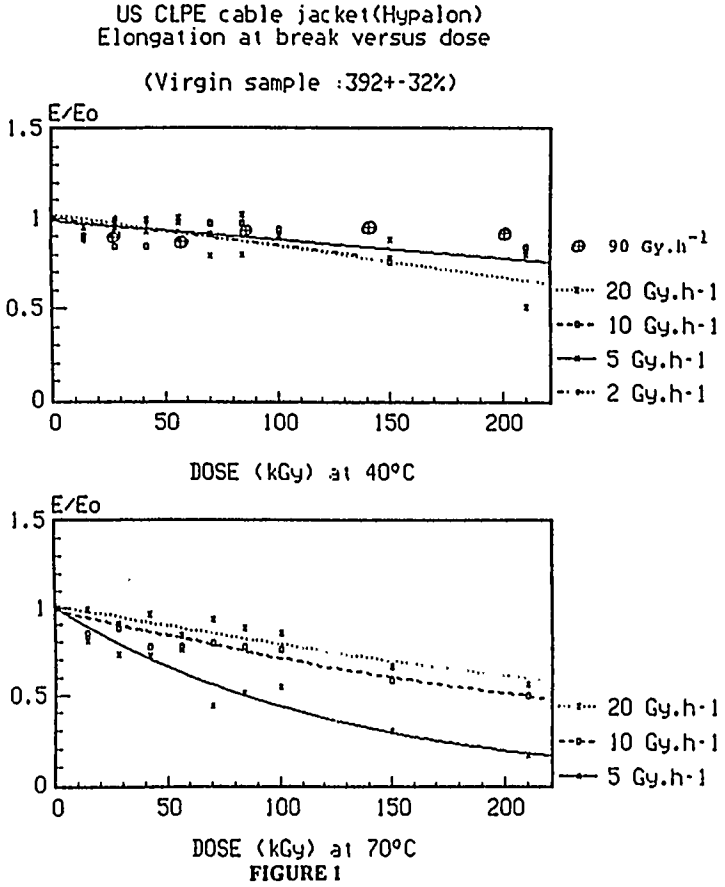

FIGURE 1

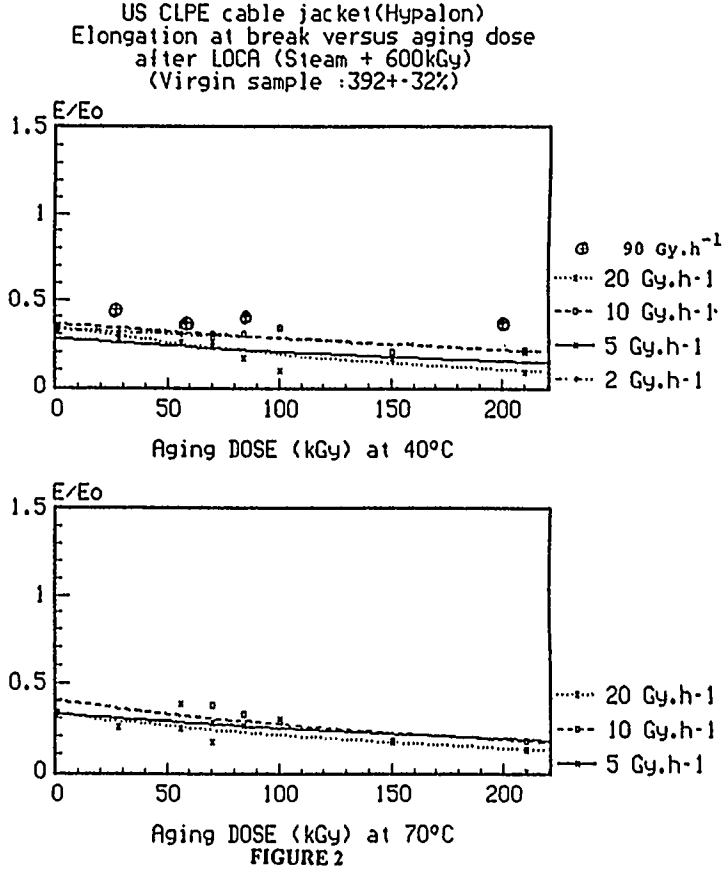

FIGURE 2

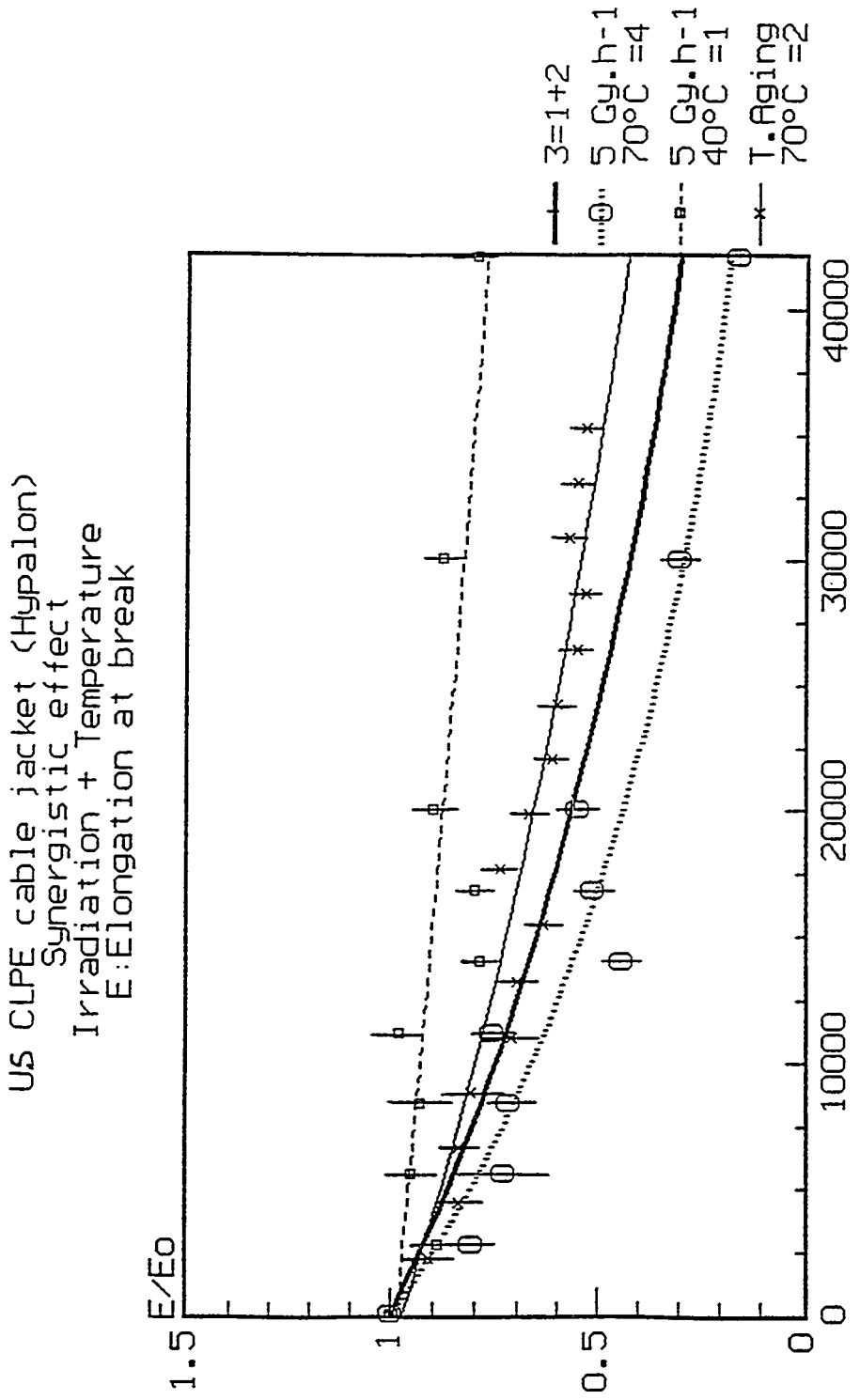
US CLPE cable jacket (Hypalon)
Synergistic effect
Irradiation + Temperature
E:Elongation at break
E/Eo
1.5
1
0.5
0
0
10000
20000
30000
40000
TIME (hours)
3=1+2
5 Gy.h-1
70°C =4
5 Gy.h-1
40°C =1
T.Aging
70°C =2

FIGURE 3

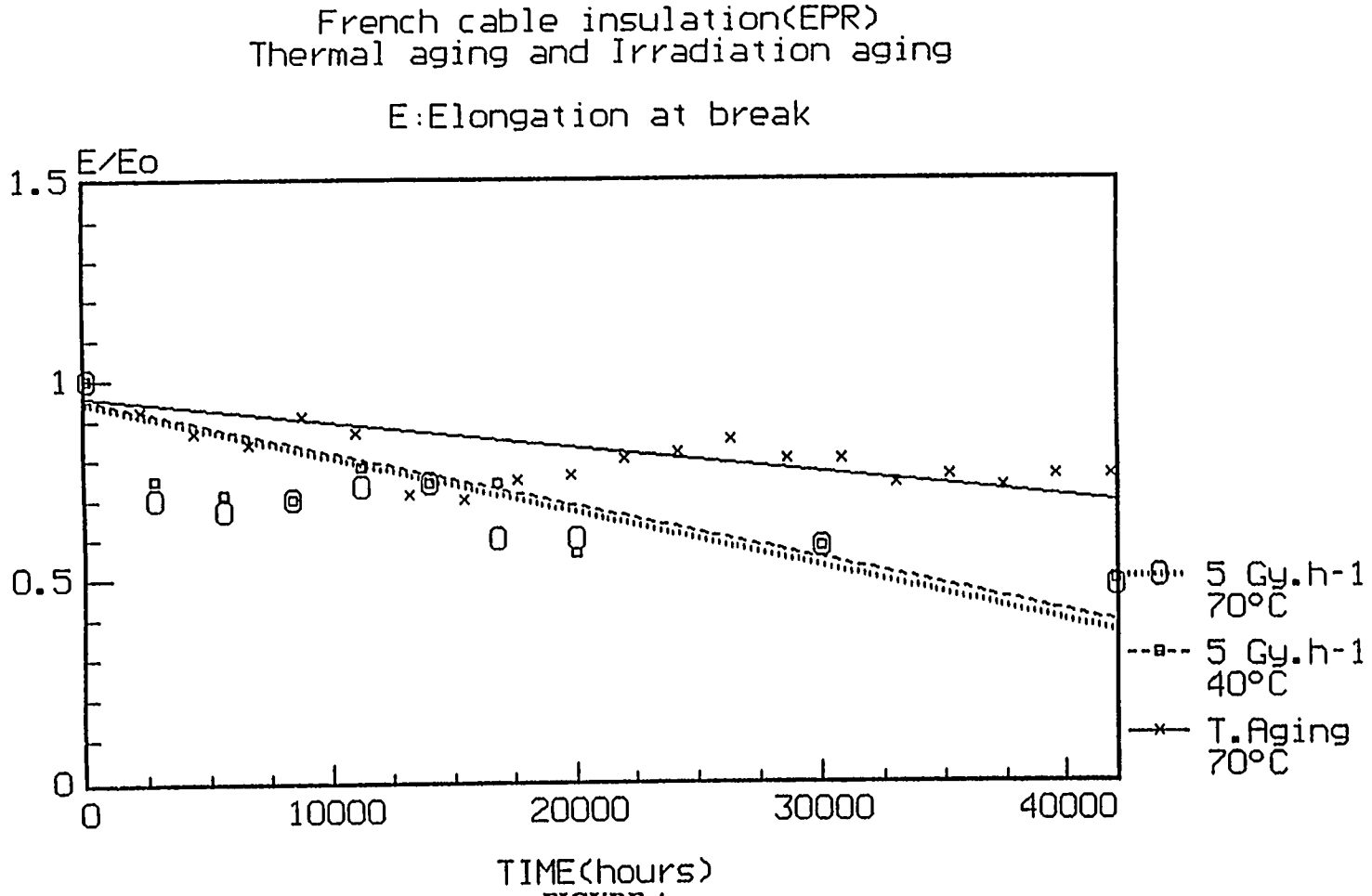
French cable insulation(EPR)
Thermal aging and Irradiation aging
E:Elongation at break
E/Eo
1.5
1
0.5
0
0
10000
20000
30000
40000
TIME(hours)
5 Gy.h-1
70°C
5 Gy.h-1
40°C
T.Aging
70°C

FIGURE 4

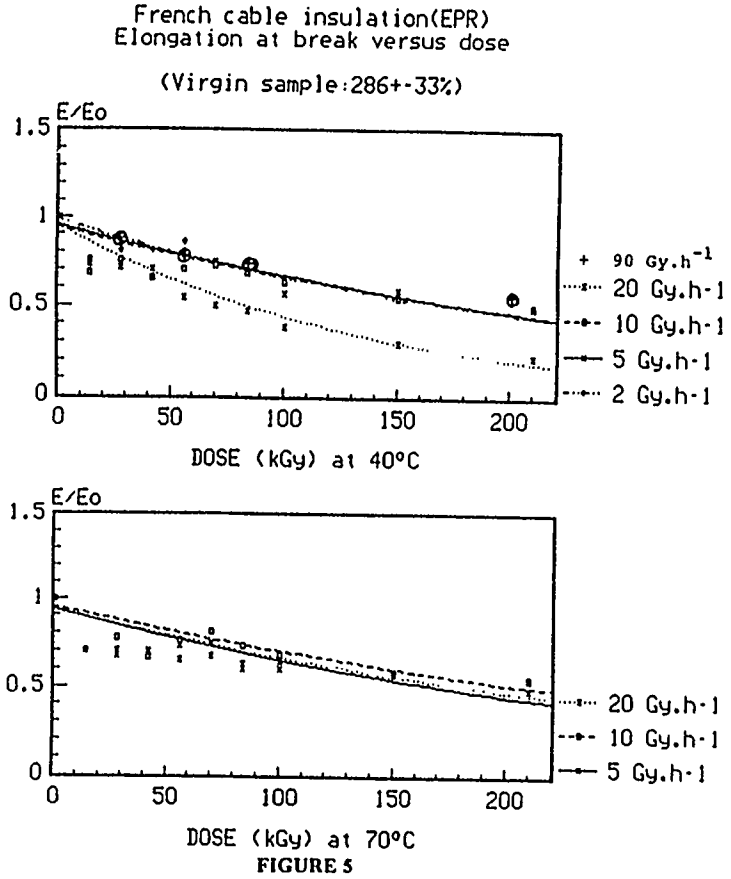

FIGURE 5

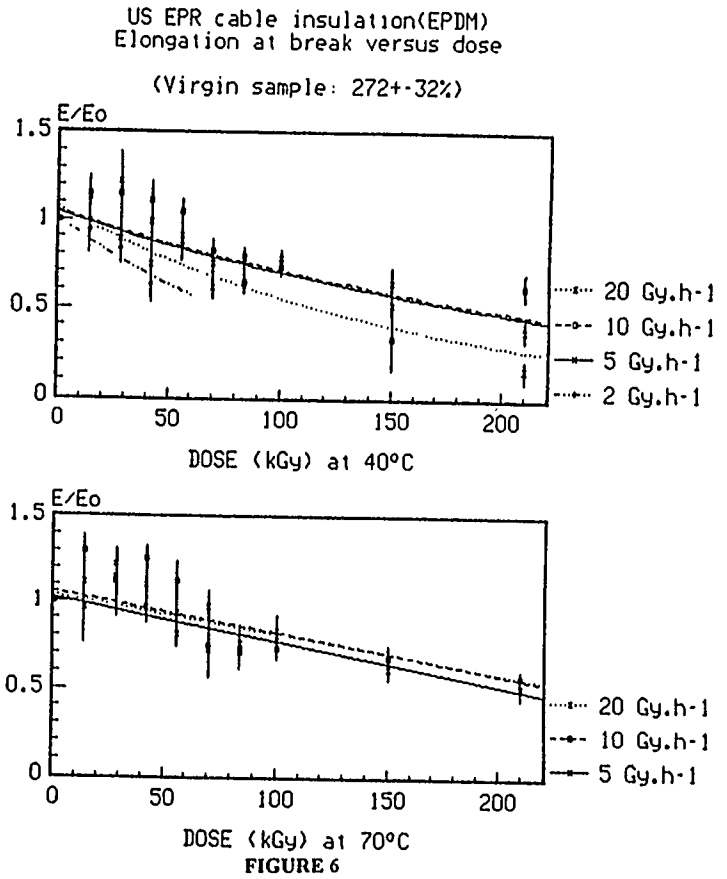

FIGURE 6

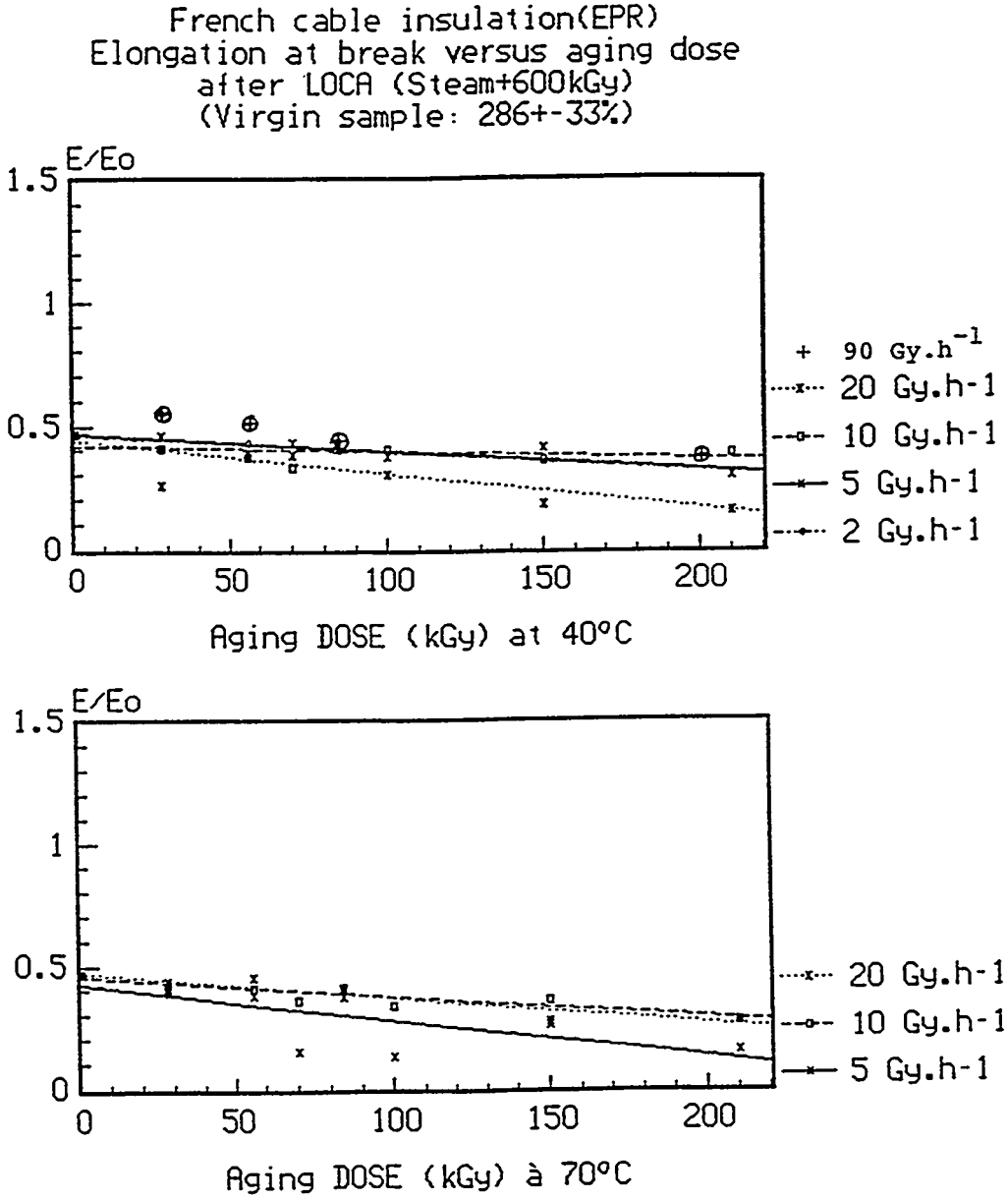
French cable insulation(EPR)
Elongation at break versus aging dose
after LOCA (Steam+600kGy)
(Virgin sample: 286+-33%)
E/Eo
1.5
1
0.5
0
0
50
100
150
200
+ 90 Gy.h-1
20 Gy.h-1
10 Gy.h-1
5 Gy.h-1
2 Gy.h-1
Aging DOSE (kGy) at 40°C
E/Eo
1.5
1
0.5
0
0
50
100
150
200
20 Gy.h-1
10 Gy.h-1
5 Gy.h-1
Aging DOSE (kGy) à 70°C

FIGURE 7

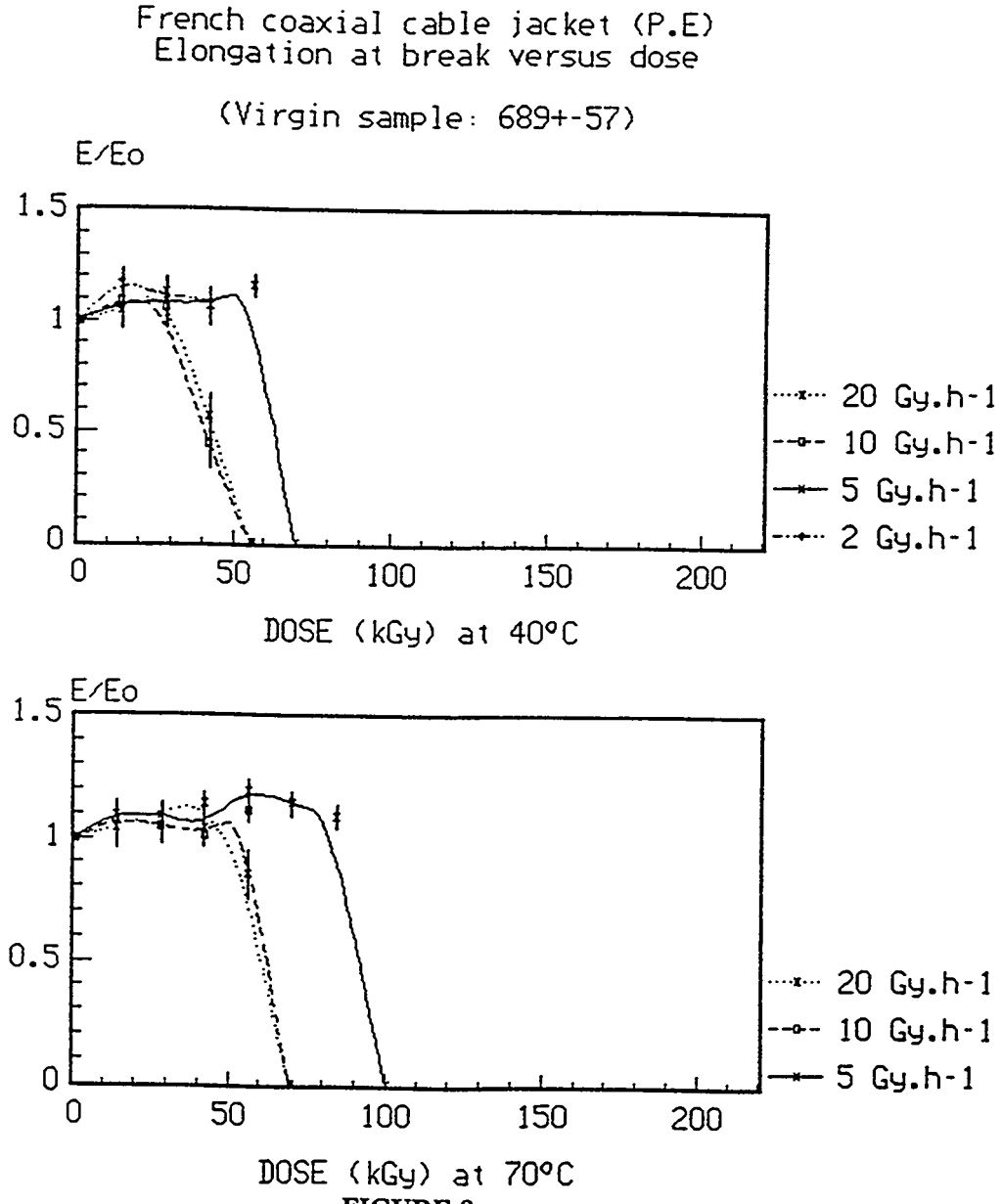
French coaxial cable jacket (P.E)
Elongation at break versus dose
(Virgin sample: 689+-57)
E/Eo
1.5
1
0.5
0
0
50
100
150
200
DOSE (kGy) at 40°C
20 Gy.h-1
10 Gy.h-1
5 Gy.h-1
2 Gy.h-1
E/Eo
1.5
1
0.5
0
0
50
100
150
200
DOSE (kGy) at 70°C
20 Gy.h-1
10 Gy.h-1
5 Gy.h-1

FIGURE 8

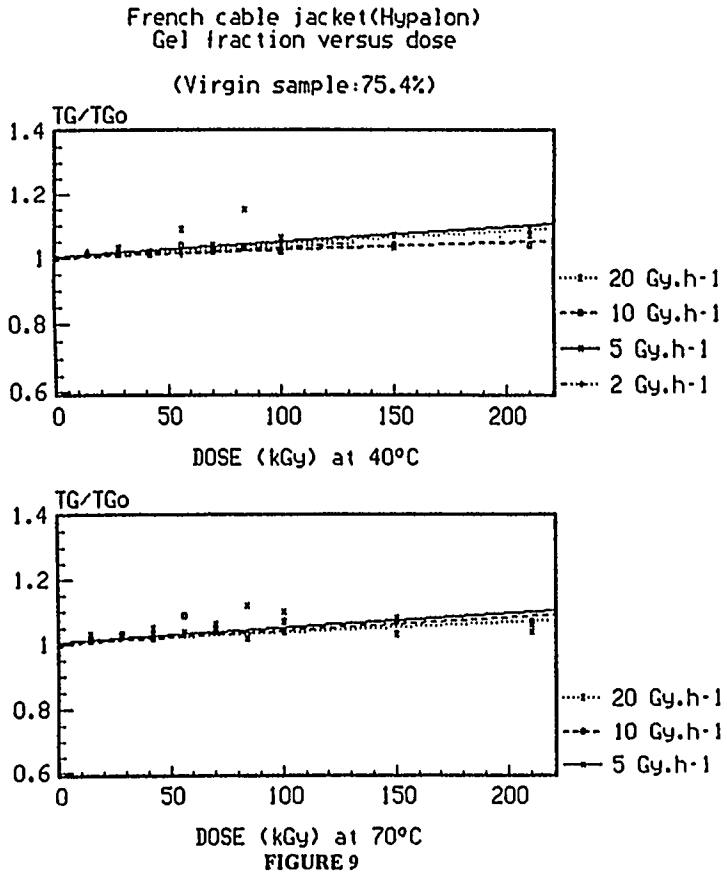

FIGURE 9

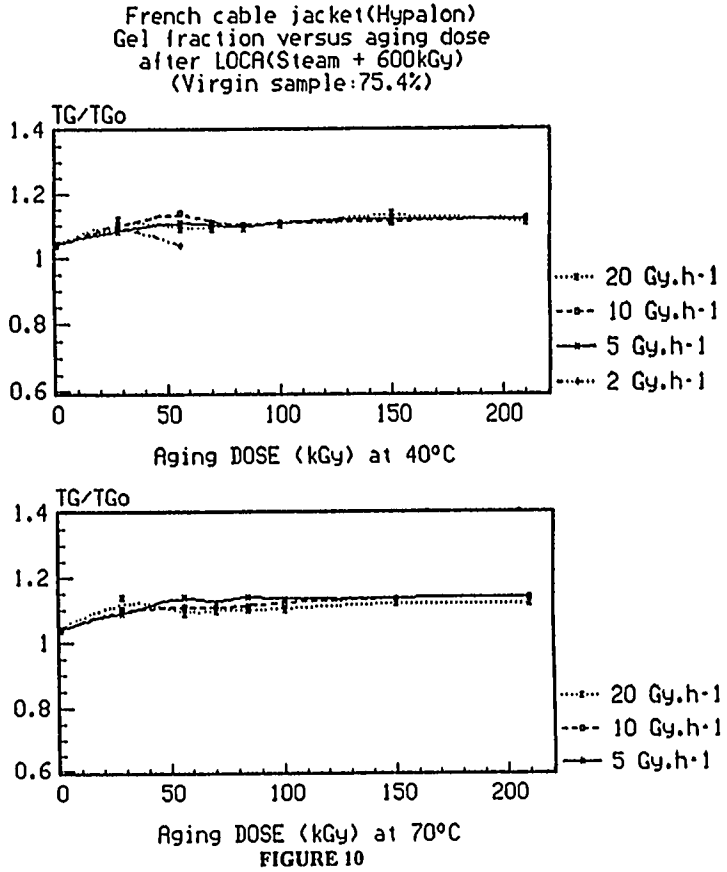

FIGURE 10

French Hypalon/EPR cable
Insulating resistance
versus dose

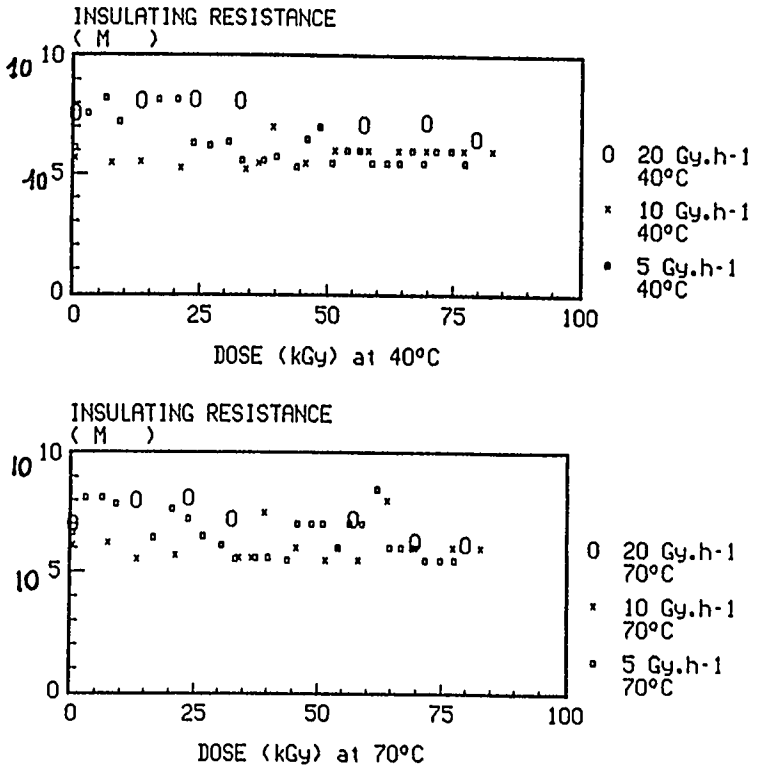

FIGURE 11

US EPR cable
Insulating resistance
versus dose

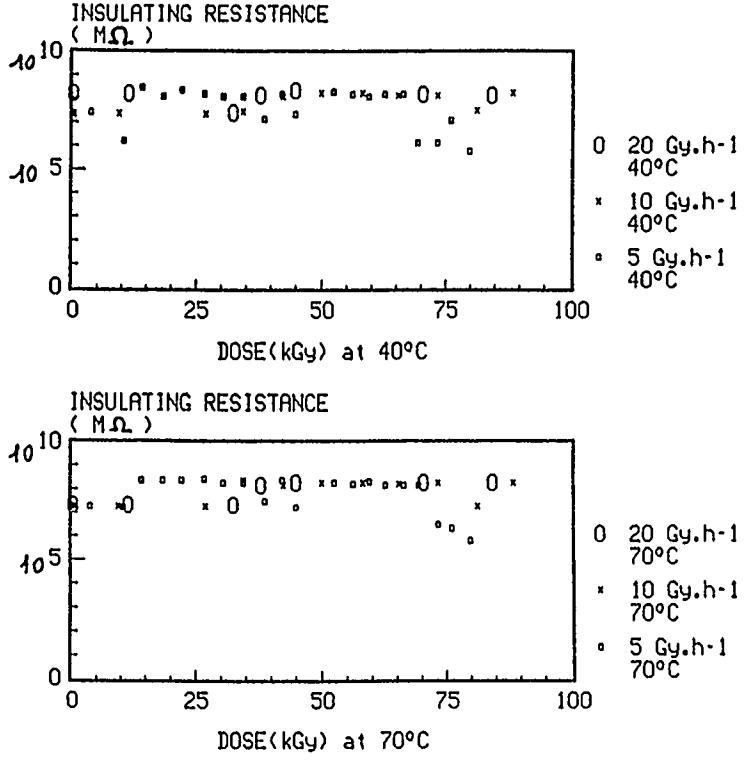

FIGURE 12

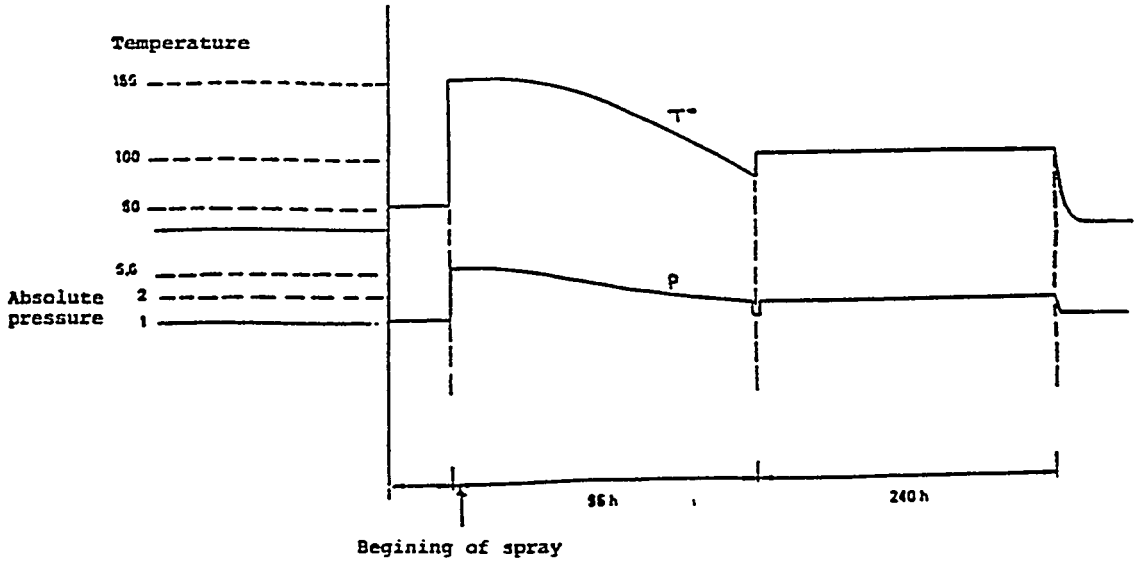

LOCA and POST LOCA profiles

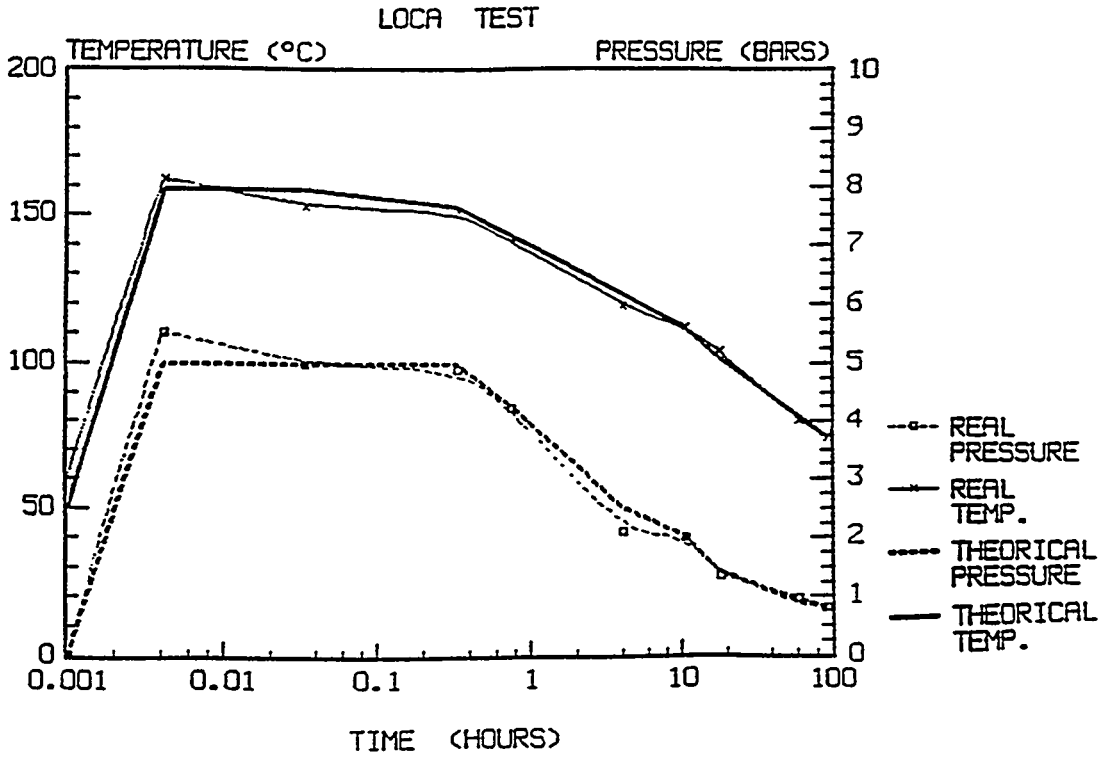

Thermodynamic profile obtained inside CESAR

FIGURE 13

REFERENCES

1. The effect of thermal and irradiation aging simulation procedures on polymer properties.
   L.D. Bustard - E. Minor - J. Chénion - F. Carlin - C. Alba - G. Gaussens - M. Lemeur.
   NUREG/CR 3629 - SAND 83-2651.

2. The effect of alternative aging and accident simulation polymer properties.
   L.D. Bustard - J. Chénion - F. Carlin - C. Alba - G. Gaussens - M. Lemeur.
   NUREG/CR 4091 - SAND 84-2291.

3. U.S. / French joint research program regarding the behavior of polymer base materials subjected to βeta radiation.
   Volume 1 - phase 1 - Normalization results
   Volume 2 - phase 2a - Screening tests
   Volume 3 - phase 2b - Expanded test results
   W.H. Buckalew - J. Chénion - F. Carlin - G. Gaussens - P. Le Tutour - M. Lemeur.
   NUREG/CR 4530 - SAND 86-0366.

4. Irradiation de veillissement des polymères. Influence du débit de dose et des séquences d'essais.
   C. Alba - F. Carlin - J. Chénion - F. Lemaire - G. Gaussens - M. Lemeur.
   SFEN - 15 et 16 mai 1984 - Paris FRANCE.

Detection of Pump Degradation

Don Casada

Oak Ridge National Laboratory
Oak Ridge, TN 37831-8038

ABSTRACT

There are a variety of stressors that can affect the operation of centrifugal pumps. Although these general stressors are active in essentially all centrifugal pumps, the stressor level and the extent of wear and degradation can vary greatly. Parameters that affect the extent of stressor activity are manifold. In order to assure the long-term operational readiness of a pump, it is important to both understand the nature and magnitude of the specific degradation mechanisms and to monitor the performance of the pump.

The most commonly applied method of monitoring the condition of not only pumps, but rotating machinery in general, is vibration analysis. Periodic or continuous spectral vibration analysis is a cornerstone of most pump monitoring programs. In the nuclear industry, non-spectral vibration monitoring of safety-related pumps is performed in accordance with the ASME code. Pump head and flow rate are also monitored, per code requirements.

Although vibration analysis has dominated the condition monitoring field for many years, there are other measures that have been historically used to help understand pump condition; advances in historically applied technologies and developing technologies offer improved monitoring capabilities. The capabilities of several technologies (including vibration analysis, dynamic pressure analysis, and motor power analysis) to detect the presence and magnitude of both stressors and resultant degradation are discussed.

1. Pump Stressors

In a study performed for the NRC on the aging and service wear of auxiliary feedwater (AFW) pumps[1] (hereinafter referred to as the "pump study"), pump stressors were classified as belonging to the following categories:

- Mechanical
- Hydraulic
- Chemical
- Tribological
- Low-relevance factors

The study was based largely on experience with similar pumps used in boiler feed service in fossil applications. It should also be noted that at the time the study was conducted, there was minimal available failure data.

The scope of the pump study did not include the pump driver. A subsequent study of the AFW system[2] (hereinafter referred to as the "system study"), indicated that pump driver-related failures were a principal source of system degradation. For purposes of this paper, the principal pump (including driver) stressor categories are slightly modified from the original pump study:

- Mechanical
- Hydraulic
- Other (including those associated with the pump driver)
- Tribological
- Chemical

The pump study indicated that the principal relevant chemical stressors for AFW pumps, oxidation of 400 series stainless steels through chemical reaction with stagnant water, was in effect a tribological factor since its relevance was primarily related to abrasive oxides. As a result, the pump study dealt with the effects of the first three stressor categories (mechanical, hydraulic, and tribological) on the various parts of the pump.

Some specific stressors within these three categories are identified in Table 1.

Table 1. Principal Stressors of Influence for AFW pumps

Mechanical	Hydraulic	Tribological
torque transmitted loads	hydraulic loads	rubbing between rotating and nonrotating members
rotor-dynamic loads	fluid impingement	bearing lubricant breakdown
piping forces	internal pressure	surface fatigue
seismic loads	cavitation	lubricant contamination and degradation
vibration (all sources)		starts and stops
		fretting
		surface oxide formation

The specific pump components that are affected by such stressors were identified in the pump study to include the items listed in Table 2.*

Table 2. Primary Components Influenced by Identified Stressors

Rotating elements	Nonrotating internals	Mechanical subsystems
shaft	diffusers/volutes	thrust bearings
impellers	return channels	radial bearings
thrust runners	wear surfaces	shaft seals
fasteners	fasteners	thrust balancer
miscellaneous spacers		coupling
		fasteners

Hydraulic and tribological factors, primarily associated with dynamic loads from hydraulic forces and cavitation, were identified as the principal stressors of significance for both rotating elements and nonrotating internals components. Tribologically-related factors, which are more diverse in nature, were identified as being the primary influence for the mechanical subsystem components. The tribological factors associated with the mechanical subsystem components identified in the pump study ranged from axial and radial hydraulic loads (both static and dynamic) to breakdown or loss of lubricant in gear couplings. Mechanical factors, such as overtightening of packing, and rotor dynamic loads were also indicated as principal stressors of influence.

The pump study also identified that the operation of AFW pumps at low flow rates was a particularly important factor in accelerated aging. This factor, as well as the inability to gain useful hydraulic data on the operating condition of the pump when tested at low flow, has led to changes in ASME code requirements.[3,4,5]

The system study, which by its nature investigated historical system failure data (as opposed to focussing on individual component stressors), found that problems with turbine drives were the largest contributor to overall system degradation. Over 80% of the turbine drive problems were associated with either the turbine's control subsystem, the trip and throttle valve, or the governor valve. Likewise, over 80% of pump motor drive problems were related to either the instrumentation and control subsystem or the motor breaker. Thus, the bulk of the pump drive problems were neither related to the drive itself (that is, either the turbine or the motor specifically) nor indirectly induced by the coupling to the pump.

A study of the dynamic loading of pumps[6] that are similar to AFW pumps indicated that for pumps that are balanced according to American Petroleum Institute Standard API 610,[7] the hydraulic unbalance force is "clearly the biggest dynamic load acting on a pump rotor during normal operating conditions." The study did note that the tight mechanical unbalance limits obtained originally (in accordance with API 610) may be difficult to maintain. The study also noted that at low flow rates, "broad band vibrations can become predominant, and can be higher than any other vibrations."

While these stressors were identified in studies on AFW pumps and systems specifically (or on pumps similar to AFW pumps in the case of Ref. 6), they are generally applicable to the broader spectrum of pumps. There are certainly other factors involved in certain applications, and the principal stressors of influence may vary with the specific design and use, but the general observations remain valid.

* Other components identified were the pressure-containment casing and the pump support. Because the stressors identified were not judged to be high-importance factors for these components, they are not included in Table 2.

2. Historically Applied Monitoring Practices

Probably the most commonly applied method for monitoring rotating equipment condition in general, and pumps in particular, has been vibration analysis. The measurement of vibration has been employed for many years. It has evolved from strictly analog devices such as vibrating reeds to digitally-based expert systems. Current expert systems compare the vibration spectra to pre-established limits and previously acquired data to: (1) indicate whether the machine is operating within the desired range, (2) indicate potential sources of problems if not, and (3) project remaining life before repair is necessary. Other commonly monitored pump parameters include head and flow, bearing temperatures, and lube oil condition.

The ASME code[8,†] requires that pump head, flow, and vibration be monitored periodically. The frequency and exact requirements depend upon the type of pump and the specific test being conducted. The vibration monitoring requirement is for a broad band, unfiltered (i.e., non-spectral) amplitude, and the required frequency response range is from one-third of pump shaft rotating speed to 1000 hz.

The current version of the code requires that all pumps be tested within $\pm$ 20% of the pump design flow, if practicable, on a biennial basis. This test is referred to as the Comprehensive Test. The Comprehensive Test, like the other tests under the current and previous code, does not require spectral vibration monitoring or trending.

Another parameter that is seldom used for routine field monitoring, but is often used in troubleshooting and in special test programs (particularly when addressing low-flow conditions or other problem pump conditions such as cavitation), is pressure pulsation.[9,10,11] Pump discharge and suction, as well as various points in the pump casing have been monitored for pressure pulsation analysis.

3. The Detection of Hydraulically-Induced Vibration

The original AFW pump study indicated that effects of low-flow-related forces could be a principal contributor to pump degradation. Subsequent failure of multiple AFW pumps[12] as well as independent studies on similar pumps[6] support the validity of this observation. Utility personnel involved in reviewing the Ref. 12 pump failures indicated that neither the ASME code monitored vibration nor spectral vibration monitoring indicated that a problem existed.

Many vibration guides are available that typically address mechanically-induced vibration components, such as unbalance, misalignment, defective bearings, worn gears, etc. Unfortunately, it is most often the case that such guides or tables fail to address pump-related components. This could well account for the failure to observe indications of degradation or sources of degradation.

The literature suggests that the effects of vibration resulting from undesired pump operational conditions may be manifested at various frequency regimes. Table 3 lists several frequency regions that have been found with field experience.

Table 3. Some Hydraulically-induced Vibration Components

Item	Frequency	Source of vibration	References
A	0-10 Hz (broadband)	Suction recirculation (Ref. 14 relates this to Gap "A", which is the gap between impeller and diffuser/volute sidewalls)	13, 14, 15
B	<15 Hz (broadband)	Unsteady flows due to recirculation or turbulence (similar to item A)	6
C	0 to 1.5 * running speed, broad band	Recirculation	6
D	0.5 to 0.95 * running speed	Rotating stall	6
E	0.6 to 0.9 * running speed	Hydraulic instability	14, 15
F	1* running speed	Hydraulic unbalance	6, 13, 14, 15
G	0.5 kHz to 10 kHz (broadband)	Cavitation	6
H	Vane pass frequency	Impeller vane to diffuser vane gap (Gap "B")	6, 13, 14, 15
I	Relatively distinct peak, 1 to 15 Hz	Surge or system instability	6

† It should be noted that the NRC has not yet, as of this writing, endorsed the 1990 version of the ASME code.

It should be noted that Table 3 is not intended to be a comprehensive listing of all vibration frequencies that may be found; specifically, there are no mechanically-related frequencies.

4. A Comparison of Monitoring and Analysis Methods

The frequency regimes identified in Table 3 are primarily based on vibration monitoring experience. Vibration monitoring is certainly the most commonly applied field diagnostic, so it is a natural result that hydraulic, as well as mechanical, stressors and degradations would be most often identified in that context. However, it is important to recognize that bearing or pump casing vibration will not necessarily represent all sources of unstable conditions. For example, significant torsional loading variations can exist without being manifested at normally monitored vibration locations.

Test data was acquired on two pumps to compare the results of vibration, motor input power, and pressure pulsations (the latter for only one pump) with each other as well as the spectral components identified in Table 3. It is important to note that the pumps tested are relatively low energy pumps. This is an important factor, since low energy pumps are less significantly affected by hydraulic forces than are high energy pumps.[6]

Nominal pump parameters for the tested pumps are provided in Table 4. Both pumps are horizontal, overhung, single suction, single stage, double volute pumps. Pump A would be generally expected to be more subject to low flow-related instabilities than Pump B because of its relatively high suction specific speed as well as larger size. It should be recognized that there are a number of nuclear pump applications that would be expected to be more sensitive to low-flow operation than either of the tested pumps.

Table 4. Nominal pump parameters for test pumps

Parameter	Industrial pump (Pump A)	Small check valve test loop pump (Pump B)
Best Efficiency Flow Rate (gpm)	2000	200
Nominal speed (rpm)	1780	3500
Best Efficiency Head (ft)	137	100
Specific speed	1990	1570
Suction specific speed	12750	10700
Motor power rating (hp)	75	7.5
Number of impeller vanes	6	5

4. A. Pump A Vibration Data Analysis

Vibration data was acquired at various flow rates for Pump A, ranging from shutoff (0 gpm) conditions to greater than best efficiency point (BEP) flow. The vibration data was acquired with accelerometers mounted on (1) the pump casing, in an axial direction, and (2) the housing of the radial bearing closest to the pump, in the horizontal, radial direction.

Figure 1 provides pump casing axial and bearing housing radial vibration velocity spectral data for Pump A at four flow rates ranging from shutoff to 105% of BEP. For the axial vibration data, the running speed peak generally increases with increasing flow, while the vane pass frequency amplitude decreases with flow, suggesting increased hydraulic imbalance with increasing flow (however, see discussion under section 4.D relative to hydraulic imbalance). These patterns are not duplicated in the radial horizontal data. For both monitored locations, the spectral region below 100 hz is somewhat noisier at the low flow conditions. Note that with the exception of a small peak occurring at around 850 hz in the radial signal, there is very little spectral energy in the velocity domain above 400 hz. The spectral displays above 1000 hz are not shown since the velocity domain spectra above 1000 hz are insignificant compared to the lower frequency components.

Figure 2 provides the same vibration source data as Figure 1, except that the vibration is presented in the acceleration domain, and displayed up to 5000 hz, since there is obviously considerable energy present. There are multiple sources of the higher frequency energy including cavitation and bearing fault frequencies. For the axial location (left column), the significantly higher amplitude of broadband noise in the 3000-5000 hz range is attributable to cavitation. The radial location peak at about 850 hz that is barely visible in the velocity domain is one of the more dominant peaks in the acceleration domain. A review of the bearing fault frequencies indicated that all four fault-related frequencies (bearing inner race, outer race, cage, and ball frequencies) for the pump thrust bearing have harmonics that converge at about 850 hz.

Figure 1. Pump A vibration spectra in the velocity domain.

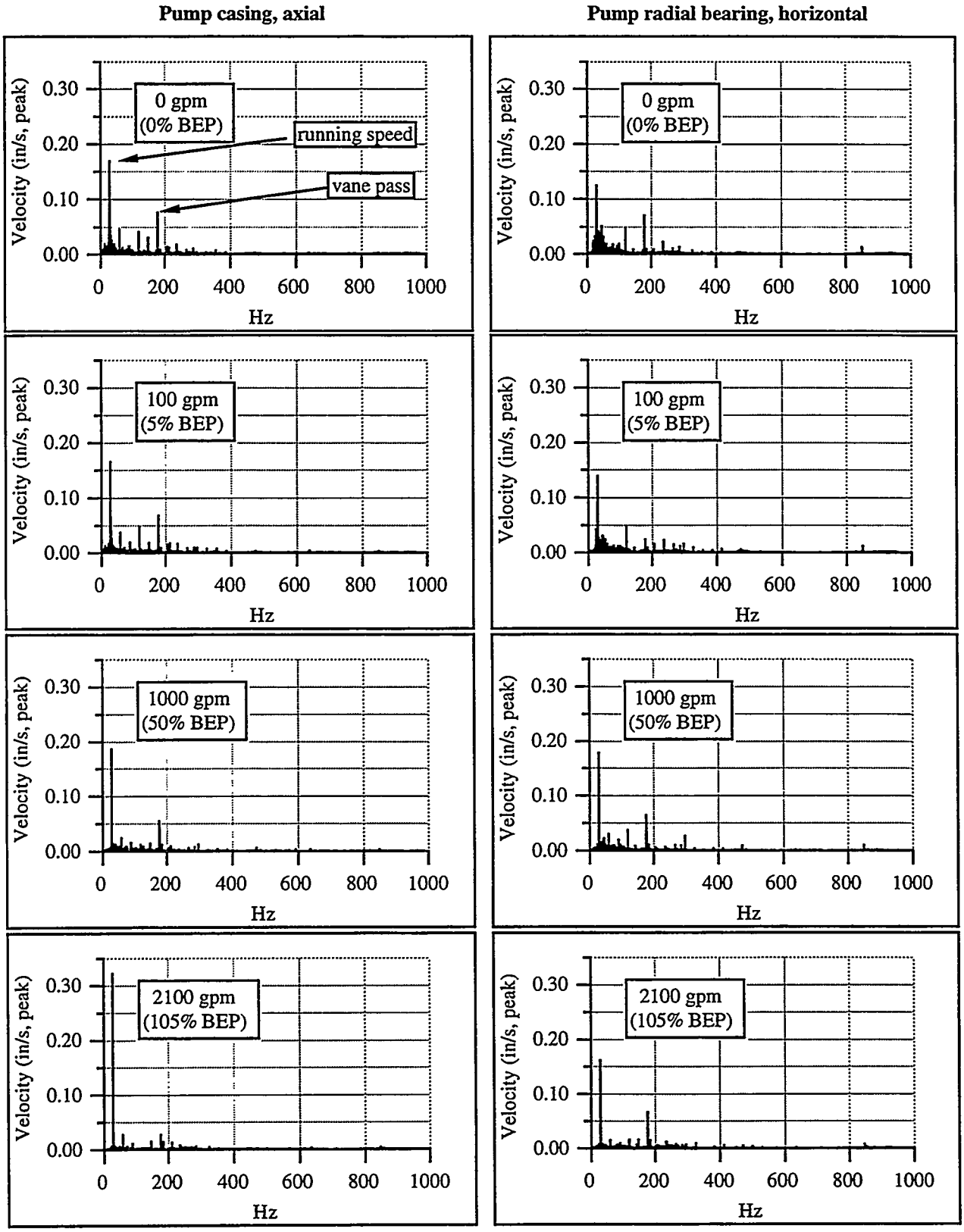

Figure 2. Pump A vibration spectra in the acceleration domain.

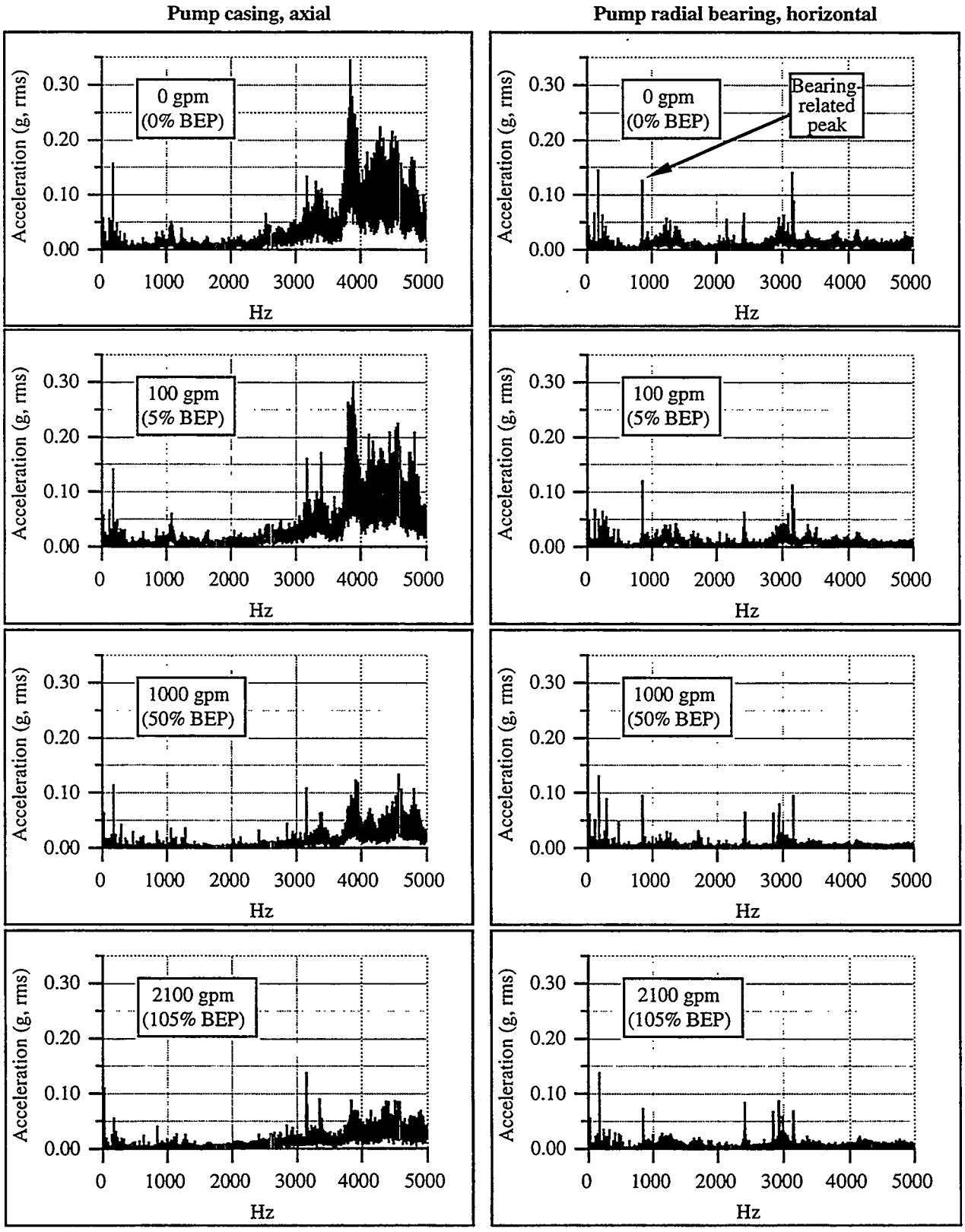

Figure 3 is the same data as shown in Figure 1, but zoomed to show more clearly the spectra from 0-200 Hz. For Figure 3, the graph tick mark labels are at harmonics of running speed. The non-harmonic peak that occurs at about 140 Hz in the radial data (right column) appears to be related to the inner race frequency of the thrust bearing. Figure 3 more clearly shows the higher level of broadband noise that exists at reduced flow conditions from about half of running speed to around four times running speed. Note that the principal areas of higher noise are somewhat different at the two locations. For the axial location (left column), most of the noise appears as sidebands of running speed, while at the radially monitored location, the noise bandwidth is somewhat broader, extending up to four times running speed.

By comparing the data observed in Figures 1-3 with the components reported in Table 3, it can be concluded that the pump shows some evidence of cavitation (broadband noise over a fairly wide band) that is stronger at low flow conditions, as well as indication of recirculation at low flow (although the range of the broadband noise extends beyond the 1.5 times rotating speed suggested in Table 3). Independently, there was audible cavitation noise when the pump was being operated at low flow conditions.

Since the ASME Code does not require spectral monitoring of vibration, the vibration waveforms were also converted to the velocity domain and analyzed. The analysis of the data went well beyond ASME requirements by not only evaluating the overall amplitude, but also determining fluctuations in the overall amplitude during the approximately fourteen seconds over which data was acquired.

Figure 4 provides the results of the analysis. Note that the two upper plots present the non-spectral, or overall amplitude as rms amplitude times 1.414. The reason for providing rms * 1.414 rather than true peak is that historical data that has been labeled "peak" has, in most cases, been actually rms * 1.414. The average pump axial amplitude slightly increases at the upper end of the flow rates monitored, while the radial vibration slightly decreases at the higher flow rates. Both locations are somewhat higher at the shutoff condition than at the intermediate flow conditions. There is little useful information that can otherwise be distilled from the average values.
The presentation of the data as rms * 1.414 rather than true peak is an important distinction, since the true peak is often several times rms *1.414. The lower left plot of Figure 4 shows the ratio of true peak to rms * 1.414 for both monitored locations as a function of flow rate.

The maximum and minimum values shown in the two upper plots are based on the calculation of rms values for one-half second snapshots of the vibration data over a total sample time of fourteen seconds. When the fluctuations in measured amplitude are considered, as opposed to simply the average rms * 1.414, a somewhat more revealing pattern emerges than the simple average rms. The lower right hand plot of Figure 4 shows the ratio of maximum to minimum values of the one-half second sets. At the lowest flow rates, there were more fluctuations in short-duration measurements, which indicate less stable overall conditions. This is qualitatively consistent with the generally noisier spectra observed at the low flow conditions.

The effect of changes in the bearing-related flaws component noted above was also explored. Using the 0 gpm radial vibration data as a source, the signal was modified in two ways. First, the accelerometer signal was digitally filtered to remove the principal frequencies that appear to be bearing-related, as well as the broadband noise above 850 Hz. Second, the bearing flaw-related energy around 850 Hz was digitally amplified by a factor of 10. Figure 5 shows the unmodified velocity domain spectrum, the spectrum with the bearing fault frequencies removed, and the spectrum with the 850 Hz component increased. While the differences are clearly evident in the spectral domain, there is minimal effect on the overall, non-spectral value. For the case where the 850 Hz bearing flaw component is increased by a factor of 10, the overall amplitude increased by less than 20%.

A real degradation in bearing condition would certainly manifest itself differently than the simple digital model used above. For instance, harmonics and/or running speed sidebands of defect frequencies might be expected as the bearing degraded. However, the point to be made is that relatively large increases in high frequency components have minimal effect on the non-spectral overall vibration velocity amplitude.

4. B. Pump B Vibration Data Analysis

Vibration data was acquired at various flow rates for Pump B, ranging from shutoff (0 gpm) conditions to approximately twice best efficiency point (BEP) flow. The vibration data was acquired with accelerometers mounted on (1) the pump casing, in an axial direction, and (2) the housing of the inboard radial bearing.

Figures 6-8 provide velocity and acceleration domain vibration spectra for both monitored locations. Some observations on the data in these figures are listed below.

Figure 3. Pump A vibration spectra in the velocity domain (zoomed).

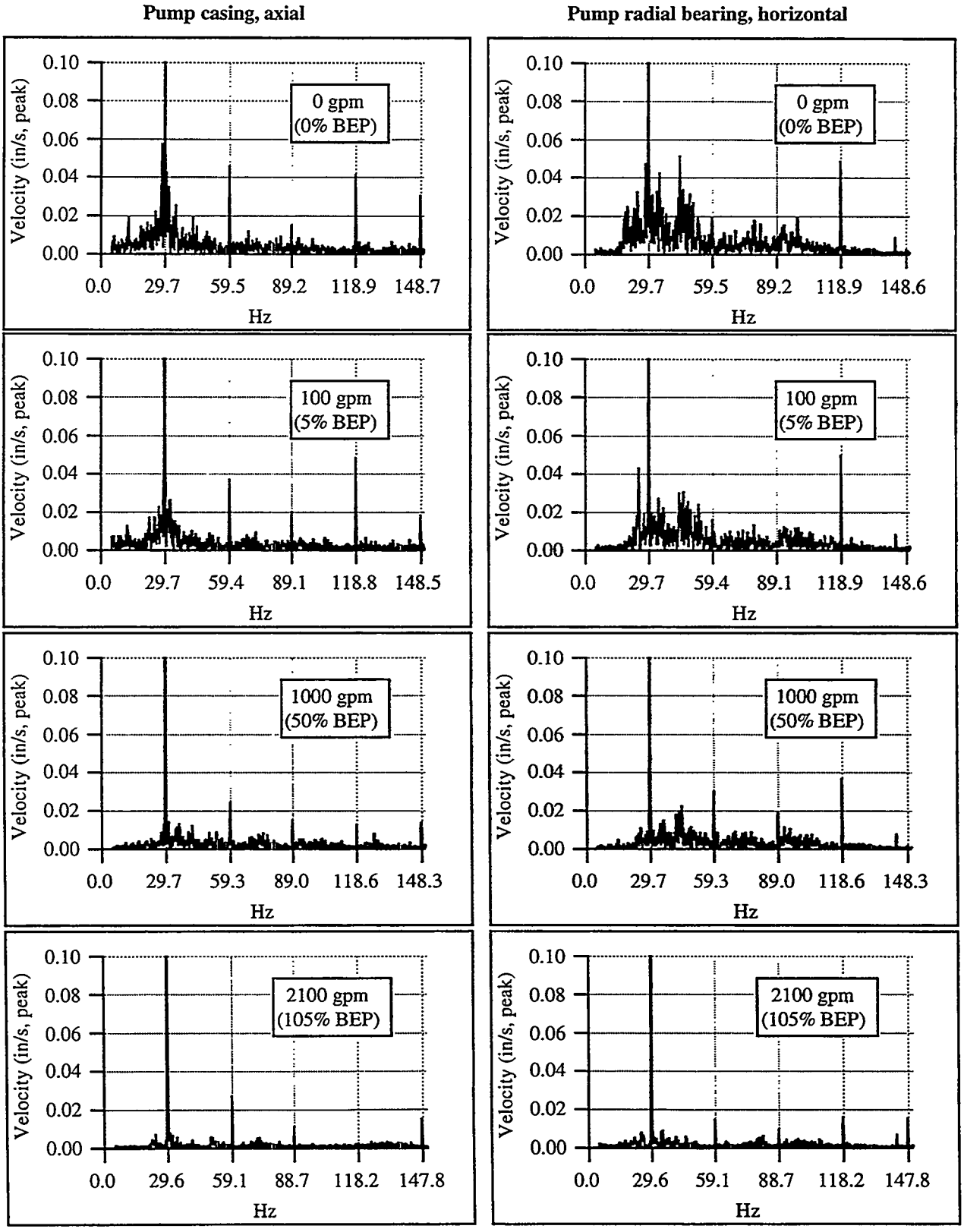

Figure 4. Summary rms vibration data for Pump A. Fourteen seconds of data were acquired; the rms values were calculated over 0.5 second intervals.

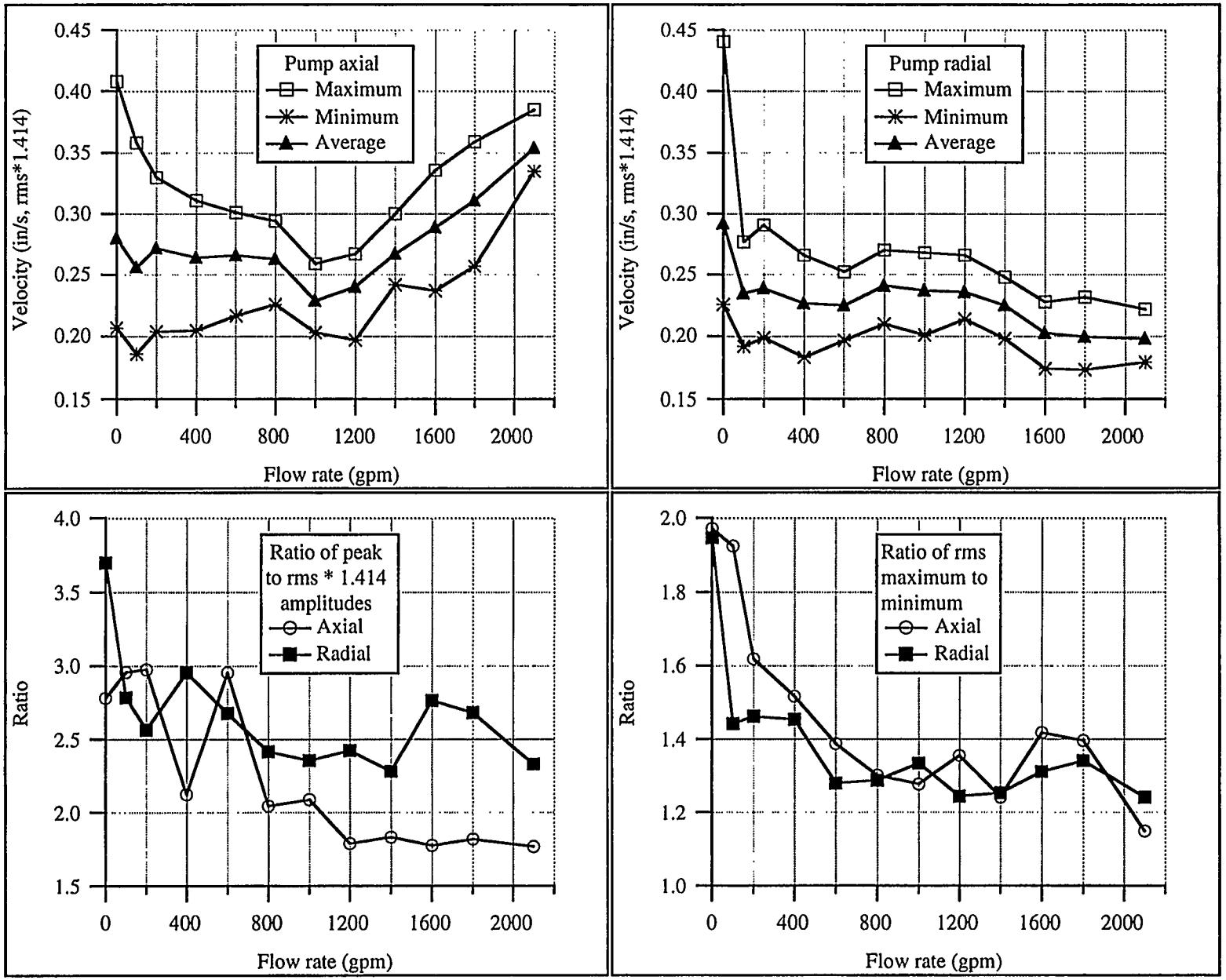

Figure 5. Pump A horizontal radial velocity spectra at 0 gpm: 1) Original data, 2) Data filtered to remove the bearing flaw and cavitation components, and 3) data modified to amplify the bearing flaw component.

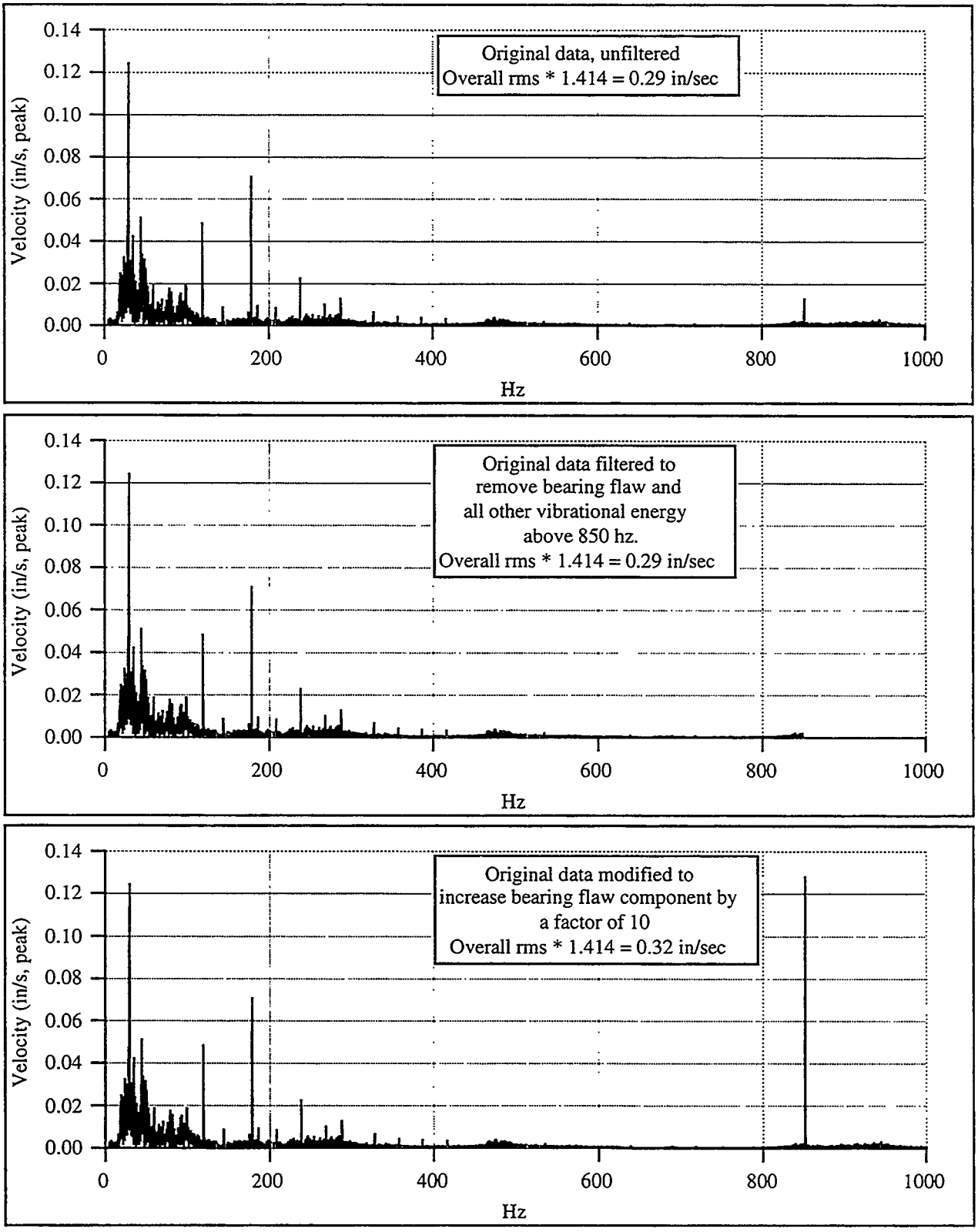

Figure 6. Pump B vibration spectra in the velocity domain.

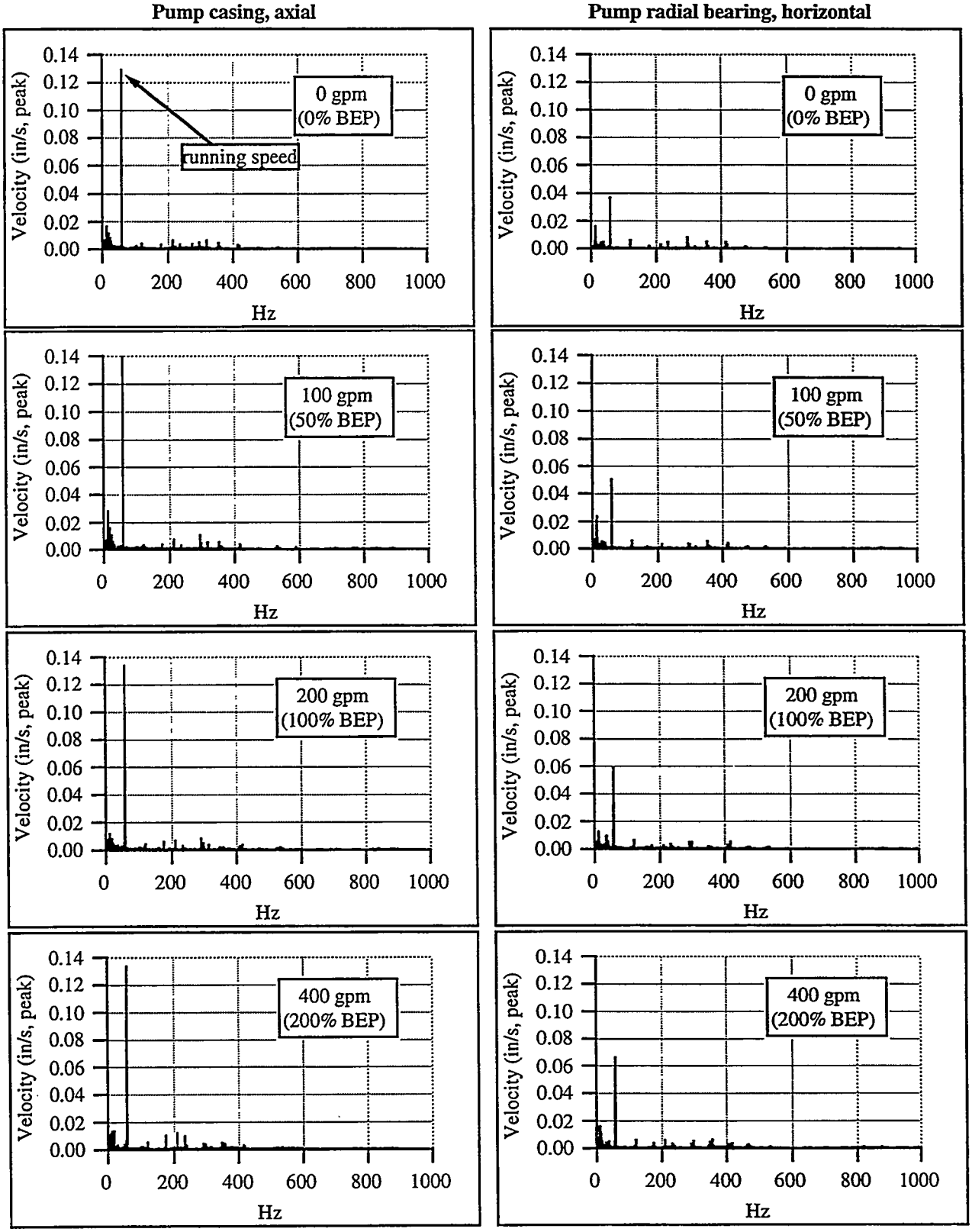

Figure 7. Pump B vibration spectra in the acceleration domain.

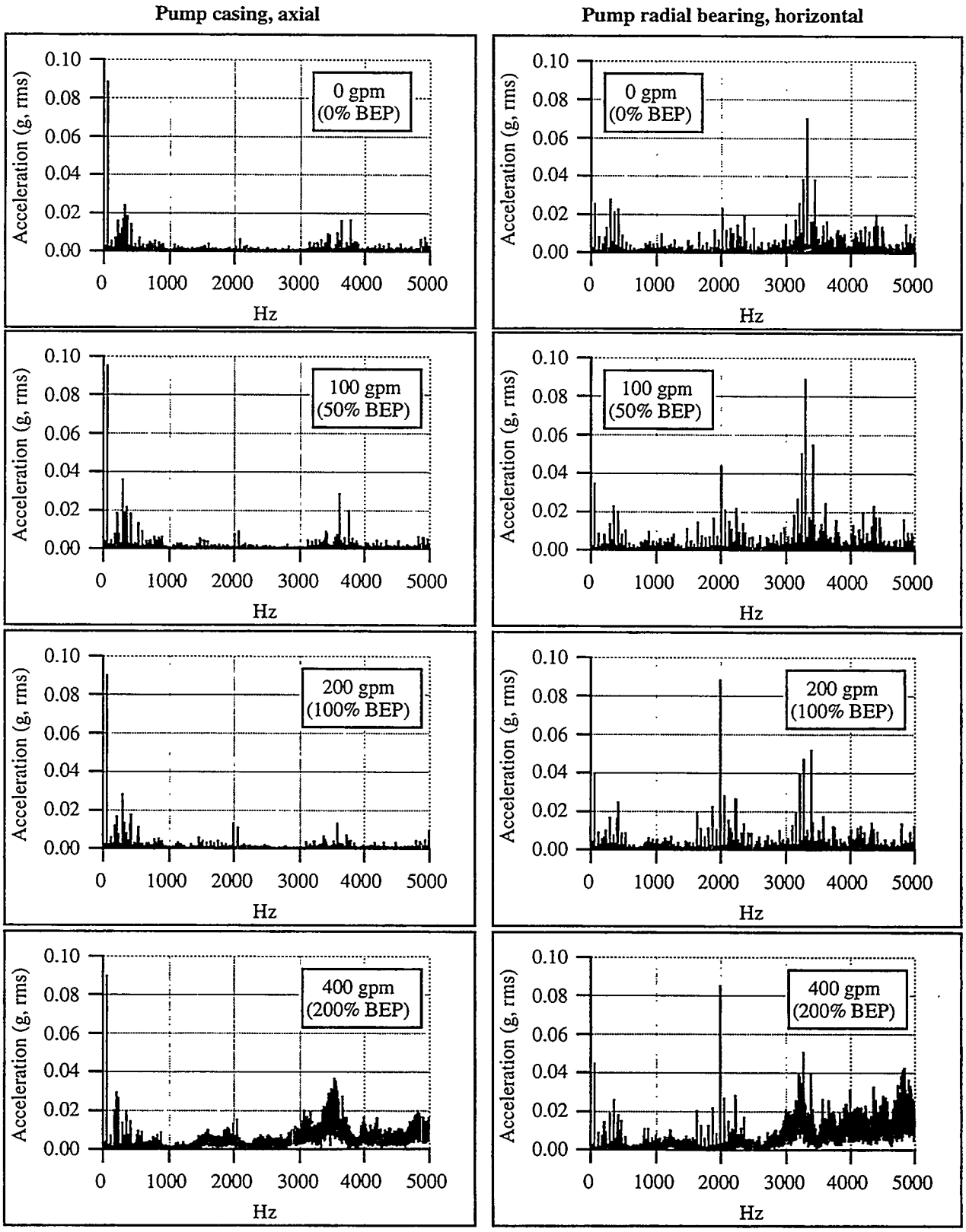

Figure 8. Pump B vibration spectra in the velocity domain (zoomed).

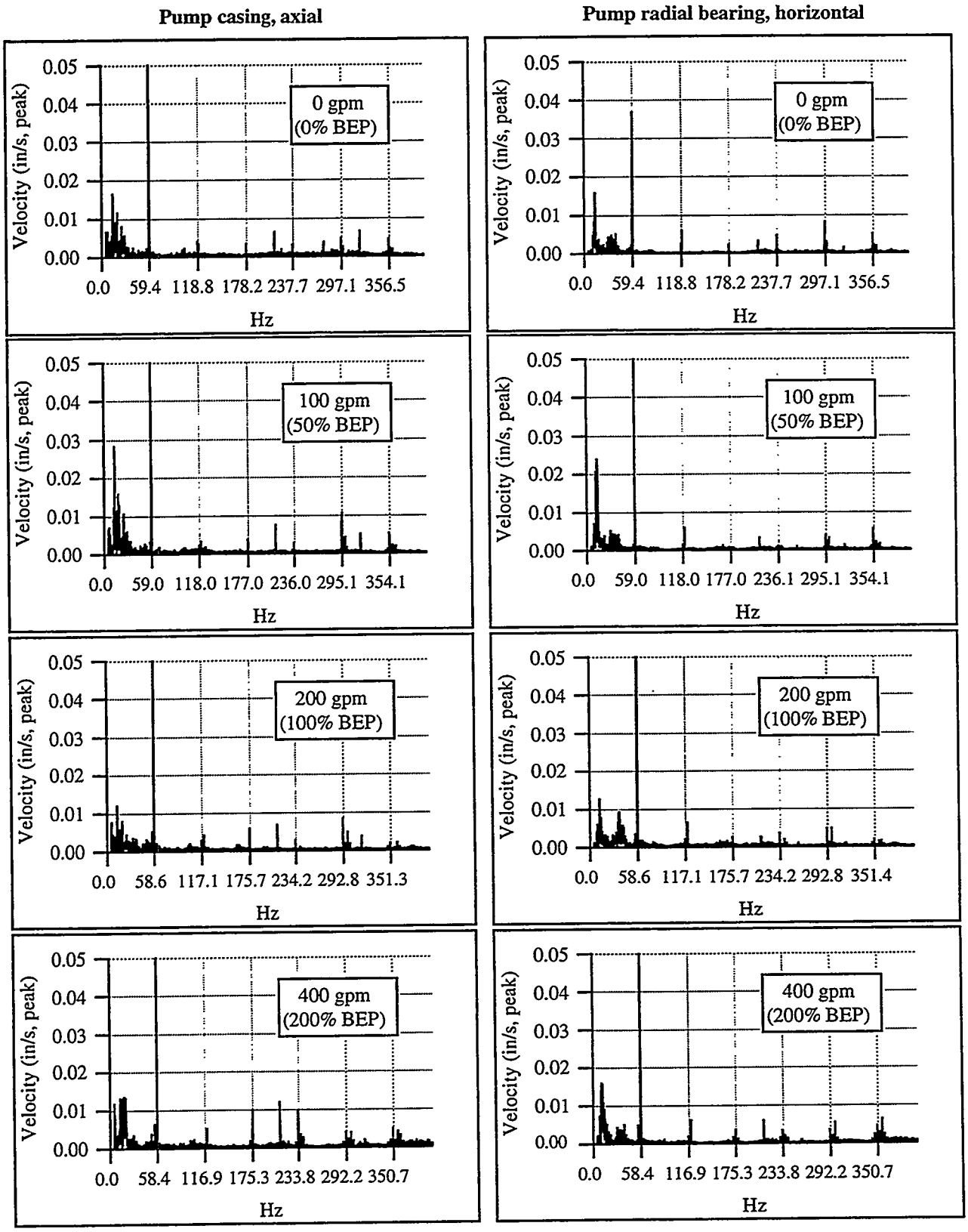

- The running speed axial velocity amplitude for Pump B (Figure 6) is relatively constant with flow rate, unlike Pump A, where the axial running speed amplitude at the highest flow rate is approximately twice that at shutoff (Figure 1).
- There is a significant level of broadband noise at both locations in the acceleration domain (Figure 7) signals at the highest flow rate (200% BEP), indicating cavitation. Although the pump and system generate a generally higher level of noise at this flow rate, cavitation is not audibly detectable.
- There are a series of relatively well defined peaks in the range of 1600-2200 Hz and also in the range of 3100-3400 Hz in the acceleration domain horizontal radial signal. More detailed analysis of the spectra indicated that these peaks originate from a combination of the rotor bar pass frequency (and second harmonic), characteristic bearing frequencies (including a harmonic convergence similar to that noted for Pump A above), and running speed and 120 Hz sidebands of these components. It is important to note that the motor used to drive this pump is a high efficiency motor. High efficiency motors have been observed to be somewhat more likely to generate electrically-related vibration (such as rotor bar pass and 120 Hz components) than conventional motors.
- The vane pass peak is least well defined in the axial vibration for the lowest and highest flow cases. In Figure 8, for which the x-axes are laid out in orders of running speed, the fifth harmonic (vane pass) of running speed can be seen to be better defined for the 50% and 100% of BEP cases than for the shutoff and 200% case.

Figure 9 presents summary, non-spectral rms vibration data for the flow rates previously discussed. For this pump, the general trend is that radial vibration generally increases with flow, while there is no consistent trend with flow for the axial vibration. The overall amplitudes, and the level of fluctuation at all flow rates, is less than that for Pump A.

Clearly, there is important information in the higher frequency region of the vibration spectrum whose effect is minimally seen in the overall, non-spectral rms amplitude, as the acceleration frequency spectra for the pumps above have shown. Figure 10 shows the waveforms of the same vibration signal, with different digital filters applied. The upper plot shows the signal with a 6000 Hz digital low-pass filter applied to the signal (which was also analog low-pass filtered at 6000 Hz nominal cutoff frequency for anti-aliasing before digitization). The lower plot of Figure 10 shows the same signal after having been low-pass filtered at 1000 Hz. The overall rms amplitude is only marginally changed. The filtering at 1000 Hz almost totally eliminates the effects of cavitation, rotor bar pass, and higher frequency bearing-generated vibration.

The significance of the 1000 Hz filter is that the ASME code requires that the frequency span to be included in vibration monitoring range from one-third of running speed to 1000 Hz. Many vibration analyzers allow the user to select the bandwidth, and then apply anti-aliasing filters to limit signals outside of the selected bandwidth. Thus, an analyzer set up to cover the exact range required by the ASME code would also filter out the higher frequency components noted above.

4. C. Pressure Pulsation Analysis

Pressure pulsations originate from various sources, including impeller vanes passing diffuser vanes or volute cutwaters, non-symmetric loading at rotational frequency, and other hydraulically-borne load variations. The vibration components listed in Table 3 are associated with hydraulic conditions, and vibration is a secondary response to the hydraulic loadings. Careful pressure analysis should be an inherently better means of monitoring the sources of hydraulically induced vibration. Of course, pressure monitoring is somewhat intrusive in nature, and is therefore not a practical tool to use as a routine field monitor.

Pressure pulsation data for Pump B was acquired and spectrally analyzed. Two pressure transducers were used – one located about 6 inches upstream of the pump suction nozzle, and the other located about two feet from the pump discharge nozzle. Both analog pressure signals were digitized. The suction pressure signal was subtracted from the discharge pressure signal to yield a pump head signal.

Figure 11 provides the pressure spectrum for the pulsations in the pump head at the same four flow conditions for which vibration data presented in Figures 6-8 was acquired. The pulsation amplitude is expressed in rms terms. The pump vane pass frequency was, for all cases except the highest flow case, the dominant component, but trended down with increasing flow rate. This is not surprising, since the overall head decreases with increasing flow rate; however, note that the decay is decidedly non-linear with average head. At shutoff conditions, the rms pressure pulsation amplitude at vane pass frequency is over 1% of the total head. At the intermediate flow conditions, the

Figure 9. Summary rms vibration data for Pump B. Seven seconds of data were acquired; the rms values were calculated over 0.5 second intervals.

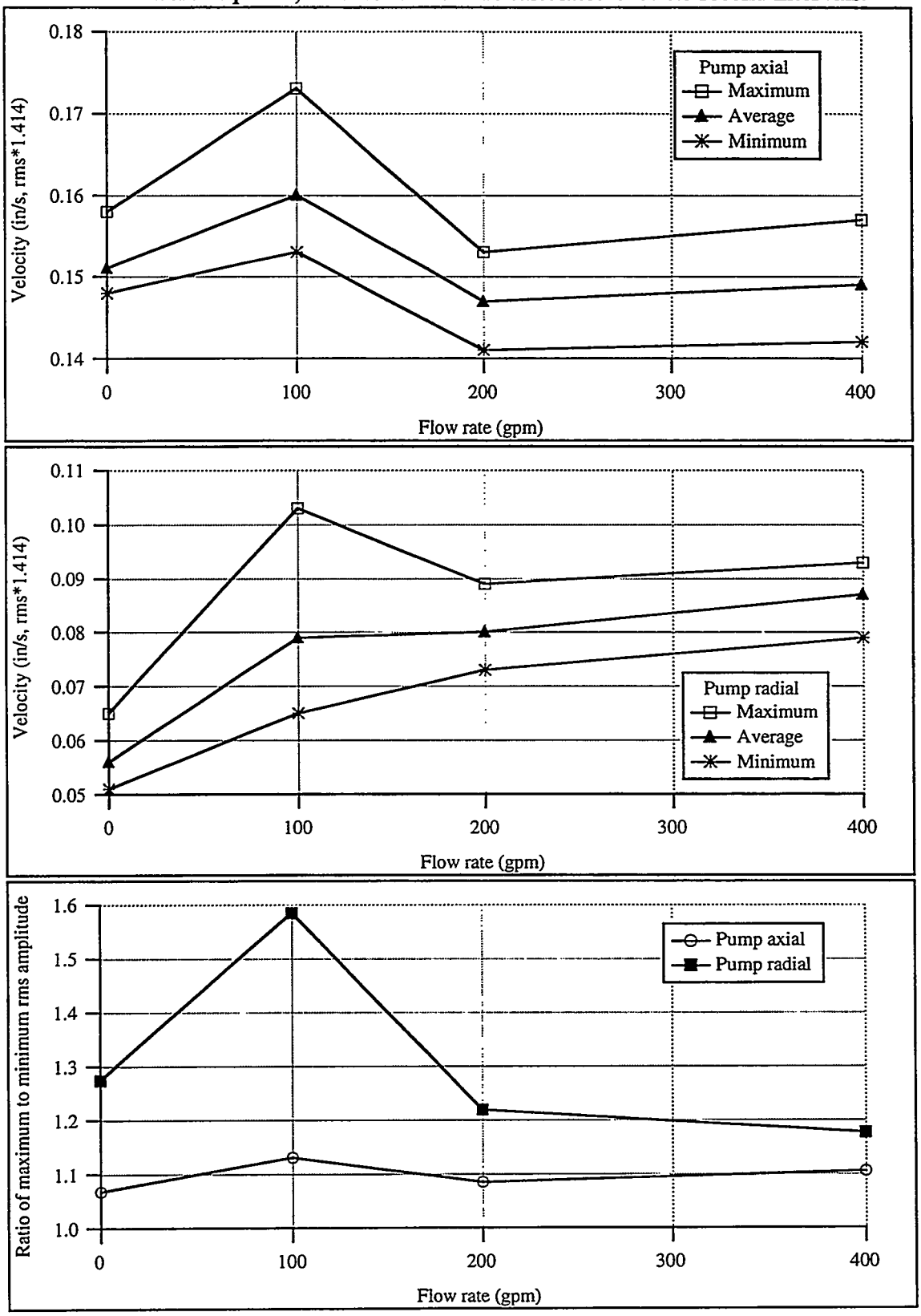

Figure 10. Radial vibration velocity waveforms for Pump B at 400 gpm for two digital low-pass filter applications.

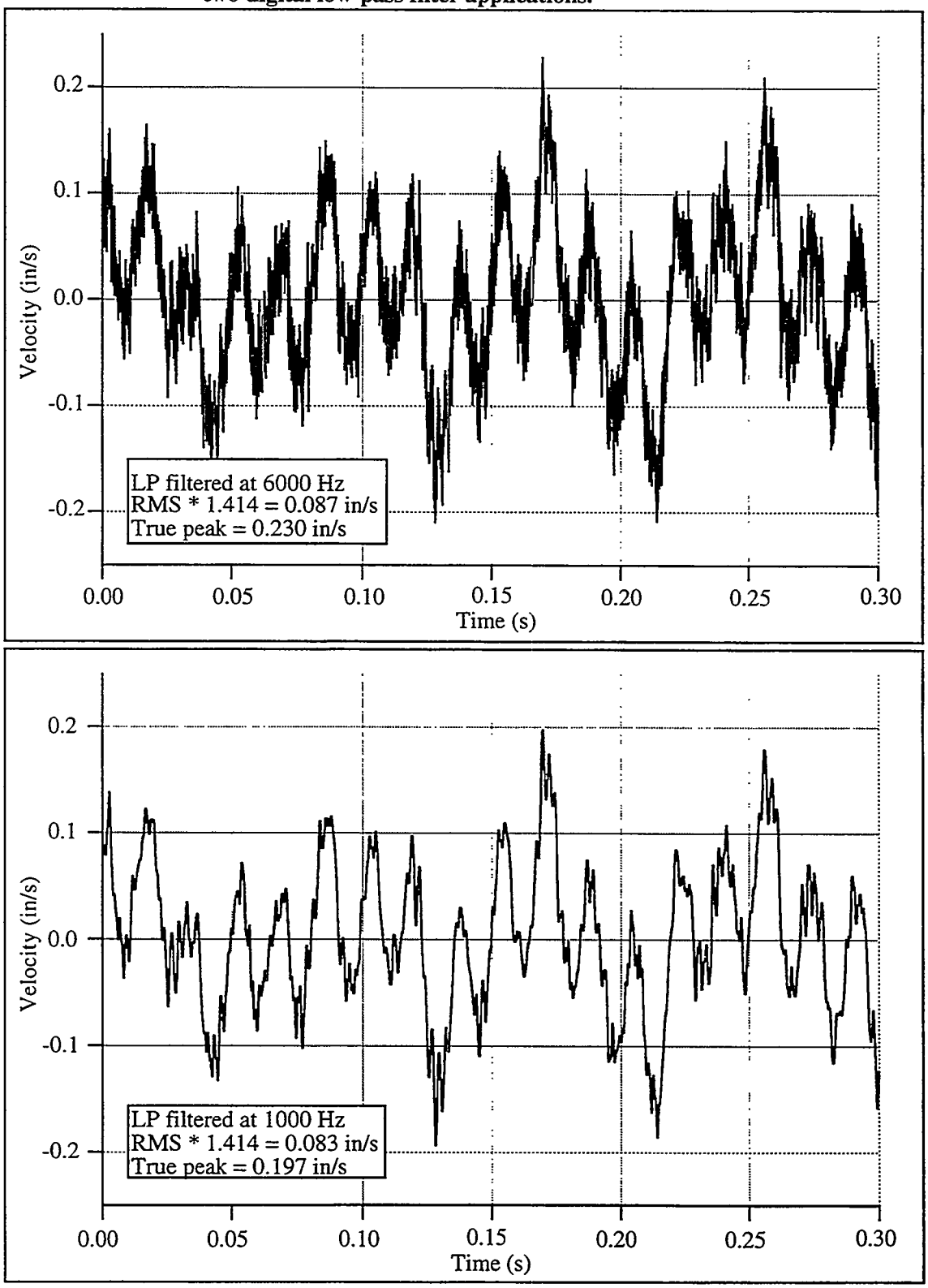

Figure 11. Pump ΔP pulsation spectra - Pump B.

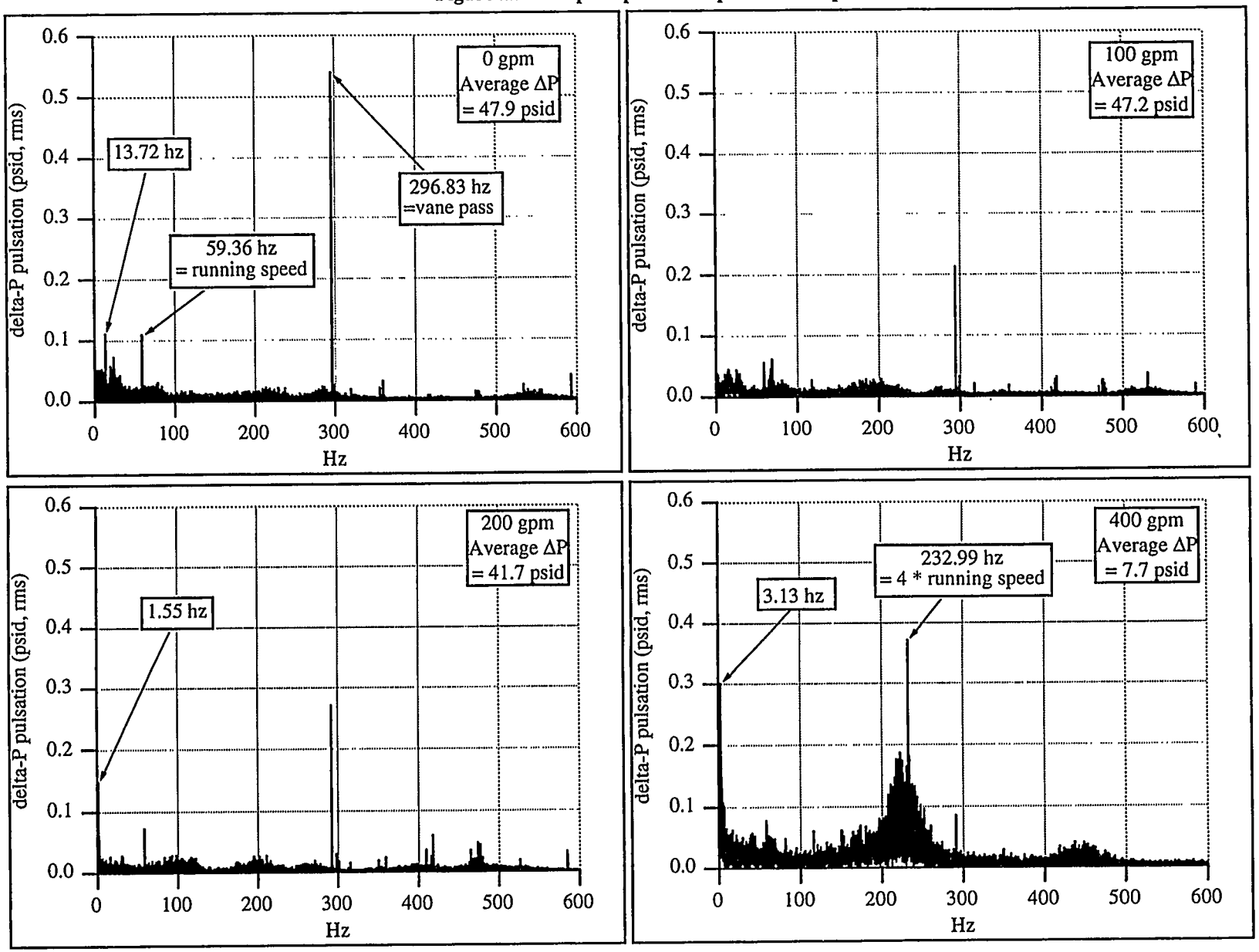

vane pass pulsation amplitude is less than 0.5% of the head. At the highest flow condition, it is again over 1% of pump head.

One particularly interesting result is the dramatic increase at four times running speed at the highest flow rate, accompanied by a general broadband noise in the spectrum in this vicinity.

Pump suction and discharge pressure pulsation spectra are shown in Figure 12. The subsynchronous suction and discharge spectra are shown in more detail in Figure 13. By comparing the total head, the suction, and the discharge spectra, certain spectral components can be tied to specific sources. For example, the dramatic change in total head at four times running speed for the highest flow case (Figure 11) is not present in the suction pressure spectrum, but is present in the discharge spectrum (Figure 12), indicating that this is a discharge-related phenomenon. Another example feature of interest can be seen at 15.3 hz in both the suction and discharge pressure spectra at 100 gpm, but is not present in the total head spectrum. This suggests that an external influence, such as a resonant frequency in the loop, affected both signals individually, and is probably not a pump-generated component. Other spectral features such as the spectral peaks at 1.55 and 3.13 hz for the 200 and 400 gpm cases, respectively are common to all three signals. It is of interest that the ratio of these two frequencies is the same as the flow ratio.

4. D. Motor Power Analysis

Motor input power was monitored on both pumps. All three phases of current were monitored using clamp-on current transformers. All three phases of voltage were monitored using dropping resistor networks. The total input power was measured by summing the products of the individual phase currents and voltages (using both analog and digital multiplication).

Motor power acts as a transducer of the motor load. Obviously, as the motor load increases, the motor input power increases to accommodate the load; thus it is sensitive to changes in pump hydraulic and mechanical loads. For most motors, the motor power is relatively linear with load, so it is a parameter that gives a reasonably representative indication of load fluctuations. Motor power does have some inherent frequency limitations when monitoring pumps due to the rotating inertia of the motor and pump, as well as the pumped fluid. In order for the motor power to change in an induction motor, the rotating speed must either increase or decrease (as the result of a load change). High frequency components, such as vane pass frequency, create load fluctuations at such a rate that the relatively large inertia of the rotating equipment and the pumped fluid essentially allow the motor to pass through these events with little or no change in speed.* However, for lower frequency load components, particularly at synchronous speed and below, the motor input power can be a relatively informative tool.

It might be noted here that motor current also responds to load changes, and has been historically used to monitor motor loads.[16] Motor current is somewhat non-linear with load for most motors (being most responsive at high loads), however, and its use to understand load fluctuations at different load conditions requires the application of a current vs. load adjustment. Current as a transducer of pump loads was not analyzed here for that reason. The ease of acquiring current (vs. power) makes it an inherently attractive parameter to monitor, and it is likely that with correction factors applied to account for non-linearities, current could also be effectively employed as a tool for understanding pump conditions.

Figure 14 provides normalized power spectra for Pumps A and B.† The normalization is performed by dividing the power spectra by the average power for the particular flow condition. For Pump A, it can be clearly seen that at the two low-flow conditions, the low frequency end of the power spectrum (up to about half of running speed) is much noisier. Also, note that the spectral peak just below 30 Hz (corresponding to running speed) decreases with increasing flow, which is exactly opposite to the pattern noted in the axial vibration data for Pump A. One possible interpretation of this apparent inconsistency emerges when it is recognized that both mechanical and hydraulic unbalance are manifested at running speed, but the phase angles of the mechanical and hydraulic unbalance components are not necessarily aligned. Since the pump motor input power is not particularly sensitive to mechanical unbalance (except at significant levels of unbalance, in our experience), but is sensitive to *torsional* load fluctuations, the data suggest that there is increased hydraulic unbalance at low flow; however, this hydraulic

---

* It might be noted that vane pass frequency has been observed in spectral analysis of motor power, however. The results to date show some promise, but have not been fully explored.

† Note that the four flow conditions for Pump B power are not identical to those shown for vibration and pressure pulsation previously. Instead, the selected flow rates for both pumps are roughly equivalent, in terms of percent of BEP.

Figure 12. Pump suction and discharge pressure pulsation spectra - Pump B.

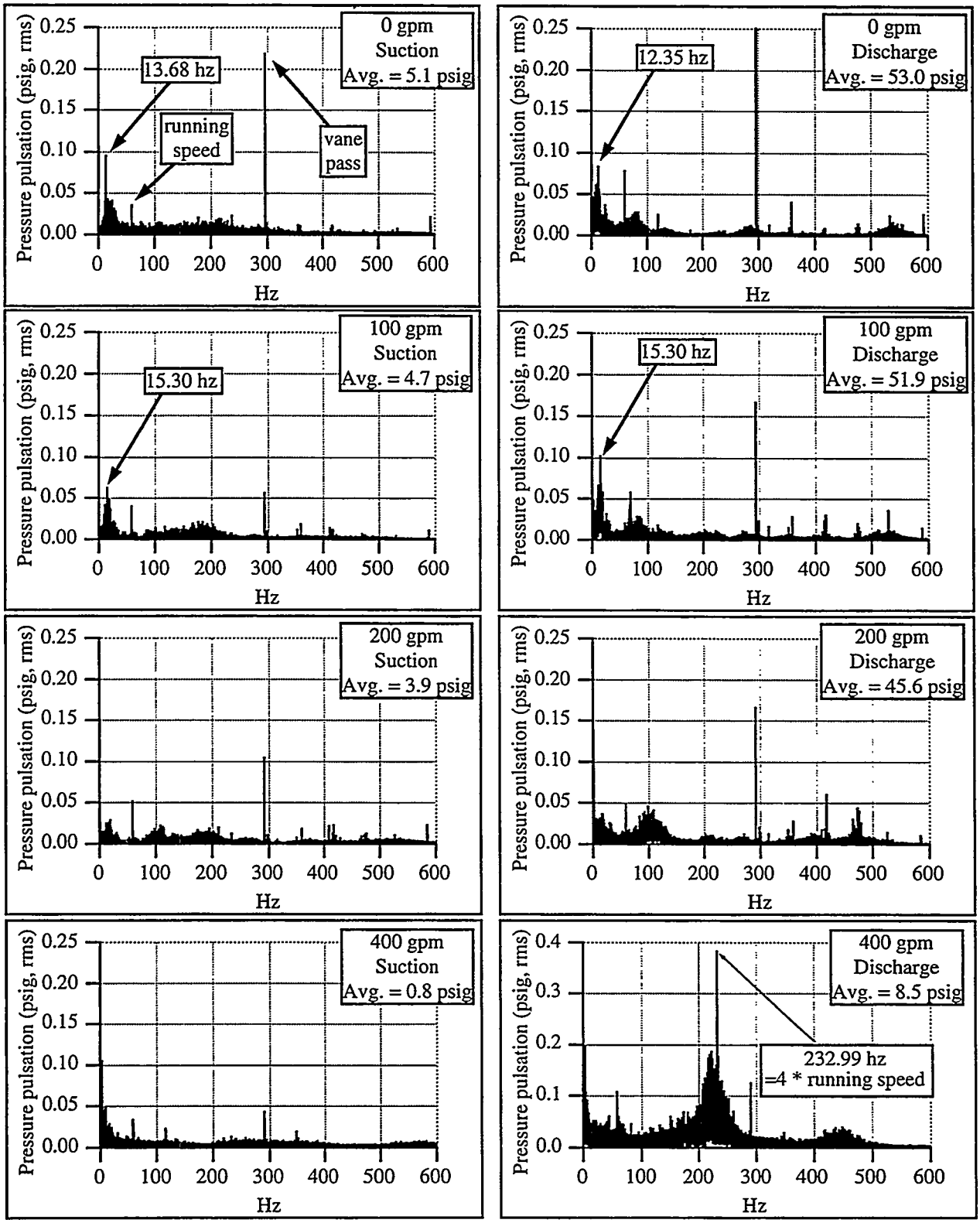

Figure 13. Pump B suction and discharge pressure low frequency pulsation spectra.

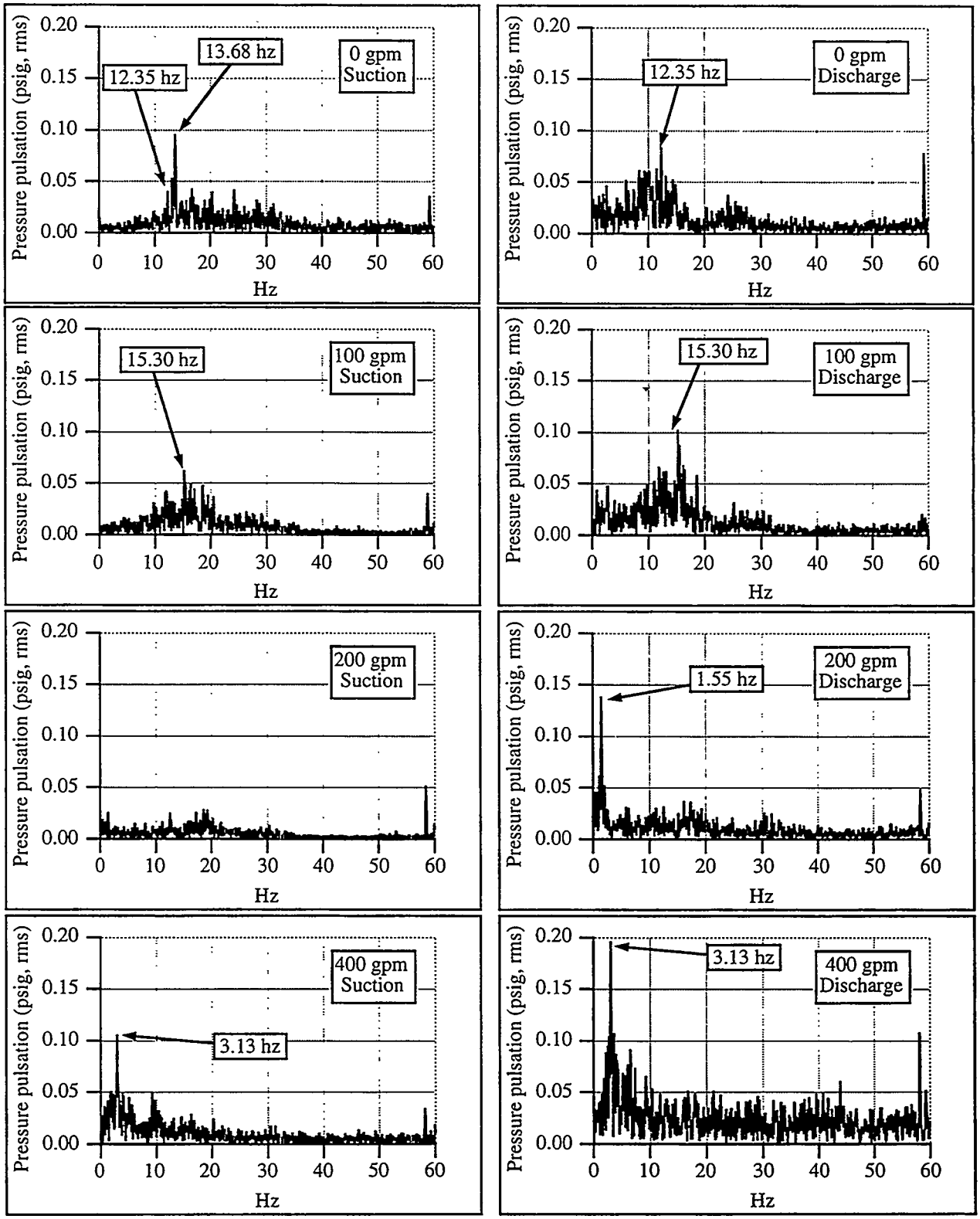

Figure 14. Normalized power spectra for Pumps A and B. The 3-phase power spectra are normalized by dividing the spectrum by the average power at the indicated flow rate.

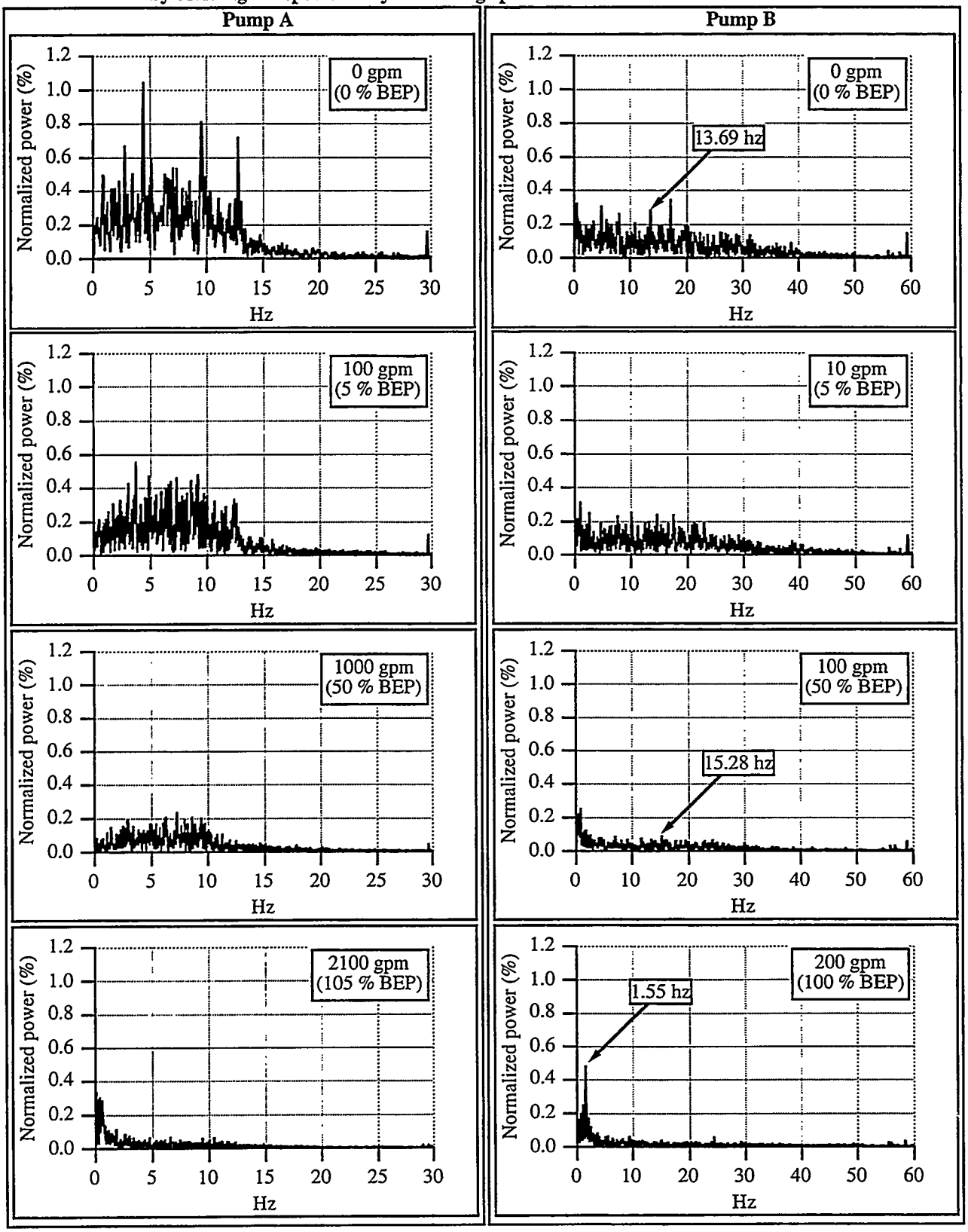

unbalance is apparently out of phase, to some extent, with the existing mechanical unbalance, resulting in decreased overall running speed vibration at low flow conditions.

Pump B also has a level of low-flow related broadband noise at low frequencies (again, up to about half of running speed), although at a significantly lower absolute level than Pump A. The amplitude of the running speed peak (at just less than 60 Hz) also diminishes with increasing flow.

As flow rate increases, there is a general trend for both pumps to develop some very low frequency (<5 Hz) energy. This can be seen for Pump A at 2100 gpm (105% BEP), and for Pump B at both 200 and 400 gpm (100% and 200% BEP, respectively). For Pump B, the energy is manifested as a more discrete peak.

Figure 15 presents a summary plot of power instability as a function of flow, including more flow conditions than have been discussed above. The motor power instability is calculated by dividing the standard deviation of the motor power by the average motor power, and is thus normalized for the different flow rates of a particular pump, as well as providing a common parameter against which to compare different pumps. The load of Pump B clearly fluctuates more at low-flow conditions than does Pump A. Both pumps have instability ratios that are comparable near the BEP, however. The test loop for Pump B is a relatively short loop which can be operated with minimal flow restrictions, thus allowing the pump to be run at flow rates significantly beyond its design condition. At the highest flow rate, the motor power exhibits more instability than at even the shutoff flow condition.

5. Comparing Results

Vibration and motor power data were recorded for Pump A. The results of the individual parameters were discussed above. The overall vibration velocity spectra (Figure 1) tend to be dominated by running speed and harmonics, making it more difficult to see the broader patterns in the acceleration domain (Figure 2). The acceleration domain spectra for Pump A (particularly axial vibration) show a considerably higher level of broadband noise at low flow rates (Figure 2). The lower frequency spectra of the vibration velocity show a marginal increase in low-flow related broadband noise from below running speed to about four times running speed. While these particular spectral components are not directly observable in the motor power signal, the results of the broadband noise are, in that the unstable flow-induced noise also causes lower frequency load variations that are manifested as input power fluctuations. It is important to note that the overall rms vibration velocity signals, measured in accordance with ASME code requirements (Figure 4), do not show the tendency toward hydraulically unstable conditions at low flow (although the variations in the rms amplitude do shed some insight).

Vibration, pressure pulsation, and motor power data were recorded for Pump B. The overall vibration amplitude was minimally affected by operation at either low or very high flow rates. The vibration acceleration spectra did show a significant increase in broadband, higher frequency noise at the highest flow rate (Figure 7).

The Pump B pressure pulsation data indicated that vane-pass frequency amplitude dropped with increasing flow rate. However, at the highest flow rate, a significant level of 4 times running speed activity was noted in the pump discharge pressure. Similar patterns were not found to exist in the vibration spectra. Some significant very low frequency peaks in the pressure pulsation data at the higher flow rates were observed. The amplitude of the running speed peak in the pump suction pressure was found to be largest at the lowest and highest flow rates.

For Pump B, as for Pump A, the motor power spectra do not show the same spectral features as vibration. However, there were identical spectral peaks in the motor power and pressure pulsation spectra at the low frequency range. For example, note the presence of spectral peaks at 1.55 hz in both the pressure and power spectra for the 200 gpm case. Although the power spectrum for the 400 gpm case is not shown, it also had a spectral peak in common with pressure pulsation (at 3.13 hz). The motor power instability was also consistent with the amplitudes at running speed in the pressure data. Likewise, for the highest flow condition, the high level of noise at four times running speed was manifested as an increased power fluctuation.

There are obviously a great number of other features that merit attention in correlating these signals. ORNL plans future activities to help better understand the signal correlations.

6. Summary and Conclusions

Previous studies indicate that the principal sources of service wear and degradation of internals for AFW pumps are hydraulic- and cavitation-related loads. Available literature indicates that various hydraulic-related stressors occur at frequencies ranging from as low as 0-10 Hz to 10 kHz (and beyond).

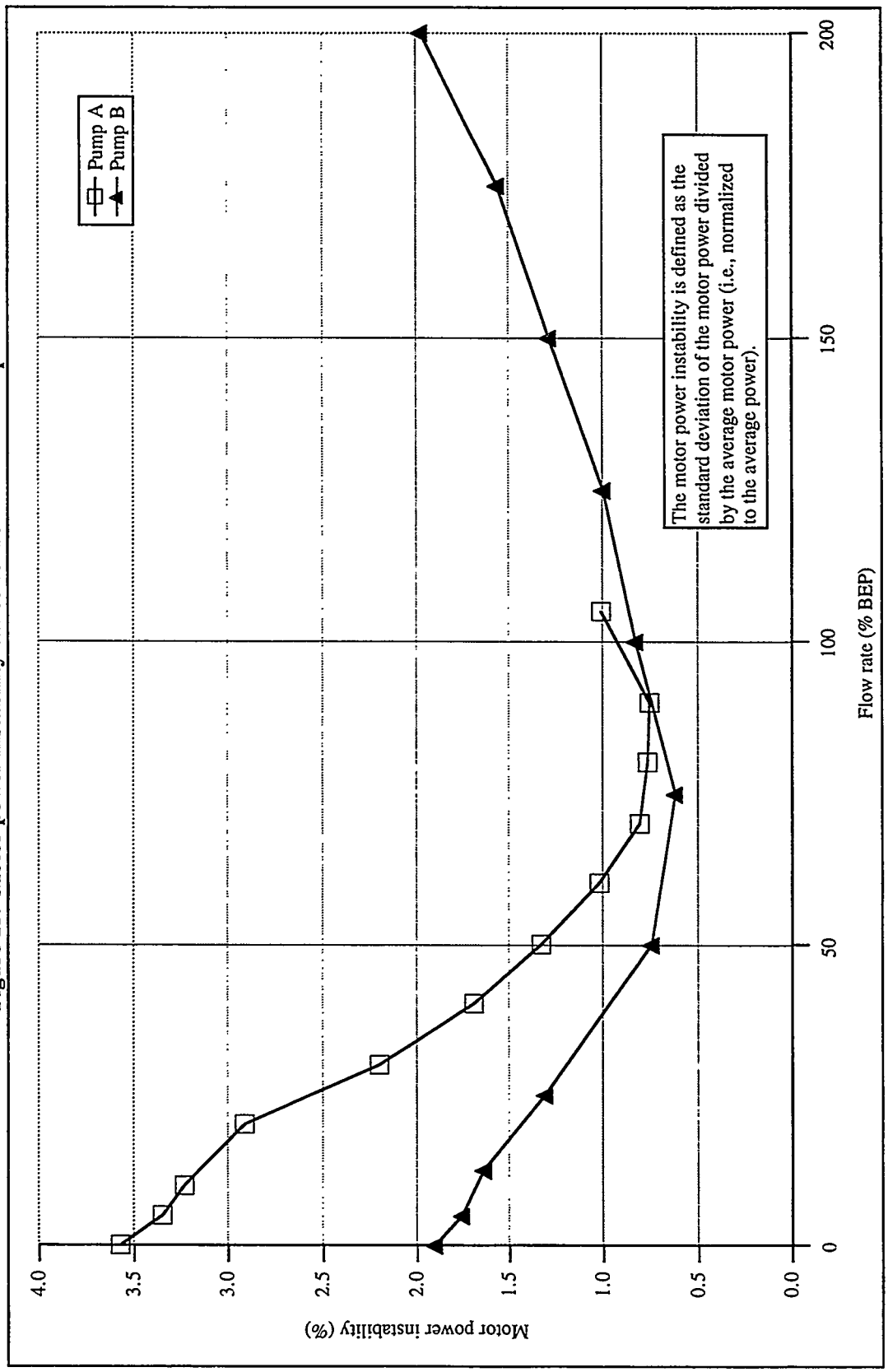

Figure 15. Motor power instability ratios vs. flow rate for Pumps A and B.

Vibration, pressure pulsation, and motor power measurements taken on two pumps indicate that there is, to a limited extent, consistency in the response of these parameters as hydraulically-related loads are changed.

The results of low flow-related hydraulic instability was clear in both the spectral vibration and motor power signals on a 2000 gpm BEP pump, and the two parameters showed generally consistent results, although the spectra were not directly comparable. The effects of low-flow instability can be recognized in both the vibration spectra and the motor power, but cannot be detected in the non-spectral vibration.

As expected, the level of instability at low flow was found to be significantly less in the smaller, 200 gpm BEP pump. Spectral vibration data provided little or no indication of instability at low flow, but clearly showed the effect of cavitation at flow rates significantly beyond BEP. Pressure pulsation spectra showed an increasing vane-pass frequency amplitude at low flow rates, and the presence of some relatively significant, very low frequency components at higher flow rates. A significant increase in four times running speed frequency, accompanied by surrounding broadband spectral noise was found in the pressure pulsation spectra. The very low frequency components present in the pressure spectra at higher flow rates were also observed in the power spectra.

The motor power instability appears to provide some useful insights into the general hydraulic stability of pumps that is complementary to that available from vibration spectra. Since radially and axially mounted vibration transducers will not necessarily be able to observe torsional fluctuations, motor power may be able to detect effects that cannot be detected by vibration (likewise, other sources of degradation, such as mechanical imbalance, may not be observed in motor power. Further study of how to best quantify and relate motor power to other parameters is needed before it can be applied more broadly.

Finally, the overall, non-spectral vibration amplitudes measured on these pumps were found to be insenstive to the hydraulic stability of the pump and to high-frequency related faults. The importance of spectral vibration monitoring was clearly borne out by the results.

References

1. Aging and Service Wear of Auxiliary Feedwater Pumps for PWR Nuclear Power Plants, NUREG/CR-4597, Vol. 1, M. L. Adams and E. Makay.
2. Auxiliary Feedwater System Aging Study, NUREG/CR-5404, Vol. 1, D. A. Casada.
3. Low-Flow Operation and Testing of Pumps in Nuclear Plants, *Proceedings of the Symposium on Inservice Testing of Pumps and Valves*, NUREG/CP-0111, W. Greenstreet.
4. Pump Testing in the Nuclear Industry: The Comprehensive Pump Test and Other Considerations, *Proceedings of the Second NRC/ASME Symposium on Pump and Valve Testing*, NUREG/CP-0123, T. Hoyle.
5. Description of Comprehensive Pump Test Change to ASME OM Code, Subsection ISTB, *Proceedings of the Third NRC/ASME Symposium on Valve and Pump Testing*, R. S. Hartley.
6. Dynamic Loading on Pumps – Causes for Vibrations, Proceedings of the Tenth International Pump Users Symposium, S. Florjancic and A. Frei.
7. Centrifugal Pumps for General Refinery Service, API Standard 610, Seventh Edition, American Petroleum Institute
8. Code for Operation and Maintenance of Nuclear Power Plants, ASME OM Code-1990, including 1994 addenda, American Society of Mechanical Engineers.
9. Control of Backflow at the Inlets of Centrifugal Pumps and Inducers, Proceedings of the First International Pump Symposium, D. P. Sloteman, P. Cooper, and J. L. Dussourd.
10. Investigation of Pressure Pulsations Arising from Impeller/Diffuser Interaction in a Large Centrifugal Pump, Proceedings of the Rotating Machinery Conference and Exposition '93, E. Makay, P. Cooper, D. P. Sloteman, and R. Gibson.
11. A Case History – Improved Hydraulic Design Lowers Cavitation Erosion and Vibrations of a Water Transport Pump, Proceedings of the Tenth International Pump Users Symposium, S. S. Florjancic, A. D. Clother, F. J. L. Chavez.
12. 10CFR21 Reportability of a Potential Safety Hazard from Broken Cast Iron Diffusor Pieces in Auxiliary Feed Water Pumps, letter to R. Fuhrmeister (USNRC) from G. Young (Ingersoll-Rand), September 19, 1991.
13. Pump Vibrations, Proceedings of the Ninth International Pump Users Symposium, W. E. Nelson and J. W. Dufour.

14. Changes in Hydraulic Component Geometries Greatly Increased Power Plant Availability and Reduced Maintenance Cost: Case Histories, Proceedings of the First International Pump Symposium, E. Makay and J. A. Barrett.
15. Trouble-Shooting High Energy Input Power Plant BFP Pumps, 1989 EPRI/MVI Centrifugal Pump Short Course Lecture Notes, E. Makay.
16. Aging and Service Wear of Electric Motor-Operated Valves Used in Engineered Safety-Feature Systems of Nuclear Power Plants, NUREG/CR-4234, Vol. 2, H. D. Haynes.

*Research sponsored by the Office of Nuclear Regulatory Research, U. S. Nuclear Regulatory Commission under Interagency Agreement DOE 1886-8082-8B with the U. S. Department of Energy under contract No. DE-AC05-840R21400 with the Martin Marietta Energy Systems, Inc.

METHODS FOR DETERMINING ATYPICAL GATE VALVE THRUST REQUIREMENTS

R. Steele, Jr.
J. C. Watkins
K. G. DeWall

Idaho National Engineering Laboratory
Idaho Falls, Idaho, U.S.A

Dr. G. H. Weidenhamer
USNRC Technical Monitor

INTRODUCTION

Evaluating the performance of rising stem, wedge type, gate valves used in nuclear power plant is not a problem when the valves can be design-basis tested and their operability margins determined diagnostically. The problem occurs when they cannot be tested because of plant system limitations or when they can be tested only at some less-than-design-basis condition. To evaluate the performance of these valves requires various analytical and/or extrapolation methods by which the design-basis stem thrust requirement can be determined. This has been typically accomplished with valve stem thrust models used to calculate the requirements or by extrapolating the results from a less-than-design-basis test. The stem thrust models used by the nuclear industry to determine the opening or closing stem thrust requirements for these gate valves have generally assumed that the highest load the valve experiences during closure (but before seating) is at flow isolation and during unwedging or before flow initiation in the opening direction. However, during full-scale valve testing conducted for the USNRC,[a] several of the valves produced stem thrust histories that showed peak closing stem forces occurring before flow isolation in the closing direction and after flow initiation in the opening direction. All of the valves that exhibited this behavior in the closing direction also showed signs of internal damage. Initially, we dismissed the early peak in the closing stem thrust requirement as damage-induced and labeled it nonpredictable behavior. Opening responses were not a priority in our early research, so that phenomenon was set aside for later evaluation.

However, in subsequent industry valve test programs and as more and more in situ valve testing were being completed in response to USNRC Generic Letter 89-10, "Safety-Related Motor-Operated Valve Testing and Surveillance," we observed a substantial number of atypical valve responses both in the opening and closing directions, and many of the valves did not show any obvious signs of internal damage.

---

a. Work supported by the U.S. Nuclear Regulatory Commission, Division of Engineering, office of Nuclear Regulatory Research, under U.S. Nuclear Regulatory Commission, Division of Engineering, Office of Nuclear Regulatory Research, under U.S. Department of Energy Contract No. DE-AC07-94ID13223, FIN A6857, Dr. G. H. Weidenhamer, USNRC Program Manager. Computer-generated graphics by Geraldine S. Reilly, technical editing by Dave Pack.

These industry test results caused us to take another look at the forces involved in the closing and opening requirements of wedge-type gate valves, particularly at that part of the valve stroke near flow isolation but where flow is still present. This is the area of the valve stroke where the early peak in the stem force occurred in the closing direction and the late peak in the stem force occurred in the opening direction. These early and late peaks in the thrust requirements had been observed to be significantly larger than the flow isolation or flow initiation thrust requirements, so they required attention. After sufficient investigation, we came to call this type of valve performance *atypical* rather than *nonpredictable* stem thrust behavior. This is in part because we came to understand the root cause of this atypical performance. The root cause is disc tipping, allowed by large internal clearances between the disc and the guides. The flow forces tip the disc during that portion of the valve stroke where the disc is not fully supported by the body seat as it is during flow isolation and seating. Without extensive internal valve measurements, this type of behavior cannot be predicted; however, it can be extrapolated from a less-than-design-basis test.

Initially, extrapolating this atypical performance was a problem because all of the industry stem force sizing models, including the one developed at the INEL, are for typically responding valves. The models are based on the assumption that pressures around the disc are uniform, and that flow isolation has occurred, upstream and downstream pressures equalize with their respective plenums, and the vertical and horizontal disc loads can be calculated or test results analyzed. However, when flow is present the pressures are not uniform around the disc because of the flow paths over and under the disc. The problem is made more complicated by a tipped disc, which further changes the pressure distribution around the disc and the resulting stem thrust requirement.

This paper presents our current understanding of the atypical valve response problem and discusses a performance-based method for evaluating the response of valves whose peak stem thrust occurs before flow isolation in the closing direction or after flow initiation in the opening direction.

BACKGROUND

The U.S. Nuclear Regulatory Commission (NRC) sponsored the Idaho National Engineering Laboratory (INEL) to conduct a wide range of valve research over the past 11 years, including full-scale field testing, single-effects laboratory testing, and data analysis. Much of this full-scale work was the first of its kind: the butterfly valve testing in 1983 and -84, the motor-operated valve (MOV) flow and pressure operation plus seismic load tests in 1986, -87, and -88, the MOV line break flow tests in 1988, the parametric and multi-fluid MOV testing in 1989, and the integrated valve load simulator work conducted in 1991, -92, and -93. From this NRC work and industry research, the classic or typical response of a flex-wedge gate valve became better understood. New models, equations, correlations, and insights for in situ testing evolved from the work, as well as a number of regulatory information notices and several supplements to Generic Letter (GL), 89-10 "Safety-Related Motor-Operated Valve Testing and Surveillance." The flexwedge gate valve research identified new vertical loads that had not been accounted for in the standard industry equation and led to the development of our stem thrust correlation. In addition to the correlation, the work identified that internal valve frictional behavior was influenced by fluid conditions and

temperature. This is particularly important because it influenced performance in a manner that was not what an intuitive analysis would predict. However, as more and more industry testing is completed, the effects of pressure and temperature are being validated. The industry test program results have not yet validated our fluid effects theory, but our belief is stronger now that we have investigated atypical opening and closing valve behavior.

Figure 1 shows classic or typical opening and closing stem force histories for a flexwedge gate valve. Figure 2 shows the same information for a atypical valve. We call it atypical because the stem force is not a linear function of the exposed disc area and the differential pressure, but, rather, results in irregular shapes: a hump in the opening direction and a hook in the closing direction of the stem force histories. As stated, the primary cause of this atypical performance is gate or disc tipping caused by flow and differential pressure forces as the valve opens or closes. Larger-than-necessary internal valve clearances between the disc and the guides allow the flow forces to tip the disc during the portion of the stroke before full seat contact in the closing direction and after coming off the seat in the opening direction. Figure 3 shows what we call a guide-restrained tipped disc; Figure 4 shows what we call a seat-restrained tipped disc. Each of these two tipped-conditions represent the worst-case tippage. The tipped disc changes the pressure distribution around the disc and, with the added mechanical interference, alters the disc's stem thrust requirements.

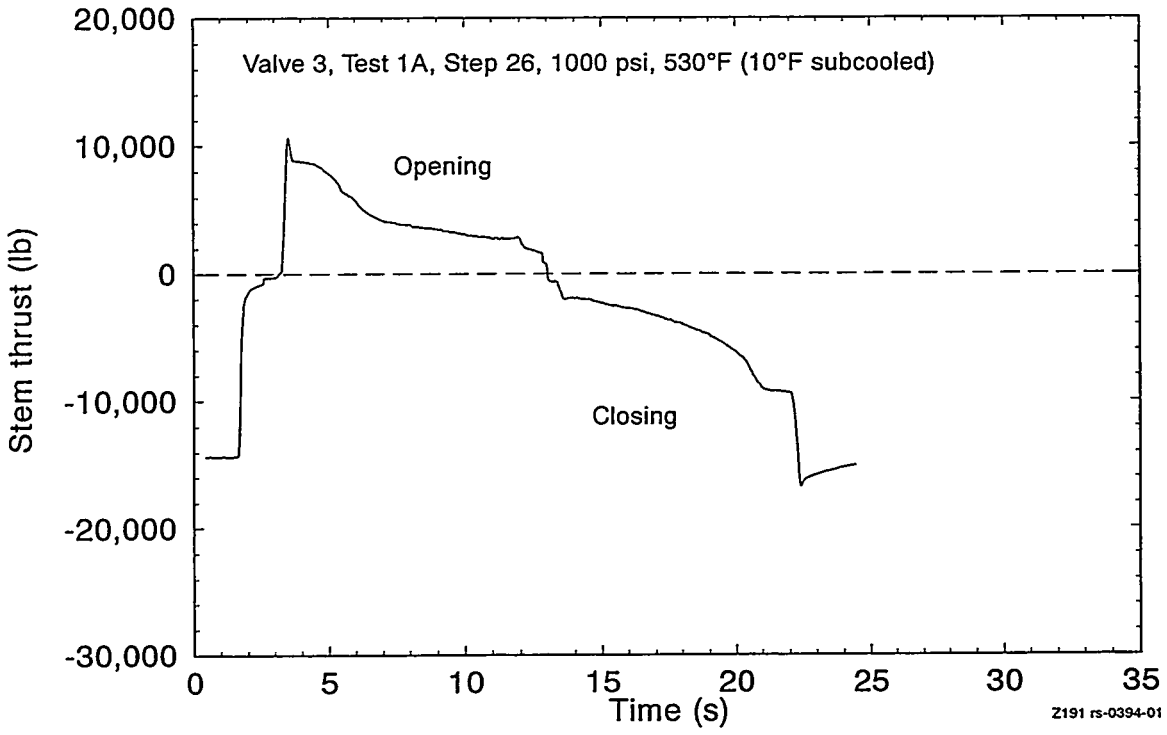

Figure 1. Six-in. flex wedge valve, opening approximately 30% at high flow and reclosing. The resulting stem force history is classic typical behavior.

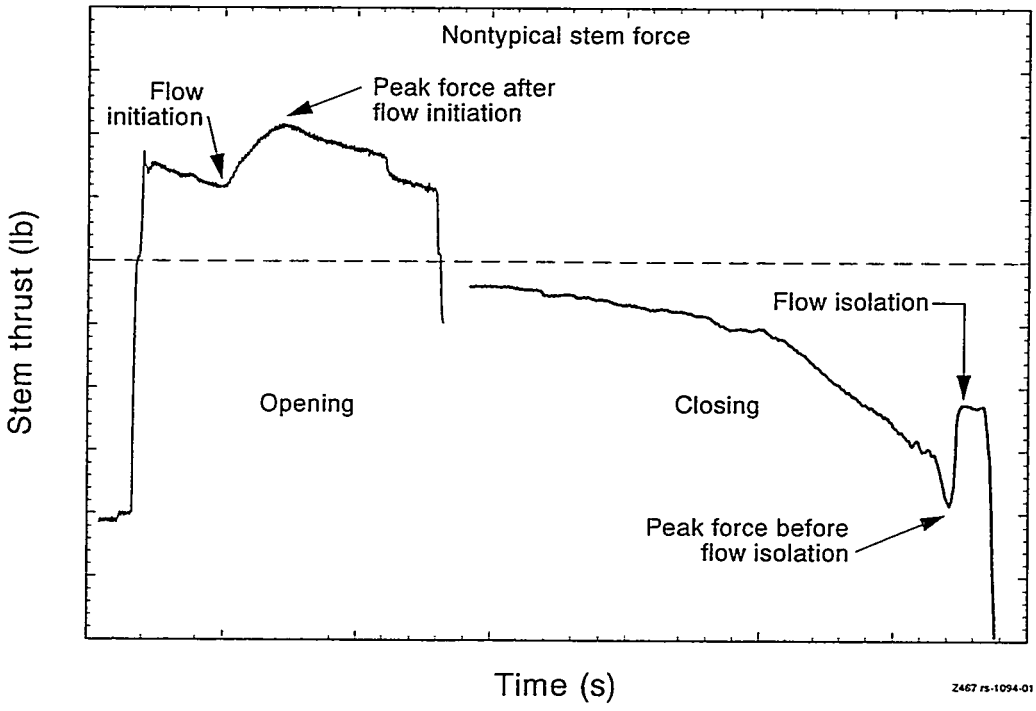

Figure 2. Flex wedge gate valve, opening and closing histories. The resulting stem force histories are representative of nontypical behavior.

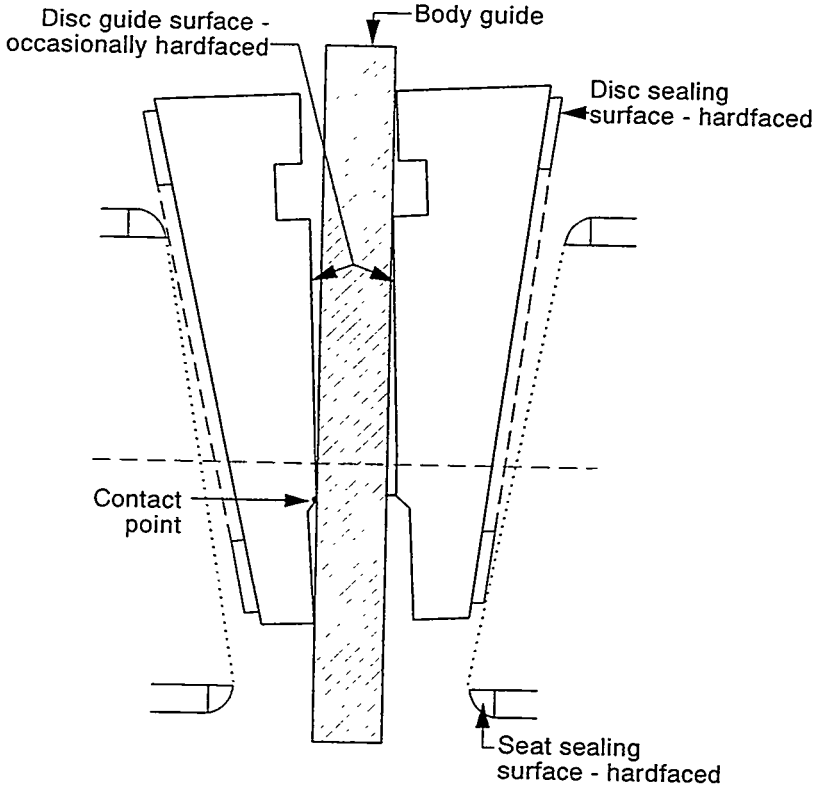

Figure 3. Larger-than-necessary disc-to-guide clearances allow disc to tip. In this example, the guides restrain the amount of tipping.

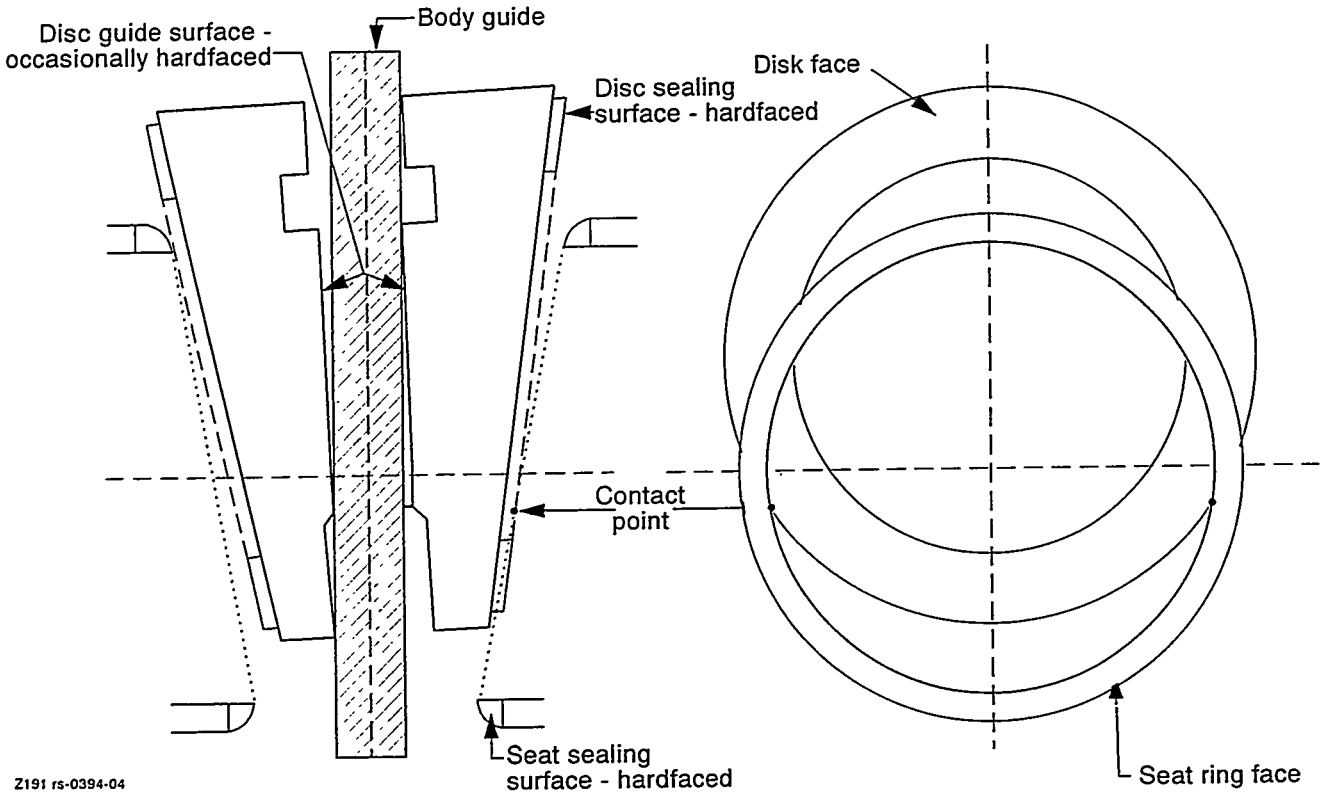

Figure 4. Larger-than-necessary disc-to-guide clearances allow disc to tip. In this example, the body seats restrain the amount of tipping.

In addition to the tipped disc's additional thrust requirement, physical damage can add to the thrust required to operate the valve. Most of the load from mechanical interference and physical damage will be in the closing direction. In the guide-restrained case, if the tippage angle is large enough the effective guide contact area will be reduced and the contact stress will be increased, which can lead to galling and plastic deformation of the guide surfaces. In the seat-restrained case, if the angle of the tipped disc is large enough and the leading edges sharp enough, the disc can machine the seat as it closes. In the worst of cases, the disc lip will not pull out of the seat bore and will mechanically lock at a partially open position in the seat bore. If the disc and seat edges are rounded enough, only mechanical interference will occur, causing added resistance.

All of the above anomalies have been observed in actual testing. Posttest inspection of the valve parts and careful analysis of the stem force histories have shown that most internal valve damage can be detected from the stem force history. Figures 5 and 6 are stem force histories from our full-scale valve testing, which show damage occurring during the valve closure. Figure 7 is a stem force history from a closing valve test where the disc tipped but no damage occurred. Figure 8 shows an opening test stem force history where the flow isolation forces are less on the seat than they are after flow is initiated. These later stem force histories that occurred without valve damage exhibit the atypical behavior we wish to discuss further in this paper.

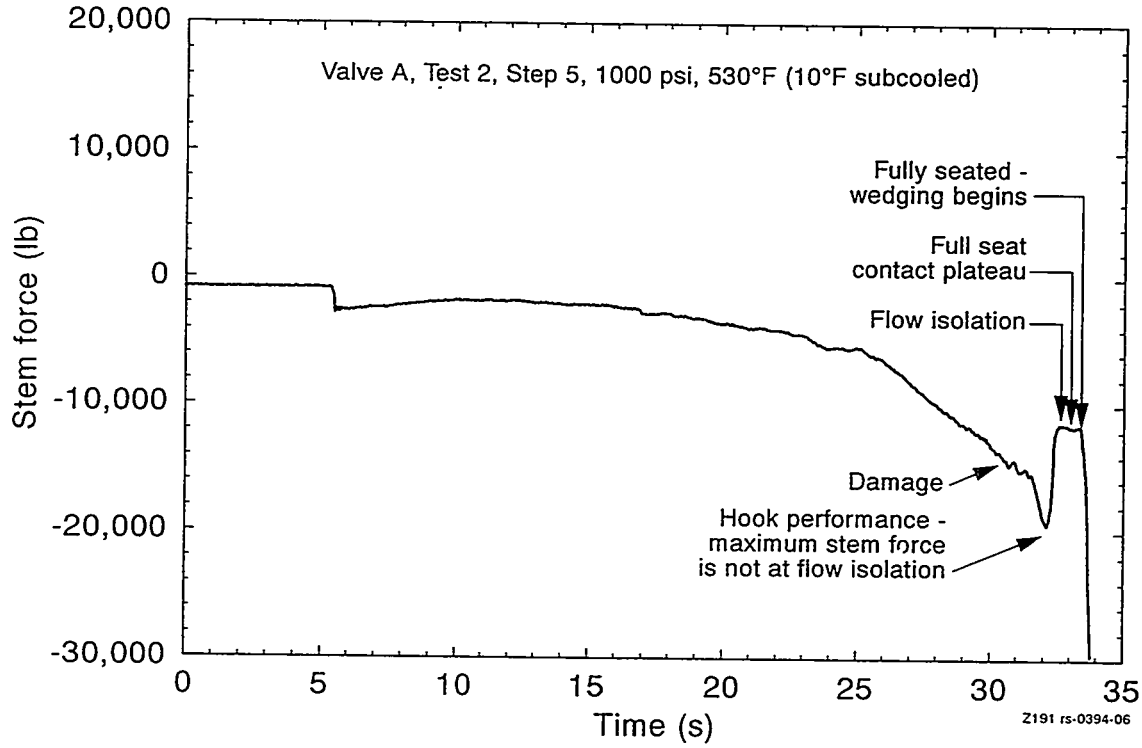

Figure 5. Six-in. flex wedge system valve, design-basis line break flow. Stem force history shows indications of damage during the loaded portion of the closing cycle.

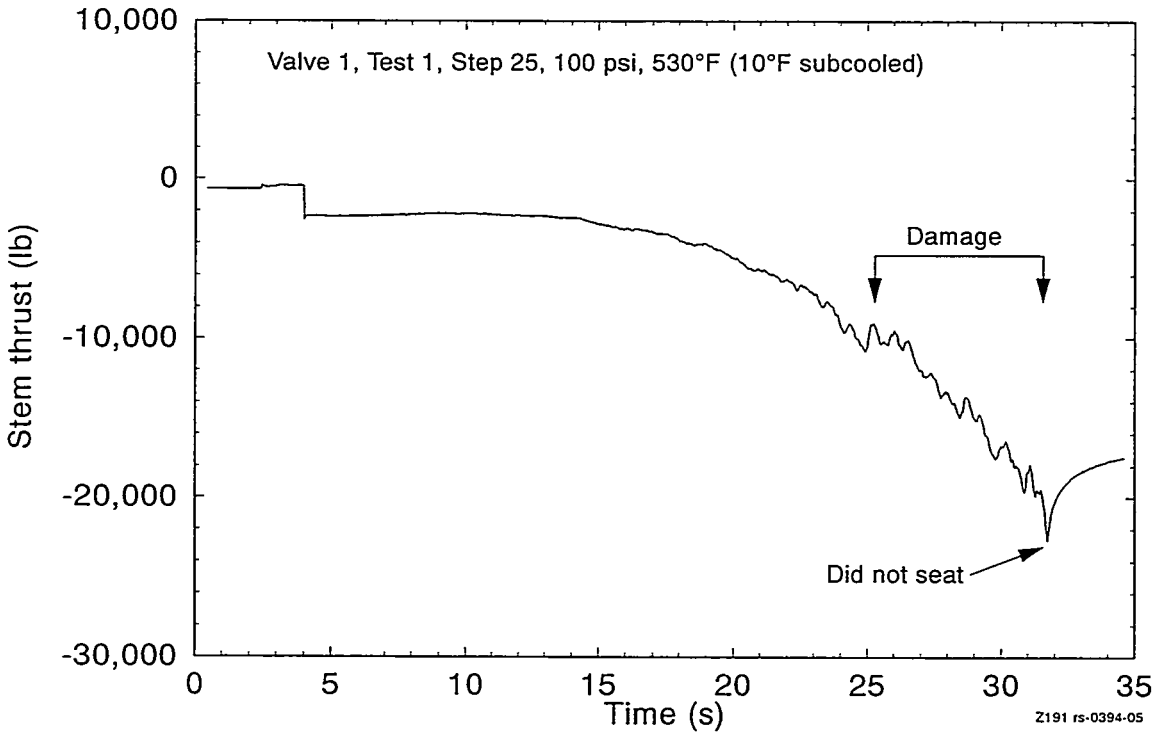

Figure 6. Six-in. flex wedge system valve, design basis line break flow. Stem force history shows indication of damage during the loaded portion of the closing cycle.

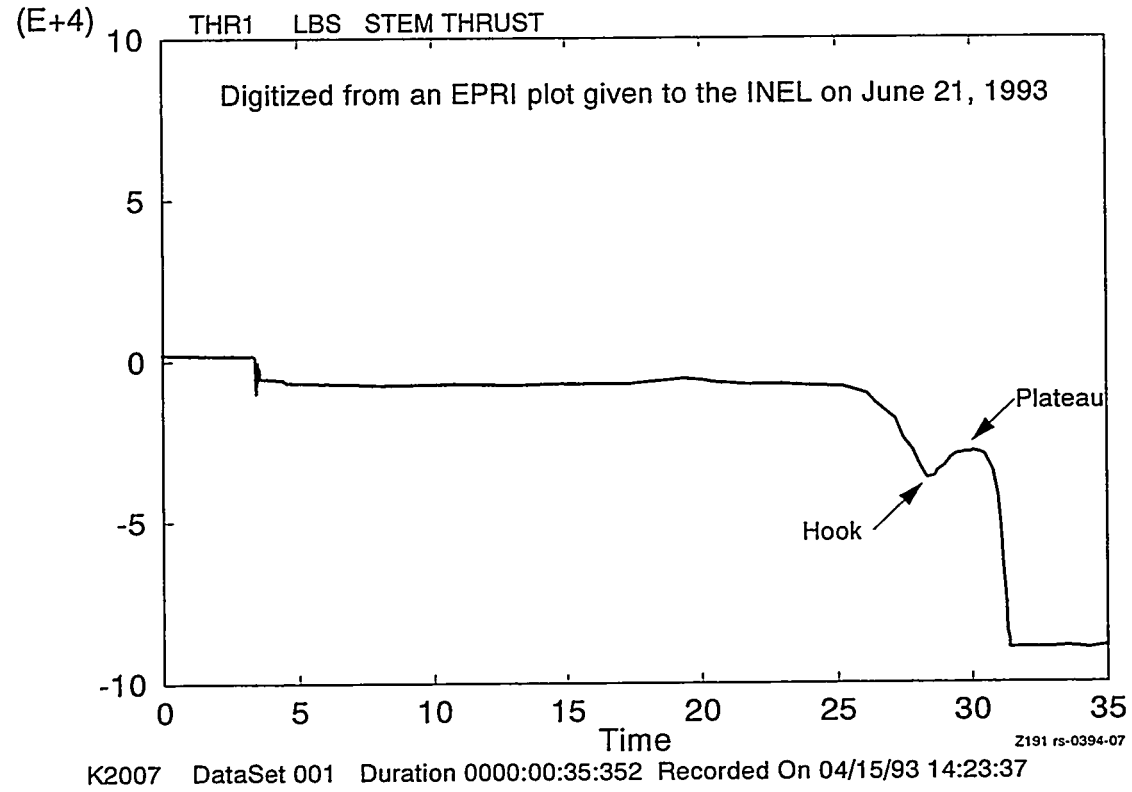

Figure 7. Six-in. service water valve closing on design basis flow. Stem force history shows nonlinear performance but no damage.

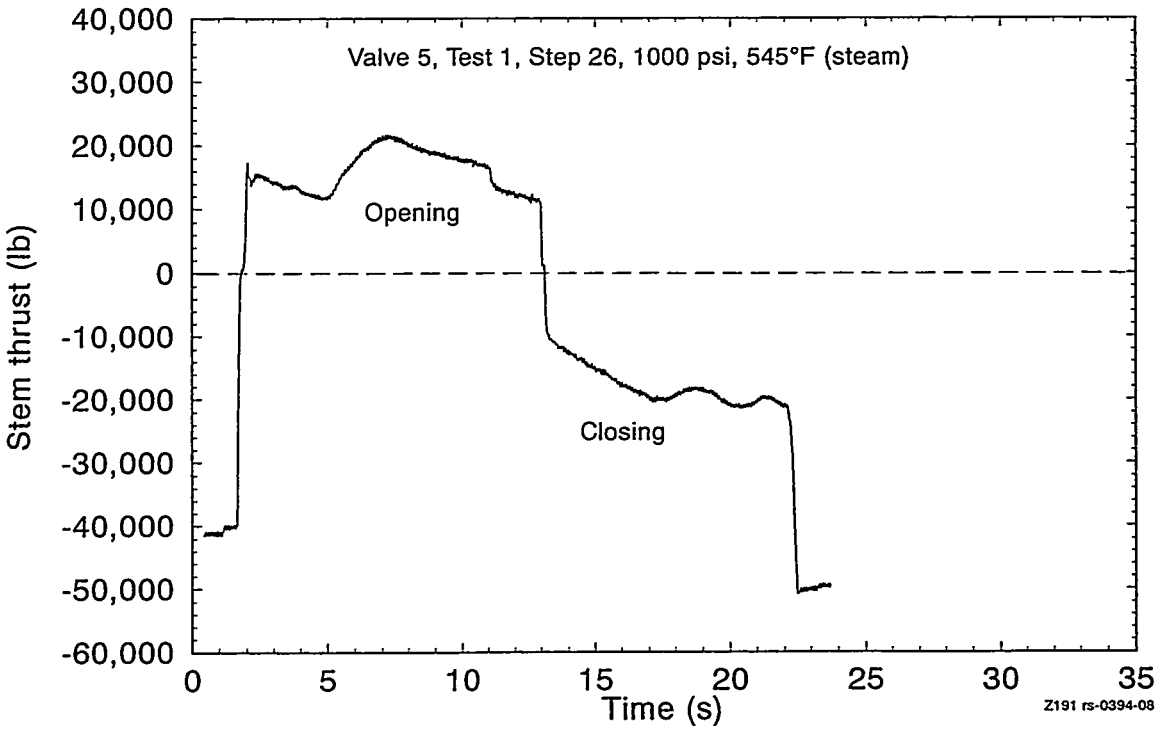

Figure 8. Ten-in. flex wedge valve, opening approximately 30% at high flow and reclosing. The stem force history in the opening direction shows a higher load after unseating.

THE PROBLEM

Manufacturing dimensions in many cases allow the disc in wedge type gate valve designs to tip under a flow load. Manufacturing tolerances within a given valve dictate the tip angle and how big the problem will be. Without very detailed internal valve measurements, analytically predicting the performance of a specific valve could require very conservative values to be assigned for the unknown stem thrust requirement. The conservative values could be reduced with a best effort in situ flow interruption test. Extrapolating classic or typical stem thrust requirements is not a problem; all of the modern stem thrust models are for analyzing stem thrust results when the highest thrust values occur at flow isolation or before flow initiation. These models have been used, however, to predict and to extrapolate atypical behavior in both the opening and closing directions, but because they do not consider flow forces, temperature, state of the fluid, pressure distribution, and valve disc tippage, they may not provide conservative predictions or the correct basis for extrapolation.

The need, then, for those valves that could be tested at less-than-design-basis conditions and that exhibit a atypical response, has been for a new model to analyze test results and then to predict or extrapolate the test results to design-basis conditions.

RESOLUTION

What We Know

The materials of construction for valve internals have been the subject of a number of friction studies. Typically, when valve responses obtained from flow and pressure testing are analyzed, the resulting friction factors will be lower than the friction factors obtained in the laboratory from material samples, particularly when temperature and pressure are involved with the test. The effects of temperature and load on the seat and disc hardfacing have been noted in the laboratory, generally lowering the friction factor. However, when evaluating the results of actual valve testing, the temperature, fluid type, and pressure all have an effect on the stem load. In the atypical opening or closing case, when the peak thrust does not occur at flow isolation or just before flow initiation in the opening direction, the load components are not easily separated because of flow effects and the pressure distribution around the disc. In such cases, instead of extracting a friction factor from the test results, a disc factor is extracted. Typically, the disc factor is a multiplying fraction, like the friction factor, but is not the result of a normal versus sliding load calculation. In other words, the disc factor contains other unknowns related to the pressure distribution around the disc and the added thrust needed to overcome the mechanical interference. Generally, the results of test analysis or calculations using a disc factor cannot be compared with those determined from a friction factor analysis which eliminates some of the unknowns, but can only be used at flow isolation on typically responding valves. For atypical responding valves the disc factor technique must be used for extrapolation or analysis. The question is whether the unknowns extrapolate in a linear manner with pressure.

As stated, a atypical response occurs in valves when the disc can tip far enough to change the pressure distribution around the disc, and in the closing direction increase the mechanical interference before it comes in full contact

with the seat. Full-seat contact in this sense is not related to wedging but to when the disc is sliding in full contact with the downstream seat. This occurs after flow isolation in the closing direction and after unwedging but before flow initiation in the opening direction. The following analysis provides insights into why we believe the tipped disc to be the cause of atypical behavior and why we believe the performance can be managed.

Figure 9 shows the horizontal and stem rejection areas where the pressure loads can act on the wedge disc. These areas and the corresponding pressure loads were the basis of the old industry gate valve sizing equation. The industry equation was basically an area times a differential pressure times a fractional disc factor, plus the packing load, plus or minus the stem rejection load (depending on whether the valve was opening or closing). The internal valve pressure is always trying to expel the stem, so the pressure load on the stem area helps during valve opening and resists during valve closing. The stem rejection load was the only vertical load considered in the early gate valve sizing equations. Valve testing and comparisons of results with the sizing equations provided the first insight that other forces were acting on the disc in wedge gate designs.

Figure 10 shows the additional disc vertical wedge areas since identified and where the internal valve pressures could produce additional loads on the disc. Reference 1 documents the study that identified these new vertical

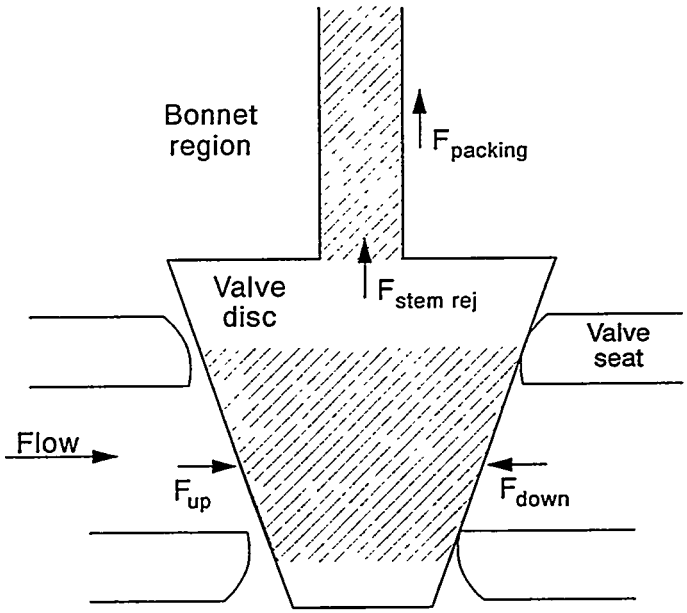

Figure 9. Valve disc cross-section, showing the unbalanced forces acting on a disc that contributes to the maximum stem force before wedging (industry equation).

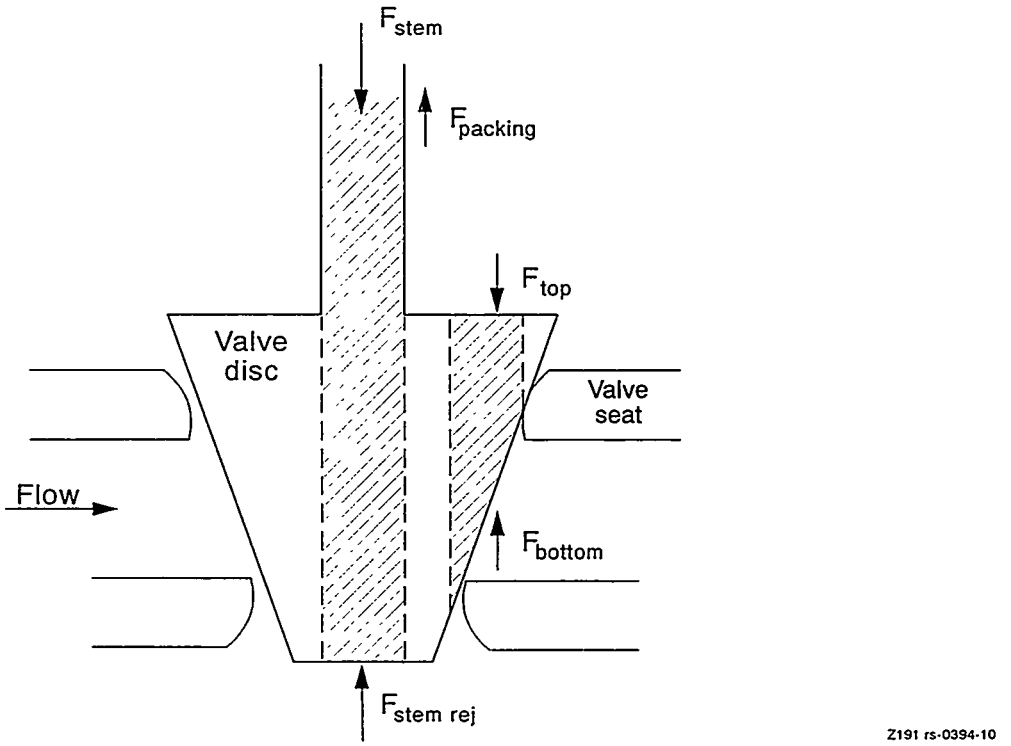

Figure 10. Valve disc cross-section, showing the unbalanced vertical forces acting on a disc that contributes to the maximum stem force before wedging.

areas. Typically, pressure forces acting on these areas in the closing direction would produce a net downward loading that would tend to offset the stem rejection load. The forces produced by pressure on these areas converge in the average 6-in. valve. The stem area force dominates in the smaller valves; the disc vertical force dominates in the larger valves. All of the previously discussed loads maintain their relationships as long as the disc is closing or opening in an untipped condition.

However, most valve discs will tip to some degree when not on the valve body seat. The degree of tipping will dictate whether it responds typically or not. Figure 11 shows how the pressure distribution loads change when the disc tips. The net downward load shown in Figure 10 begins to get smaller, and a new upstream vertical disc area term becomes larger as the tippage of the disc increases, resulting in a net upward force that resists valve closure. The mechanical interference between the disc and the downstream valve body seat also increases as the disc tips further. The decrease in the stem thrust just before flow isolation, shown in Figure 7, is caused by the disc coming into full contact with the seat and straightening up. This changes the pressure distribution back to a normal distribution and the mechanical interference is reduced to normal sliding friction.

Every atypical response will be different and no two valves where the disc can tip will exhibit the same response. However, a valve tested at less-than-design-basis conditions but at the same fluid subcooling should exhibit all the signs of its atypical response. The tippage, pressure distribution, and fluid effects will all be there, and it should only be a matter of analysis, and predicting or extrapolating the results. We say this even though there are yet some unknowns.

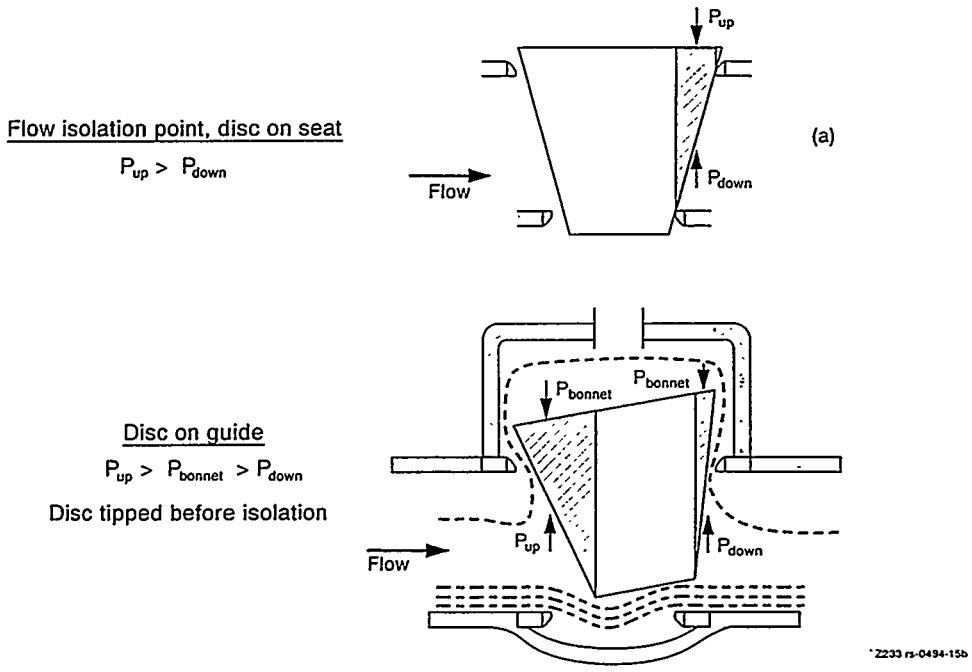

Figure 11. Change in disc areas that the various pressures act on as a result of tippage.

What We Do Not Know

We do not know (a) why the larger valves appear to be so pressure insensitive in the opening direction (it may have to do with the vertical area ratios), (b) why the stem thrust necessary to move the disc across the seat prior to initiating flow in the valves is so low when tested with high pressure steam, yet after flow initiation the forces return to expected levels, (c) why the valve opening responses are closer to a mirror image of closing responses with low pressure cold water or fluids that can flash yet not so with the single-phase fluid mentioned in (b) above.

NEW METHODS

The Atypical (Hook) Response in the Closing Direction

The atypical closing response, or hook response, is the result of a tipped disc and may include mechanical interference between the disc and the guides the downstream valve seat, or both. Figure 7 show a typical hooked valve response in the closing direction from an industry test program. This valve and several other valves from INEL and industry test programs have shown hooks in the closing direction. Some of these hooked responses required an additional 20 to 30% increase in force over the force required at flow isolation. This is not a trivial unknown and provides an incentive for a best-effort flow test to reduce the conservatism that would be required to account for the worst-case performance. Our analysis of test data indicates that a valve tested at any reasonable differential pressure load in relation to its design basis differential pressure (50% in low pressure cases, 20% in higher pressure cases, but no more than 400 psid in any case) should cause the

valve to exhibit all the signs of its atypical design basis response, provided the fluid subcooling is about the same as the design basis subcooling.

Once a best-effort closing flow test has been performed and a hook response identified, the force history should be examined for a jagged appearance. Figures 6 and 2 (INEL test valves) show stem force histories where damage occurred during the closing stroke. Figure 1 (also an INEL test valve) shows a clean stem force history. During our testing, we were always able to tell from the stem force history when major damage occurred during a closing test. Some of the more subtle damage, such as bent guides, were identified from posttest inspection. That response can also be seen in the stem force history now that we know what to look for. A posttest seat leakage test can also help identify damage. Another good indicator of seat damage is if the flow test is repeated and the hook is smaller in the second test. This usually indicates that the disc has machined the seat. The first test removes the sharp edges from the disc and rounds the machined area on the disc seat. Figure 12 (INEL valve repeat design basis test) is a good example of a hook that is less pronounced during the second test than during the first (see Figure 13). If no damage is found, the hooked response will increase linearly as the valve pressure load is increased. This is because the disc closing geometry does not change after the flow forces become large enough to overcome the weight of the disc. The mechanical interference friction factor will remain constant because it is geometry dependent, not pressure dependent. For the pressure-dependent load producing areas of the disc, the only variable is the differential pressure that can be extrapolated using the ratio of the differential pressure during a best-effort flow test and the design-basis differential pressure. The design-basis load can be estimated by extrapolating a best-effort flow test using the following equation:

$$F_{stem} = C_{hooking}\,\Delta P + P_{up}\,A_{stem} + F_{packing} \qquad (1)$$

where

F_{stem} = valve stem thrust

$C_{hooking}$ = hooking factor

ΔP = valve differential pressure

P_{up} = upstream pressure

A_{stem} = $1/4\ \pi\ (D_{stem})^2$

D_{stem} = valve stem diameter

$F_{packing}$ = packing drag.

We believe this to be conservative because, for wedge gate valves, the ratio of stem force to differential pressure typically drops as the pressure increases, all other things remaining the same.

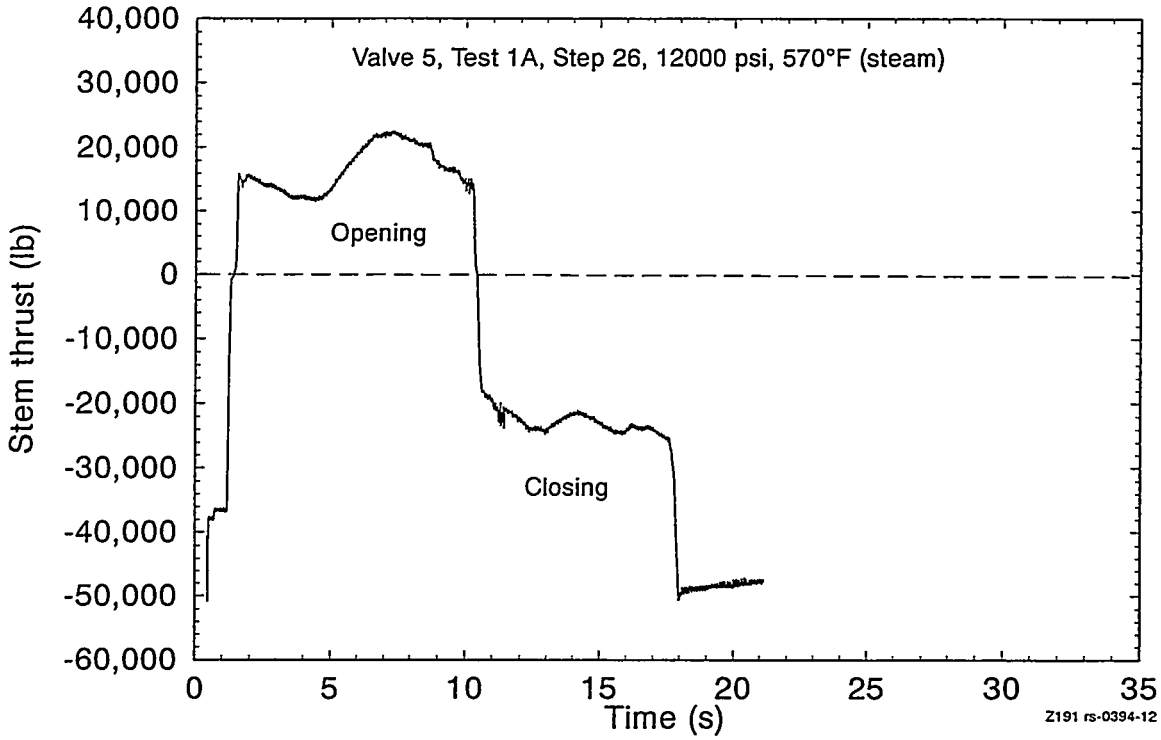

Figure 12. Ten-in. flex wedge system valve, 30% reopen and closing at high flow. Stem force history shows less of a hook in the second line break flow closing load.

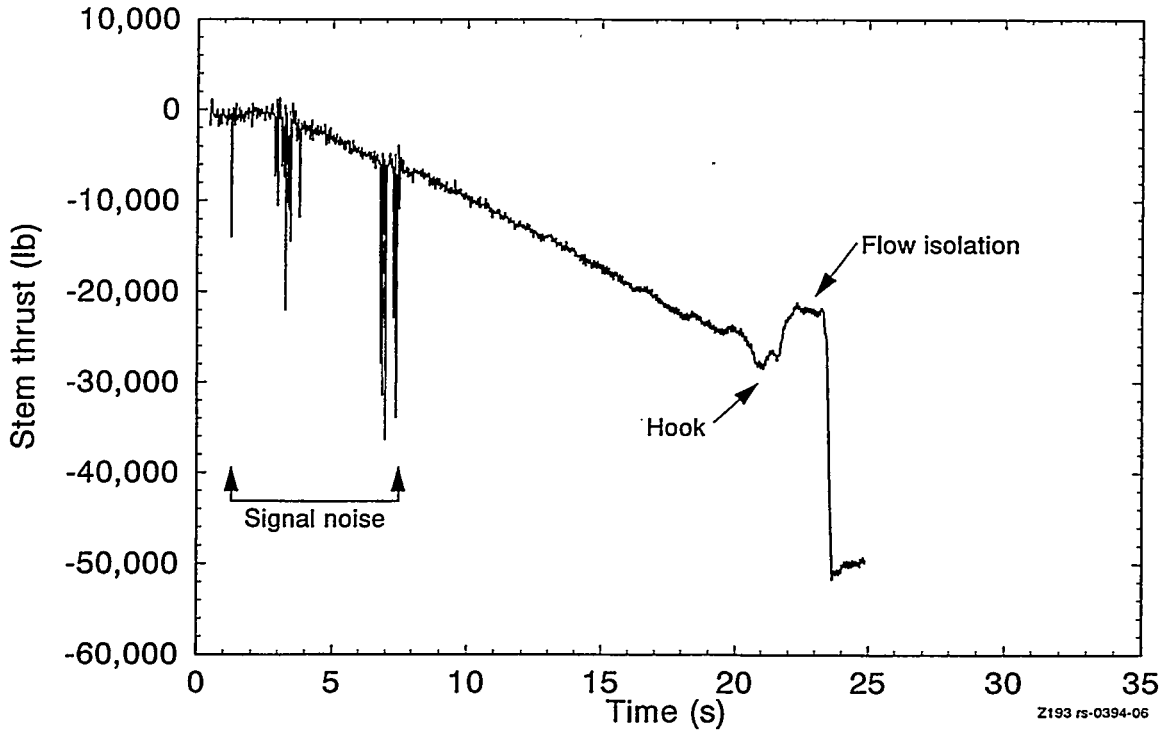

Figure 13. Ten-in. flex wedge system valve. Closing against line break flow in the first test shows a significant hook just before flow isolation.

Extrapolation of Atypical Opening Response

Prior to the NRC-sponsored INEL valve testing program, there were not many high-energy gate valve test results in the public domain. There may have been some proprietary data in Europe, but virtually none in the United States, particularly in the opening direction. Most of the analysis presented in the opening section is from our work. Since then, we have reviewed a number of industry test programs, and the results of their work does not conflict with the results presented here.

In both phases of our full-scale test programs, we wrote the test procedures to require the valve to be reopened about 20 to 30% under full-blowdown conditions and then reclosed. This testing was performed as soon as the preceding blowdown test had been evaluated against the specified conditions (pressure, temperature, etc.), typically about 5 to 30 minutes later. We opened and closed the valves under other flow loads, but, typically, the highest flow tests are better for analysis because the load components are easier to separate. What might have been a subtle influence in a lower differential pressure test stood out during the higher load test.

For us, initially predicting the opening loads and analyzing the test results from the opening tests was a less-than-absolute science. Industry has always calculated the valve opening stem thrust like the valve closing stem thrust, except that the sign on the valve stem term is reversed because the stem is traveling in the opposite direction. Industry, for the most part, has been more concerned about the unwedging load than they have been about flow loads in the opening direction. Our test results questioned industry's opening model as it did the closing model.

However, before discussing the atypical opening valve response it is necessary to observe that unlike a atypical valve closing that results in more required thrust, atypical valve opening results in initially less thrust while the disc is riding on the valve seat; thus, it cannot be extrapolated from a less-than-design-basis test; it can only be evaluated and then predicted with a correlation based on typical opening behavior. The worst cases of atypical opening behavior have been observed on valves operating in a steam environment and high velocity cold water applications. In-high energy hot water and low-velocity cold water applications, the opening response appears to be a mirror image of closing.

Opening loads that are not a mirror image of the closing loads with a few changes in signs, such the stem rejection load. These opening responses present a completely different problem. Stem force history plots for the three 10-in. valves we tested in a steam environment show that flow loads after unseating were higher than the unseating loads, which in turn looked like a hump in the stem force after unseating. This means that not only was there a hook in the closing direction, but possibly a corresponding hump in the opening direction. This was further compounded in some cases by mechanical interference between the disc and the seat, which added resistance in the closing direction but not in the opening direction. In addition, in the opening direction the fluid and pressure effects seemed to act quite differently than observed in the closing direction. There were always a number of individual forces influencing the opening responses, and separating these opening forces was a different challenge than for the closing direction.

After a preliminary analysis phase trying to analyze the data by separating the forces and solving for the friction factor, we created a computer model that represented what we thought should be going on within the valve in the opening direction and then analyzed all of our close-to-open-to-close test data against this model. The model was based on the INEL closing equation, refitted for the opening direction, with the added capability to address disc tippage. The model used actual valve dimensions and the actual test pressures recorded during the test on a real-time basis to make response estimations. It was not our intent during this initial effort to tweak the model until it provided exact response predictions, but to look at all of our high-flow reopening and reclosing data against a common set of predictions based on what we thought was going on. We made a number of assumptions in the model, but as long as they were constant from test to test, it met our needs

Figure 14 shows the stem force plotted against calculations for a 10-in. Wm. Powell flexwedge gate valve during the high flow opening and closing cycle discussed above. In this figure, the upper two plots are the actual stem force history and the calculated stem force history for valve opening; both plots travel from left to right on the page, whereas the lower plots, actual and calculated stem force histories, are for valve closing and travel right to left on the page. The actual and calculated stem force histories have been plotted against stem position, and the fully closed valve position for both opening and closing is on the left. The zero stem position corresponds to the disc position where the visual flow path through the valve is first blocked. The calculated plots are the estimated responses based on the actual test pressures but assuming a specific disc friction factor based on experience and adding slight disc tippage after the disc came off the seat based on internal valve measurements that verified all of the tested valve discs could tip. Except for the initial, on-the-seat response for the valve in the opening

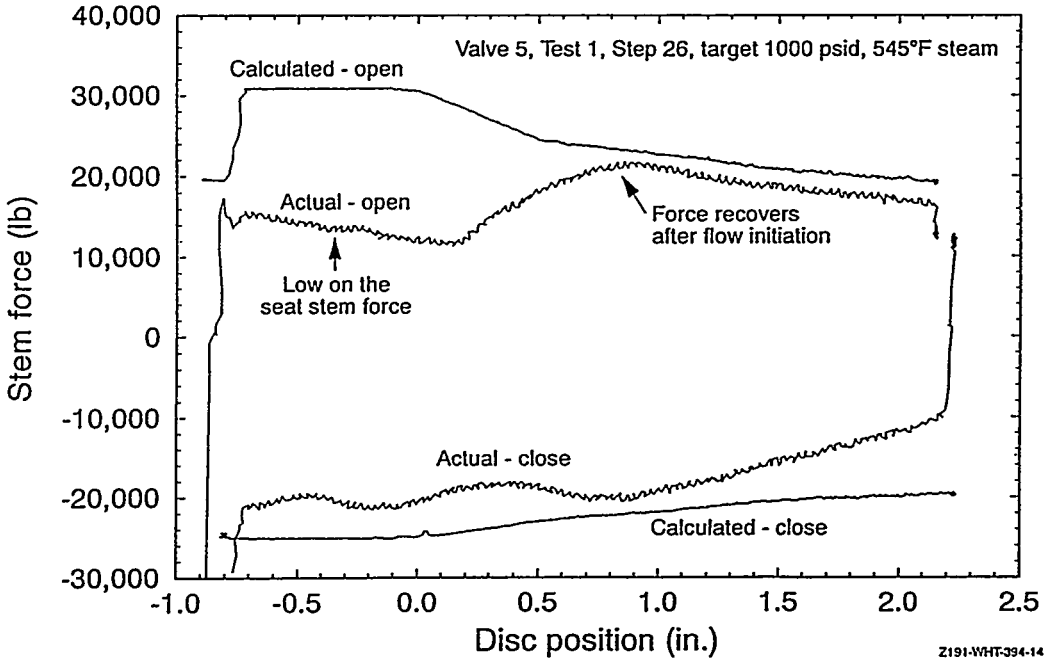

Figure 14. Valve 5, 10-in. flex wedge valve opening, 30% on a steam flow and reclosing, shown against calculated loads.

direction, the force estimates for opening and closing are slightly conservative. However, once the disc moves off the seat and flow is initiated, the opening response increases and matches the prediction quite well.

We also note that these particular estimations begin to overpredict the stem thrust at about the 1.5-in. stem position. This is the result of the model assuming a constant disc area after unseating. We did this because it made the model simpler to implement and because our primary interest was in the response of the valve during the unseating and initial flow portion of the valve opening stroke when nearly the full area of the disc was exposed to flow. Within this limit, what the opening estimation tells us is that the stem thrust is lower than predicted while the disc is riding on the seat, but as soon as flow is initiated, the disc load increases and starts to respond more as the model would predict it to. This implies that the hump in the opening direction is not a new load but rather the appearance of the load we expected to be there. In our test program, the three larger valves (10-in.) were dynamically tested with steam, and the responses of all three were similar to the example shown here. This type of opening load will be discussed further under the extrapolation of atypical opening response presented below.

The smaller, 6-in., valves were exposed to a number of fluid conditions and pressure parametric tests. The low on-the-seat opening response observed during the 10-in. valve testing was also present during the 6-in. valvetesting but only with the single-phase fluids (high velocity cold water and steam) as shown in Figures 15 and 16 for a 6-in. Velan flexwedge gate valve. Conversely, Figure 17 for the same valve shows the response of the valve while opening and closing against 10°F subcooled water at about 1000 psid. This opening response is much closer to a mirror image of closing.

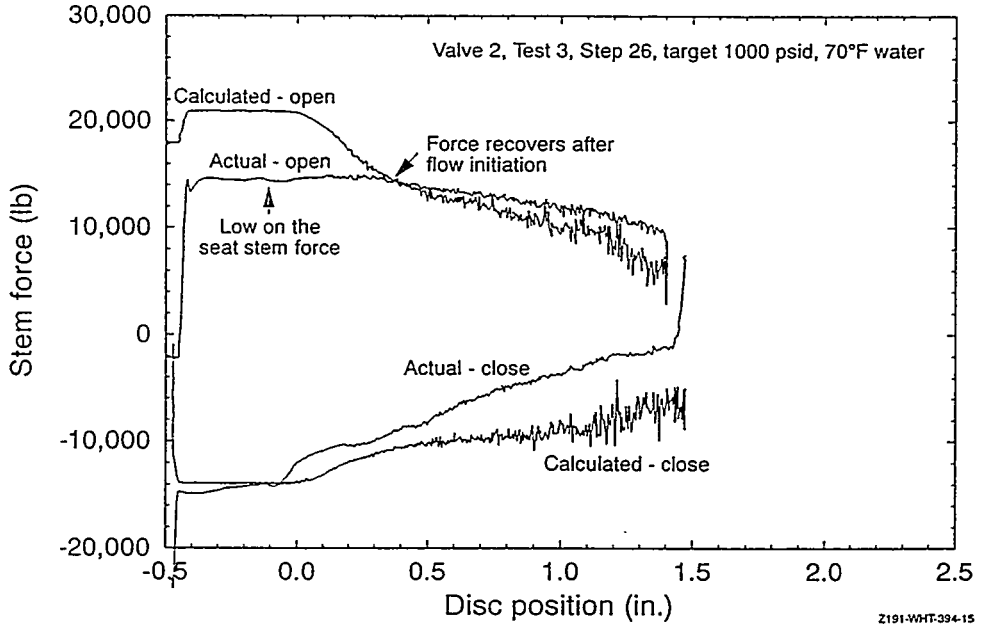

Figure 15. Valve 2, 6-in. flex wedge valve opening, 30% on 10°F subcooled water and reclosing, shown against calculations.

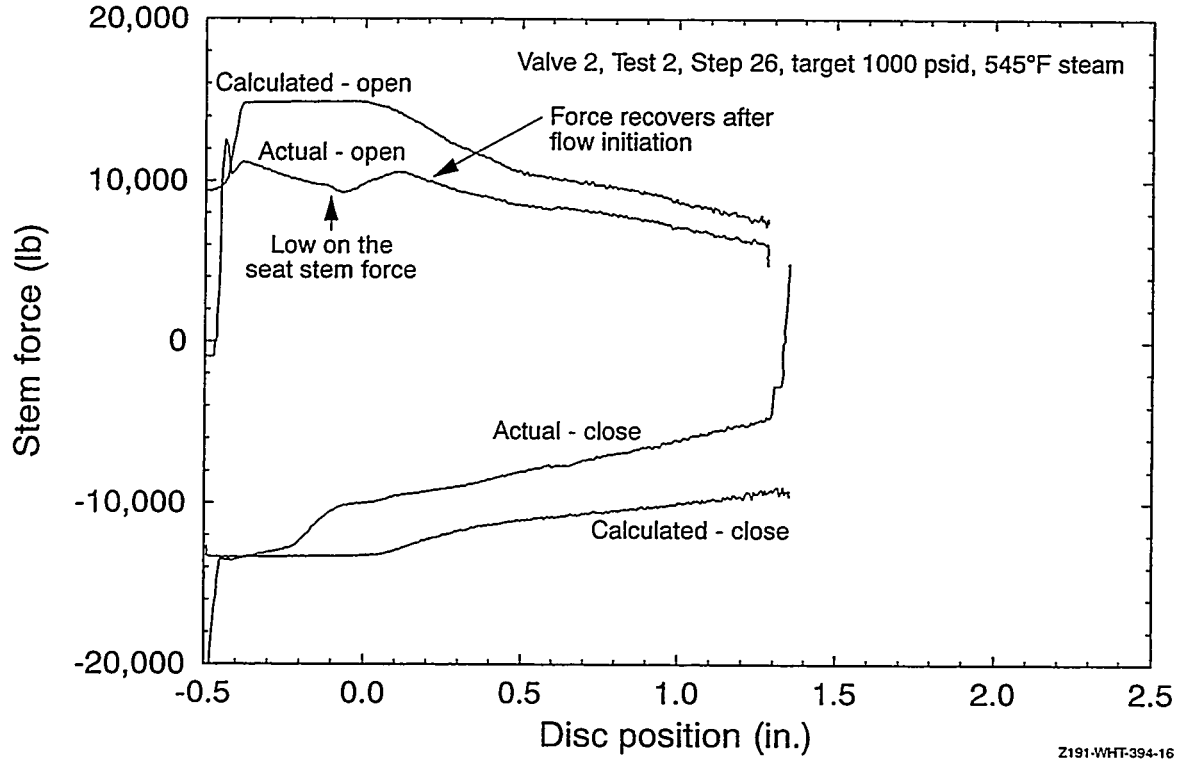

Figure 16. Valve 2, 6-in. flex wedge valve opening 30% on ambient temperature water and reclosing shown against calculations.

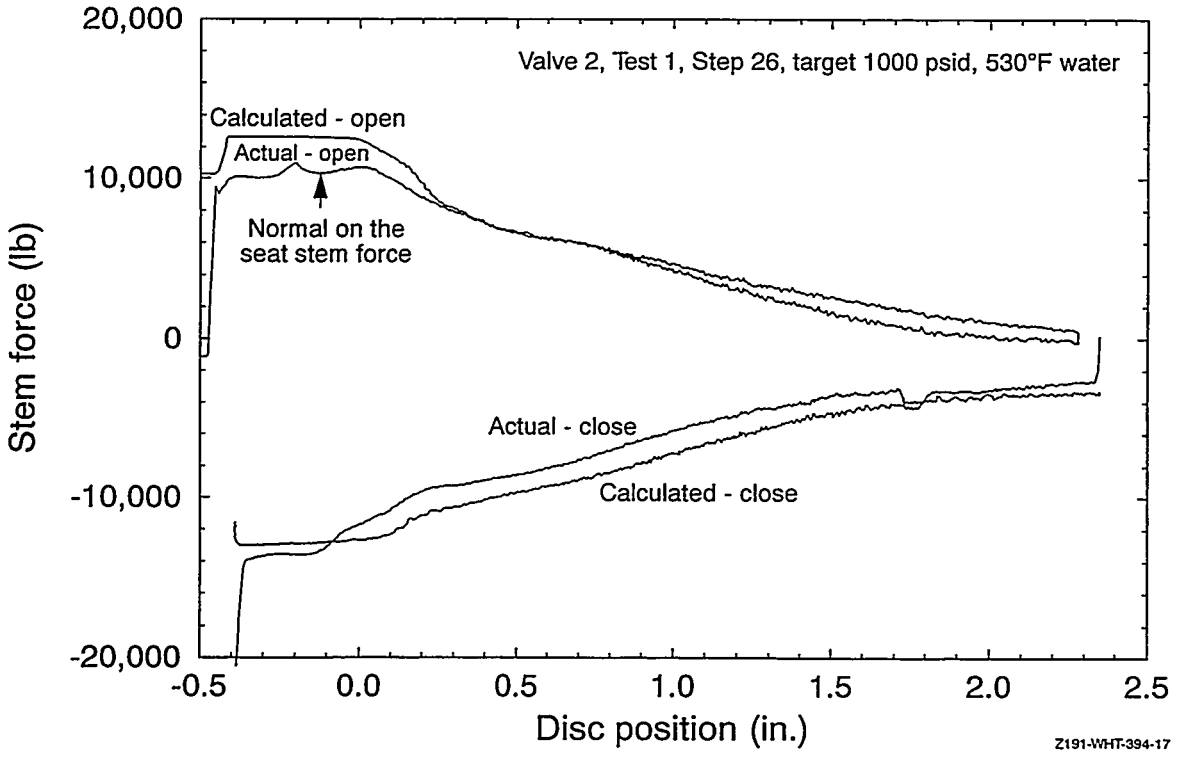

Figure 17. Valve 2, 6-in. flex wedge valve opening, 30% on steam flow and reclosing, shown against calculations.

Other opening responses for the 6-in. Velan, where the fluid could flash downstream of the closing disc, show the same general tendencies; the opening mirrors the closing response. Industry testing shows the same is true for low-velocity cold water; the opening responses are a mirror image of closing.

A 6-in. Walworth flexwedge gate valve was parametrically pressure-tested with 10°F subcooled water and exhibited the same general opening shapes as the valve described above when tested with flashing fluids. These test results show that for a fluid that can flash, the opening direction develops a response much like that seen in the closing direction. The pressure effect was also observed for both 6-in. valves in the opening direction; as we increased the valve inlet pressure, the corresponding stem thrust was less per pound differential pressure.

The pressure and fluid effects in the opening direction are not unexpected, but the magnitude of the effects while the disc was riding on the seat in the steam environment are surprising. We had previously observed the pressure effect in the closing direction, but to a much smaller degree, and the fluid effect in the closing direction required the INEL closing correlation to have two different disc friction factors, one for fluids under 70°F subcooled and another for fluids over 70°F subcooled. So, while the fluid and pressure effects were not unexpected, what we cannot explain is why the seat friction factors are so low for the identified single-phase fluids. While it is a curiosity, the fact remains that once flow starts, the response recovers to a more predictable value. This dictates that we must predict the response without regard for the unexplained low friction while the disc is on the seat for certain fluids.

Once we understood that the fluid type and pressure effects had a larger impact in the opening direction than in the closing direction, and that the hump in the opening direction was not a new flow load, but only recovering to where it should have been, we were able to start understanding the opening response. After examining our test results in light of the effect that fluid type, pressure, and velocity had on the peak response of the valve, we extracted the results of those tests where the opening was a typical response (mirror image of closing). These results bound the observed responses of all of the valves, including those that respond atypically, and avoid the difficulties of dealing with the unexplained low on the seat friction factors prior to flow initiation under some fluid conditions. Using these opening typical data, we were able to estimate the normal and sliding loads acting on the disc and to correlate them over a wide range of differential pressure conditions. Figure 18 is a plot of the sliding versus normal loads for the valves used to develop our opening correlations. Less-than-design-basis opening tests results can be evaluated using Equations 2 or 3 below as applicable. If the test results fit within the bounding values of Figure 18, or the test results show the valve to exhibit a atypical response with a very low on the seat stem thrust, then the design-basis thrust may be estimated using the applicable equation below.

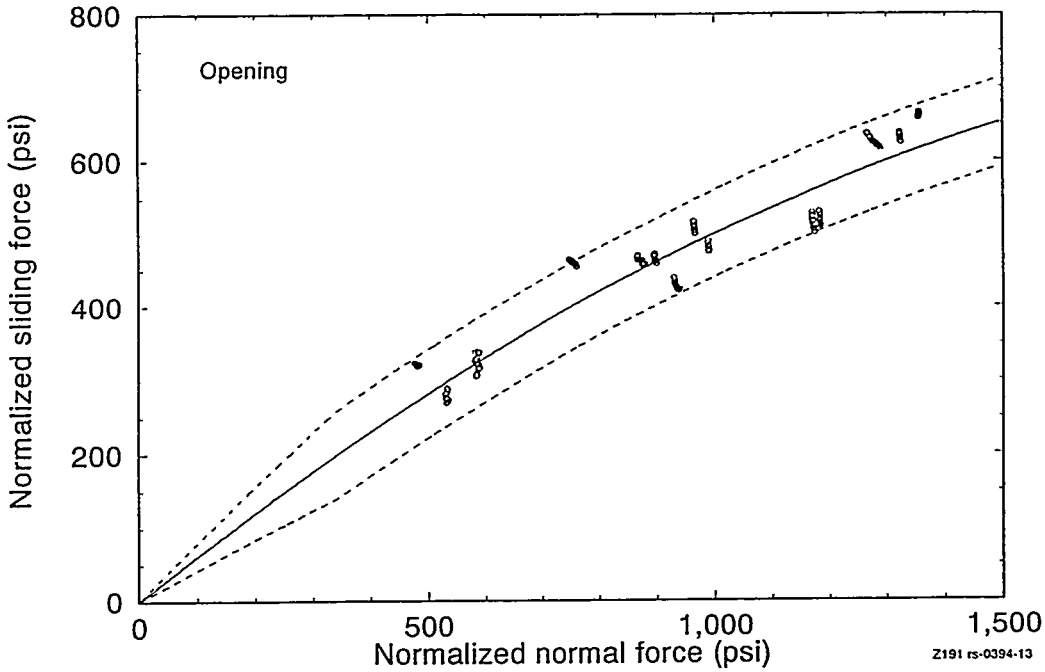

Figure 18. Flexwedge gate valve opening, normal versus sliding correlation.

For $\Delta P >= 350$ psi:

$$F_{stem} = F_{packing} + F_{top} - F_{bot} - F_{sr} + \frac{(\sin\alpha + f_o\cos\alpha)(F_{up} - F_{dn}) - \frac{f f_o \cos^2\alpha}{A_{ms}}(F_{up} - F_{dn})^2 \pm 60 A_{ms}}{(\cos\alpha - f_o\sin\alpha) + \frac{2 f f_o \cos\alpha \sin\alpha}{A_{ms}}(F_{up} - F_{dn})} \quad (2)$$

For $\Delta P < 350$ psi

$$F_{stem} = F_{packing} + F_{top} - F_{bot} - F_{sr} + \frac{(\sin\alpha + 1.3 f_o\cos\alpha)(F_{up} - F_{dn}) - \frac{1.3\ f f_o \cos^2\alpha}{A_{ms}}(F_{up} - F_{dn})^2}{(\cos\alpha - 1.3 f_o\sin\alpha) + \frac{2.6 f f_o \cos\alpha \sin\alpha}{A_{ms}}(F_{up} - F_{dn})} \quad (3)$$

where

F_{stem}	=	Valve stem thrust
$F_{packing}$	=	packing drag
F_{top}	=	$P_{up} * A_{ms} * \tan\alpha$
F_{bot}	=	$P_{dn} * A_{ms} * \tan\alpha$
F_{sr}	=	$P_{up} * A_{stem}$
F_{up}	=	$P_{up} * A_{ms}$
F_{dn}	=	$P_{dn} * A_{ms}$

α = valve seat angle

A_{ms} = $\frac{1}{4}\ \pi\ (\text{Seat MD})^2$

A_{stem} = $\frac{1}{4}\ \pi\ (D_{stem})^2$

and

Seat MD = valve mean seat diameter

D_{stem} = valve stem diameter

P_{up} = upstream pressure

P_{dn} = downstream pressure

f_o = 0.63

ff_o = 0.00013.

Unlike the INEL's linear correlation for closing, Figure 18 (the extended closing correlation discussed below), the opening correlation is a quadratic. In effect, this results in a larger friction factor when the valve is lightly loaded (around 0.63), and the friction factor decreases as the valve load increases. Another difference between the closing correlation and the opening correlation can be seen in the limits of the data scatter at higher loadings. The closing correlation bounded the response with a ±50 psi band, whereas the opening correlation bounds the data with a ±60 psi band. These values represent the term necessary to conservatively bound actual valve performance. However, for all the differences between the opening and closing methodologies, the on-the-seat typical responses are quite similar, which adds to our confidence that the opening correlations are valid.

EXTENDING THE INEL CLOSING CORRELATION

We know from our original high-pressure high-flow work used in developing our closing correlation that the data scatter below a disc loading of about 400 psi became dominant. As such, we originally limited the use of the correlations to 400 psi and above. It was not known at the time if valve responses below 400 psi were linear or not, and that is why we have included this discussion of typical behavior in this mostly atypical response paper. While data scatter prevents direct comparison or extrapolation of low-pressure testing in many cases, the results do provide a value that can be compared with the upper limit of the data scatter used in the development of the correlation. If the upper limit is exceeded, the extended INEL correlation should not be used to predict the design-basis load using a less-than-design basis test. The following analysis documents the extension of the INEL correlation to loads less than 400 psi.

Data from an Industry Valve Test Program

A classic example of this low-pressure data scatter is shown in the results of the analysis of a 14-in. 600-lb valve tested recently as part of an industry test program. A quick look at the test results provided by them

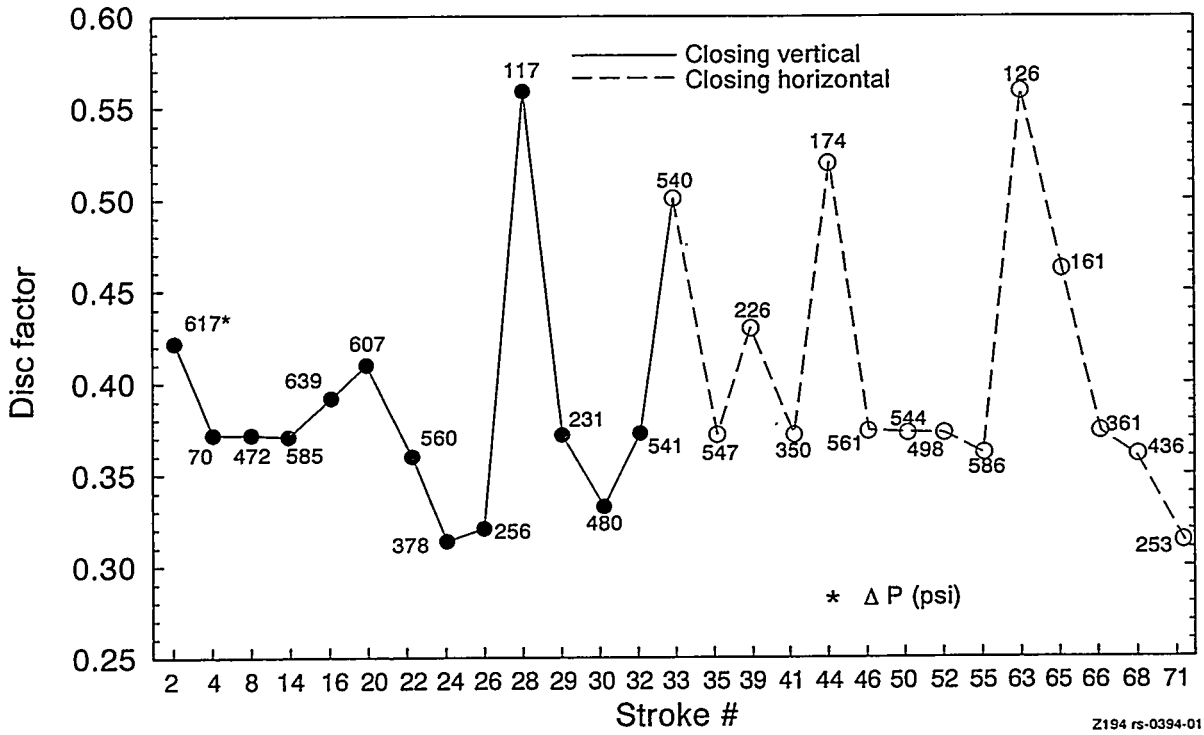

Figure 19. Results from testing a 14-in. 600-lb valve.

is shown in Figure 19, which plots the calculated disc factor versus stroke number. These tests were all performed with the same valve. Each of the circles represents results from a closing test, and the number next to the circle is the differential pressure for that test at flow isolation. The solid circles are from tests with the valve mounted in the vertical position, and the clear circles are from tests with the valve mounted in the horizontal position. This preliminary view of the test results indicates the data scatter mentioned above.

The presentation in Figure 20, with disc factor plotted against differential pressure, gives a better indication of the data scatter. As a general trend, the tests at a higher differential pressure show a more consistent disc factor than do the tests at a lower differential pressure. The EPRI-NMAC and standard industry equations were used in analyzing the data in the figure.

Looking at the data in a different way, as shown in Figures 21 and 22, we see a much better correlation of the data. What appeared to be a lot of scatter in the data takes on a more linear appearance. This is the same valve in all of the testing, so this simplified method of looking at the data will work. (Most of the current industry gate valve models can be used to analyze single valve for trending against itself; a model must be more precise, though, if the results from one valve are used to predict the response of another valve, and that is not the case here.) What the analyst has done in Figure 21 is to divide the dynamic load in the stem (total stem thrust minus the stem rejection load and the packing load) by the pressure load on the disc (disc area times differential pressure) to calculate a disc factor. The

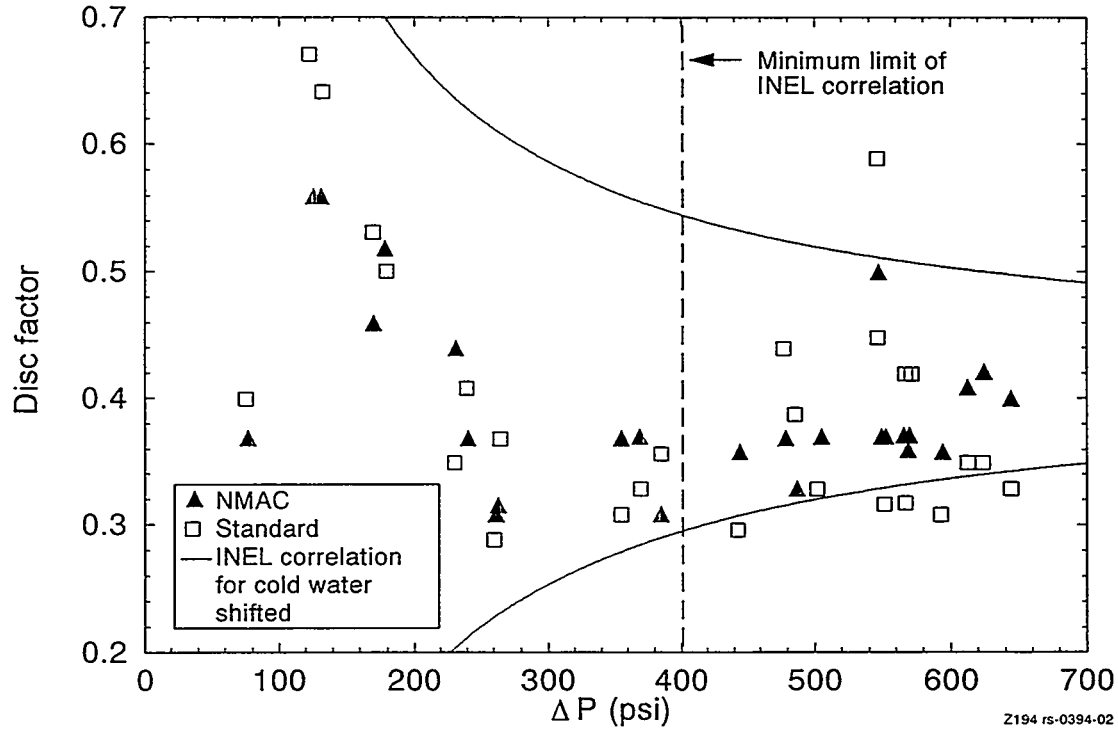

Figure 20. Disc factor plotted against differential pressure for the 14-in. valve. Tests at higher differential pressure show a more consistent disc factor.

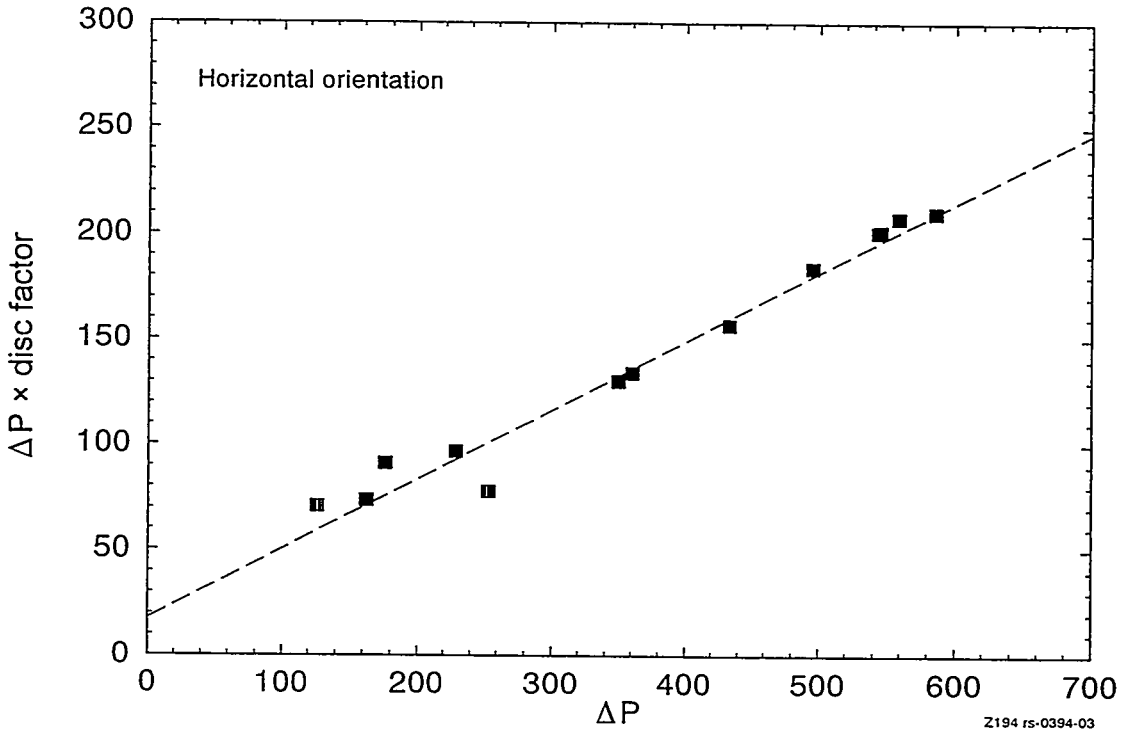

Figure 21. Disc load versus dynamic stem load; data fit for tests performed with th valve in the horizontal position.

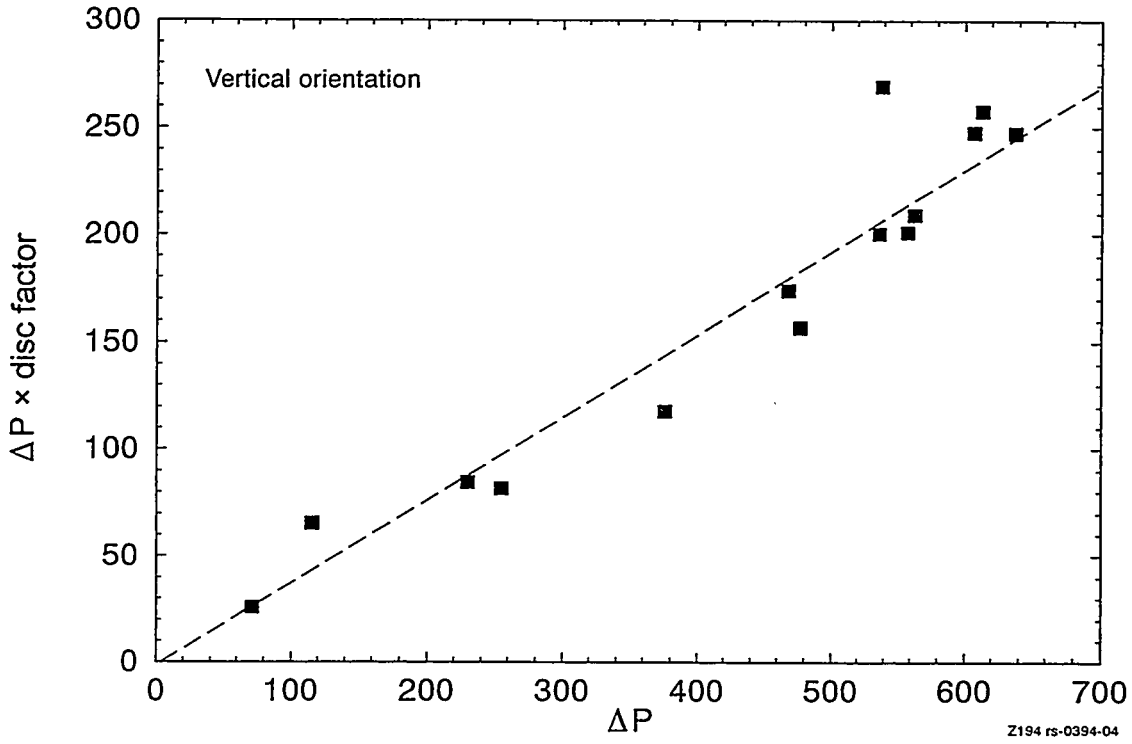

Figure 22. Disc load versus dynamic stem load; data fit for tests performed with the valve in the horizontal position.

results presented in Figures 21 and 22 is a simplified analysis similar to that used in the INEL correlation; the y axis represents the dynamic stem thrust load (the y axis, though labeled differently, equals the dynamic stem thrust divided by the disc area), the x axis represents the disc load (the x axis equals the disc load divided by the disc area), and the slope of the trace represents the disc factor. Unlike the INEL correlation, however, this analysis does not result in a true normal versus sliding load because it does not account for the 5-degree (nominal) angle of the disc and seat. Again, this kind of simplified analysis works only for analyzing a single valve for trending against itself.

As stated, the low differential pressure tests that we performed as part of our full-scale testing show a similar degree of scatter in the disc factor data. For this reason, we initially limited the application of the INEL correlation to loads above about 400 psid. The data we had at the time was very limited and did not support extending the correlation any lower. However, from what we now see in the INEL data, our review of selected tests performed at the Trojan Nuclear Power Station, and other data we have looked at, it is evident that there is a linear trend running through a set of data scatter. Based on these observations, we have extended the INEL correlation below 400 psi. The extended correlation is presented below and shown in Figure 23. When using the INEL extended correlation above a normalized normal load of approximately 415 psi, the first correlation should be used, whereas below this load the second correlation should be used.

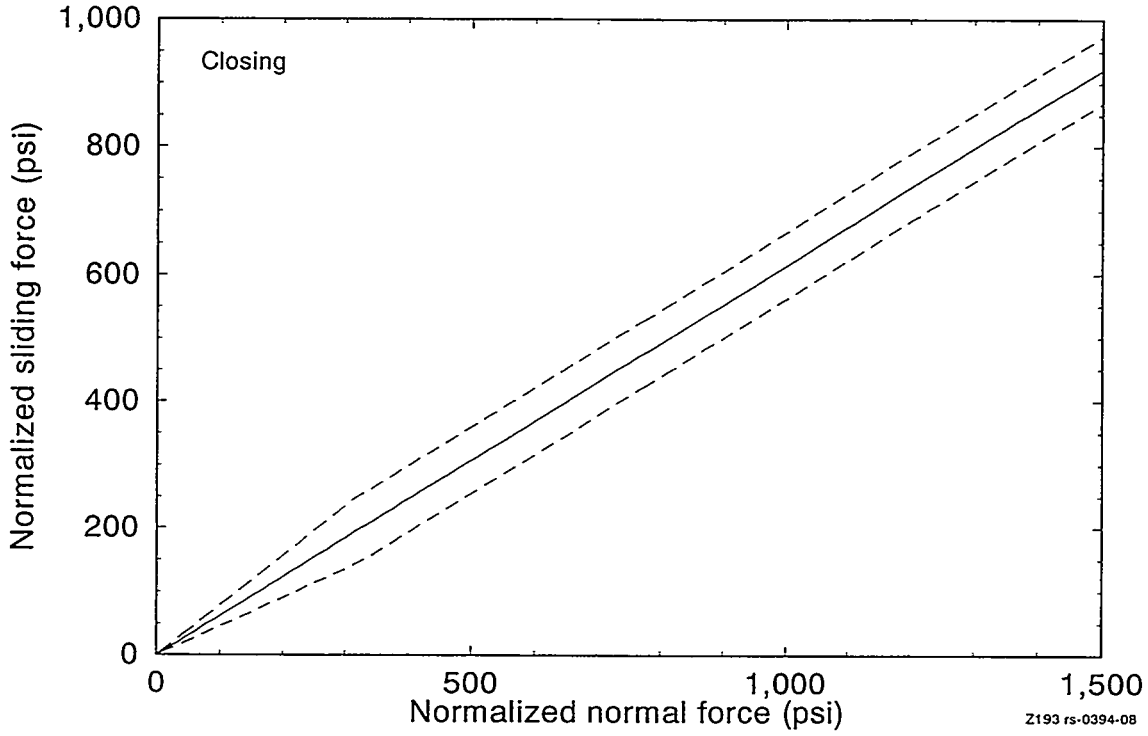

Figure 23. Normalized sliding force versus normalized normal force for gate valves.

For $\Delta P >= 415$ psi:

$$F_{stem} = F_{packing} + F_{sr} - F_{top} + F_{bot} + \frac{(\sin\alpha + f_c \cos\alpha)(F_{up} - F_{dn}) \pm 50 A_{ms}}{(\cos\alpha - f_c \sin\alpha)}$$

For $\Delta P < 415$ psi:

$$F_{stem} = F_{packing} + F_{sr} - F_{top} + F_{bot} + \frac{(\sin\alpha + 1.3 f_c \cos\alpha)(F_{up} - F_{dn})}{(\cos\alpha - 1.3 f_c \sin\alpha)}$$

where

F_{stem} = Valve stem thrust

$F_{packing}$ = packing drag

F_{top} = $P_{up} * A_{ms} * \tan \alpha$

F_{bot} = $P_{dn} * A_{ms} * \tan \alpha$

F_{sr} = $P_{up} * A_{stem}$

F_{up} = $P_{up} * A_{ms}$

F_{dn} = $P_{dn} * A_{ms}$

α = valve seat angle

A_{ms} = $\frac{1}{4} \pi$ (Seat MD)^2

A_{stem} = $\frac{1}{4} \pi$ (D_{stem})^2

and

Seat MD = valve mean seat diameter

D_{stem} = valve stem diameter

P_{up} = upstream pressure

P_{dn} = downstream pressure

f_c = 0.40 for less than 70°F subcooled water
0.50 for 70°F for greater subcooled water

It is our opinion that if a valve cannot be tested at its design-basis differential pressure, the valve control switches should be set using the best information available and a justifiable friction factor or disc factor for the design basis loads. Then, the valve should be tested at the highest differential pressure possible and the results checked for anomalous behavior.

Use of the extended correlation is the same as for the original INEL closing correlation used in the IVA software package. The correlation still requires that a test be performed for verification. If a test cannot be conducted at the design-basis differential pressure, we recommend that a test be conducted at the highest differential pressure possible. The results of that test can then be used to evaluate the valve against the extended INEL correlation. As stated at the beginning of this discussion, if the results of the low-load test fall below the upper bound shown in Figure 19, the extended INEL correlation is considered applicable. This evaluation verifies that the response of the valve is typical of the valve responses used to develop the correlation. If the extended correlation is applicable, the correlation can be used to estimate the response of the valve at design-basis conditions. We placed the upper bound on the extended correlation to establish the upper limit on what we consider sliding friction. Disc factors or friction factors above 0.65 do not represent sliding friction alone, but include mechanical interference. We know of no way to predict responses caused by mechanical interference, particularly when at higher loads it may involve damage.

Note that with either the original INEL correlation or the extended INEL correlation, the procedure is not a true extrapolation, though it appears to be such and though it is sometimes referred to as such. The prediction of the design-basis stem force requirements is a straightforward calculation using a friction factor provided by the correlation and using known values for the valve dimensions and the design-basis conditions. The calculation itself is independent of the low-load test results. The low-load test results do not

provide a base from which to extrapolate; instead, they provide confidence in the applicability and accuracy of the prediction.

PRECONDITIONING

Some of the scatter in the disc factor data (Figure 19) can be attributed to a lack of *preconditioning*. *Preconditioning* refers to the breaking-in of a new valve or a recently overhauled valve. New gate valves and gate valves that have recently been overhauled might temporarily have lower than-normal-disc friction coefficients. This phenomenon may be the result, for example, of machining oil residue left on the disc and seat surfaces. As a general trend for industry testing, tests performed earlier in a test series produced lower disc factors than those performed later in the series. This explains why, in Figure 19, the disc factors for stroke numbers 28 and 33 (at differential pressures of 117 and 540 psid) appear to be abnormally high; they were run out of turn, later in the test series.

Data scatter caused by the lack of preconditioning has appeared in other test results as well. Following our Phase 2 testing, it was observed that exposing a new or overhauled valve to hot water or steam conditions stabilized the friction coefficient immediately. In recent industry testing, researchers observed that under ambient temperature water conditions, many cycles were necessary to age the friction surfaces enough to yield a stable friction coefficient. It appears that disc friction values derived from recently overhauled valves operated in ambient temperature water may not be reliable. It would be better to use the friction values obtained before the overhaul, or values from similar valves with aged surfaces.

CONCLUSION

Atypical behavior, whether in the opening or closing direction without damage, is a manageable condition. Performing a best-effort differential flow test in either direction will help reduce unnecessary conservatism.

REFERENCES

1. R. Steele Jr., J. C. Watkins, K. G. DeWall, and M. J. Russell, NUREG/CR-5720, Motor-Operated Valve Research Update, EGG-2643, 1992.

NOTICE

PERFORMANCE-BASED INSPECTION AND MAINTENANCE STRATEGIES

W. E. Vesely
Science Applications International Corporation

Abstract

Performance-based inspection and maintenance strategies utilize measures of equipment performance to help guide inspection and maintenance activities. A relevant measure of performance for safety system components is component unavailability. The component unavailability can also be input into a plant risk model such as a Probabilistic Risk Assessment (PRA) to determine the associated plant risk performance. Based on the present and projected unavailability performance, or the present and projected risk performance, the effectiveness of current maintenance activities can be evaluated and this information can be used to plan future maintenance activities.

A significant amount of information other than downtimes or failure times is collected or can be collected when an inspection or maintenance is conducted which can be used to estimate the component unavailability. This information generally involves observations on the condition or state of the component or component piecepart. The information can be detailed such as the amount of corrosion buildup or can be general such as the general state of the component described as "high degradation", "moderate degradation", or "low degradation". Much of the information collected in maintenance logs is qualitative and fuzzy.

As part of an NRC Research program on performance-based engineering modeling, approaches have been developed to apply Fuzzy Set Theory to information collected on the state of the component to determine the implied component or component piecepart unavailability. Fuzzy Set Theory is a formal approach for handling qualitative information and fuzzy information in models and in evaluations. When the information is qualitative or fuzzy, then the results which are produced are also qualitative and fuzzy, consisting of categorized descriptions. As the information becomes more quantitative and precise, Fuzzy Set Theory results converge to standard numerical results.

Demonstrations of the applications of Fuzzy Set Theory are presented utilizing information from plant maintenance logs. The demonstrations show the power of Fuzzy Set Theory in translating engineering information to reliability and risk implications.

PERFORMANCE-BASED INSPECTION AND MAINTENANCE STRATEGIES

W. E. Vesely
Science Applications International Corporation

Introduction

This paper reports on a study sponsored by the Division of Engineering of the Office of Nuclear Regulatory Research of the U.S. Nuclear Regulatory Commission. The objective of the study was to identify approaches for utilizing inspection and maintenance information in order to determine component and plant performance implications, and particularly reliability and risk implications. The inspection and maintenance information of prime interest was engineering-related information and the study focused on how this information would be used to indicate the reliability performance of the equipment.

During inspection and maintenance, observations are generally recorded of the conditions of the component or component pieceparts. These observations include descriptions of the amount of wear, amount of corrosion, or amount of contamination which is occurring. The observations represent important engineering information. In fact, most maintenance and inspection information is of this type. There is sufficient information that individual components can be tracked in terms of their performance. The problem with this information is that it is often qualitative or semi-quantitative in nature. For example, in one plant's maintenance log that was examined, the amount of erosion buildup in a motor operated valve was characterized as being "small", "moderate" or "significant" with accompanying descriptions.

The objective of the work described here is to identify a systematic process which will utilize this engineering information on the general deterioration state of the component or component pieceparts and predict the implications on the component performance. Of particular interest are predictions of the implications on component reliability and plant risk. These implications can then be used to help evaluate the effectiveness of the inspection or maintenance program and to identify when further inspection or maintenance actions are needed.

Applicability of Fuzzy Set Theory

Because inspection or maintenance information recorded on the conditions of the component or component piecepart is often qualitative or semi-quantitative in nature, such as described by categorizing the deteriorations, the process for evaluating the performance implications of the observed conditions should be able to handle this type of information. Furthermore, since the information can also be quantitative, such as measurements of the amount of pipe wall-thinning which is occurring, the process must be able to also handle quantitative information.

One approach which has the capability of systematically processing both qualitative and quantitative information is Fuzzy Set Theory. Fuzzy Set Theory is so called because it is a theory which formally deals with fuzzy, qualitative information. Fuzzy Set Theory was developed in 1965 by Lofti Zadeh (1). Fuzzy Set Theory, or FST as it shall be denoted for short, is now employed in a wide variety of engineering applications. These applications utilize qualitative and semi-quantitative information to derive engineering implications and systems implications. References on the basic methodology of FST and its engineering applications are (2,3,4,5,6,7). All these references have extensive bibliographies which identify many further references. Also, the journal Fuzzy Sets and Systems is published periodically and contains many articles on FST methods and applications.

Application of Fuzzy Set Theory to Inspection and Maintenance Information

The basic steps of FST as applied to the evaluation of inspection and maintenance information are shown in Table 1.

TABLE 1. BASIC STEPS OF APPLYING FST TO ANALYZE INSPECTION AND MAINTENANCE INFORMATION

Step 1.	Define the descriptive categories which describe the deterioration state of the component or component piecepart
Step 2.	Construct an FST description (a membership function) for each category
Step 3.	If risk implications are also to be determined, determine the risk importances for the components
Step 4.	At each inspection or maintenance categorize the condition of the component or component piecepart using the descriptive categories
Step 5.	Use the FST methodology to determine the reliability and risk implications by determining the reliability or risk category describing the size of impact.
Step 6.	Use the reliability and risk results to help identify when future maintenance actions and overhauls are required.

For inspection and maintenance applications, a more appropriate name for FST is *descriptive category analysis* since information and results are represented in terms of descriptive categories such as "small deterioration", "moderate deterioration", or "large deterioration". The description of the reliability implications is similarly described in terms of broad descriptive categories. The categories can be defined to correspond to different approximate ranges of size as will be seen in the example.

Demonstration of FST Applications to Inspection and Maintenance

Figure 1 shows the results of a demonstration of FST. In this example, valve body erosion is monitored in one MOV in the Auxiliary Feedwater System in a given plant. The recorded observations were used to determine the reliability and risk implications of the erosion. The plot shows the predicted unavailability implication of the observed erosion conditions.

FIGURE 1. UNAVAILABILITY INCREASE VERSUS VALVE AGE

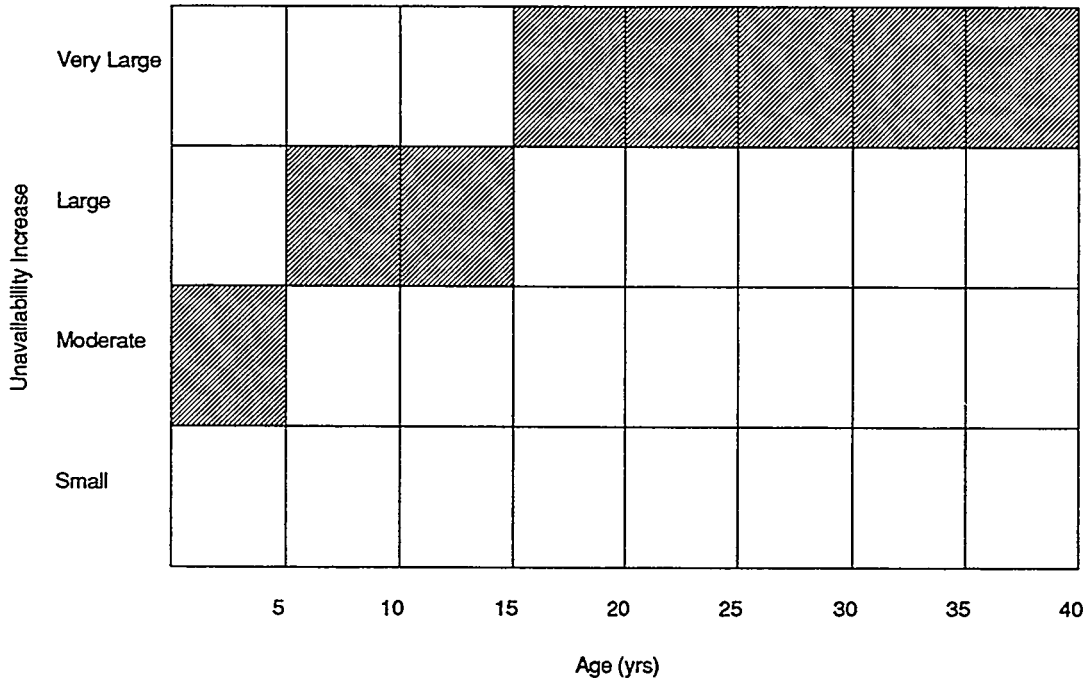

Figure 1 shows the predicted relative increase in unavailability of the valve versus future valve age due to the observed erosion conditions affecting the valve. The erosion conditions were categorized into appropriate descriptive categories by visually examining the valve, piping, and water conditions. Note that because of the descriptive nature of the observations the unavailability results obtained are in terms of descriptive categories, i.e. "small unavailability increase", "moderate unavailability increase", etc.

Figure 1 was obtained in the following manner. Based on successive observations of the valve conditions, the degradation or erosion rate of the valve was classified into one of four descriptive categories. The descriptive categories were defined to represent different degrees of valve

degradation and were described by the labels "small degradation", "moderate degradation", "large degradation", and "very small degradation". What category was selected was based on general criteria used by maintenance personnel. Using FST the descriptive categories for the degradation conditions were then translated to unavailability implications as a function of future valve age.

To determine the unavailability implications, the relative degradation rate categories were translated to similar failure rate increase categories. The relative increase in the failure rate was thus defined to be proportional to the relative increase in the valve degradation. The failure rate increase categories were then translated to unavailability increase categories using standard unavailability formulas. The unavailability increase categories were defined to correspond to the following general sizes of increase:

Small Increase	~ 10%
Moderate Increase	~ 30%
Large Increase	~ 100%
Very Large Increase	~ 300%.

Figure 2 shows the implications of the valve degradation descriptions on the relative core damage frequency (CDF) using the valve risk importance value determined from the plant PRA. The CDF increase categories were defined to have the same general sizes as the above unavailability categories, e.g. a small CDF increase corresponded to roughly a 10% increase in the CDF. Note again that the results are in terms of descriptive categories and not numbers. Note also that the PRA was only used to obtain the risk importance value for the MOV which was used to translate valve unavailability impacts to CDF impacts.

FIGURE 2. CORE DAMAGE FREQUENCY INCREASE VERSUS VALVE AGE

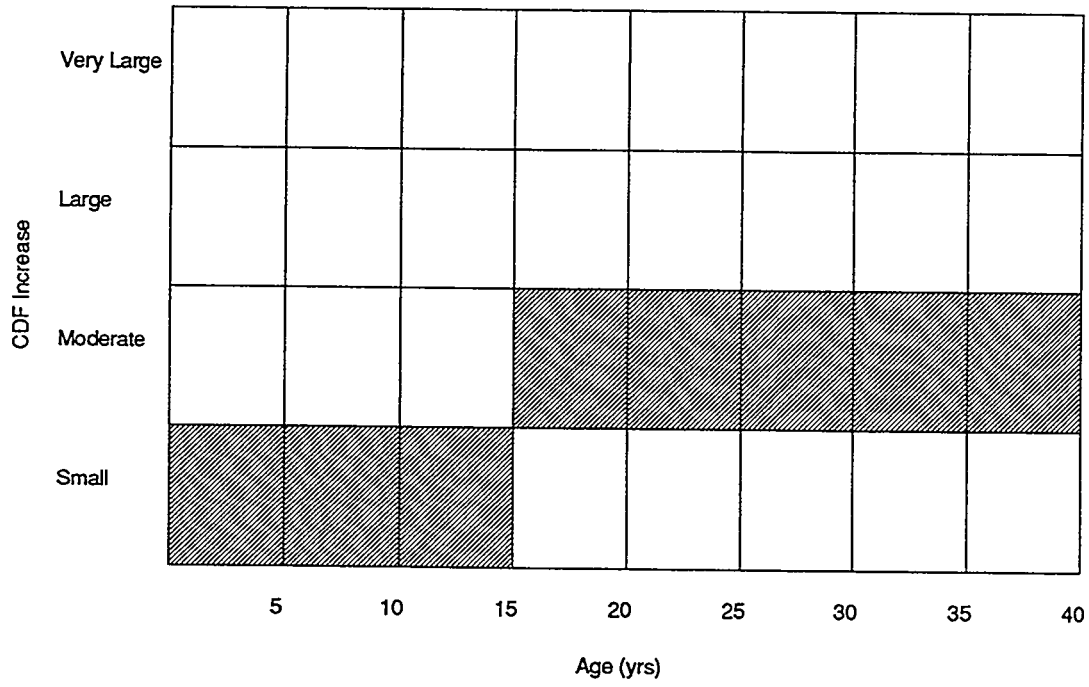

One of the principal objectives for determining the unavailability implications and CDF implications is to identify when more complete maintenance or overhaul on the valve is needed so that reliability and risk are controlled. The CDF profile in Figure 2 indicates that if overhaul is carried out within 15 years then the impact on the CDF would remain small. The unavailability profile in Figure 1 indicates that if overhaul is carried out within 15 years, the impact on the valve unavailability would at most be large, but would not be very large, i.e. would at most result in a factor of 2 increase in the unavailability (~100% increase). The large impact in unavailability does not translate to a large impact in the CDF because of the relative small importance of the valve as determined by the PRA.

The tables below show more detailed evaluations of the maximum unavailability increase and maximum CDF increase as a function of different overhaul periods on the valve in two year intervals. These results were consistent with engineering judgment at the plant but provided more substantive information for inspection and maintenance planning.

TABLE 2. MAXIMUM UNAVAILABILITY INCREASE FOR DIFFERENT OVERHAUL INTERVALS

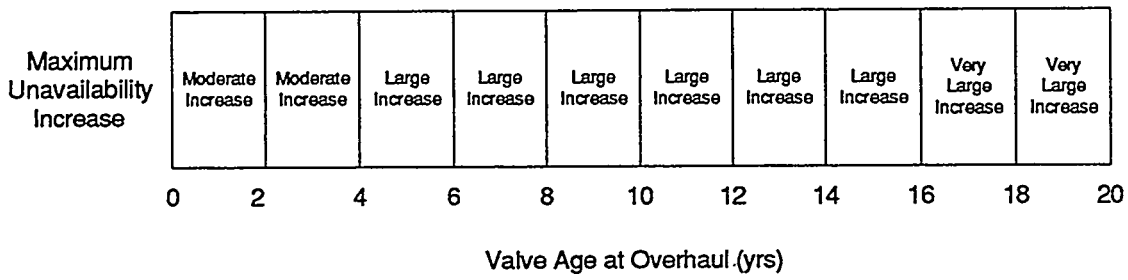

TABLE 3. MAXIMUM CORE DAMAGE FREQUENCY (CDF) INCREASE FOR DIFFERENT OVERHAUL INTERVALS

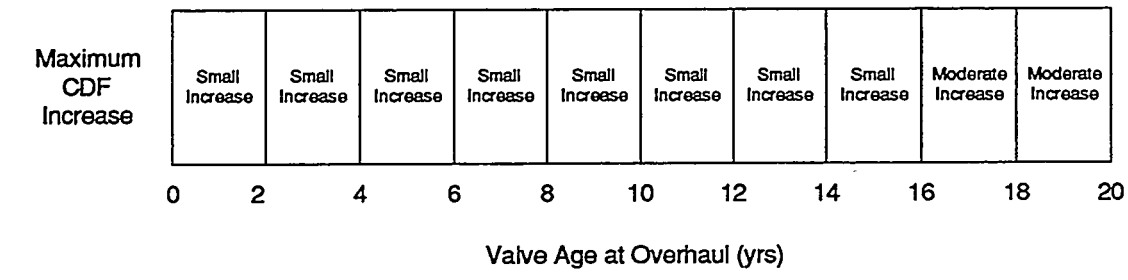

Conclusions

FST, as was used here, appears to be a potentially important tool for translating qualitative and semi-quantitative inspection and maintenance information into reliability and risk implications. Even though the reliability and risk implications were obtained in terms of descriptive categories they were sufficiently informative to indicate the order of magnitude impacts which is all that is needed for inspection and maintenance evaluation and planning. However, further work needs to be done before FST, or a variant of FST, can be confidently used in plant or regulatory applications.

The results of FST are dependent on the categories of information that are used and the way the categories are related to general sizes of values associated with the categories. For the inspection and maintenance applications, the FST results are dependent on the categories of degradations that are defined and their general relationship to measures of degradation size.

The criteria used for the categories in the study were rather subjective, based on plant personnel judgments. More objective criteria need to be defined as to what constitutes small degradation, moderate degradation, and large degradation (or very large degradation) for different degradation mechanisms and different component pieceparts. Reports issued by the NRC's Nuclear Plant Aging Research (NPAR) Program contain information on degradation conditions and degradation effects which can be used as inputs along with maintenance log information for the degradation categorizations. (See for example, references (8,9)).

Simple linear relationships were used in the study between the amount of degradation occurring and the reliability impact (unavailability). These relationships need to be better calibrated by categorizing degradations where failure histories also exist.

As indicated, there is a great deal of information that exists at the plants and at NRC that relates to the engineering performance of equipment which is not translated to reliability and risk implications because of the qualitative nature of the information. In fact, the majority of information which is collected by the plants and by the NRC is of this nature. FST can provide a tool for translating this information to its reliability and risk implications. A key advantage of FST is that component degradation conditions can be used to determine reliability and risk implications--failures don't have to occur first. Furthermore, performance can be evaluated for individual components as was done for the individual MOV that was tracked--data for different components doesn't have to be aggregated. Even though the results that are produced are not precise, they are practical and useable. Thus, by using condition information and engineering information, practical and powerful tools can be developed for maintenance and inspection applications.

ACKNOWLEDGMENT

Acknowledgment is given to Dr. G. H. Weidenhamer, the NRC Project Monitor, who has provided significant inputs to the work and whose comments greatly improved this paper.

REFERENCES

1. L. A. Zadeh, "Fuzzy Sets", Information and Control, 8, pp. 338-353, 1965. Reprinted in Fuzzy Models for Pattern Recognition, J. C. Bezdek and S. K. Pal, eds., IEEE Press, 1992.

2. D. Dubois and H. Prade, Fuzzy Sets and Systems, Theory and Applications, Academic Press, 1980.

3. A. Kondel, Fuzzy Techniques in Pattern Recognition, Wiley and Sons, 1982.

4. A. Kaufmann and M. M. Gupta, Fuzzy Mathematical Models in Engineering and Management Science, North-Holland, 1991.

5. T. Terano, K. Asai, and M. Sugeno, Fuzzy Systems Theory and Its Applications, Academic Press, 1992.

6. D. Dubois, H. Prade, and R. R. Yager, Fuzzy Sets for Intelligent Systems, Morgan Kaufmann Publishers, 1993.

7. R. R. Yager and L. Zadeh, Fuzzy Sets, Neural Networks, and Soft Computing, Van Nostrand Reinhold, 1994.

8. B. M. Meale and D. G. Satterwhite, "An Aging Failure Survey of Light Water Reactor Safety Systems and Components", NUREG/CR-4747, July 1988.

9. USNRC, "Nuclear Plant Aging Research (NPAR) Program Plan", NUREG-1144, Rev. 2, June 1991.

FATIGUE MONITORING IN NUCLEAR POWER PLANTS[a]

A. G. Ware and V. N. Shah
Idaho National Engineering Laboratory
Lockheed Idaho Technologies Company
Idaho Falls, Idaho

ABSTRACT

This paper summarizes fatigue monitoring methods and surveys their application in the nuclear power industry. The paper is based on a review of the technical literature. Two main reasons for fatigue monitoring are more frequent occurrence of some transients than that assumed in the fatigue design analysis and the discovery of stressors that were not included in the fatigue design analysis but may cause significant fatigue damage at some locations. One fatigue monitoring method involves use of plant operating data and procedures to update the fatigue usage. Another method involves monitoring of plant operating parameters using existing, or if needed, supplementary plant instrumentation for online computation of fatigue usage. Use of fatigue monitoring has better defined the operational transients. Most operational transients have been found less severe and fewer in numbers than anticipated in the design fatigue analysis. Use of fatigue monitoring has assisted in quantifying newly discovered stressors and has helped in detecting the presence of thermal stratification at unsuspected locations.

1 INTRODUCTION

This paper is a survey of fatigue monitoring methods developed by the nuclear industry. It presents a review of the technical literature relating to the transients that cause fatigue damage, locations susceptible to such damage, approaches developed for monitoring the transients, and monitoring systems developed for field applications. The paper describes the monitoring techniques developed and applied by the nuclear industry. It does not deal with the acceptance of these techniques by the Nuclear Regulatory Commission nor with the regulatory positions relating to fatigue.

Fatigue monitoring includes monitoring of the plant operating parameters such as temperature, pressure, and flow rate so that the operating transients can be estimated and the cumulative usage factor at a location can be computed. Proper use of the key operating parameters can provide a more accurate estimate of the transients than those assumed in the design fatigue analyses, and this, in turn, can result in more reliable prediction of cumulative usage factors. Fatigue monitoring may assist in identifying both conservative and nonconservative assumptions made in the design fatigue

---

a. Work supported by the U.S. Nuclear Regulatory Commission, Office of Nuclear Regulatory Research, under DOE Idaho Operations Office Contract No. DE-AC07-941013223; Dr. G. H. Weidenhamer, Technical Monitor.

analysis. Fatigue monitoring can also assist in directing inservice inspection efforts and identifying mitigative actions and assessing their effectiveness.

This paper first provides a background of fatigue design analysis of nuclear power plant components. Next it discusses why fatigue monitoring of the components is needed. Then it identifies the component locations that are potential candidates for fatigue monitoring. Then the paper describes two fatigue monitoring methods that have been developed by the industry for more accurate predictions of cumulative usage factors. This is followed by the applications of these methods at nuclear power plants. Finally, the paper summarizes the benefits that may be realized from the use of fatigue monitoring.

2 BACKGROUND

Nuclear power plant components in the early U.S. plants were designed with little or no fatigue analysis. Nuclear vessels and piping were designed using ASME Section VIII and United States of America Standard (USAS) B31.1, respectively. Fatigue design analysis requirements were developed in the 1960s and incorporated in the codes. In 1963, the requirements for vessels were published in ASME Section III. In 1969, the requirements for Class 1 piping were published in USAS B31.7. In 1971, these requirements for piping were incorporated in ASME Section III. All fatigue analyses of vessels and Class 1 piping use design basis transients.

The purpose of the fatigue design analysis was not to calculate the actual cumulative usage factor, but to demonstrate that a component would have a cumulative usage factor of less than 1.0 at the end of its 40-year design life. Therefore, several simplifying and conservative assumptions were made to reduce the effort required for the fatigue design analysis. The simplified assumptions were related to design basis transients, heat transfer and stress analyses required for the fatigue analyses, and calculation of cumulative usage factors. In addition, a given number of occurrences for each transient were assumed in order to calculate the cumulative usage factors. Transients are counted according to the plant technical specifications to ensure that the design numbers are not exceeded.

Design basis transients were represented by simplified operating transients. For example, a simplified cooldown transient for a PWR cold leg is shown in Figure 1. The cooldown rate for the design transient [~56°C/h (100°F/h] is about three times higher than the maximum rate for the actual transient [~19°C/h (34°F/h)]. Such a design transient will introduce a much steeper thermal gradient through the pipe wall and, therefore, significantly higher stresses. The actual transient produces a fraction of the design-basis usage factor; thus, it is equivalent to a partial design transient.

Examples of simplifying assumptions used in heat transfer analyses include use of one-dimensional heat transfer models and use of an upper-bound surface heat transfer coefficient (Deardorff and Smith 1994). The one-dimensional models allow heat transfer in the radial but not the axial direction. These models may give conservative results at a junction of two components with different thicknesses; for example, a thinner-wall component may experience higher stresses during a transient with increasing temperatures. The use of an upper-bound heat transfer coefficient will give a higher thermal gradient across the component wall thickness.

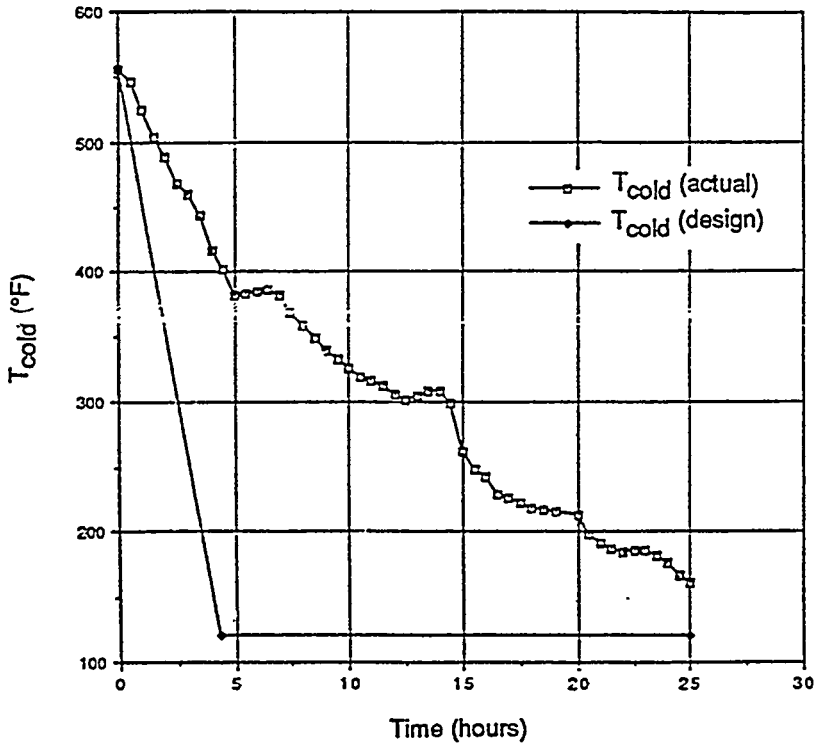

Figure 1. Example of actual versus design basis cooldown transient.

Examples of simplifying assumptions used in stress analyses include use of formulas for stresses caused by a thermal gradient across the piping wall thickness. These formulas do not take into account thermal expansion of the piping cross section and, therefore, give conservatively high estimates for the stresses. The simplified stress analyses also assume linear elastic behavior for piping material.

Examples of simplifying assumptions used in calculations of cumulative usage factors include groupings of design transients. Each grouping may combine several design transients with a worst-case transient, which then conservatively represents all the transients in the grouping. Such a combination results in an artificially high cumulative usage factor. Also, in the calculation of fatigue usage factors, generally no time phasing was considered between different components of thermal stresses in piping. This produces conservative estimates of thermal stresses and, therefore, higher cumulative usage factors.

3 REASONS FOR FATIGUE MONITORING

Most plant locations do not require fatigue monitoring because their cumulative usage factors were conservatively calculated to be less than 1.0. However, field experience has identified several

locations where the use of fatigue monitoring may be warranted. Two main reasons for fatigue monitoring are more frequent occurrence of some transients than that assumed in the fatigue design analysis and the discovery of stressors that were not included in the fatigue design analysis but may cause significant fatigue damage at some locations. Some of these stressors have caused fatigue cracking in the field. Fatigue monitoring is performed to quantify the magnitude, frequency, and duration of these stressors so that cumulative usage factors can be calculated more accurately.

The overall experience of light water reactor (LWR) vendors has been that most operational transients have been less severe and the number of cycles fewer than specified in the design basis (Gosselin et al. 1989, Stevens and Rangnath 1989). However, for some transients and for several plants, the numbers of cycles projected to the end of life may exceed the numbers in the design basis. For example, projected number of cycles associated with the testing of pressurized water reactor (PWR) charging and letdown system valve circuitry exceed the corresponding number in the design basis analysis (Barbier and Bond 1992). In many of these cases, the cumulative usage factor was proportionately increased to account for the actual number of cycles, and the resulting usage factor has been shown to be less than 1.0. In cases where such simple recalculation does not provide a usage factor of less than 1.0, fatigue monitoring can be used to determine the actual magnitude of the transient, which may produce a cumulative usage factor of less than 1.0, even with higher numbers of cycles. Thus, fatigue monitoring can be used to justify continued operation (Sakai et al. 1993).

The newly discovered stressors for Class 1 components include thermal stratification, thermal striping, thermal cycling, and turbulent mixing. Although the presence of thermal stratification in LWR feedwater piping was recognized as early as 1979, its presence in the PWR primary coolant piping was not recognized until 1988 (Su 1990, USNRC 1988). Similarly, thermal striping and turbulent mixing were discovered after the original plant design analyses but have been investigated for a number of years (Snaider 1980, Su 1990). Thermal cycling is a more recently discovered stressor (Kim et al. 1993).

Thermal Stratification. Thermal stratification is a condition in which two volumes of fluid in a horizontal segment of piping separate into layers without appreciable mixing because of different temperatures and low flow velocities. In this situation, the lighter, warmer fluid will stay above the heavier, cooler fluid without appreciable mixing of the two layers; generally one layer will be stagnant and the other layer will have a small flow velocity. Affected safety systems in the primary reactor coolant systems include safety injection, residual heat removal, and pressurizer surge and spray lines. Experience at domestic and foreign nuclear plants indicates that thermal stratification has caused pipe cracks, damaged supports, and loosened flanges in different high-energy safety systems.

Thermal Striping. Thermal stratification can induce local cyclic stresses in the portion of the pipe near the inside surface in contact with the interface between the hot and cold coolant layers, if the relative flow velocity is high. These stresses are caused by oscillation of the fluid temperature at the interface resulting from turbulent mixing of the hot and cold fluids. The stressor associated with such interfacial mixing is called thermal striping. The cyclic changes in the metal temperatures caused by thermal striping are highest on the pipe inside surface and attenuate rapidly through the thickness because of thermal conductance inertia; the pipe outside surface does not experience any temperature change. The magnitude of the stresses associated with thermal striping is greatest on

the inside surface and decreases rapidly through the thickness, so high-cycle damage is limited to the pipe inside surface adjacent to the interface.

Thermal striping has been investigated in laboratory tests. Wolf et al. (1987) have conducted thermal stratification tests in horizontal feedwater lines at the HDR (Heissdampfreaktor) test facility in Germany. Thermal striping was observed only at relatively high flow rates (Deardorff 1990). The onset of the interface mixing that leads to thermal striping occurs when inertial forces overcome stratifying density differences between the fluid layers. The gradient Richardson number, which is the ratio of the density gradient and the horizontal velocity gradient, has been used to quantify when thermal striping is apt to take place. Test results and theory indicate that thermal striping is present when the gradient Richardson number at the interface is less than 0.25 (Hafner and Spurk 1990).

Thermal Cycling. Cyclic axial movement of an interface between hot and cold fluids is called thermal cycling. Such cycling takes place when a column of hot turbulent fluid penetrates a branch line and interacts with a cooler stratified fluid, which could be produced by valve leakage. The turbulent flow in the main reactor coolant piping generates the turbulent penetration in a branch line as shown in Figure 2. The turbulence intensity decays exponentially from the header pipe into the branch line, but the temperature remains fairly constant over the length of several diameters and then decays. The length of turbulent penetration changes with time, and is greater for a higher flow velocity in the header and smaller for an increasing stratified flow in the branch line. The length of turbulent penetration also changes when the reactor coolant system undergoes an operational transient such as a change in power. Cyclic changes in the length and intensity of turbulent penetration produces corresponding changes in the length of the stratified fluid layer. As a result, the

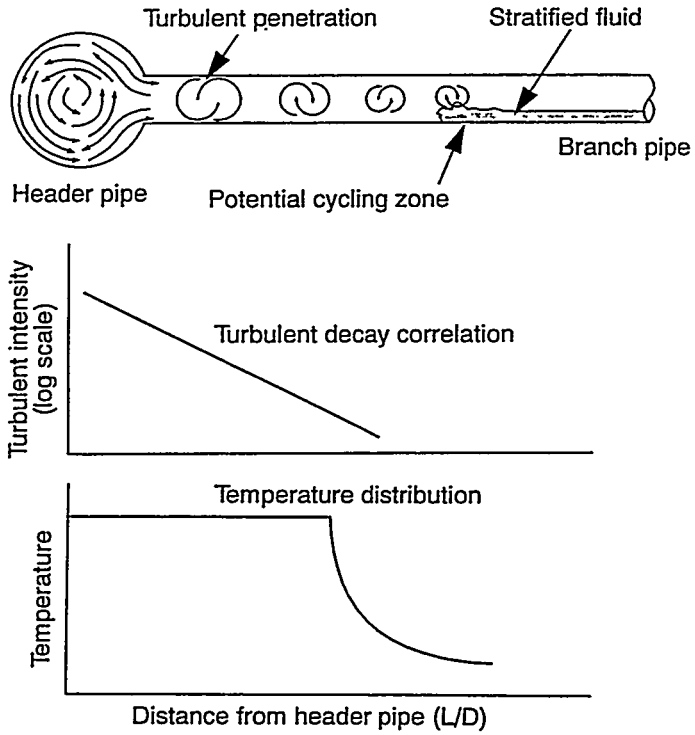

Figure 2. Thermal cycling caused by interaction between turbulent penetration and stratified fluid.

pipe adjacent to the interface experiences stress cycling, (and therefore fatigue damage) resulting from the presence and absence of stratified fluid (Kim et al. 1993).

It appears that turbulent penetration alone could produce thermal cycling (from the periodic presence and absence of stratified fluid) in a branch line under certain operating conditions and piping layout. The presence of thermally stratified fluid, in the absence of any valve leakage, has been detected in a branch line of a PWR plant, as illustrated in Figure 3 (Lubin et al. 1994). The branch line contains stagnant fluid. It extends vertically from the main coolant loop and then runs horizontally. Turbulent penetration has initially developed in the vertical section of the branch line, as shown in Figure 3(a). Then, an operational transient such as a power change causes the turbulence to penetrate the full length of the vertical section and produce stratification in the elbow at the end and in the adjacent horizontal section of the branch line, as shown in Figure 3(b). With further changes in power, the length of the turbulent penetration could recede and the stratified layer would no longer be present.

Turbulent Mixing. Turbulent mixing of hot and cold coolants has resulted in cyclic changes in the coolant temperatures and imposed high-frequency thermal cycles in the adjacent component wall. Turbulent mixing has been mainly reported in BWR plants where bypass leakage of cold feedwater has mixed with relatively hot coolant in the vessel downcomer and imposed cyclic changes in the feedwater nozzle wall temperatures. Turbulent mixing has been also reported at one PWR steam generator feedwater nozzle. The high-frequency thermal cycles contribute to crack initiation. The magnitude of the temperatures and stresses associated with turbulent mixing decrease rapidly through the thickness, so the presence of turbulent mixing cannot be detected by measuring the temperature of the outside surface of the feedwater nozzle and the high-cycle fatigue damage is limited to the inside surface.

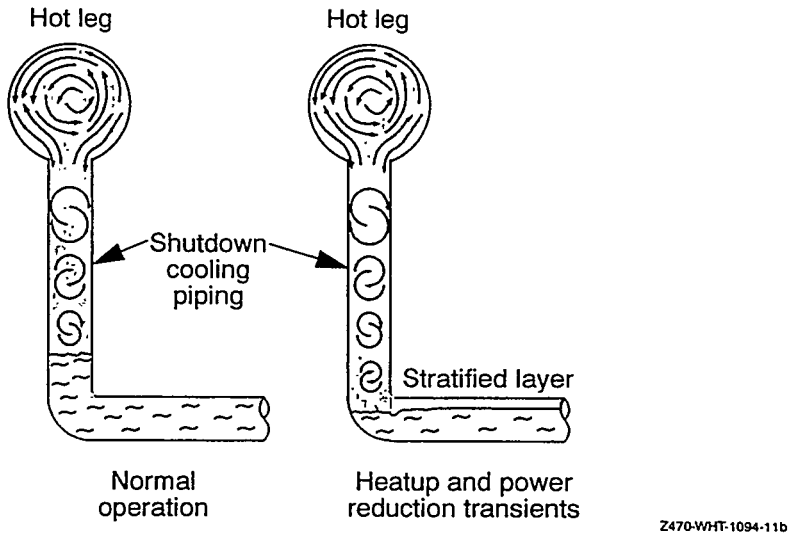

Figure 3. A change in the penetration depth of turbulence from power variations can cause thermal stratification and cycling in a branch line.

4 LOCATIONS FOR FATIGUE MONITORING

Locations having a high cumulative usage factor or ones that have experienced field fatigue cracking are the candidates for fatigue monitoring. Fatigue is generally a concern at locations with high thermal gradients and high cyclic stresses; at geometric discontinuities or stress concentrations; and at welds, including dissimilar metal welds. Locations that are subjected to stressors of uncertain magnitudes, frequency, and duration are also prime candidates for fatigue monitoring. One example of such stressors is thermal stratification. Locations such as reactor internals and instrumentation line connections susceptible to high-cycle mechanical fatigue are unsuitable as potential fatigue monitoring locations. Vibration monitoring may be used to detect the severity of the associated stressor, that is, flow-induced vibration, at these locations.

Locations for fatigue monitoring are identified in Figures 4 and 5 for pressurized water reactor (PWR) and boiling water reactor (BWR) plants, respectively (Ware 1990, Ware and Shah 1992, Ware 1994). Cumulative usage factors listed in parentheses are from a review of the fatigue design analyses reports for a few BWR and PWR plants, and are, therefore, not intended to cover all LWRs. These locations are currently being monitored in one or more countries, including the United States, Germany, France, and Japan. Fatigue monitoring systems have been installed at two new Japanese BWRs prior to their operation.

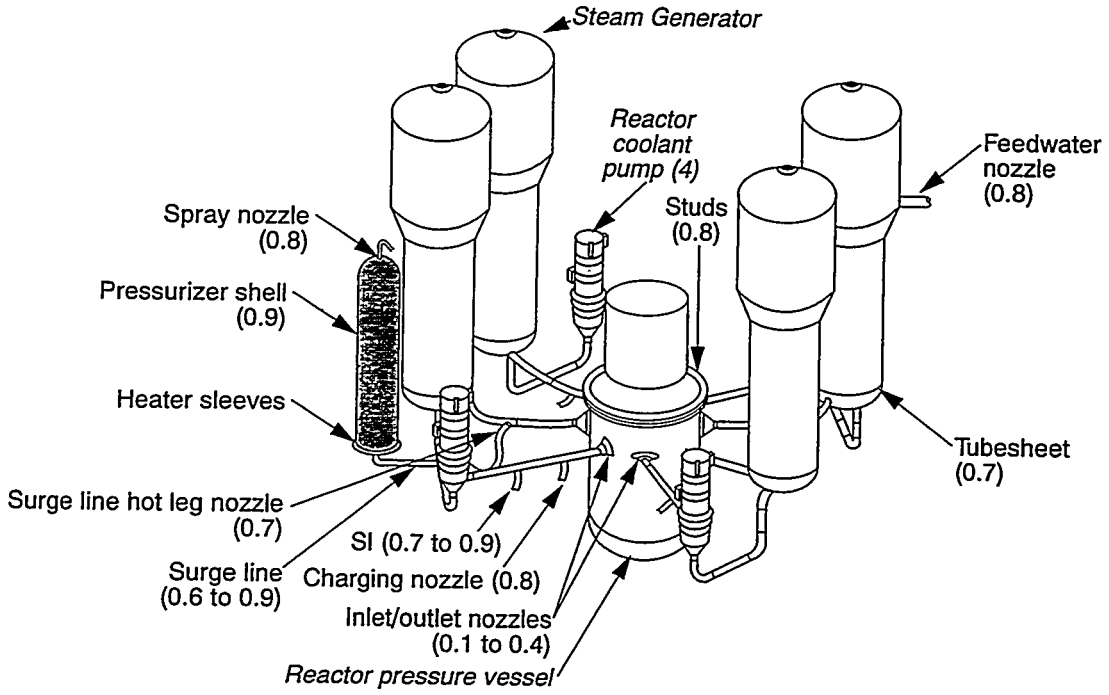

Figure 4. Potential locations for fatigue monitoring in PWR plants. Cumulative usage factors are listed in parentheses.

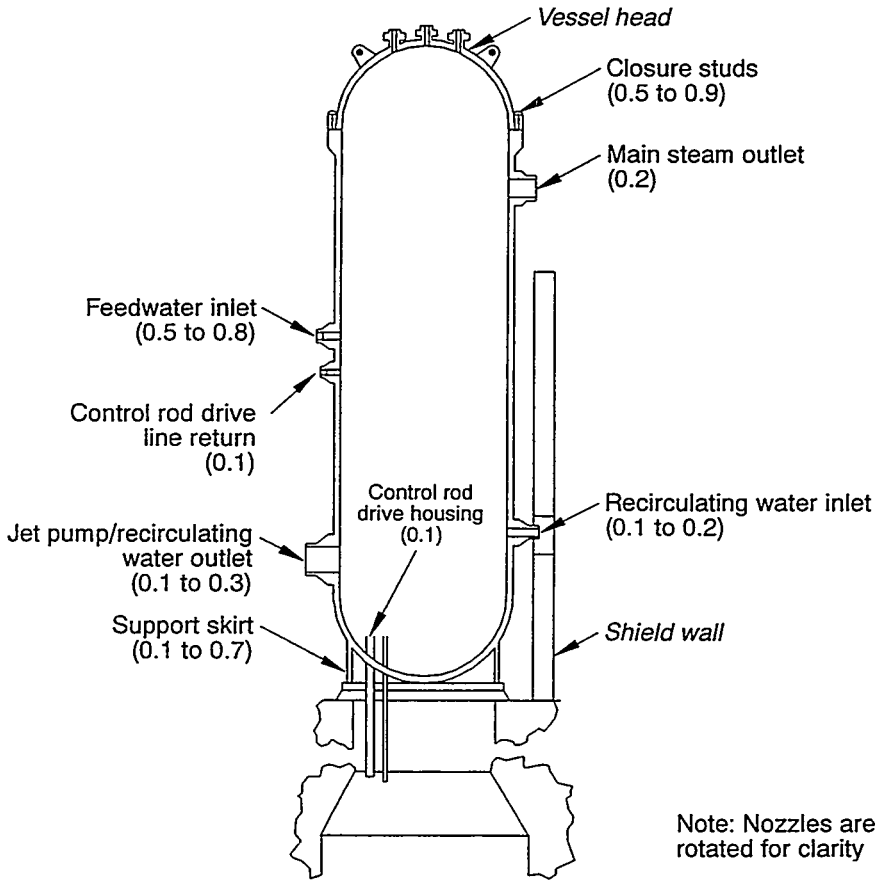

Figure 5. Potential locations for fatigue monitoring in BWR pressure vessels. Cumulative usage factors are listed in parentheses.

5 FATIGUE MONITORING METHODS

Fatigue monitoring methods developed for more accurate prediction of cumulative usage factors take two different forms: (a) design basis monitoring, which includes review of the plant historical data for operating transients, and (b) online monitoring of plant parameters using existing, or if needed, supplementary plant instrumentation.

Use of fatigue monitoring methods generally require an estimate of the past fatigue usage, that is, the fatigue usage prior to implementation of the monitoring methods, and then update of the usage as additional cycles occur in the future. Either or both of these methods can be used to estimate the actual fatigue usage to date. Because past operating logs are available and plant operation may have changed over the years, the first consideration is generally to consult and systematically catalog the categories, numbers, and severity of the transients from the records of past plant operation. Past usage can be estimated by reviewing plant logs, refining analysis assumptions as necessary to conform to actual parameters, performing stress analyses again if necessary, and computing the cumulative usage factor based on the actual number and severity of the cycles. Redefinition of transients can be extrapolated to predict future usage.

In the second method, the stresses induced by transients can be computed online as they occur by taking into account the plant process parameters measured during the various transients. This method can be useful in determining the ongoing fatigue usage at key locations. It can also be used to assess the past usage, assuming that the past transients have induced the same stresses as the present transients. However, this second method may not be as acceptable as the first for estimating past usage because plant operating procedures may have changed, and extrapolating backward in time is not likely to produce as accurate a result without review of the plant records. Unfortunately, in some cases the required information on past operation may not be available, and the past usage can only be estimated from current operation. A combination of the two methods appears to offer the best prospect for accurate estimation of the overall fatigue usage.

5.1 Design Basis Fatigue Monitoring

The design basis monitoring method involves use of historical plant operating data and procedures to update the fatigue usage. The sources for historical operating data include plant operating logs and procedures, strip charts, hot functional and startup test summaries, licensee event reports, monthly reports to the NRC, and operator interviews. The advantages of this method are as follows:

- The transients can be classified according to actual number and severity. The method can account for partial cycles, which results in a reduced cumulative usage factor.
- The assumptions used in the stress analyses can be refined.
- The fatigue analysis can be revised to account for changes in operating procedures and design.
- Fatigue damage caused by newly discovered transients can be estimated.
- In many cases, the existing stress models can be used.

Programs relying solely on operating data are still not entirely rigorous because the plant parameters needed to determine the presence and severity of previously unidentified stressors such as thermal stratification, thermal striping, turbulent mixing, and thermal cycling may not be recorded. However, present knowledge of conditions (temperatures and flow rates) and plant operations that cause or accompany abnormal transients can assist in identifying instances during which these transients might have occurred, and in estimating their severity.

The successful use of this method depends on the accessibility and accuracy of a plant's logs. The logs may not contain sufficient detail, or the entries may not be clear enough to provide the desired accuracy for determining the temperature changes during the transient. Significant personnel time may be involved in reviewing data and updating the cumulative usage factor.

5.2 Online Fatigue Monitoring

Several vendors have developed online fatigue monitoring systems that directly query the plant process information system and more precisely define the thermal stresses causing fatigue usage. These systems also provide an automated method to track the fatigue usage being accumulated at key locations. This method generally involves global monitoring of plant parameters using existing instrumentation, which is usually sufficient for most of the stressors associated with low-cycle fatigue. However, for certain stressors, such as thermal stratification, this method also employs local monitoring of relevant plant parameters. Some vendors have combined the use of laboratory-developed frequency spectra with global monitoring for high-cycle thermal fatigue.

Once the online fatigue monitoring system is in operation, calculation of fatigue usage is much less labor-intensive than manual cataloging of the plant process data required by the design basis monitoring method. For each location chosen to be monitored, an analytical model is developed to compute the stress and fatigue usage. The model relies on the results of a few representative thermal and stress analyses, and on predicting the fatigue usage for a given transient by using the results from the analysis that most closely matches the transient. Cycle counting methods such as the rainflow method or the ordered overall range method are used to determine stress ranges. The fatigue usage algorithm (based on the ASME Code Section III method) is general, but the stress model must be component-specific. Fatigue usage calculations are performed offline or with multitasking computers so that significant transients are not missed while calculations are being carried out.

Online fatigue monitoring methods use linear-elastic analyses for calculating stresses from the measured plant parameters. These methods generally take full advantage of the linearity of the problem in reducing the computational cost for calculating stresses. For some effects, such as pressure or thermal expansion, the stresses can be computed directly using closed-form solutions. However, for stresses caused by thermal gradients such as through nozzle walls, the Green's (influence) function technique is used.

Generally, the *global monitoring* approach using the Green's function technique is applied to piping having a fluid with a uniform temperature. However, at a branch nozzle connection, for example, there could be a fluid of one temperature in the main pipe and incoming fluid of another temperature in the branch pipe. Chen and Kuo (1991) have developed a Green's function technique to solve this problem by linearly superimposing the results of the two flows, and they found good agreement with finite element analysis. This superposition technique can be extended to cover thermal loadings from multiple locations, such as in areas of several branch connections.

Some vendors have carried out extensive *local monitoring* of thermal stratification in nuclear power plant piping. Figure 6 shows an example of local monitoring on pressurizer surge line piping in a Babcock & Wilcox plant. The only instrument originally installed on the surge line was a single thermocouple, which is generally mounted on the side of the pipe. For this local monitoring program, 54 surface-mounted thermocouples and 12 linear variable displacement transducers were installed to monitor temperatures and displacements for thermal stratification. The results of the local program, reviews of the plant operating procedures, and a review of the plant logs were used to relate the measured thermal stratification conditions to the design transients.

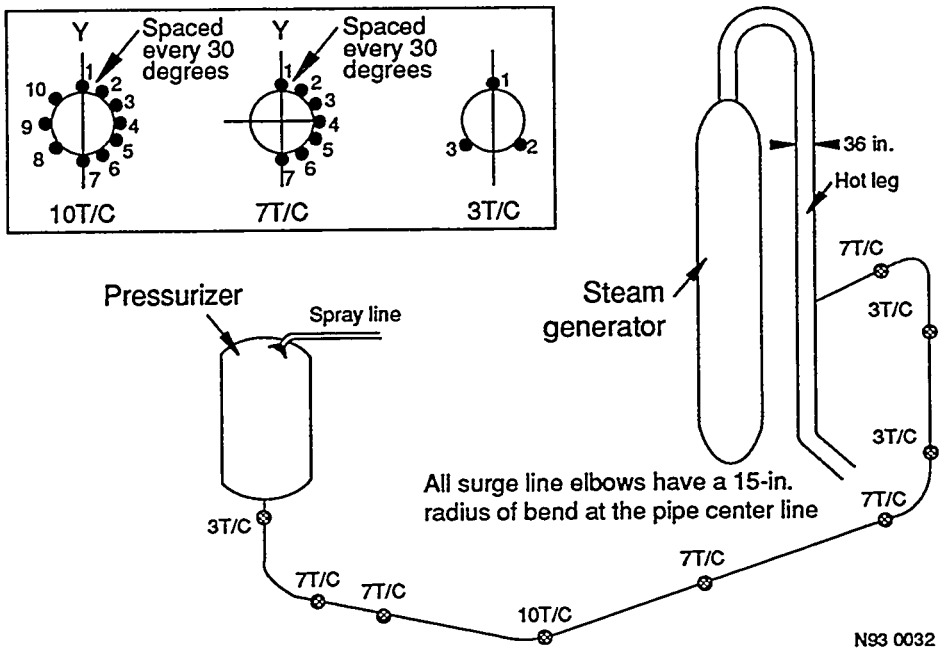

Figure 6. Example of instrumentation for local monitoring of thermal stratification in a PWR surge line.

For high-frequency stressors such as thermal striping or turbulent mixing, the *frequency spectrum* approach may be used. While thermal stratification can be measured by thermocouples or resistance temperature detectors mounted on the outside surface of the piping, thermal striping or turbulent mixing cannot be monitored in this manner because the high-frequency temperature fluctuations on the interior of the pipe wall will not be detected. Thus, thermal striping and turbulent mixing must be accounted for indirectly. One method is to use spectra generated from laboratory tests to approximate the stresses produced by these high-frequency stressors. The amplitude of the temperature variation can be used to determine the magnitude of the corresponding stress cycling on the inside surface of the component wall. Such data can then be used to generate spectra of stress amplitude versus frequency. The length of time during which the stressor is present may be determined by monitoring the relevant plant parameters. Then one can estimate the total number of cycles and the associated fatigue usage by combining the frequency spectrum data and the estimated length of time during which the stressor is present.

Deardorff et al. (1990) demonstrate how such a frequency-spectrum approach could be applied to determine fatigue usage for a surge line because of thermal striping. Data from several tests conducted at the HDR facility in Germany were used for the development. One interesting conclusion from this work is that, apparently, thermal striping does not occur below certain flow rates, depending on the temperature difference between the pressurizer and the hot leg.

In practice, the method would be applied as follows. First determine the flow velocity from the pressurizer spray flow rate and the rate of change of pressurizer level. Then, determine the temperature difference between the pressurizer and the hot leg. This information assists in selecting an appropriate spectra for the fatigue usage calculation. Finally, calculate the fatigue usage using the

spectrum for the number of hours over which the thermal striping is judged to have occurred. The number of hours may be determined from the flow velocity estimates.

Another kind of high-frequency stress cycling that cannot be measured with existing plant instrumentation and for which local monitoring is impractical is turbulent mixing. An example is turbulent mixing of relatively cold BWR feedwater with the hotter reactor coolant when a small portion of the incoming feedwater leaks past the thermal sleeve in the feedwater nozzle. The magnitude of the temperature range of the cycling is assumed to be proportional to the difference in feedwater and reactor water temperatures, and proportional to a leakage-efficiency factor based on the design of the thermal sleeve (older designs allowed more leakage than newer ones). Extensive experimentation by the General Electric Company with BWR feedwater nozzles in the late 1970s indicates that the cycling caused by turbulent mixing can be represented by a frequency spectrum (Riccardella et al. 1989). Frequency spectra could be developed for each geometry and transient condition (flow rate, etc.) for which turbulent mixing fatigue calculations are needed. The number of hours during which turbulent mixing is present may be estimated by monitoring the feedwater leakage, the presence of which can be determined by monitoring the outside surface temperature of the feedwater nozzle.

5.3 Cycle Counting

Cycle counting methods that have been adapted for online fatigue monitoring are based on methods developed in the transportation industry (aerospace and automotive) for random loadings. This cycle counting approach is different than the one used in the original fatigue design analysis performed according to the ASME Code, Section III, where numbers of transients were combined for the entire lifetime of the plant and worst-case combinations were considered in the analysis.

A number of different methods have been developed for cycle counting; examples are the range-pair counting method, the Hayes method, the original rainflow method, the racetrack counting method, and the hysteresis loop counting method. If the load history begins and ends with its maximum peak, or with its minimum valley, all of these counting methods give identical results. In other cases, the counts are similar, but results are not identical (Society of Automotive Engineers, 1988).

Two counting methods have been adapted for use in nuclear plant online fatigue monitoring systems: the rainflow counting method and the ordered overall range method, which is a simplified rainflow method (Fuchs and Stephens, 1980). The ordered overall range method is used to condense the cycles to only those that produce the major damage. In practice, these methods do not generally allow the maximum stress ranges for the life of the plant to be determined directly but rather focus on the fatigue usage for the limited length of time in which the online system has been in operation. However, this type of fatigue monitoring allows fatigue computation for lower stress range cycles within the main transient that might be overlooked in the traditional manual fatigue analysis.

6 FATIGUE MONITORING PROGRAMS

There are at least five active developers of fatigue monitoring programs in the United States: four nuclear steam supply system (NSSS) vendors and a consulting company that developed a program sponsored by the Electric Power Research Institute (EPRI). There are also several overseas

developers. Some of these programs use a design basis fatigue monitoring method, whereas others use online fatigue monitoring methods.

6.1 Design Basis Approach to Fatigue Monitoring

These programs combine the transient data from plant operating logs with the results of the original stress analyses to estimate fatigue usage. This estimate of the cumulative usage factor is more accurate than that can be obtained from counting the design basis transients alone. To accomplish this, the severity and number of events recorded in the operating logs are compared with the design basis events to estimate the numbers of full and partial cycles. The stresses have already been calculated in the component stress analysis for the design basis events; therefore, this approach is termed a *design basis* approach. Two examples of design-basis approaches are described, along with examples of how local fatigue monitoring has be used to provide additional information for surge lines.

6.1.1 Application to Babcock & Wilcox Plants

The first example of a design-basis fatigue monitoring program, called the Allowable Operating Transient Cycles Program, is described by Tally (1985). The program was applied to a 3-unit Babcock & Wilcox 177-fuel assembly plant. Its objective was to demonstrate the adequacy of critical reactor coolant system components for the 40-year design life, given the operating conditions and procedures experienced to date. A major element of the program was to establish a transient logging program, which included reviewing records from several years of operation, classifying and numbering the significant transients that had occurred, and updating the stress analyses as necessary.

A PC-based system called the Transient Cycles Logging System (TCLS) has been written for monitoring transients (Babcock & Wilcox, 1987). The system keeps track of the number of transient cycles for key components and compares that number to the number of design cycles. The Transient Cycles Logging System can deal with complex events composed of more than one design transient. The operator inputs the appropriate data for the transient event, and the system classifies the event and conditions, stores key plant data event by event, and tracks the number of thermal cycles for each key component.

In response to USNRC Bulletin 88-11 (Pressurizer Surge Line Thermal Stratification), design basis fatigue monitoring and an extensive local online fatigue monitoring of the surge line was carried out. The instrumentation for the local monitoring is shown in Figure 6. Indepth fatigue analyses were performed including elastic-plastic stress analyses of a surge line elbow (Matthews et al. 1990). Thermal striping was treated using the HDR test results that were considered to be relevant to the surge lines. The ordered overall range method of cycle counting was used.

6.1.2 Application to Combustion Engineering Plants

A second example of design-basis fatigue monitoring program is described by Gosselin et al. (1989). The program was developed to more accurately estimate the stressors associated with actual

plant operations and to use them in the cumulative usage factor calculations. The program sequence is as follows:

- Identify the systems necessary for maintaining safe operation and shutdown of the plant.
- Review all components within these systems and identify the key locations susceptible to significant fatigue damage.
- Review the design basis stress reports to identify the controlling design basis transients.
- Lump the noncontrolling transients together, and assume all these events have occurred according to the design basis. These events are not considered part of the fatigue monitoring.
- Develop analytical models for the key locations and recompute the fatigue usage for the controlling transients at these locations based on plant operation.

The first application of the program was the fatigue analysis of the safety injection nozzle (located on the cold leg of the reactor coolant system) in a newer vintage Combustion Engineering plant. The key location was determined to be the inside surface of the nozzle safe end. The shutdown cooling transient accounted for about 98% of the cumulative usage factor in the fatigue design analysis. The Combustion Engineering approach was to retain the design basis transients for all but the shutdown cooling transient, and to recompute the fatigue usage associated with that transient using an effective (or partial) cycle counting method based on the severity of the transient. The design basis transient assumed a worst–case shutdown cooling thermal shock of 154°C (310°F), whereas the typical temperature difference is approximately one–half the maximum, which results in an effective cycle that contributes only about 10 to 15% of the usage of the full cycle.

In response to USNRC Bulletin 88–11, local monitoring of pressurizer surge lines was conducted for three Combustion Engineering plants (Combustion Engineering 1989). Two plants were instrumented with surface–mounted thermocouples, and the third with resistance temperature detectors to measure the temperatures. Linear potentiometers were also used to measure deflections. Thermal–hydraulic models based on the measured outside wall temperatures were employed to estimate the temperature distribution in the fluid and the pipe wall. This temperature distribution was used in the stress analysis and fatigue usage calculations. In addition, the design basis transients were modified to include thermal stratification conditions. The revised conditions were derived from a review of the local monitoring results, plant records, and plant procedures. A literature survey was used to develop a conservative thermal striping model based on the maximum potential temperature differences. The stress range for thermal striping was calculated to be well below the stainless steel fatigue curve at 10^{11} cycles, and a crack growth analysis showed that thermal striping would not appreciably propagate an existing crack into the wall.

6.2 Online Fatigue Monitoring Systems in Use at U.S. Plants

These programs use various amounts of online operational data from the plant instrumentation and computer algorithms to determine the fatigue usage accumulated during the transients. The fatigue usage calculated by the online monitoring system is combined with the fatigue usage

accumulated before the use of the online system was initiated, which is generally estimated using the design basis approach. Three examples of online fatigue monitoring programs that have been used in the United States are described below; examples of online fatigue monitoring programs in France, Germany, and Japan are described in Section 6.3.

6.2.1 The General Electric Fatigue Monitoring System

A personal-computer-based online fatigue monitoring system (GEFMS) developed by General Electric for BWR plants was first used to calculate fatigue usage of the feedwater nozzle of a BWR/3 plant (Stevens and Ranganath 1989). The location chosen for this demonstration was the safe end of the feedwater nozzle because it has the highest cumulative usage factor (0.9) among all the components analyzed in the original design analysis report (Stancavage 1989a). A rainflow cycle counting method was used. Following the demonstration, the GEFMS system has been or is in the process of being installed on several other U.S. and overseas BWRs. One feature of the system is to monitor for leakage past the redesigned thermal sleeve in BWR feedwater nozzles to ensure that the turbulent mixing stressor is not present. Stancavage (1989b) considers that in addition to the feedwater nozzle safe end, the following locations are candidates for fatigue monitoring: the CRD return nozzles (if they have not been capped), the recirculation line inlet and outlet nozzles, the CRD penetration, the reactor vessel support skirt, and the reactor vessel closure studs.

The system has also been applied to Tsuruga 1, the oldest BWR in Japan, having been in operation over 20 years. The unit has strip charts and operation records but no database of the actual fatigue usage for critical components such as the feedwater nozzle. The yearly occurrences of some cycles were found to be greater than assumed in the design basis, so a General Electric system called the Thermal Cycle Monitor was installed (Sakai et al. 1993). Existing plant instrumentation was augmented by installation of a signal cable that monitored the high-pressure core injection system valve position. Based on the data from online monitoring for two fuel cycles, the cumulative usage factor for the feedwater nozzle is estimated to be 0.0074, whereas the design basis cumulative usage factor for the nozzle was 0.387.

6.2.2 The FatiguePro System

In 1984, the Electric Power Research Institute began to sponsor development of a fatigue monitoring program for critical nuclear power plant locations that could be used in both BWR and PWR plants. The program includes a personal-computer-based online monitoring system that uses existing plant instrumentation for data input. The computer software, called FatiguePro, uses a Green's function and an ordered overall range counting method to process the data (Gustin et al. 1988, Deardorff et al. 1988, Riccardella et al. 1989). Plant instrumentation data such as pressure, temperature, valve position, and flow rates are used along with the influence functions to determine stress versus time at the key locations. The cycle-counting method is used to develop a stress/frequency spectrum based on the stress history. The spectrum is then combined with the ASME Code S-N curve to determine the fatigue usage.

The first demonstration project was at a newer vintage Combustion Engineering PWR (Deardorff et al. 1988). The charging system, which returns water from the chemical and volume control system to the reactor coolant system, was selected. Nine plant process instrument sensors were used for online monitoring during a six to seven month demonstration. The monitoring results were used to

calculate the fatigue usage at the charging system nozzles. It was concluded that the charging system nozzle fatigue usage was negligible during this time. A similar demonstration was carried out on a BWR/3 feedwater nozzle (Riccardella et al. 1989).

Other fatigue monitoring projects using FatiguePro include the charging nozzles at a Westinghouse PWR, the feedwater and control rod drive return line at a BWR/2 plant, and the feedwater nozzles and control rod drive bottom head penetrations at a BWR/4 plant (Deardorff et al. 1988). This monitoring system has been or is in the process of being installed at selected locations in twelve more BWR and PWR plants. The locations selected in the PWR plants include the charging nozzle, pressurizer shell, surge and spray nozzles, instrument nozzle, feedwater nozzle, and safety injection nozzle. The locations selected in the BWR plants include the feedwater nozzle, control rod drive return line nozzle, and control rod drive bottom head penetration.

6.2.3 The Cycle Monitoring System

Pepka and Bond (1987) describe a third automated fatigue monitoring system designed for PWR plants, called the Cycle Monitoring System . The data acquisition module is designed to continuously monitor existing plant instruments, to identify the onset and end of individual transients, to sample data at a rate consistent with the resolution required for the particular transient, and to return to a more sparse sampling rate once the transient is over. Bond et al. (1987) consider that the existing sensors and instrumentation in a nuclear power plant are, in most cases, adequate to supply the information needed to determine the fatigue usage. The system uses a modified rainflow cycle counting approach, has the capability of performing online fatigue usage calculations, and includes transient recognition and classification capabilities (Pepka and Bond 1987).

The system has been implemented at a 4–loop Westinghouse plant (Barbier and Bond 1992). Initially, the system will monitor the pressurizer surge line, including its hot leg nozzle, and the normal and alternate charging lines and their nozzles. Thirteen other locations have been identified as potential locations for fatigue monitoring. Additional capability to the system may be added over time if needed and plant resources permit. The system uses a global–to–local parameter data transformation, which has been benchmarked with experimental data. The global parameters measured by the plant instruments are used to estimate the local temperature distributions needed for stress calculations.

Local monitoring has been performed at key locations to supplement the data collected by the system. Applications of local monitoring include monitoring for thermal stratification in surge lines (Hirschberg and Antaki 1989); thermal stratification and thermal striping in a feedwater nozzle (Capra 1988); and the safety injection and residual heat removal piping at the first check valve upstream of the cold leg nozzle (Strauch et al. 1990). In the last application, ten resistance temperature detectors and five accelerometers were mounted on the outside pipe wall at locations on both sides of the check valve. The accelerometers measured only small vibrations, but the temperature monitoring results indicated the presence of thermally stratified fluid with a top–to–bottom temperature difference of about 100°C (215°F) measured at the pipe outside surface.

6.3 Online Fatigue Monitoring Systems in Use at Overseas Plants

Online fatigue monitoring systems have been implemented at operating power plants worldwide. In some newer plants, they have been installed prior to operation. Some examples of fatigue monitoring systems being used in France, Germany, and Japan are described below.

6.3.1 French Plants

Électricité de France (EDF) was perhaps the first to implement fatigue monitoring in nuclear plants and has one of the most mature programs in the world. The first EDF program, the Transient Monitoring and Logging Procedure (TMLP), was initiated with the commissioning of its earliest plants (in 1977) and consisted of a bookkeeping method. The actual transients were logged and checked, case by case, to ensure they were not more severe than the design basis.

Even though the monitoring and logging procedure worked for many of the plant components, EDF realized that advanced fatigue monitoring systems were required for more critical locations. Consequently, EDF developed a system called the *Fatiguemeter* and, in 1985, installed it on a 900-MW PWR charging line nozzle for a real-time evaluation of the fatigue usage. Plant instrumentation for measuring temperature, pressure, flow rate, and valve position (open or closed) were used; no additional instrumentation was required. An influence function approach for estimating thermal stresses, rainflow counting, and Miner's linear damage rule were used. Although the manual-bookkeeping used as a part of the Transient Monitoring and Logging Procedure reduced the cumulative usage factor substantially, the use of the Fatiguemeter system resulted in an even further reduction in the cumulative usage factor (Bimont and Aufort 1987, Bimont and Cordier 1989).

The second application of the Fatiguemeter was at several key locations in another 900-MW PWR plant. The key locations include the pressurizer and hot leg surge line nozzles, the charging nozzle, and the steam generator feedwater nozzle. Previous measurements at another nuclear plant were used to establish correlations between the measured plant parameters and the surge line piping temperatures resulting from thermal stratification.

After more than ten years of experience with the Transient Monitoring and Logging Procedure and six years with the Fatiguemeter, EDF, in collaboration with Framatome, has developed an integrated system called SYSFAC (Systéme de Surveillance en Fatigue de la Chaudiére). This system incorporates the lessons learned from the previous two approaches, the logging system to review overall plant fatigue usage and the more detailed approach using the Fatiguemeter at key locations (Bimont and Cordier 1989). The EDF standardized plant design is helpful in developing this system because there are few plant-to-plant variations that have to be considered, and the lessons learned from one plant can be directly applied to others. The first SYSFAC installation began in 1992 for a 900-MW PWR plant (L'Huby et al. 1991). Five specific locations are monitored: (1) hot leg surge line nozzle, (2) pressurizer surge line nozzle, (3) charging line nozzle, (4) pressurizer heater sleeves, and (5) residual heat removal line nozzle. SYSFAC has been installed at all French PWRs and is undergoing the final phase of testing (Kergoat et al. 1994).

6.3.2 German Plants

Fatigue monitoring systems developed in Germany rely more heavily on local monitoring systems, which are specifically installed for the purpose of fatigue monitoring, than do systems developed in other countries. For example, in a monitoring program for a PWR plant that began in 1980, 29 locations on the regenerative heat exchanger alone are monitored (Bartonicek et al. 1993). Several primary pressure boundary locations are being monitored. These include the reactor pressure vessel flange and bolts, reactor coolant pump suction nozzles, steam generator tubesheet, charging system nozzle, main and auxiliary spray lines, safety injection and residual heat removal system nozzles, and the surge line and its nozzles. Other locations include regenerative heat exchangers, and the feedwater and steam systems, including locations both inside the containment and in the auxiliary buildings.

The FAMOS (Fatigue Monitoring System) system was first installed on a 1300–MW PWR plant (Miksch et al. 1988). In addition to the existing instrumentation, a total of 109 strain gages and 224 thermocouples were installed. The system uses both a global and a local monitoring approach. In the global monitoring approach, normal plant process parameters have proven sufficient to give accurate stress predictions for components such as the reactor pressure vessel and steam generator shells. However, Miksch et al. (1988) determined that the global monitoring approach did not supply sufficient details of the parameters to accurately compute the stresses at other locations, so additional instrumentation was used in a local monitoring approach.

The temperature profiles for the pipe wall, which were estimated by measuring the outside surface temperatures using local instrumentation, were compared to profiles calculated in advance. This comparison showed that the thermocouple readings from the outside surface can be applied to obtain accurate temperatures for wall thicknesses up to about 50 mm (2 in.) (Miksch et al. 1988). The temperature profiles for the pipe wall may be estimated by a method developed by Miksch and Schücktanz (1990). This method matches the measured outside wall surface temperatures with the calculated temperature profiles using a regression analysis. These profiles were calculated by superposing assumed triangular temperature distributions at the inside surface. This method for estimating the temperature profiles has the advantage that it requires solution of purely a heat conduction problem, and knowledge of the fluid temperatures and of the convective heat transfer coefficient on the inside wall is not needed.

The FAMOS system has been applied at two other German PWR plants where 80 thermocouples are installed for local monitoring of sixteen structural components (Miksch et al. 1988). In addition, 11 other structural components, which include, for example, the reactor vessel bolts, the steam generator tubesheet, and the reactor coolant pump suction nozzle, are monitored with the global monitoring approach. Use of the FAMOS system in Germany is increasing; in total, it is now installed at 11 PWR and one BWR plants (Golembiewski and Miksch 1993).

6.3.3 Japanese Plants

Mitsubishi Heavy Industries, Ltd., has developed a system called FAMS (Fatigue Monitoring System) to monitor fatigue in PWRs using existing instrumentation (Kato et al., 1993). The system includes use of Green's functions for calculating stresses from measured temperatures and use of the rainflow cycle counting method to estimate the stress ranges. The system is designed to monitor the

locations subject to significant stressors such as thermal stratification, high thermal gradients, or thermal shock and have relatively high calculated cumulative usage factors. These locations include the steam generator feedwater nozzle, pressurizer surge and spray lines and their nozzles, charging line nozzle, and reactor coolant pumps.

The Japan Power Engineering and Inspection Corporation (JAPEIC) has been active in developing fatigue monitoring programs for Japanese BWRs (Takahashi et al. 1991). An online plant process data acquisition system (OPDAS) has been developed and applied to two units of a newly constructed BWR. Three different reactor pressure vessel locations with high cumulative usage factors were chosen to being monitored: the feedwater nozzle, skirt support (bottom head), and closure studs. Several different parameters were monitored for each location. For example, fatigue monitoring for the closure studs include online monitoring of the temperatures for the pressure vessel head, flange, main studs, and shell, and of the temperature and flow rate for main steam.

7 BENEFITS OF FATIGUE MONITORING

Use of fatigue monitoring methods have resulted in several benefits for nuclear power plants. Most operational transients have been found less severe and fewer in numbers than anticipated in the design fatigue analysis. However, for a few PWR transients such as full power trips and charging system operation, the number of cycles to end-of-life may exceed the design basis numbers. Similarly, for a few BWR transients such as feedwater operation, the number of cycles to end-of-life may also exceed the design basis numbers. The severity of these transients needs to be assessed so that their impact on the cumulative usage factor can be estimated.

Use of fatigue monitoring has better defined the operational transients such as heatups and cooldowns. Use of global and local monitoring has assisted in quantifying newly discovered stressors such as thermal stratification. Use of fatigue monitoring has also helped in detecting the presence of thermal stratification at unsuspected locations. Monitoring of temperatures and relative flow rates along with laboratory-generated spectra can assist in estimating fatigue usage caused by thermal striping and turbulent mixing.

Fatigue monitoring of operational data could support changes to some inspection requirements. For example, monitoring of BWR feedwater nozzle outside surface temperature is being considered to change the requirement for surface inspection of the nozzle inside corner.

REFERENCES

Babcock & Wilcox, 1987, "Transient Cycles Logging System," PB 281 1M, Lynchburg, VA.

Barbier, C. C., and C. B. Bond, 1992, "Implementation of a Transient and Fatigue Cycle Monitoring Program at Virgil C. Summer Plant," *Service Experience and Life Management in Operating Plants*, PVP-Volume 240, American Society of Mechanical Engineers, New York, NY, pp. 95–102.

Bimont, G., and P. Aufort, 1987, "Fatigue Monitoring in Nuclear Power Plant," *Transactions of the 9th International Conference on Smirt, Lausanne, Switzerland*, Volume D, pp. 133–140.

Bimont, G., and G. Cordier, G., 1989, "A New Approach for NSSS Fatigue Life Assessment," *Transactions of the 10th International Conference on Smirt, Anaheim, CA*, Volume D, pp. 37–47.

Bond, C. B., W. T. Bogard, and S. S. Palusamy, 1987, "The Role of Monitoring in Plant Life Extension and Maintenance," *The International Meeting on Nuclear Power Plant Operation, Chicago, IL, August 30-September 3, 1987, Transactions of the American Nuclear Society*, Supplement to Volume 54, Number 1.

Capra, R. A., (USNRC) 1988 letter to S. B. Bram (Consolidated Edison), 1988, "Steam Generator Girth Weld Repair Safety Evaluation for Indian Point Nuclear Generating Unit No. 2," October 28, 1988.

Chen, K. L., and A. Y. Kuo, "Green's Function Technique for Structures Subjected to Multiple Site Thermal Loading," *Transactions of the 11th International Conference on Smirt, Tokyo, Japan*, Volume D, pp. 353–358.

Combustion Engineering, 1989, *Pressurizer Surge Line Flow Stratification Evaluation*, CEN 387–NP, Windsor, CT.

Deardorff, A. F. and J. K. Smith, 1994, *Evaluation of Conservatisms and Environmental Effects in ASME Code, Section III, Class 1 Fatigue Analysis,* SAND94–0187, Sandial National Laboratory, pp. 3–1 to 3–10.

Deardorff, A. F., et al., 1990, "Development of a Thermal Striping Spectrum for use in Evaluating Pressurizer Surge Line Fatigue," *Advances in Dynamics of Piping and Structural Components,* PVP-Volume 198, The American Society of Mechanical Engineers, New York, NY, pp. 23–28.

Deardorff, A. F., et al., 1988, "An Approach for Long-Term NSSS Fatigue Life Assessment/Validation, *ANS/ENS Topical Meeting on Nuclear Plant Life Extension," Snowbird, UT*, pp. 591-598.

Fuchs, H. O., and R. I. Stephens, 1980, *Metal Fatigue in Engineering 4,* John Wiley & Sons, New York, NY, 1980.

Gerber, D. A., and P. Hirschberg, 1991, "Transient Monitoring Program at Diablo Canyon Units 1 and 2," *International Power Generation Conference, San Diego, CA*, ASME 91–JPGC–NE–2.

Golemliewski, H.–J., and M. Miksch, 1993, "Fatigue Monitoring in German Nuclear Power Plants," *Nuclear Engineering and Design 144*, pp. 409–421.

Gosselin, S. R., R. O. Doney, and E. A. Siegel, 1989, "Thermal Transient and Fatigue Monitoring," *Life Assessment and Life Extension of Power Plant Components,* PVP–Volume 171, The American Society of Mechanical Engineers, New York, NY, pp. 133–136.

Gustin, H. L., et al., 1988, "On-Line Fatigue Monitoring of Feedwater Nozzles in Boiling Water Reactors and Pressurized Water Reactors," *Life Extension and Assessment: Nuclear and Fossil Power Plant Components,* PVP-Volume 138, NDE-Volume 4, The American Society of Mechanical Engineers, New York, NY, pp. 189–192.

Hirschberg, P., and G. A. Antaki, 1989, "Measurement of Stratification in the Pressurizer Surge Line," *Design and Analysis of Piping and Components,* PVP–Volume 169, The American Society of Mechanical Engineers, New York, NY, pp. 85–90.

Jaske, C. E., and R. Viswanathan, 1990, "Predict Remaining Life for High Temperature/Pressure Service," *T–8 Symposium on Refining Industry Corrosion, April 23–27, 1990, Las Vegas, NV,* Corrosion 90, NACE, Paper Number 213.

Kato, A., et al., 1993, "Outline of On–Line Fatigue Monitoring System for Nuclear Power Plant," *Service Experience and Life Management: Nuclear, Fossil, and Petrochemical Plants,* PVP–Volume 261, The American Society of Mechanical Engineers, New York, NY, pp. 321–329.

Kergoat, M., et al., "Fatigue Monitoring of PWR Primary Loop and Unclassified Transients," *Developments in Pressure Vessels and Piping,* PVP–Volume 278, The American Society of Mechanical Engineers, New York, NY, p. 85–88.

Kim, J. H., et al., 1993. "Thermal Stratification and Reactor Piping Integrity," *Nuclear Engineering and Design, 139,* pp. 83–95.

Lapides, M. E., et al., 1994, "Measuring Precrack Initiation Fatigue State in Reactor Pressure Vessel Steels," *Plant Systems/Components Aging Management,* PVP–Volume 283, The American Society of Mechanical Engineers, New York, NY, pp. 23–28.

L'Huby, Y., et al., "New Developments in French Transient Monitoring: SYSFAC," *Transactions of the 11th International Conference on Smirt, Tokyo, Japan,* Volume D, pp. 345–351.

Lubin, B. T., et al., 1994, "Structural Evaluation of a Shutdown Cooling Line Subjected to Thermal Stratification due to Turbulent Penetration," *Changing Priorties of Codes and Standards; Failure, Fatigue, and Creep,* PVP–Volume 286, The American Society of Mechanical Engineers, New York, NY, pp. 45–48.

Matthews, M. T., et al. 1990. *Final Submittal in Response to Nuclear Regulatory Commission Bulletin 88–11 "Pressurizer Surge Line Thermal Stratification,"* BAW–2127, Babcock & Wilcox, Lynchburg, VA.

Miksch, M., G. Schon, and B. Thomas, 1988, "FAMOS - A Tool for Transient Recording and Fatigue Monitoring," *Life Extension and Assessment: Nuclear and Fossil Power - Plant Components,* PVP–Volume 138, NDE-Volume 4, The American Society of Mechanical Engineers, New York, NY, pp. 27–34.

Miksch, M., and G. Schücktanz, 1990, "Evaluation of Fatigue in Reactor Components by On–Line Monitoring of Transients," *Nuclear Engineering and Design 119,* pp. 239–247.

Pepka, J. M., and C. B. Bond, 1987, "CMS Records Transient Data and Performs On-Line Analysis," *Nuclear Engineering International,* July, pp. 44–45.

Riccardella, P. C., et al., 1989, *FATIGUEPRO™ On-Line Fatigue Monitoring System: Demonstration at the Quad Cities BWR*, EPRI NP-6170-SD, Electric Power Research Institute, Palo Alto, CA.

Sakai, T., et al., 1993, "Implementation of Automated, On-Line Fatigue Monitoring in a Boiling Water Reactor," *Plant Systems/Components Aging Management,* PVP-Volume 252, American Society of Mechanical Engineers, New York, NY, pp. 67–74.

Shah, V. N. and A. G. Ware, 1994. "Inservice Inspection of Base-Metal Sites Susceptible to Thermal Fatigue Damage," *Changing Priorities of Codes and Standards: Failure, Fatigue, and Creep,* PVP-Vol. 286, American Society of Mechanical Engineers, New York, NY, pp. 9–18.

Society of Automotive Engineers, 1988, *Fatigue Design Handbook, AE-10*, Second Edition.

Stancavage, P. P., 1989a, "The Longevity of BWR Vessels and Internals," *1989 ASME Pressure Vessels and Piping Conference, Honolulu, HI*, PVP-Volume 171, pp. 77–80.

Stancavage, P. P., 1989b, "Integrated Monitoring for BWR Life Extension," *Nuclear Plant Availability Improvement Conference, Madrid, Spain, April 10–14, 1989.*

Stevens, G. L., and S. Ranganath, 1989, "Use of On-Line Fatigue Monitoring of Nuclear Reactor Components as a Tool for Plant Life Extension," *Life Assessment and Life Extension of Power Plant Components,* PVP-Volume 171, American Society of Mechanical Engineers, New York, NY, pp. 85–92.

Strauch, P. L., D. H. Roarty, and L. L. Palusamy, 1990, "Stratification Issues and Experience in Operating Power Plants," *High Pressure Technology, Fracture, Mechanics, and Service Experience in Operating Power Plants,* American Society of Mechanical Engineers, New York, NY, PVP-Volume 192, pp. 85–92.

Su, N. T., 1990, "Review of Thermal Stratification Operating Experience," AEOD/S902, USNRC, Washington, DC.

Takahashi, Y., et al., 1991, "Application of Plant Data Acquisition System to Kashiwazaki-Kariwa N.P.S. Units 3 and 4," *Transactions of the 11th International Conference on Smirt, Tokyo, Japan*, Volume D, pp. 359–364.

Tally, C. W., 1985, "Ensuring the Design Life of a Nuclear Steam Supply System," *Power Engineering*, April.

USNRC, 1990, *BWR Feedwater Nozzle and Control Rod Drive Return Line Cracking*, NUREG-0619.

Ware, A. G., 1994, *Fatigue Monitoring for Aging Assessment of Major LWR Components (Draft)*, NUREG/CR-5824, INEL/94-0089, October 1994.

Ware, A. G., 1990, "Mechanical Damage Experience in Major LWR Systems," *Advances in Dynamics of Piping and Structural Components,* PVP-Volume 198, American Society of Mechanical Engineers, pp. 7–14.

Ware, A. G., and V. N. Shah, 1992, "Lessons Learned from Fatigue Failures in Major LWR Components," *NRC Aging Research Information Conference, March 24–27, 1992, Rockville, MD*, NUREG/CP–0122, Volume 1, pp. 275–295.

NOTICE

NRC FORM 335 (2-89) NRCM 1102, 3201, 3202

U.S. NUCLEAR REGULATORY COMMISSION

BIBLIOGRAPHIC DATA SHEET

(See instructions on the reverse)

1. REPORT NUMBER (Assigned by NRC. Add Vol., Supp., Rev., and Addendum Numbers, if any.)
NUREG/CP-0140
Vol. 3

2. TITLE AND SUBTITLE
Proceedings of the Twenty-Second Water Reactor Safety Information Meeting
Primary Systems Integrity, Structural and Seismic Engineering, Aging Research, Products and Applications

3. DATE REPORT PUBLISHED
MONTH: April
YEAR: 1995

4. FIN OR GRANT NUMBER
A3988

5. AUTHOR(S)
Compiled by Susan Monteleone, BNL

6. TYPE OF REPORT
Conference Proceedings

7. PERIOD COVERED *(Inclusive Dates)*
October 24-26, 1994

8. PERFORMING ORGANIZATION – NAME AND ADDRESS *(If NRC, provide Division, Office or Region, U.S. Nuclear Regulatory Commission, and mailing address; if contractor, provide name and mailing address.)*
Office of Nuclear Regulatory Research
U. S. Nuclear Regulatory Commission
Washington, DC 20555-0001

9. SPONSORING ORGANIZATION – NAME AND ADDRESS *(If NRC, type "Same as above"; if contractor, provide NRC Division, Office or Region, U.S. Nuclear Regulatory Commission, and mailing address.)*
Same as Item 8 above

10. SUPPLEMENTARY NOTES
Proceedings prepared by Brookhaven National Laboratory

11. ABSTRACT *(200 words or less)*

This three-volume report contains papers presented at the Twenty-Second Water Reactor Safety Information Meeting held at the Bethesda Marriott Hotel, Bethesda, Maryland, during the week of October 24-26, 1994. The papers are printed in the order of their presentation in each session and describe progress and results of programs in nuclear safety research conducted in this country and abroad. Foreign participation in the meeting included papers presented by researchers from Finland, France, Italy, Japan, Russia and United Kingdom. The titles of the papers and the names of the authors have been updated and may differ from those that appeared in the final program of the meeting.

12. KEY WORDS/DESCRIPTORS *(List words or phrases that will assist researchers in locating the report.)*
BWR type reactors-reactor safety, international organizations-meetings, PWR type reactors-reactor safety, water cooled reactors-proceedings, Human Factors, Leading Abstract, Reactor Control Systems, Reactor Instrumentation, Probabilistic Estimation, Risk Assessment

13. AVAILABILITY STATEMENT
Unlimited

14. SECURITY CLASSIFICATION
(This Page)
Unclassified
(This Report)
Unclassified

15. NUMBER OF PAGES

16. PRICE

NRC FORM 335 (2-89)